Circ 0 NOV 9 - 1932

U. S. DEPARTMENT OF COMMERCE

BUREAU OF STANDARDS JOURNAL OF RESEARCH

Vol. 9 AUGUST, 1932 No. 2

CONTENTS

RP. No.	TITLE AND AUTHOR	Page
461.	A vacuum tube amplifier for feeble pulses. L. F. Curtiss	115
462.	Infra-red spectra of helium. William F. Meggers and G. H. Dieke	121
463.	Tests of cellular sheet-steel flooring. J. M. Frankland and H. L. Whittemore	131
464.	The influence of temperature on the evolution of hydrogen sulphide from vulcanized rubber. A. D. Cummings	163
465.	Some of the factors which affect the measurement of sound absorption. V. L. Chrisler and Catherine E. Miller	175
466.	The reciprocal spherical aberration of an optical system including higher orders. Harold F. Bennett	187
467.	An attachment for turning approximately spherical surfaces of small curvature on a lathe. I. C. Gardner	227
468.	Wave lengths and Zeeman effects in lanthanum spectra. William F. Meggers	239
469.	Note on the freezing point of "iso-octane" (2, 2, 4-trimethylpentane). Johannes H. Bruun and Mildred M. Hicks-Bruun	269
470.	A twin-bomb method for the accurate determination of pressure-volume-temperature data and a simple method for the accurate measurement of high pressures. Edward W. Washburn	271

BUREAU OF STANDARDS JOURNAL OF RESEARCH

CONTENTS OF RECENT NUMBERS

February, 1932 (Vol. 8, No. 2)

RP407. Deteriorative effect of sulphur dioxide upon paper in an atmosphere of constant humidity and temperature. Arthur E. Kimberly. Price, 10 cents.

RP408. Tensile properties of rail steels at elevated temperatures. G. Willard Quick. Price, 5 cents.

RP409. The resistance to impact of rail steels at elevated temperatures. G. Willard Quick. Price, 5 cents.

RP410. Kaolins; effect of firing temperature on some of their physical properties. R. A. Heindl, W. L. Pendergast, and L. E. Mong. Price, 5 cents.

RP411. Composite-coil electrodynamic instruments. F. B. Silsbee. Price, 10 cents.

RP412. Some studies of radio transmission over long paths made on the Byrd Antarctic expedition. L. V. Berkner. Price, 10 cents.

RP413. Phase equilibra in the system SiO_2-ZnO-Al_2O_3. E. N. Bunting. Price, 5 cents.

RP414. System CaO-Na_2O-Al_2O_3. L. T. Brownmiller and R. H. Bogue. Price, 5 cents.

RP415. Determination of tin in iron and steels. J. A. Scherrer. Price, 5 cents.

March, 1932 (Vol. 8, No. 3)

RP416. Heat of vaporization of water at 50°, 70°, and 90° C. E. F. Fiock and D. C. Ginnings. Price, 5 cents.

RP417. Note on international comparison of X-ray standards. Lauriston S. Taylor.

RP418. The course of the oxidation of the aldose sugars by bromine water. H. S. Isbell and C. S. Hudson. Price, 5 cents.

RP419. Fluctuations of the rate of emissions of α particles for weak sources and large solid angles. L. F. Curtiss.

RP420. Gases obtained from commercial feldspars heated in vacuo. G. R. Shelton and H. H. Holscher. Price, 5 cents.

RP421. Experiments on the emission and absorption of radiation by metallic silver. F. L. Mohler.

RP422. Accelerated weathering tests of soldered and tinned sheet copper. Peter R. Kosting. Price, 5 cents.

RP423. The chromium oxide and the vanadium oxide band spectra. W. F. C. Ferguson. Price, 5 cents.

RP424. Air density corrections for X-ray ionization chambers. Lauriston S. Taylor and George Singer.

RP425. The arc spectrum of phosphorus. C. C. Kiess. Price, 10 cents.

RP426. Some physical properties of levulose and its estimation by copper reduction methods. Richard F. Jackson and Joseph A. Mathews.

April, 1932 (Vol. 8, No. 4)

RP427. The optical requirements of airplane mapping. I. C. Gardner.

RP428. Note on the moving boundary method for measuring transference numbers. A pycnometer for determining the volume change occurring at an electrode and its application to a cathode of silver chloride in a solution of potassium chloride. E. R. Smith.

RP429. Radio field intensity measurements at frequencies from 285 to 5,400 kilocycles per second. S. S. Kirby and K. A. Norton.

RP430. The photographic emulsion: Silver ion and hydrogen ion concentrations and sensitivity. Burt H. Carroll and Donald Hubbard. Price, 10 cents.

RP431. Capacitance and power factor of a mica capacitor as measured at the Bureau of Standards and the National Physical Laboratory. Harvey L. Curtis, C. Matilda Sparks, L. Hartshorn, and N. F. Astbury.

RP432. Isolation and determination of normal heptane and of methylcyclohexane in a mid-continent petroleum. Including a determination of the phase equilibrium diagram for the condensed system normal heptane-methylcyclohexane. Mildred M. Hicks-Bruun and Johannes H. Bruun.

RP433. The spectral erythemic reaction of the untanned human skin to ultra-violet radiation. W. W. Coblentz, R. Stair, and J. M. Hogue.

Research papers, where price is given, are already available, and others will be available in the near future as separates for purchase from the Superintendent of Documents, United States Government Printing Office, Washington, D. C.

U. S. DEPARTMENT OF COMMERCE
R. P. LAMONT, Secretary
BUREAU OF STANDARDS
LYMAN J. BRIGGS, Acting Director

BUREAU OF STANDARDS JOURNAL OF RESEARCH

August, 1932
Vol. 9, No. 2

UNITED STATES
GOVERNMENT PRINTING OFFICE
WASHINGTON : 1932

For sale by the Superintendent of Documents, Washington, D. C. - - - - - - - - $3 per year on subscription

For a partial list of previous research papers appearing in BUREAU OF STANDARDS JOURNAL OF RESEARCH see pages 2 and 3 of the cover

RP461

A VACUUM TUBE AMPLIFIER FOR FEEBLE PULSES

By L. F. Curtiss

ABSTRACT

A resistance-capacity coupled 5-stage amplifier is described which is suitable for automatic registration of the primary ionization pulses produced when corpuscular rays pass through a shallow ionization chamber. A discussion of an improved type of ionization chamber is given.

CONTENTS

	Page
I. Introduction	115
II. Description of the amplifier	116
III. The ionization chamber	119
IV. Acknowledgments	120

I. INTRODUCTION

It has long been recognized that a direct method of recording current pulses produced by ionizing particles, such as α or H rays, would be of great value in the study of this type of radiation. By such a procedure, in which the current pulse occurring in an ionization chamber is amplified linearly and recorded, a decided advance over the now familiar Geiger counter is achieved in that the particle is not only counted, but also the ionization which it produces as it passes through the ionization chamber is instantaneously measured and recorded. In view of the fact that an α ray passing through a chamber 5 mm in depth would produce on the average only about 10^4 ions, the rise in potential of the insulated collector of the ionization chamber can not be much greater than 10^{-4} volt for any practicable value of the capacity of the collector. The problem is therefore to amplify this potential pulse up to the order of 20 volts before applying it to the grid of the output tube of the amplifier. This is very difficult or impossible to do with ordinary radio tubes, since poor grid insulation, large grid currents, large grid capacity, and other undesirable characteristics serve to obliterate entirely the effect of the arrival of such a small charge to the grid. It is not surprising, therefore, that this form of registration has not rapidly replaced the Geiger counter in which the primary ionization is amplified by impact ionization 10^7 times in the counter itself. This augmented ionization current is then easily handled by a very simple amplifier. Thus, once given a satisfactory counter, it is a comparatively simple matter to record the entrance of particles into the counter. However, in the counter the primary ionization serves only as a trigger to set off a much larger impact

ionization which can never be more than very roughly proportional to the primary ionization.

Greinacher [1] first demonstrated that it was possible to amplify directly the primary ionization of a single particle. For this purpose he used an ionization chamber with electric field only sufficiently intense to insure rapid and complete collection of the primary ions. Later developments of this arrangement led to vacuum-tube circuits of many stages of amplification which were not only difficult to operate but risked a serious sacrifice of the linear characteristics required to make the amplifier of value.

More recently the development of amplifiers which meet the requirements of linearity and reasonable convenience of operation have been undertaken by Wynn-Williams and Ward [2] and by Leprince-Ringuet.[3] Although accomplishing the same result the two circuits differ considerably in details. Unfortunately neither circuit is readily available to investigators working in this country, since the tubes used are of foreign manufacture, therefore it is difficult to procure or to replace them, or to secure information to enable one to select from tubes available here those which would have similar characteristics. For these reasons the writer, in undertaking to construct an amplifier, was faced with the necessity of working out an arrangement based on the principles outlined by Wynn-Williams and Ward, but making use of entirely different types of tubes with the exception of the output tube. In doing this it was found possible to use commercial radio tubes in all stages except the first. The tube used here is so simple in construction that it can be made in almost any laboratory, and full details of its construction are given.

Since a complete discussion of the principles involved in the design of such circuits is given by Wynn-Williams and Ward and the theory of the operation is very adequately discussed by Ortner and Stetter,[4] these matters are not discussed here.

II. DESCRIPTION OF THE AMPLIFIER

As pointed out by Leprince-Ringuet, the essential difficulty met with in amplifying these primary ion pulses is that of conserving the small quantity of charge and converting the sudden rise in potential produced when this charge is driven on to the collecting system of the ionization chamber into a current pulse which can be readily amplified. No ordinary radio tube is suitable for this purpose, since the grid in such tube is not insulated sufficiently to deal successfully with such small quantities of charge. Since neither the tube used by Wynn-Williams and Ward nor by Leprince-Ringuet was available, the writer constructed a simple tube from the description given by Leprince-Ringuet. Figure 1 shows a sketch of this tube. It is a 3-electrode tube which departs from the usual arrangement in that the filament is located between the grid G and the plate P, the grid in this case being a plane electrode like the plate. The filament (an oxide-coated nickel ribbon operating on 0.4 ampere and 0.6 volt) is stretched parallel to the plane of these electrodes. The filament and plate leads are taken out

[1] H. Greinacher, ZS. f. Phys., vol. 36, p. 364, 1926.
[2] C. E. Wynn-Williams and F. A. B. Ward, Proc. Roy. Soc., vol. 131, p. 391, 1931.
[3] L. Leprince-Ringuet, Annales des P. T. T., vol. 20, p. 480, 1931.
[4] G. Ortner and G. Stetter, ZS. f. Phys., vol. 54, p. 449, 1929.

through a press seal at the lower end of the tube, the grid lead being brought out separately at the top. This arrangement provides for better insulation of the grid which is further increased by making the tube of pyrex glass. Other features of this tube which make it particularly suited to this work are a a low grid-ground capacity and a filament emission limited by space charge. The high insulation and low capacity of the grid, a plate about 1 cm square, make possible the rapid and sufficient rise of potential of the grid required to produce a current pulse in the plate circuit. The space-charge characteristics of this tube are of great value in cutting down the shot effect. With several succeeding stages of amplification, the shot effect becomes one of the limiting factors in the operation of the amplifier. This effect is so large in ordinary tubes that they can not be used in the first stage since the current pulses resulting from it mask entirely the pulses which come from the ionization chamber.

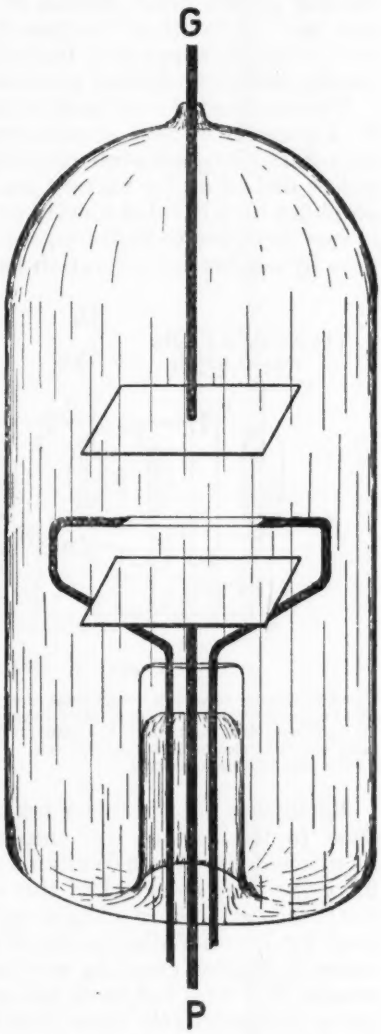

FIGURE 1.—*Diagram of special electrometer tube*

G=grid lead; *P*=plate lead

It is quite possible that other types of electrometer tubes, for example the FP54, would serve here, but the tube described is much simpler in construction and operation and likewise less expensive.

Having determined the type of tube for the input stage, the remainder of the amplifier becomes more or less routine radio practice as related to audio-frequency resistance-capacity coupled amplifiers. The complete circuit is shown in the wiring diagram reproduced in Figure 2. It has five stages, four of which use commercial radio tubes. In order to obtain as much amplification per stage as possible, thus reducing the required number of stages, screen grid alternating current amplifier tubes (type 224) were selected for the three amplifying stages. Following Wynn-Williams and Ward, a pentode was used in the output stage and the time constants of all these stages were made large. The amplifying constant of the 224 tubes connected as shown is 1,000. Naturally the amplification per stage does not attain such a high value, but with the resistances here used it is reasonable to

expect an over-all amplification of about 100 per stage. This high degree of amplification is necessary since, as Leprince-Ringuet points out, the input tube does not amplify the potential applied to it. In fact, the potential surge produced at the plate end of the plate circuit resistor by the plate current of this tube is probably of the order of one one-hundredth of the rise of potential of its grid. However, this is a potential surge in a battery-fed current which can be amplified readily without unusual precautions regarding insulation.

The constants for all parts of the circuit are given below the diagram in Figure 2. Those condensers not designated by a letter are 2 microfarad by-pass condensers to shield the amplifier from extraneous pulses picked up by battery leads. Thorough shielding of the whole amplifier by a divided metal box is of course essential. The amplifier is very sensitive to high-frequency oscillations which ruin its effectiveness by setting up relaxation oscillations in the coupling condensers.

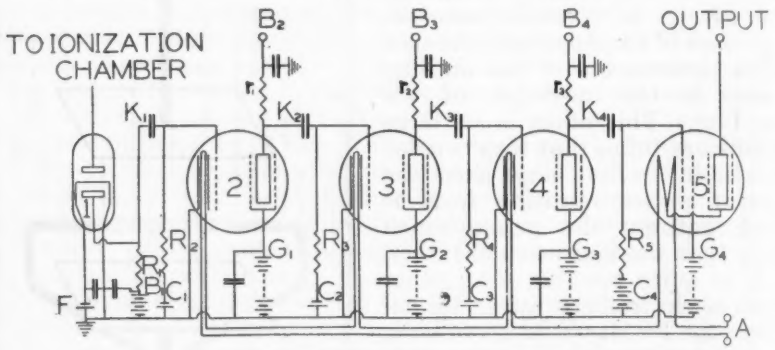

FIGURE 2.—*Wiring diagram of amplifier*

1=Electrometer tube; 2, 3, 4=224 tubes; 5=247 tube; r_1, r_2, r_3=250,000 ohms; R_3, R_4, R_5=1 megohm; R_2=2 megohms; R_1=250,000 ohms; B_1=4.5 volts; B_2, B_3, B_4=250 volts; G_1, G_2, G_3=25 volts; G_4=250 volts; C_1, C_2, C_3=1.5 volts; C_4=25 volts; K_1=0.0005 microfarad; K_2, K_3=0.1 microfarad; K_4=2 microfarad. F(filament battery for electrometer tube)=0.6 volt. A=10 volts (1.75 amperes). Condensers not designated are 2 microfarad by-pass condensers.

Particular note is to be taken of the coupling of the electrometer tube to the rest of the amplifier. This is the "distorting" stage mentioned by Wynn-Williams and Ward. It is very important to have the time constant of this circuit small. The value used here is 0.001 second. Since a higher value of grid leak was required than that used by Wynn-Williams and Ward, this small constant is secured by using a smaller coupling condenser (0.0005 microfarad). For some reason that does not seem self-evident, Leprince Ringuet was able to use a comparatively slow circuit at this point (0.04 second). However, he does not give a diagram of his complete circuit so that he may have introduced the "disotrtion" at a later stage. It may be well to emphasize that it is not safe to depend merely on the values of the resistances and capacities given and to construct an amplifier without testing its performance thoroughly by means of an oscillograph. This is particularly important, of course, when other forms of recording are to be used. The writer's experience indicates that only by taking careful oscillograph records can it be made certain that the amplifier is functioning properly.

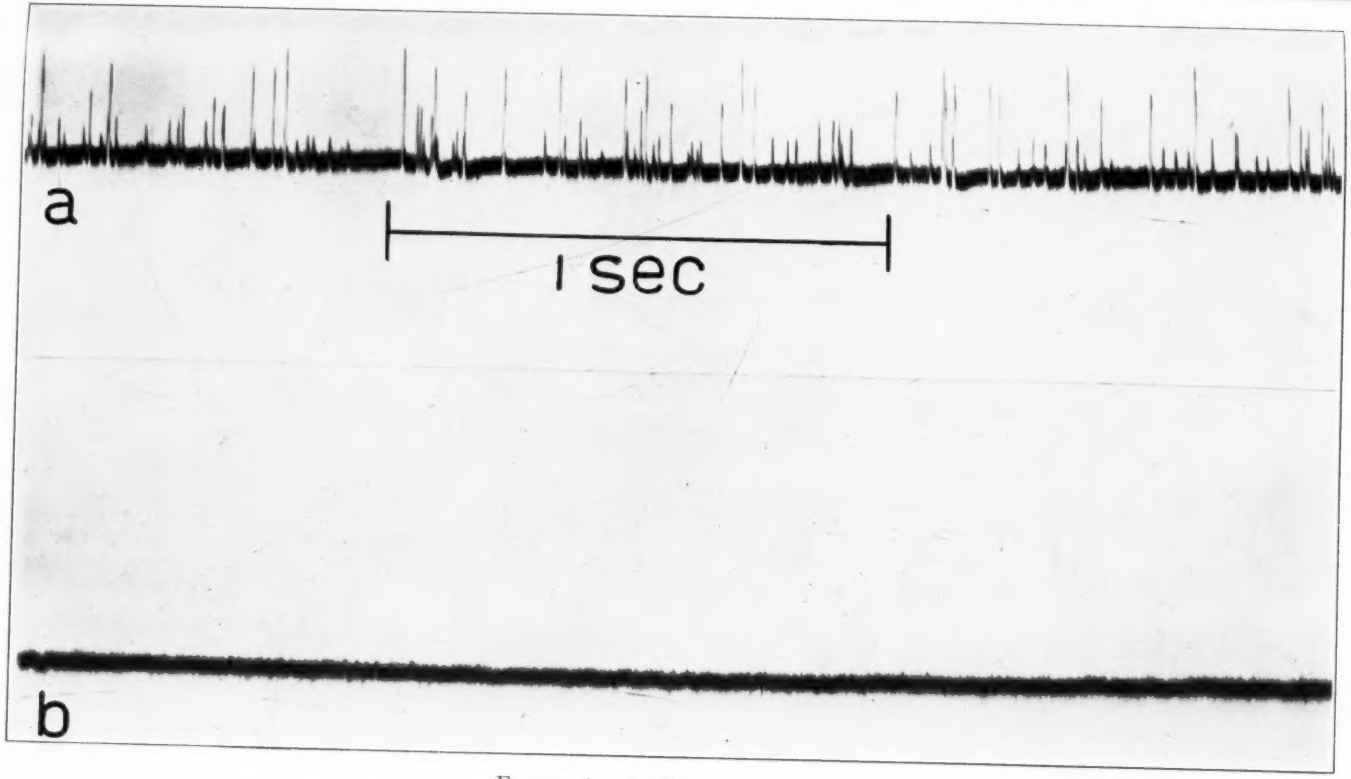

UNIV. OF MICH.

FIGURE 4.—*Oscillograph records*

a, α particles in presence of β and H particles; *b*, zero line in absence of radiation.

III. THE IONIZATION CHAMBER

Wynn-Williams and Ward describe the precautions to be taken in designing ionization chambers for use with an amplifier of this kind. The guard-ring type of chamber is particularly suited for this use, but in the form which they describe the "parasitic" capacity has not been reduced to a minimum. Their design is shown in Figure 3(*a*). The capacity of this system consists of (1) that between the window, *W*, and the electrode, *E;* (2) that of the cylindrical condenser formed between the guard ring, *G*, and the electrode, *E*; and (3) the capacity of the lead, *L*, mainly located at the point where it passes through the insulator, *S*. The capacity (1), is that of the ionization chamber itself and can not be reduced without reducing the effective volume of the chamber. The other two, however, are not associated with the volume of the chamber and any means of reducing them will increase the sensitivity of the arrangement. Of these, (2), that represented by the cylindrical condenser between the electrode, *E*,

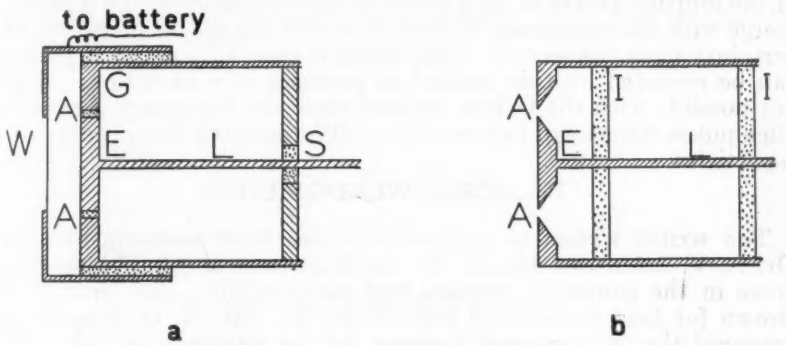

FIGURE 3.—*Section of ionization chambers*

and the guard ring, *G*, is by far the largest. In fact, it may be several times larger than the rest of the capacity of the system, particularly when, as in the chamber described by Wynn-Williams and Ward, insulating material is inserted in the annular gap to support the electrode, *E*. This difficulty may be greatly reduced by modifying the internal parts of the ionization chamber as shown in Figure 3 (*b*). The electrode, *E*, and the guard ring here have tapered edges which reduce the capacity at this point to a minimum. The insulator is removed entirely. The lead, *L*, is supported by two large insulators, *I*, at points where the capacity is a minimum. This requires the lead, *L*, to be stiffer and, therefore, of larger diameter, but the actual increase in capacity between, say, 0.5 millimeters and a 1.5-millimeter rod at this point is small compared with the reduction of capacity effected by the modification.

As examples of the kind of records that may be obtained with this amplifier and ionization chamber, reproductions of oscillograph records are shown in Figure 4 (*a*) and (*b*). Figure 4 (*a*) is a record of α particles obtained in the presence of β and H radiation and indicates the ease with which different types of radiation may be identified. Figure 4 (*b*) a blank record on the same time scale, indicates the nature of the zero line in the absence of radiation. The

unsteadiness in this line is made up of a combination of effects, such as shot effect in the first tube, sound vibrations in the ionization chamber, and mechanical shock, all of which may set up small pulses in the amplifier. The ionization chamber with a thin metal window is a sensitive microphone which must be shielded as far as possible from all sound. The zero line is much less steady than that shown if reasonable precautions are not taken to shield the complete amplifier from noise and mechanical shock.

The tallest peaks in Figure 4 (*a*) are due to α particles and vary slightly in height as a result of differences in speeds and in lengths of paths of the particles as they traverse the ionization chamber in different directions. The shortest sharp peaks are produced by H particles and are roughly of one-fourth the height of the peaks due to α particles. Since a high-speed α particle produces about the same ionization as a low-speed H particle, there are some peaks of intermediate height which could not be identified merely by a study of the record. Since a β particle has only about one two-hundredth of the ionizing power of an α particle, the ionization of the β particles merge with the extraneous disturbances and can not be identified with certainty from the record. This makes it clear why α and H particles can be recorded by this method in presence of γ radiation. This is not possible with the Geiger counter since the secondary β rays produce pulses which can not readily be differentiated from those due to α particles.

IV. ACKNOWLEDGMENTS

The writer wishes to acknowledge aid from consultations with Dr. A. V. Astin and Dr. G. W. Gardiner regarding problems which arose in the course of constructing the amplifier, and from B. W. Brown for help in building and testing it. Mr. R. G. Kenedy, jr., prepared the oxide-coated filament for the electrometer tube. The writer is particularly grateful to Dr. F. West and to Dr. C. F. Burnam, of the Howard A. Kelly Hospital of Baltimore, for the material from which the polonium source used in testing the amplifier was extracted.

WASHINGTON, May 16, 1932.

RP462

INFRA-RED SPECTRA OF HELIUM

By William F. Meggers and G. H. Dieke [1]

ABSTRACT

Employing Xenocyanine photographic plates to explore the infra-red spectra of helium emitted by a Geissler tube used "end-on" about 120 new lines were recorded in the spectral interval 8,361 to 11,045 A. Analysis of these data shows that 32 of the lines belong to the arc spectrum of neutral He atoms (He I) and the remainder are ascribed to the band spectrum of the He_2 molecule. The He I lines are accounted for as combinations of previously known terms and as extensions to the fundamental series, while the He_2 lines for the most part represent hitherto lacking intercombinations between groups of terms which account for the visible bands of helium.

CONTENTS

	Page
I. Introduction	121
II. Experimental	121
III. Results	122
1. The He I spectrum	122
2. The He_2 spectrum	124
3. Constants	126

I. INTRODUCTION

The spectra of helium have been investigated [2] so extensively that they would appear to have been exhausted. However, the recent discovery of a remarkable new infra-red sensitizer, Xenocyanine, by the Eastman Kodak Research Laboratories [3] has greatly extended the photographic range of spectra, and use of these plates at the Bureau of Standards has revealed many new lines in the emission spectra of chemical elements. Up to the present, the longest published wave length observed photographically from helium was 7,281 A, but with Xenocyanine plates 120 lines have been recorded in the infra-red between 8,361 and 11,045 A. In this range, only the reasonance line at 10,830 A was known, since its detection radiometrically by Paschen [4] in 1908. Analysis shows that 32 of the above lines belong to the He I spectrum, while the remainder are ascribed to the band spectrum of the He_2 molecule.

II. EXPERIMENTAL

The source of the infra-red He spectra described in this paper was a Geissler tube made by Robert Goetze in Leipzig. It had a narrow capillary and was designed for end-on projection of the light into the

[1] Associate Professor of Physics, The Johns Hopkins University.
[2] H. Kayser, Handbuch der Spectroscopie, vol. 5, p. 508, 1912. H. Kayser, and H. Konen, Handbuch der Spectroscopie, vol. 7, p. 606, 1930.
[3] C. E. K. Mees, J. Opt. Soc. Am., vol. 22, p. 204, 1932.
[4] F. Paschen, Ann. der Phys. (4), vol. 27, p. 537, 1908.

spectrograph. The tube was operated with uncondensed discharges from a 40,000-volt transformer, the primary of which was fed by 5 or 6 amperes, 60 cycle, alternating current, 110 volts.

A concave grating spectrograph in Wadsworth mounting[5] was employed in recording the spectra on Xenocyanine plates, the He exposure being made in the first order spectrum in which the dispersion is 10.26 A per millimeter. Comparison spectra of the iron arc were photographed in the second order of the grating, above and below the He exposure, and wave-length measurements were based on the internationally adopted secondary standards.[6] The duration of exposure averaged 16 hours for He and 2 minutes for Fe.

The appearance of such a large number of new lines in the He exposures first suggested the presence of impurities or spurious lines, but careful examination showed that the O I triplet at 9,260.9, 9,262.8, and 9,266.1 A was the only impurity, and no evidence of Lyman ghosts was found. It was immediately suspected that most of the lines in this region must be due to the He_2 molecule, but the production of this band spectrum under the conditions of excitation employed was somewhat surprising. It is well known that the ordinary Geissler tube of He excited by uncondensed discharges shows only the so-called arc spectrum, He I. The band spectrum of the He_2 molecule is excited with great intensity by using a higher pressure of He in a discharge tube with a large bore in place of the usual capillary, and passing through it discharges from an induction coil or transformer with a condenser in parallel and a small spark gap in series with the tube,[7] but it appears also with uncondensed discharges in tubes with a very fine constriction in the bore.[8] The latter conditions are approximated by the tube described above, and probably account for the production of the observed mixture of He I and He_2 spectra.

III. RESULTS

1. THE He I SPECTRUM

The Bohr model of a neutral He atom consists of a nucleus and two electrons so that its characteristic spectrum must resemble that of alkaline earths with two valence electrons. Its energy states must comprise a system of singlet terms and a system of triplet terms, among which singlet S (1^1S_o) represents the normal state of the atom.

Analysis of the structure of the He I spectrum has been summarized in treatises on spectral series[9] in which singlet and doublet systems are described. In the last treatise, it is shown that the doublet system is in reality a triplet system in which the level separations are so small that they are difficult to detect. Partial resolution of the ^3P terms gave the impression of doublets in the spectrum. Since the new infra-red (He I) lines are all accounted for as combinations of known terms or extensions of known series we are presenting our results in Table 1 in Grotrian's modern notation. Table 1 may,

[5] W. F. Meggers and K. Burns, B. S. Sci. Paper (No. 441), vol. 18, p. 191, 1922.
[6] Trans. Internat. Astron. Union, vol. 3, p. 86, 1928.
[7] W. E. Curtis, Proc. Roy. Soc. A 89, p. 146, 1913.
[8] T. R. Merton and J. G. Pilley, Proc. Roy. Soc. A 109, p. 267, 1925.
[9] A. Fowler, Series in Line Spectra, p. 91, Fleetway Press, London, 1922. F. Paschen and R. Goetze, Seriengesetze der Linienspektren, p. 26, Julius Springer, Berlin, 1922. W. Grotrian, Handbuch der Astrophysik, vol. 3, p. 555, Julius Springer, Berlin, 1930.

however, be regarded as an extension to the He tables in any of the above-mentioned reports.

TABLE 1.—*He I*

Fundamental series $3^1D = 12{,}205.09$. $3^1D - m^1F$

λ_{air}	Intensity	ν_{vac}	m	m^1F
18,693.4	2	5,348.0	4	6,857.1
12,792.2	1	7,815.1	5	4,390.0
10,917.0	3	9,157.5	6	3,047.6
10,031.16	15	9,966.20	7	2,038.9
9,529.27	4	10,491.10	8	1,714.0
9,213.1	1	10,851.1	9	1,354.0

Fundamental series $3^3D = 12{,}209.10$. $3^3D - m^3F$

18,684.2	3	5,350.71	4	6,858.39
12,784.6	1	7,819.89	5	4,389.21
10,912.95	6	9,160.92	6	3,049.82
10,027.73	40	9,969.61	7	2,239.49
9,526.17	10	10,494.52	8	1,714.58
9,210.28	6	10,854.46	9	1,354.64
8,996.7	2	11,112.1	10	1,097.0
8,845.0	1	11,302.7	11	906.4

Combinations

λ_{air}	Intensity	ν_{vac}	Combination
10,233.0	2	9,769.6	$3^1P - 7^1S$
9,682.4	1	10,325.2	$3^1P - 8^1S$
11,045.1	1	9,051.3	$3^1P - 6^1D$
10,138.50	10	9,860.69	$3^1P - 7^1D$
9,625.80	3	10,385.90	$3^1P - 8^1D$
9,303.2	2	10,746.0	$3^1P - 9^1D$
9,085.6	1	11,003.4	$3^1P - 10^1D$
11,013.1	1	9,077.6	$3^1S - 5^1P$
9,603.50	6	10,410.01	$3^1S - 6^1P$
8,914.7	2	11,214.4	$3^1S - 7^1P$
10,667.62	4	9,371.60	$3^3P - 6^3S$
9,702.66	10	10,303.63	$3^3P - 7^3S$
9,346.2	2	10,896.6	$3^3P - 8^3S$
10,311.32	40	9,695.43	$3^3P - 6^3D$
9,516.70	30	10,504.97	$3^3P - 7^3D$
9,063.40	6	11,030.36	$3^3P - 8^3D$
10,072.10	2	9,925.70	$3^3D - 7^3P$
9,552.8	1	10,465.3	$3^3D - 8^3P$
9,463.66	60	10,563.84	$3^3S - 5^3P$
8,361.7	3	11,956.0	$3^3S - 6^3P$

The so-called fundamental (hydrogenlike) series of He have been extended from 2 to 6 members in the singlet system and from 2 to 8 in the triplet system, the first two lines of each series representing the radiometric observations of Paschen, so that the intensities of these are not to be compared with the photographic estimates of the remainder. The third line of each series lies close to 11,000 A, and to compensate for declining photographic sensitivity their estimated intensities should be multiplied by 10 or more to make them comparable with the succeeding lines.

2. THE He_2 BANDS

The known energy levels of the helium molecule [10] may be regarded as originating from a single valence electron and may therefore, be classified as $s\Sigma$, $p\Sigma$, $p\Pi$, $d\Delta$, etc., levels in which the s, p, d mean, as in atomic spectra, that the orbital moment of the valence electron is 0, 1, 2, whereas the symbols Σ, Π, Δ designate the component Λ of this orbital momentum along the internuclear axis. The low levels which are the final states in the transitions which give rise to the visible helium bands are $2s\Sigma$, $2p\Pi$, and $2p\Sigma$. The negative s and d levels combine with the $2p\Sigma$ and $2p\Pi$ levels, whereas the positive p levels combine with the $2s\Sigma$ level. This fact divides the terms of the helium molecule into two groups, the $2s\Sigma$ level and those terms which combine with it on the one hand and the $2p\Sigma$ and $2p\Pi$ levels and those terms which combine with them on the other hand. The relative term values in each group can be determined with the accuracy of the wave-length measurements, but the relative position of the two groups can only be determined by calculating the limits of two Rydberg series. This is due to the fact that all the intercombinations between the two groups which are allowed by the selection rules must fall in the infra-red and were not observed so far.

The new lines in the infra-red given in the present paper are partly due to just such transitions.[11] The most prominent band in this region has its head at 9,123 A and is due to a transition $2p\Sigma \rightarrow 2s\Sigma$. (See Table 2.)

TABLE 2.—*He_2*

Band at 9,123 A $2p\Sigma \rightarrow 2s\Sigma$

K	P branch			R branch		
	λ	I	ν	λ	I	ν
1	9,193.55	4	10,874.21	9,158.92	7	10,915.32
3	9,222.96	10	839.53	42.23	12	935.25
5	57.50	20	799.09	30.66	10	949.11
7	97.14	20	753.05	24.29	8	956.75
9	9,341.91	15	701.51	23.17	6	958.10
11	91.90	10	644.55	27.34	5	953.09
13	9,447.12	8	582.34	37.00	5	941.51
15	9,507.74	8	514.86	52.23	5	923.30
17	73.90	7	442.20	73.18	5	898.36
19	9,645.68	7	364.49	9,200.00	5	866.59
21	9,723.33	6	281.72	33.03	3	827.71
23	9,807.13	5	193.87	72.60	2	781.50
25	97.47	3	100.82	----------	----------	----------
27	9,994.6	1	002.7	----------	----------	----------

Band at 9,346 A $2p\Sigma^1 \rightarrow 2s\Sigma^1$

1	----------	----------	----------	9,376.6	1	10,661.9
3	9,441.6	2	10,588.5	60.67	2	680.07
5	77.72	3	548.17	50.50	2	691.69
7	9,519.39	3	501.99	46.2	2	696.6
9	67.08	3	449.64	48.0	2	694.5
11	9,620.88	2	391.21	55.70	2	685.74
13	80.54	2	327.17	69.8	1	669.7
15	9,746.64	2	257.13	90.3	1	646.4
17	9,819.18	2	181.36	----------	----------	----------
19	98.67	2	099.60	----------	----------	----------
21	9,985.43	1	011.85	----------	----------	----------

[10] All the bands discussed in this paper belong to the triplet system. The triplet separation, however, is so small that the lines appear single, except in some cases under very high dispersion. The singlet system is weaker and much less completely known. No singlet bands were found in the region under investigation.

[11] On photographs sent to one of us two years ago by Prof. T. Takamine which were taken on Neocya nine plates under low dispersion, the presence of bands in the infra-red could be seen. The dispersion was not large enough, however, to permit an analysis.

Both the initial and the final state of this band are already known. The final state is that of the so-called main series [12] ($2s-np$ in the old notation) which contains the most prominent bands of the spectrum. The initial state $2p\Sigma$ is the final state of a group of bands, the first of which was discovered by Merton and Pilley [13] and which are described in full elsewhere.[14]

The combination relations given in Table 3 prove the identity of the band. The second column (marked new) gives the rotational differences of the final state

$$R(K-1)-P(K+1)=2s\Sigma(K+1)-2s\Sigma(K-1)$$

The next column gives the average of the same differences obtained from the bands of the main series.[15] The agreement is very good which proves that $2s\Sigma$ must be the final state of the band.

In the same way we prove from the agreement of the differences

$$R(K)-P(K)=2p\Sigma(K+1)-2p\Sigma(K-1)$$

given in column 7 for the new band and in column 8 for the previously known bands which have $2p\Sigma$ as final state that $2p\Sigma$ is the initial state of the new band. The band has only a P and R branch as must be expected for a $\Sigma \rightarrow \Sigma$ transition.

There is a fainter band of exactly the same structure with its head at 9,346 A. (See Table 2.) It is the $2p\Sigma\,^1 \rightarrow 2s\Sigma\,^1$ band which has the same electronic transition as the band at 9,123 A mentioned above, but a $1 \rightarrow 1$ vibrational transition (instead of $0 \rightarrow 0$ for λ 9,123). The columns 4 and 5 of Table 3 prove in the same way as explained above for the main band that $2s\Sigma\,^1$ is actually the final state. The initial state $2p\Sigma\,^1$ was not known before.

TABLE 3.—*Combination relations*

K	$2s\Sigma(K+1)-2s\Sigma(K-1)$				K	$2p\Sigma(K+1)-2p\Sigma(K-1)$		
	$v=0$		$v=1$			$v=0$		$v=1$ (new)
	New		New			New		
2	75.79	75.80	73.4	73.39	1	41.11	41.07	--------
4	136.16	136.20	131.90	131.87	3	95.72	95.69	91.57
6	196.06	196.06	189.70	189.84	5	150.02	150.00	143.52
8	255.24	255.22	247.0	247.08	7	203.70	203.69	194.61
10	313.55	313.49	303.3	303.47	9	256.59	256.61	248.86
12	370.75	370.76	358.57	358.63	11	308.54	308.56	294.53
14	426.65	426.63	412.6	412.60	13	359.17	359.14	342.53
16	481.10	481.07	465.0	465.03	15	408.44	408.22	389.27
18	533.87	533.85	----------	----------	17	456.16	456.45	--------
20	584.87	584.91	----------	----------	19	502.10	----------	--------
22	633.84	633	----------	----------	21	545.99	----------	--------
24	680.68	680	----------	----------	23	587.63	----------	--------

Besides the two bands given above, we must expect in this region the bands $3s\Sigma \rightarrow 2p\Sigma$ and the whole $3d \rightarrow 2p\Sigma$ complex. Only a few lines of the $3s\Sigma \rightarrow 2p\Sigma$ band could be identified near 10,400 A. The sensitiveness of the photographic plate in this region is already too

[12] W. E. Curtis and R. G. Long, Proc. Roy. Soc., A 108, p. 513, 1925.
[13] T. R. Merton and F. G. Pilley, Proc. Roy. Soc., A 109, p. 267, 1925.
[14] G. H. Dieke, S. Imanishi, and T. Takamine, ZS. f. Phys., vol. 57, p. 305 1929
[15] Mainly from unpublished data in the possession of one of the authors

weak to allow also the weaker lines to be recorded. The $3d \rightarrow 2p\Sigma$ complex is completely present, it is given in Table 4. The calculated frequencies are obtained with the help of the known differences between the $2p\Sigma$ and the $2p\Pi$ states. This band complex shows the same characteristics as the $4d \rightarrow 2p\Sigma$ complex.[16] The P branch of $3d\Sigma \rightarrow 2p\Sigma$ is practically absent, and the R branch of $3d\Pi \rightarrow 2p\Sigma$ can not be found at all. This is due to the decoupling of the orbital momentum. The band $3d\Delta \rightarrow 2p\Sigma$ is entirely absent. It is forbidden if the orbital momentum is coupled to the internuclear axis, as Λ would change by two units. For the $3d\Delta$ states the decoupling is still very small. For the $4d\Delta$ and $5d\Delta$ states it is much bigger, and, therefore, the transitions from these states to the $2p\Sigma$ state are present, though with faint intensity.

Also the $5p\Pi$, $6p\Pi$, etc., $\rightarrow 3s\Sigma$ transitions have to be expected in this region. But they are apparently much weaker than the bands mentioned above and were not found.

TABLE 4.

$3d\ \Sigma \rightarrow 2p\Sigma$

K	P branch			R branch		
	Vcalc.	I	Vobs.	Vcalc.	I	Vobs.
0				10,667.76	1	10,667.6
2	10,626.67			71.75	3	71.58
4	576.05	[1] 2d	10,576.3	65.26	4	65.17
6	515.25	[2] 8	514.86	53.90	5	53.72
8	450.20	[3] 3	449.64	40.11	4	40.09
10	383.51	1	383.38	26.02	4	26.03
12	317.47	1–	317.5	12.13	3	12.05
14	252.97	1–	252.8	599.29	2	599.03
16	190.86			87.44	2	87.6
18					2	76.3

[1] Confused with R_{18}.
[2] Masked by P_{13} of 9,123.
[3] From P_9 of λ 9,346.

$3d\ \Pi \rightarrow 2p\Sigma$

K	P branch			Q branch			R branch		
	Vcalc.	I	Vobs.	Vcalc.	I	Vobs.	Vcalc.	I	Vobs.
0							10,897.18		
2	10,853.09			10,863.77	2	10,863.8	932.61		
4	37.24	1	10,837.14	60.16	2	60.02	990.40		
6	40.42		(1)	54.84	[3] 6	54.46	11,050.84		
8	46.96	2	46.8	48.36	2	48.32	110.86		
10	54.42	[2] 6	54.46	41.57	1	41.2	169.68		
12	60.98	1	60.9	34.69	1	34.44	226.19		
14	67.05		(2)	28.43	1	28.4	280.75		
16	72.10	1	71.9	23.17	1	23.2	333.25		
18					1	19.2			

[1] Too close to P_3 of λ 9,123.
[2] P_{10}, Q_8, and 3^1D—9^1F.
[3] Too close to R_{19}.

3. CONSTANTS

The constants which can be calculated from the bands at 9,123 and 9,346 Å are

$$\lambda\ 9{,}123 : 2s\Sigma \rightarrow 2p\Sigma \qquad \nu_0 = 10{,}889.59$$
$$\lambda\ 9{,}346 : 2s\Sigma^1 \rightarrow 2p\Sigma \qquad \nu_0 = 10{,}637.8$$

[16] G. H. Dieke, ZS. f. Phys., vol. 57, p. 71, 1929.

From these values for the origins of the bands it follows that the difference between the first and second vibrational state of the initial electronic level is

$$\text{for } 2p\Sigma \qquad \omega = 1{,}481.0$$

if the value of ω for $2s\Sigma$ is 1,732.8.

The rotational constants are

$$\begin{array}{lll} 2p\Sigma\ v=0 & B=6.851 & \beta = 5.42 \cdot 10^{-4} \\ \quad v=1 & B=6.55 & \end{array}$$

in which B and β are the constants in the formula

$$B(K+\tfrac{1}{2})^2 - \beta(K+\tfrac{1}{2})^4$$

for the rotational energy.

It is interesting to note that the values B and ω for the $2p\Sigma$ state are the smallest of all levels observed so far. This means that the bond which holds the two atoms together is weakest for the $2p\Sigma$ state. It is weaker than for the He_2^+ ion for which the constants are

$$B = 7.10\ ^{17}$$
$$\omega = 1{,}627.2\ ^{18\ 19}$$

As stated above it is possible now with the help of the $2p\Sigma \rightarrow 2s\Sigma$ band to calculate all the relative term values of the triplet system with the accuracy of the wave-length measurements. In order to obtain the absolute energy values it is necessary to calculate the limit of one Rydberg series. We take

$$2s = 34{,}301.8$$

which is the value which Curtis and Long [20] calculated from the limit of the series $np\Pi \rightarrow 2s\Sigma$.[21] Then we get for the other low terms

$$2p\Pi = 29{,}533.7$$
$$2p\Sigma = 23{,}412.2$$

All other terms can then be easily calculated from the zero lines of the bands which have the level in question as initial level.

The $2p\Pi$ term can also be directly calculated as head of the $ns\Sigma \rightarrow 2p\Pi$ series. The value obtained in this way is $2p\Pi = 29{,}530.7$.[22] The difference of only 3 cm^{-1} between this value and the value given above shows how well the terms can be represented by a Rydberg series.

Finally, all of the infra-red He lines observed photographically are presented in order of increasing wave length in Table 5, in which the column headings are either self-explanatory or given by the key to the classifications.

---

[17] See footnote 16, p. 126.
[18] W. Weizel and E. Pestel, ZS. f. Phys., vol. 56, p. 197, 1929.
[19] S. Imanishi, Sc. Pa. Inst. Phys. Chem. Res., vol. 11, p. 139, 1929.
[20] See footnote 12, p. 125.
[21] If we assume the value calculated in the usual way from the head of a Rydberg series we assume that the actual levels which have half a quantum of vibrational energy follow the Rydberg law. It looks more plausible to assume that the actual electronic levels; that is, the levels extrapolated to no vibrational energy are the ones which obey the Rydberg formula more closely. Imanishi (see footnote 19) has calculated the limit of the $np\Pi \rightarrow 2s\Sigma$ series under this assumption and found a somewhat different value for $2s\Sigma$. But also this procedure is open to objections as the different orientation for the orbital momentum cause a shift and splitting up of the levels. (The $s\Sigma$ terms would be free from this objection.) On account of this complication, and because the absolute values of the energies are of very little importance for most purposes anyway, we have chosen the old value of Curtis and Long rather than that of Imanishi.
[22] G. H. Dieke, Phys. Rev., vol. 38, p. 646, 1931.

TABLE 5.—*Infra-red He spectra*

Key to the classification of the He_2 lines:

A: $2p\Sigma \rightarrow 2s\Sigma$.
B: $2p\Sigma^1 \rightarrow 2s\Sigma^1$.
C: $3d\Pi \rightarrow 2p\Sigma$.
D: $3d\Sigma \rightarrow 2p\Sigma$.
E: $3s\Sigma \rightarrow 2p\Sigma$.

Intensity	λ_{air} I. A.	ν_{vac} cm^{-1}	He I	He_2				
				A	B	C	D	E
3	8,361.7	11,956.0	3^3S-6^3P					
3	8,776.69	403.41						
1	8,845.0	302.7	3^3D-11^3F					
2	8,914.7	214.4	3^1S-7^1P					
2	8,996.7	112.1	3^3D-10^3F					
1–	8,997.6	111.0						
6	9,063.40	030.36	3^3P-8^3D					
1	82.9	006.7						
1	85.6	11,003.4	3^1P-10^1D					
1	9,094.90	10,992.16						
6	23.17	958.10		R_9				
8	24.29	956.75		R_7				
5	27.34	953.09		R_{11}				
10	30.66	949.11		R_5				
5	37.00	941.51		R_{13}				
12	42.23	935.25		R_3				
5	52.23	923.30		R_{15}				
7	58.92	915.32		R_1				
5	73.18	898.36		R_{17}				
2	74.6	896.7	3^3P-8^3S					
4	93.55	874.21		P_1				
1	9,195.5	871.9				P_{15}		
5	9,200.00	866.59		R_{19}				
2	02.4	863.8				Q_3		
1	04.8	860.9				P_{14}		
2	05.56	860.02				Q_4		
6	10.28	854.46	3^3D-9^3F			Q_6; P_{10}		
1	213.1	851.1	3^1D-9^1F					
2	15.49	848.32				Q_8		
2	16.8	846.8				P_8		
1	21.5	841.2				Q_{10}		
10	22.96	839.53		P_3				
1	25.00	837.14				P_4		
1	27.29	834.44				Q_{12}		
1	32.5	828.4				Q_{14}		
3	33.03	827.71		R_{21}				
1	36.9	823.2				Q_{16}		
1	40.3	819.2				Q_{18}		
1	49.6	808.3						
20	57.50	799.09		P_5				
2	60.91	795.11						
3	62.78	792.94						
4	66.10	789.07						
2	72.60	781.50		R_{23}				
20	9,297.14	753.05		P_7				
1	9,303.2	746.0	3^1P-9^1D					
15	41.91	701.51		P_9				
2	46.2	696.6			R_7			
2	48.0	694.5			R_9			
2	50.50	691.69			R_5			
2	55.70	685.74			R_{11}			
2	60.67	680.07			R_3			
3	68.12	671.58					R_2	
1	69.8	669.7			R_{15}			
1	71.6	667.6					R_0	
4	73.75	665.17					R_4	
1	76.6	661.9			R_1			
5	83.82	653.72					R_6	
1	9,390.3	10,646.4			R_{13}			

TABLE 5.—*Infra-red He spectra*—Continued

Intensity	λ_{air} I. A.	ν_{vac} cm^{-1}	He I	He_2				
				A	B	C	D	E
10	9,391.90	10,644.55		P_{11}				
4	9,395.84	640.09					R_8	
4	9,408.27	626.03					R_{10}	
1	17.73	615.36						
3	20.67	612.05					R_{12}	
2	32.24	599.03					R_{14}	
2	41.6	588.5			P_3			
2	42.4	587.6					R_{16}	
8	47.12	582.34		P_{13}				
2	52.5d	576.3					P_4; R_{18}	
60	63.66	563.84	3^3S–5^3P					
3	9,477.72	548.17			P_5			
8	9,507.74	514.86		P_{15}			P_6	
30	16.70	504.97	3^3P–7^3D					
3	19.39	501.99			P_7			
10	26.17	494.52	3^3D–8^3F					
4	29.27	491.10	3^1D–8^1F					
1	52.8	465.3	3^3D–8^3P					
3	67.08	449.64			P_9		P_8	
7	9,573.90	442.20		P_{17}				
6	9,603.50	410.01	3^1S–6^1P					
2	20.88	391.21			P_{11}			
3	25.80	385.90	3^1P–8^1D					
1	28.14	383.38					P_{10}	
7	45.68	364.49		P_{19}				
2	80.54	327.17			P_{13}			
1	82.4	325.2	3^1P–8^1S					
1	9,687.6	317.5					P_{12}	
10	9,702.66	303.63	3^3P–7^3S					
6	23.33	281.72		P_{21}				
2	46.64	257.13			P_{15}			
1	50.8	252.8					P_{14}	
1	9,782.7	219.3						
5	9,807.13	193.87		P_{23}				
2	19.18	181.36			P_{17}			
3	97.47	100.82		P_{25}				
2	9,898.67	099.60			P_{19}			
1	9,985.43	011.85			P_{21}			
1	9,994.6	10,002.7		P_{27}				
40	10,027.73	9,969.61	3^3D–7^3F					
15	31.16	966.20	3^1D–7^1F					
2	72.10	925.70	3^3D–7^3P					
10	10,138.50	860.69	3^1P–7^1D					
2	10,233.0	769.6	3^1P–7^1S					
1	258.8	745.1						R_{13}
40	10,311.32	695.43	3^3P–6^3D					
1	50.9	658.4						R_8
1	393.3	618.9						R_6
1	10,433.1	582.2						R_4
1	10,599.2	432.1						P_4
4	10,667.62	371.60	3^3P–6^3S					
2	10,714.4	330.7						
100	10,829.09	231.86	2^3S–2^3P_0					
500	10,830.30	230.83	2^3S–$2^3P_{1,2}$					
6	10,912.95	160.92	3^3D–6^3F					
3	917.0	157.5	3^1D–6^1F					
1	11,013.1	077.6	3^1S–5^1P					
1	11,045.1	9,051.3	3^1P–6^1D					

WASHINGTON, May 28, 1932.

TESTS OF CELLULAR SHEET-STEEL FLOORING

By J. M. Frankland[1] and H. L. Whittemore

ABSTRACT

The strength and elastic properties of a new type of cellular steel structural floor were determined. The floor panels were made from 12, 14, 16, and 18 United States standard gage special corrugated sheets which were spot-welded together into panels 2 feet wide and about 11 feet long. The weights ranged from 8 to 16 lbs./ft.[2] The specimens were tested under transverse loading at the quarter points, measurements of strain and deflection being taken at mid-span. It was found that the Euler-Bernoulli theory commonly used in designing beams could be applied satisfactorily to predict the elastic behavior. On 10-foot spans, the floor panels behaved elastically under loads equal to or greater than those which would produce a deflection of one-three hundred and sixtieth of the span. The maximum load was in all cases considerably higher than the limit of elasticity of the panels and assured a considerable margin of safety against overloading. The sections were very stable under the concentrated loads and reactions.

The tensile properties and Young's modulus of elasticity were determined for the sheet steel used in the floor specimens, as was also the shearing strength of the spot welds.

CONTENTS

	Page
I. Introduction	131
1. General	131
2. The cellular floor	132
II. Acknowledgments	133
III. Description of the specimens	133
IV. Tensile tests of the material	136
1. Methods of tests	136
2. Results	137
V. Shearing strength of the welds	141
1. General	141
2. Methods of testing	141
3. Results	142
VI. Method of testing floor panels	144
1. Information desired	144
2. Test procedure	144
VII. Results of the panel tests	147
VIII. Discussion of the test results of the panels	153
1. Specimens of types A and B	153
(*a*) Elastic behavior	153
(*b*) Neutral axis	156
(*c*) Welds	158
(*d*) Cell heights at the supports	158
(*e*) Failure of the panels	159
2. Specimens of type C	161
IX. Conclusions	161

I. INTRODUCTION

1. GENERAL

Modern practice in building construction often provides a structural steel frame on which is carried the walls and floors. The walls provide protection against weather, the floors carry the actual weight of the occupancy. The floor beams inclose areas usually 15 to 25 feet square

[1] Research Associate representing the American Institute of Steel Construction, New York, N. Y.

which are filled in with a variety of constructions. A concrete slab is often used, with or without the use of steel or concrete secondary beams. Tile arches with reinforcement are sometimes used, or else a combination of concrete and tile construction. For all these constructions the weight of the floor is usually greater than the live load it is designed to carry, often considerably so. The cost of the steel frame and the foundations is therefore greatly influenced by the weight of the floor construction. Consequently many engineers and manufacturers are endeavoring to design and produce a load-carrying member for a floor which will be lighter and more convenient than these already in use. It would be desirable to have a lightweight unit which would lend itself to the possibilities of mass production and at the same time could be economically shipped to the site and laid rapidly in place, affording workmen at once a working floor and a place for storing materials. At present the greatest possibilities seem to lie in metal construction.

The advantages to be gained by the use of a lightweight floor in buildings are apparent. For bridges also such a floor would be desirable. As W. H. Thorpe has shown [2] for a bridge of given general type, the load-carrying capacity per pound of structure depends primarily on the span and the ratio of live load to weight of the floor system. For long-span bridges and tall buildings the weight of floors has a cumulative effect. If the dead loads due to the floor system can be reduced, it will result in a much greater reduction in the total weight of the structure, making possible very appreciable economies in material in these two fields.

2. THE CELLULAR FLOOR

Sheet steel, which is now one of the leading products of the steel industry, can be readily formed into corrugated sheets in thicknesses up to 7 gage.[3] The load-carrying properties of these sheets may be materially increased by adding another sheet, flat or corrugated, to form a cellular construction. The two sheets may be either riveted or welded together, the latter process being particularly adapted to large-scale production. A panel made in such a way would be characterized by longitudinal stiffening cells. Such a construction lends itself to an economic use of the material, as much of it as possible being stressed to the allowable working stress, resulting in a beam of high strength in proportion to its weight.

Panels of this sort seem well suited for the construction of floors. They could be shop fabricated and shipped to the construction site where they would be available for rapid placing to form a continuous working floor as soon as the beams were erected to carry them. The cellular structure provides also a system of ducts which appears to offer possibilities of considerable economy in running plumbing, heating and ventilating, electrical, and compressed-air lines.

Experiments by a manufacturer resulted in the development of two types of sheet steel cellular floor panels which appeared to have sufficient strength. These are shown in Figures 1 and 2. The panels are 2 feet wide and any desired length up to 12 feet. The sheets are joined by spot welds.

---

[2] Steel Bridge Weights, Engineering, vol. 120, p. 534, 1925.
[3] 0.188 inch. United States standard gage for sheet, plate, iron, and steel.

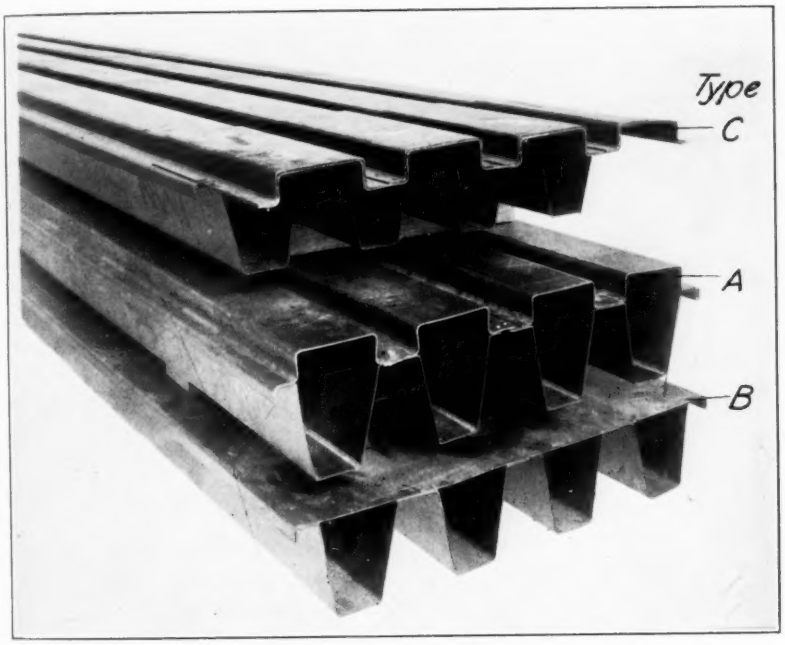

FIGURE 1.—*End view of floor types A, B, and C*

UNIV OF MICH.

The manufacturer's experiments indicated that panels weighing in the neighborhood of 10 lbs./ft.^{2} would be adequate for most floor loads. The dead load of such a floor would consequently be due for the major part to the fireproofing and floor finish. It has been estimated that with this construction there can be saved about one-half of the dead load due to the floor compared to constructions now in common use, this saving varying somewhat with the live load and being subject to modification according to local requirements for fireproofing.

Before putting such a new construction into service, it was considered advisable to make a thorough study of the panels under load

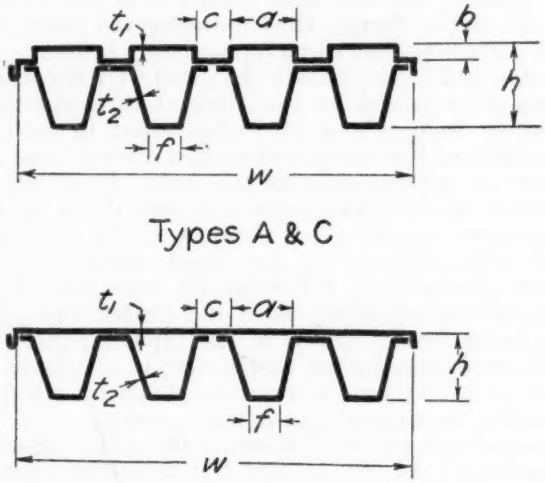

FIGURE 2.—*Sections of floor panels*

The average numerical values of the dimensions indicated by letters are given in Table 2 for each specimen.

to see how closely their performance could be predicted by conventional engineering theory.

II. ACKNOWLEDGMENTS

The American Institute of Steel Construction sponsored the investigation, which was made under the research associate plan at the Bureau of Standards. The specimens were designed and manufactured by the H. H. Robertson Co., Pittsburgh, Pa. Dr. A. H. Stang and L. R. Sweetman, of the bureau staff, assisted in the analysis of the problem and in making the tests.

III. DESCRIPTION OF THE SPECIMENS

The specimens were of three types, sections of which are shown in Figure 2. Types A and C consisted of two corrugated sheets and type B of one corrugated sheet and a flat sheet, the bottom sheets being of the same dimensions for each type. The corrugated upper surface was designed to bind with a surface slab of concrete or similar

material. The troughs in the top sheet also offer certain advantages in laying pipes and ducts. If a concrete slab is not used, the troughs can be covered with sheet-metal channels to give a smooth upper panel surface. Cork, rubber tile, or linoleum may be laid directly on the flat top sheet of the panels of type B. Different strengths were obtained by varying the thicknesses of top and bottom sheets. Type C differed from type A in having the lower corrugations cut away for a distance of 6 inches from each end, the projecting portion of the top sheeting being reinforced in the manner shown in Figure 1. There was no reinforcement of the welds at the ends of the bottom corrugations. The object of this design was to enable this type of panel to be framed into the floor beams with the top sheet lying directly on the upper flange, thus reducing the distance from the finished floor surface to the ceiling immediately below.

Where the top and bottom sheets of a panel were in contact between the cells, they were joined by two rows of three-eighths-inch spot welds, the welds being about 1½ inches apart in each row. The horizontal portion of the assembled section where these welds occur will be spoken of subsequently as the web. In all specimens the bottom sheet was made in two parts separated down the center web. In all the specimens numbered X through XXIV the top sheet was in one piece, this representing the latest manufacturing method. The top sheets of specimens I through IX were made in two pieces with the separation occurring down the center web, this type of construction being clearly shown in the type A panel of Figure 1. In all type B specimens the top sheets were in one piece.

The top sheet of the panels was bent down on either side for a lateral connection to adjacent panels when erected.

The specimens were uncoated showing the mill scale on the sheets except for numbers I, VI, X, XI, and XII, which had been given one coat of paint, inside the cells as well as on the outside surface.

All specimens were 24 inches wide and either 10 or 11 feet long. The cells were spaced 6 inches on centers and in types A and C were 5⅝ inches deep, in type B, 4⅜ inches deep.

A specimen will be described hereafter by its type letter, followed by the gage numbers of the top and bottom sheets, respectively. The gage used is the United States standard gage for sheet, plate, iron, and steel. The nominal thicknesses in inches, together with the maximum and minimum values observed may be found in Table 1. The relative variation of thickness in any one sheet was much less. When the bottom corrugations were made from material lighter than 16 gage, preliminary experiments by the manufacturer had shown that the cell bottoms are liable to crumple over the support. To avoid this the cell bottoms of the A16–18 specimens tested were reinforced at the ends by pieces of 18 gage sheet of the same shape and 6 inches long which were welded to the webs, giving in effect a double cell bottom over the supports.

The first group of specimens, numbered I to XII, were manufactured on a power cornice brake, the dimensions being obtained by hand setting of the sheet in the machine. These will be referred to later as "hand-set specimens." They were characterized by a certain irregularity in the dimensions and a lack of evenness in the

load-bearing surfaces. Specimens XII to XXIV were formed in the same machine over dies which gave much more uniform dimensions.

TABLE 1.—*Thickness of sheets*

Gage No.	Nominal thickness	Actual Thickness	
		(Minimum)	(Maximum)
	Inch	*Inch*	*Inch*
12	0.107	0.097	0.114
14	.077	.069	.083
16	.061	.056	.066
18	.049	.044	.051

The sheets were joined in all cases by resistance spot welding with three-eighths inch diameter welds. In the form of spot welding used, projection welding, small projections are formed on one of the sheets at the places where the welds are to be made. A hand-operated machine making one weld at a time and with the current controlled by a time switch was used on the first 12 specimens. The remaining specimens were welded on a multiple machine with full automatic control. Specimens XV, XXII, XXIII, and XXIV were welded on the automatic machine after its operation had been improved.

The dimensions of each cell and web were taken at both ends of a specimen and the results averaged to obtain data from which the moment of inertia and neutral axis location could be calculated. The measurements were taken to the nearest sixteenth of an inch, and the averaged results expressed to the nearest hundredth. Average dimensions and descriptions of the specimens are given in Table 2. Since the deviations in the dimensions of the most irregular panels did not produce differences of more than 2 per cent in the moments of inertia calculated cell by cell and from the averaged dimensions, it was not felt worth while to list the dimensions of the particular parts.

TABLE 2.—*Description and dimensions of floor specimens*

[The dimensions designated by letters are shown in fig. 2]

Panel	Type	*a*	*b*	*c*	*f*	*h*	*w*	t_1	t_2	Length	Nominal weight
		Inches	*Inches*	*Inches*	*Inches*	*Inches*	*Inches*	*Inch*	*Inch*	*Feet*	*Lbs./ft.*[1]
I	A14-16	3.86	1.29	2.04	2.09	5.64	24.78	0.074	0.060	11	10.50
II	A14-16	3.91	1.29	2.16	2.16	5.65	24.44	.075	.062	11	10.50
III	A14-16	3.90	1.32	2.07	2.13	5.69	24.31	.074	.061	11	10.50
IV	A16-18	3.89	1.29	2.12	2.13	5.64	------	.060	.049	11	8.50
V	A16-18	3.88	1.31	2.15	2.12	5.60	24.50	.060	.047	11	8.50
VI	A16-18	3.90	1.28	2.08	2.11	5.66	24.44	.061	.049	11	8.50
VII	C14-16	3.88	1.29	2.14	2.18	[1] 5.66	24.47	.075	.062	11	10.50
VIII	C14-16	3.84	1.29	2.09	2.12	[1] 5.66	24.50	.075	.062	11	10.50
IX	C14-16	3.88	1.31	2.10	2.16	[1] 5.66	24.03	.079	.062	11	10.50
X	B16-16	3.76	0	2.10	2.16	4.35	24.22	.057	.060	11	8.25
XI	B16-16	3.80	0	2.07	2.12	4.35	24.34	.060	.059	11	8.25
XII	B16-16	3.72	0	2.11	2.18	4.37	24.13	.060	.060	11	8.25
XIII	A14-16	3.94	1.26	2.05	2.06	5.70	24.00	.076	.065	11	10.50
XIV	A16-18	3.81	1.23	2.22	2.12	5.64	24.38	.063	.049	11	8.50
XV	B16-16	3.82	0	2.12	2.20	4.34	24.00	.061	.060	11	8.25
XVI	A14-14	3.88	1.24	2.10	2.17	5.71	24.50	.077	.079	11	11.50
XVII	A14-14	3.91	1.27	2.10	2.15	5.71	24.12	.077	.079	11	11.50
XVIII	A14-14	3.91	1.25	2.11	2.14	5.70	24.12	.077	.079	11	11.50
XIX	A12-12	3.91	1.24	2.15	2.32	5.53	24.25	.108	.105	10	16.10
XX	A12-12	3.92	1.25	2.11	2.28	5.57	24.00	.113	.100	10	16.10
XXI	A12-12	3.88	1.25	2.11	2.27	5.61	24.06	.108	.101	10	16.10
XXII	A14-16	3.92	1.25	1.98	2.19	5.64	23.88	.080	.064	11	10.50
XXIII	A14-16	3.88	1.24	2.00	2.12	5.66	23.75	.080	.064	11	10.50
XXIV	A14-16	3.87	1.24	2.02	2.14	5.66	23.81	.079	.064	11	10.50

[1] Calculated from average height of hand-set A14-16 specimens.

IV. TENSILE TESTS OF THE MATERIAL

1. METHODS OF TEST

The principal requirements of the usual commercial grades of black sheet steel are that the sheets should have a good surface and a high ductility to undergo various forming operations. They are not primarily intended for structural purposes. It was, therefore, desirable to investigate the structural properties, tensile strength, yield point and Young's modulus of elasticity of the material used in these floor panels.

A screw-power beam testing machine having a capacity of 20,000 pounds was used, the machine having two load ranges, one up to 2,000 pounds and the other up to 20,000 pounds. The former range was used for all specimens except the thickest (12 gage).

The specimen used is illustrated in Figure 3 and conforms to the requirements of the sheet tensile specimen recommended by the American Society for Testing Materials in their Tentative Methods

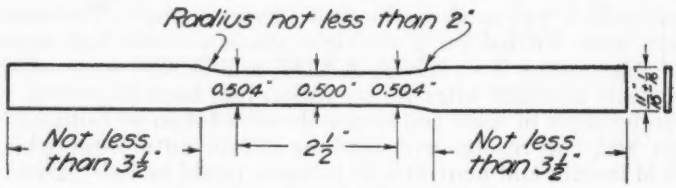

FIGURE 3.—*Sheet tensile specimen*

of Testing of Metallic Materials (Specification E8–27T, Proc., vol. 27, I, p. 1067). The gage length was 2 inches.

One hundred and twelve specimens were tested, 9 of 12 gage, 26 of 14 gage, 65 of 16 gage, and 12 of 18 gage. Stress-strain measurements were taken for 7 specimens of 14 gage, 6 of 16 gage, and 6 of 18 gage.

The tensile specimens were taken from coupons cut from the end of each sheet prior to forming. Tests were made both in the direction of rolling and transverse to this direction, these specimens being marked respectively *L* and *T*. Ninety-three specimens were taken from panels I through XII and furnished information as to the properties of practically all the sheets entering into those panels. Nineteen specimens were taken from the remaining panels.

The stress-strain curves were obtained with a Ewing extensometer of 2-inch gage length mounted on the edges of the specimen. The load was maintained until any drift in extensometer readings appeared to cease and then the reading recorded.

For the remainder of the specimens only yield point, tensile strength, and elongation were determined. A slow machine speed was used as it was found that the values obtained were to a considerable degree dependent on the rate of extension. In some cases a preliminary load of roughly one-half the yield point was applied more rapidly and the rest of the test continued at the slower speed. The speeds adopted were 0.01 inch per minute until the load began to pick up after the yield point, and 0.09 inch per minute for the remainder of the test. These speeds were measured on the movable crosshead of the

machine under no load. The yield points were determined by "drop of beam."

The cross section of the specimens was measured at the ends and at the center of the gage length. As will be seen from Figure 3, the width of the specimen is less at the center to assure fracture near the middle of the gage length. The minimum of the three areas measured was used to compute yield point and tensile strength. The effective area for the determinations of Young's modulus was obtained by assuming that the area could be represented by a quadratic function of the position in the gage length. The effective area will then be given very closely by

$$A = \tfrac{1}{6}\,(A_1 + 4A_0 + A_2)$$

where A_0 is the area at the center and A_1 and A_2 the areas at the ends of the gage length. The formula will be recognized as Simpson's rule. The area so obtained is a closer approximation than would be obtained by the use of the average area.

From the stress-strain data were determined Young's modulus and the proportional limit, using the method of differences proposed by Dr. L. B. Tuckerman, of the Bureau of Standards.[4] A trial modulus of elasticity of 30,000,000 lbs./in.^{2} was assumed and differences between the observed strain and that calculated from the trial modulus were plotted in a difference curve. A straight line was drawn through the points on the difference curve in such a way as to include the most points within a range of one hundred-thousandth inch per inch strain on either side of the line. Slight irregularities at the lowest loads were disregarded. From the slopes of these lines were derived the actual moduli of the specimens. The proportional limit was taken as the stress at which the difference began to depart from the straight line by more than one-hundred-thousandth inch per inch strain. In a few cases, the permanent set was measured after each load.

2. RESULTS

Figures 4 and 5 are typical stress-strain curves up to the yield point. Though these figures show results for two transverse specimens, the curves are representative of the results found for all specimens. Table 3 gives the results derived from the stress-strain measurements. The values of the proportional limit there assigned are to be considered as dependent on the width of the error band that was assumed. The measurements indicated that the material was not perfectly elastic at low loads, but these departures from elasticity were of the same order as the random error in the readings, so that it remained uncertain to what extent this inelasticity was real. In any case, inelastic behavior before the yield point is of little significance in estimating the suitability of a material for structrual purposes. The yield point may therefore be taken as a measure of the safe working stress of the material.[5]

[4] See Determination and Significance of the Proportional Limit in the Testing of Metals, R. L. Templin, and discussion, Proc., Am. Soc. Testing Materials, vol. 29, II, p. 523, 1929. Discussion, p. 538.
[5] See note 4.

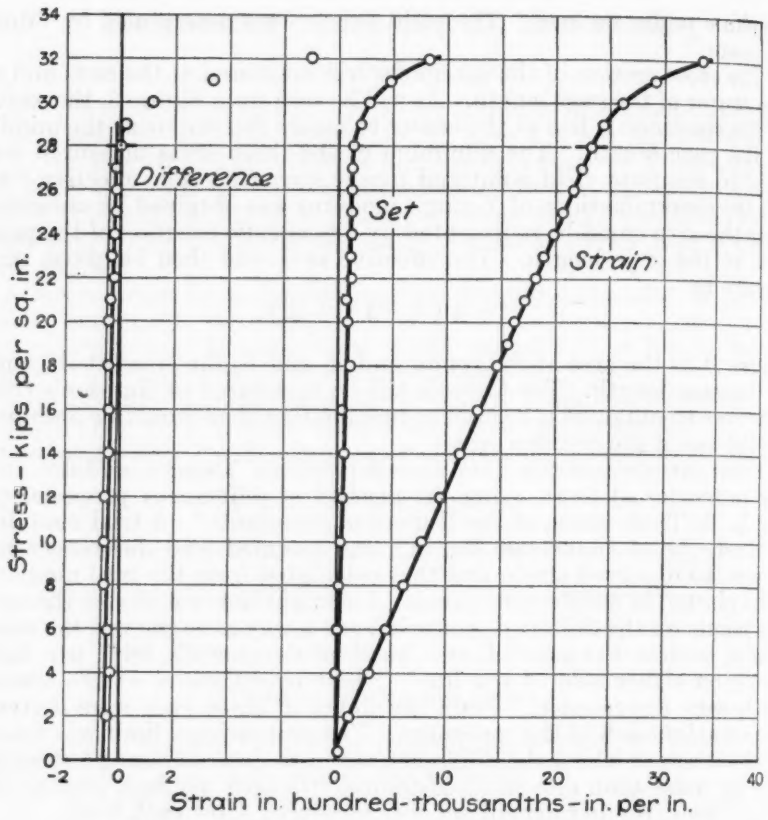

FIGURE 4.—*Stress-strain curves for tensile specimen 9T*

TABLE 3.—*Results of stress-strain measurements on tensile specimens*

Specimen	Thickness	Proportional limit	Yield point	Tensile strength	Young's modulus	Elongation in 2 inches
	Inch	*Kips/in.²*	*Kips/in.²*	*Kips/in.²*	*Kips/in.²*	*Per cent*
1 L [1]	0.078	14.7	21.6	39.7	27,600	38
2 T	.080	17.0	22.7	44.7	29,600	33
3 L [1, 2]	.069	8.6	19.0	39.9	27,500	
4 T	.073	10.0	21.2	43.3	29,100	33
5 L	.063	20.1	21.0	40.2	28,700	31
6 L	.064	12.4	21.1	39.4	28,700	32
7 T	.064	17.1	29.0	48.7	28,900	27
8 L	.048	27.4	35.1	51.4	28,400	25
9 T	.050	28.0	33.9	56.0	29,800	25
10 T	.073	20.2	24.6	45.2	29,400	38
11 L	.075	16.0	21.0	40.7	28,000	36
12 T	.076	20.6	27.8	45.0	29,900	35
13 L	.059	29.0	30.4	43.7	28,800	31
14 T	.061	29.7	35.2	45.1	29,300	40
15 L	.062	18.0	32.9	46.2	29,900	36
16 L [3]	.045	20.1	25.1	46.0	28,400	
17 T	.047	15.4	31.3	55.8	31,400	25
18 L	.049	25.0	25.0	47.6	28,600	33
19 T	.050	24.6	28.5	51.4	30,600	30

[1] Considerable set at low loads.

[3] Broke near gage mark.

The average for 10 specimens of Young's modulus in the direction of rolling was 28,500,000 lbs./in.^{2}, and transverse to the direction of rolling the average of nine tests was 29,700,000 lbs./in.^{2} A value of 28,700,000 lbs./in.^{2} was taken for the longitudinal modulus, this being arrived at by neglecting two specimens (1L and 3L), for which the elastic limit appeared to be particularly low.

Based on strength and yield-point determinations, the material was of three types:

1. Sheets having yield points of 20 to 28 kips/in.^{2} (one kip equals 1,000 pounds) and tensile strengths of 38 to 48 kips/in.^{2} The elonga-

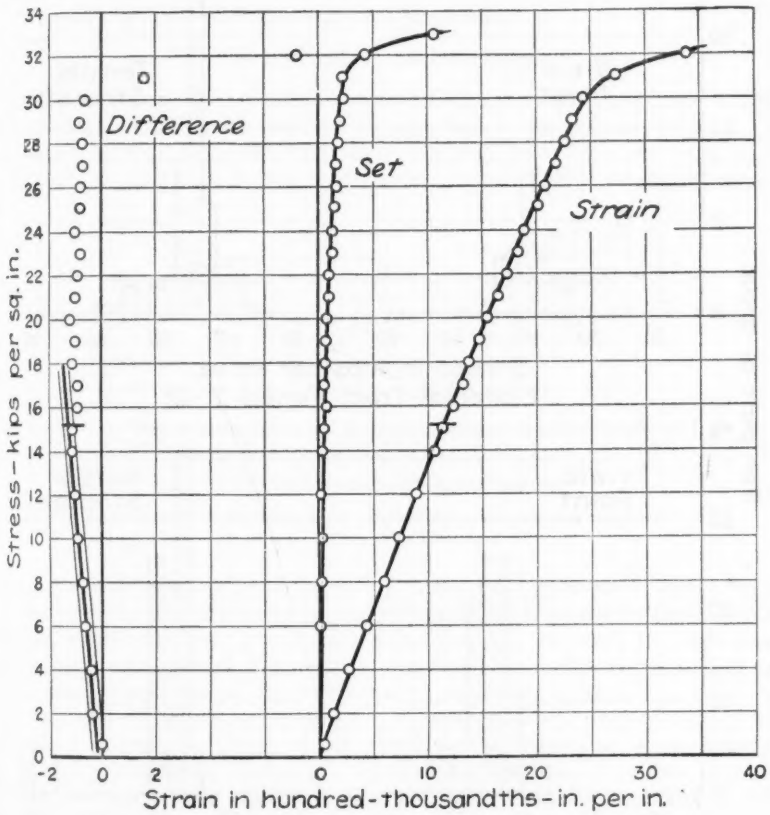

FIGURE 5.—*Stress-strain curves for tensile specimen 17T*

tion in 2 inches ranged from 30 to 40 per cent. At the yield point there was a sharp drop of beam, the load falling off considerably;

2. Sheets having yield points of 35 to 47 kips/in.^{2} and tensile strengths of 46 to 50 kips/in.^{2} There was a marked drop in load at the yield point. The elongation was as great as for the first type;

3. Sheets having tensile strengths of 50 up to 70 kips/in.^{2} and a lower elongation than the preceding types. The yield points ranged from 29 to 52 kips/in.^{2} The elongations were in the neighborhood of 25 per cent. At the yield point the drop of beam was not so pronounced and occasionally the load remained nearly constant.

Only a small proportion of the specimens were of the third type and these were all from 16 and 18 gage material. The higher strength appears to be due to cold working at the mill. The second type of sheet was made from open-hearth steel rolled on a continuous strip mill.

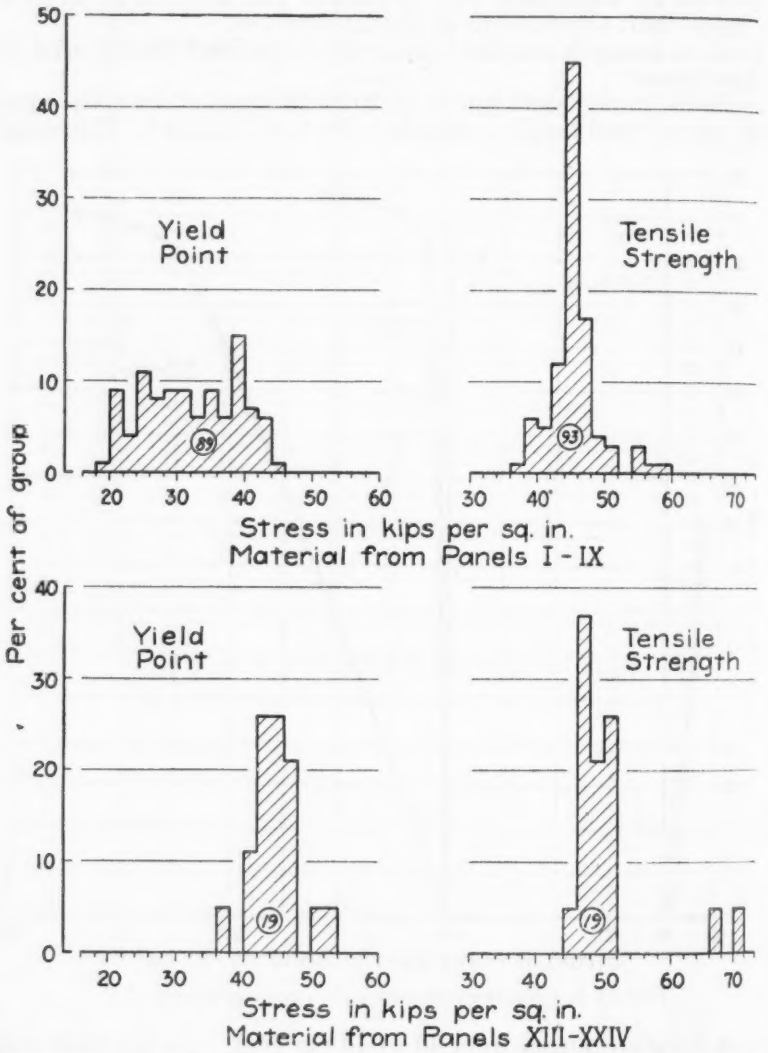

FIGURE 6.—*Distribution of yield point and tensile strength among the specimens*

The first type of material was found only in the first 12 panels, which also included some of the second type. All but one of the tensile coupons taken from panels XII through XXIV were of the second type, the exception being a 16-gage sheet of the third type.

Figure 6 shows graphically how the yield point and tensile strength were distributed among the specimens.

The ordinate represents the per cent of the group which falls within the range of 2 kips/in.^{2} indicated on the horizontal scale. The ringed number is the total of specimens in each group.

V. SHEARING STRENGTH OF THE WELDS

1. GENERAL

The loads applied to the top surface of the floor panels caused shearing forces on the welds joining the top and bottom elements. It is obviously of importance to know what shears may be safely applied to spot welds such as those used in the cellular floor. A series of tests were conducted to obtain data on this point.

2. METHODS OF TESTING

The test of a spot-welded joint in shear alone presents certain difficulties. If a joint with a single lap is pulled in tension, the eccentric loading produces a couple tending to rotate the join of the two parts. In sheet metal this tends to split the joint apart and to

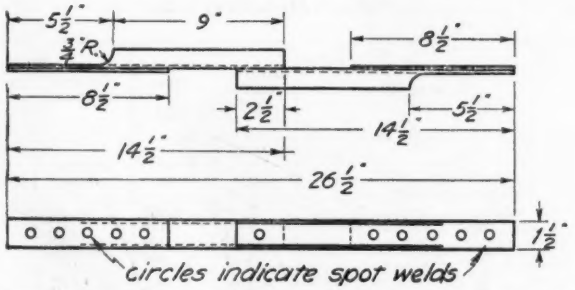

FIGURE 7.—*Specimen for determining shearing strength of welds*

produce buckles about the weld. If a double lap is used, the strength of the joint is considerably increased and fracture may occur outside of the welds; in fact, double lap joints in 14, 16, and 18 gage sheet containing two ⅜-inch diameter welds were tested to destruction and all broke by tearing of the strip inside the cover plates.

A variety of joints containing 1, 2, and 3 welds were obtained and tested in tension. From these results a satisfactory specimen was designed as shown in Figure 7. It consists essentially of two channel-shaped sections from the steel sheet lapped back to back and welded with a single spot. In order to grip the specimen in the jaws of the testing machine, the channel flanges were cut away at the ends. It was found necessary to reinforce the gripped portion of the specimen by welding on a strip along the back of each channel. The specimens were projection welded using a technique as close as possible to the welding methods used in fabricating floor. Such specimens in 14, 16, and 18 gage sheet containing one ⅜-inch diameter spot weld fractured in the weld without appreciable bending of the channels or buckling of the sheet about the weld.

The specimens were tested in tension in a 100,000-pound Amsler machine using the 10,000-pound range. The autographic recording apparatus supplied with the machine was used on an 8-inch gage length, so that a load-extension curve was obtained in each case.

3. RESULTS

The specimens described in the preceding section are noted below by the type letter G, followed by the gage number of the sheet, and an individual specimen number to distinguish those of the same gage. Six specimens each of 14, 16, and 18 gage sheet were tested. The results are summarized in Table 4.

The gross area of the fractured surface of welds was estimated by assuming an elliptical shape and measuring two perpendicular diameters to the nearest 0.01 inch. The net area was obtained from the gross area by deducting for the larger blowholes. Both figures are, of course, only approximate, as are also in corresponding degree the stresses derived from them. The maximum load is definitely the more significant figure.

The autographic records showed that failures were preceded by little or no plastic deformation. The single exception to this was G18–3, which failed by the weld tearing out of the sheet. The ultimate strength of the weld is therefore a measure of the permissible design loads.

TABLE 4.—*Strength of welds*

Specimen	Type of failure	Maximum load	Gross area of weld	Net area of weld	Shearing strength on gross area	Shearing strength on net area
		Kips	*Square inch*	*Square inch*	*Kips/in.²*	*Kips/in.²*
G14–1	Negative bearing	4.59				
G14–2	Shear	3.39	0.105	0.102	32.3	33.2
G14–3	do	4.02	.119	.117	33.8	34.4
G14–4	do	3.86	.101	.099	38.2	39.0
G14–5	do	3.64	.095	.087	38.3	41.8
G14–6	do	3.75	.108	.104	34.7	36.1
G16–1	do	2.94	.075	.074	39.2	39.7
G16–2	Negative bearing	2.61				
G16–3	do	2.57				
G16–4	do	2.24				
G16–5	do	2.43				
G16–6	Shear	2.49	.058	.055	42.9	45.3
G18–1	Negative bearing	2.91				
G18–2	Shear	2.83	.104	0.057–0.090	27.2	31.4–49.6
G18–3	Negative bearing	2.81				
G18–4	do	3.09				
G18–5	do	2.87				
G18–6	do	3.14				

Those specimens in which the weld metal itself did not shear failed by the weld spot tearing out of the sheet. On the side of a weld toward the gripped end of that portion of the specimen there exists a concentrated tensile "negative bearing stress," analogous to the compressive bearing stress in the plate of a riveted joint. Where compressive failure occurs in the plate in the riveted joint, the material in each sheet parts in tension in the welded joint. Failure progresses by the welded regions twisting and tearing out of the sheets. Figure 8 shows late stages in the failure in "negative bearing" of two 16-gage specimens, one single-lap and one channel type. Some of the failures of this kind appeared to start in defective material near the edge of the weld and then spread to the edge of the unfused material.

U. S. Journal of Research, RP463

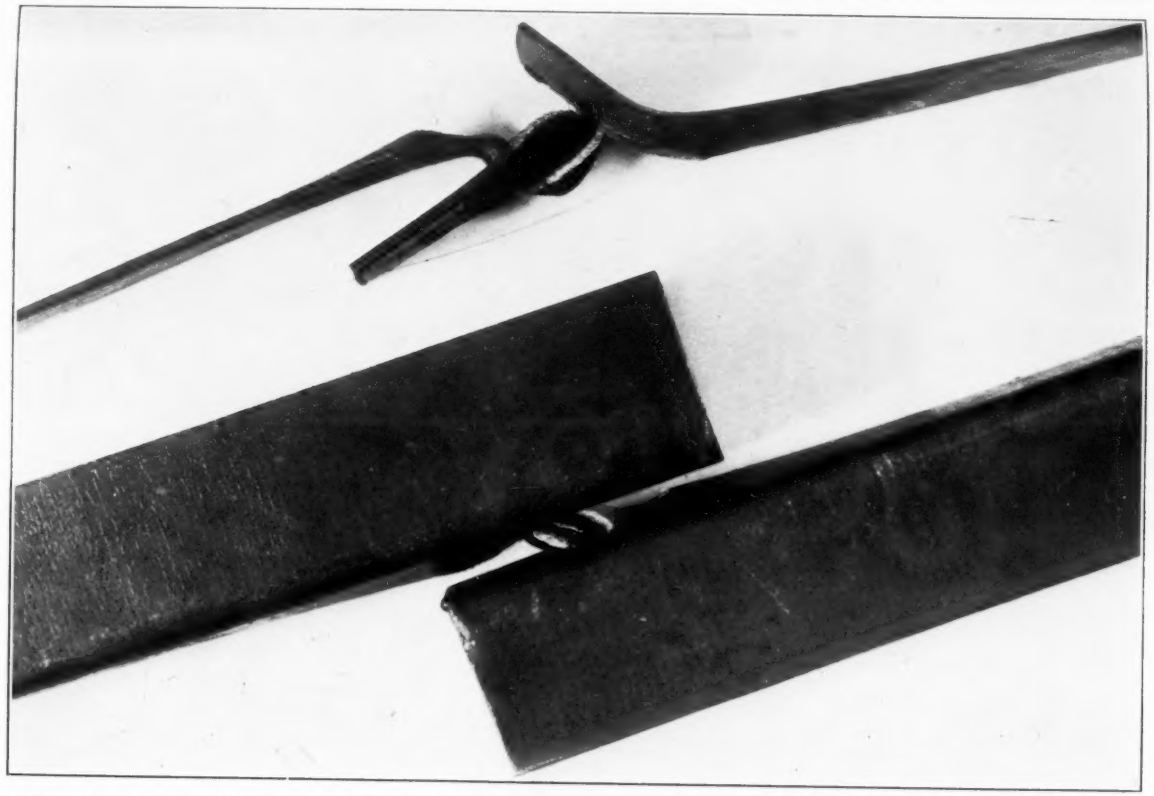

FIGURE 8.—*Typical failures of spot welds in negative bearing for channel-type (see fig. 7) and single-lap specimens*

UNIV OF MICH.

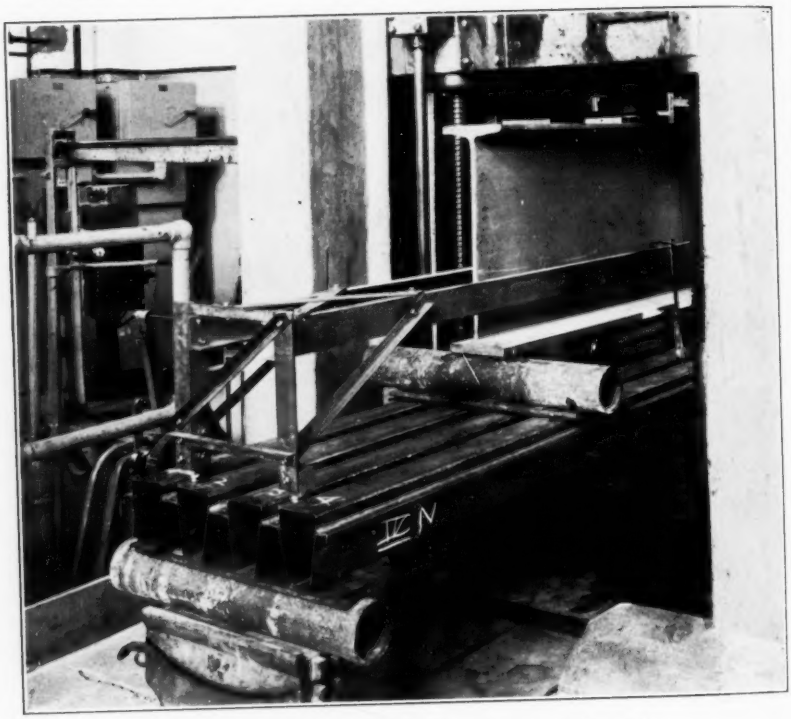

FIGURE 9.—*View of a floor panel ready for test*

The fractures of welds that broke in shear presented a variety of appearances. The welding of specimens G16–1 and G16–6 was defective, the former containing three weld spots of gross areas 0.019, 0.008, and 0.048 square inch, and the latter containing two spots of gross areas 0.013 and 0.045 square inch. Apparently the sheets were in good electric contact at more than one place due to a poorly made projection or to uneven surfaces. The welds in both specimens contained oxide inclusions. The weld in G18–2 contained coarse radial blowholes about the periphery, there being also a central region with large voids. Tarnish in the center suggests that there was poor adhesion in that portion, but the tarnish may possibly have occurred following fracture. In the 14-gage specimens all the sheared welds contained blowholes, in some cases only one at the center, while in others there were many fine radial blowholes. In the latter cases the surface of fracture showed considerable curvature through points of weakness. Where the weld contained only a few circular blowholes, the fracture presented the appearance of a broken piece of coarse-grained ductile material.

Application of conclusions drawn from these tests must necessarily be restricted to material of the same grade of sheet steel and to welds of the same size made under similar conditions. Higher-strength material would be expected to show higher values, at least in negative bearing.

It is evident that the gage and the tensile strength of the sheet determine whether shearing or negative bearing failure will occur. Below a certain thickness the concentration of tensile stress at the edge of the weld will produce negative bearing failure before the shearing strength of the weld is reached. Above this thickness the load required to shear the weld will not produce the requisite tensile stress to produce a failure in negative bearing. The specimens may be distinguished on this basis. The 16 and 18 gage specimens all broke in negative bearing with the exception of G16–1, G16–6, and G18–2, in which the welds were defective. The 14-gage specimens broke by shearing of the weld, the sole exception to this being G14–1, in which the weld was evidently of much greater shearing strength. In general, then, material of 14 gage or heavier may be expected to develop the full shearing strength of these welds while lighter gages will fail at lower loads in negative bearing.

The shearing strength developed in a welded joint thus depends upon the gage of the sheet when the gage is below a certain critical thickness. Above that thickness the strength should be independent of the gage. Though the tensile properties of the sheet used in the weld specimens were not determined, there was general evidence through the tests that the 16-gage material was of rather low strength, so that the low figures for the 16-gage specimens compared to the 18-gage specimens is probably to be explained on these grounds. The specimen of lowest strength was G16–4 which broke at 2.24 kips in negative bearing, this being a lower breaking load than observed from the specimens with defective welds previously described. Two kips would thus be a conservative figure for the strength of a single one of these spot welds in shear.

VI. METHOD OF TESTING FLOOR PANELS

1. INFORMATION DESIRED

The most important points to be ascertained in the tests of the floor panels themselves were: First, how closely do the deflections and stresses agree with those calculated by the Euler-Bernoulli theory, which is usually used in designing engineering structures; and second, under what range of loads does the floor behave elastically? It is further of importance to know how failure occurs and what are the points of structural weakness with their effects on the response of the panel to load.

It was decided therefore to make transverse tests to destruction of the individual floor panels, measuring deflections and strains at suitable locations in order to correlate these with the loads.

2. TEST PROCEDURE

The test panels were mounted at the ends on roller supports. The A12–12 specimens were 10 feet in length and were tested on a span of 9 feet 8 inches; the remaining panels were 11 feet long and were tested when possible on a span of 10 feet, it being necessary to use a span of 10 feet 6 inches for the type C specimens and the type A specimens with reinforcing at the ends of the cell bottoms (A16–18). In each case the specimen had a length of bearing of 4 inches. Equal loads were applied at the quarter points of the span in a screw power-testing machine of 600,000-pound capacity, using a poise giving a 300,000-pound range. By loading at the quarter points the bending moment between the loads was uniform and equal to the maximum moment which would be produced by the load uniformly distributed. The maximum shear is likewise equal to the maximum shear produced by uniform loading. The computed deflection at mid-span, however, is 10 per cent greater than would have been produced by uniform loading. Since the maximum bending moment is developed over the middle half of the span and the maximum shear is developed over the portions of the specimen between the loads and the supports, inhomogeneities in the structure will be more liable to discovery than if the panel were uniformly loaded.

Steel bearing plates with pads of ¼-inch canvas belting were used to distribute the loads and reactions to the specimen. The plates were 4 inches wide and one-half inch thick and extended across the specimen, the pads being cut to the same size and placed between the specimen and the bearing plate. The load was transmitted to the specimen from the movable cross head of the machine by an I beam carried on a spherical bearing, rollers being placed between the loading beam and the bearing plates. This arrangement can be seen in the typical set-up shown in Figure 9. In the figure it will be noticed that the end bearings are free to accommodate themselves to small twists in the specimen by means of a cylindrical seating.

The deflection at mid-span was measured at each load by means of dial micrometers accurate to 0.002 inch. These dials were mounted on a stiff frame supported at the horizontal webs of the panel immediately over the supports. The frame was carried on 3 steel balls in such a way that 1 foot was free to rotate about a point, 1 to move along a line, and 1 to move in a plane, the support being therefore

FIGURE 10.—*A floor panel showing apparatus for taking strain and deflection measurements*

UNIV. OF MICH.

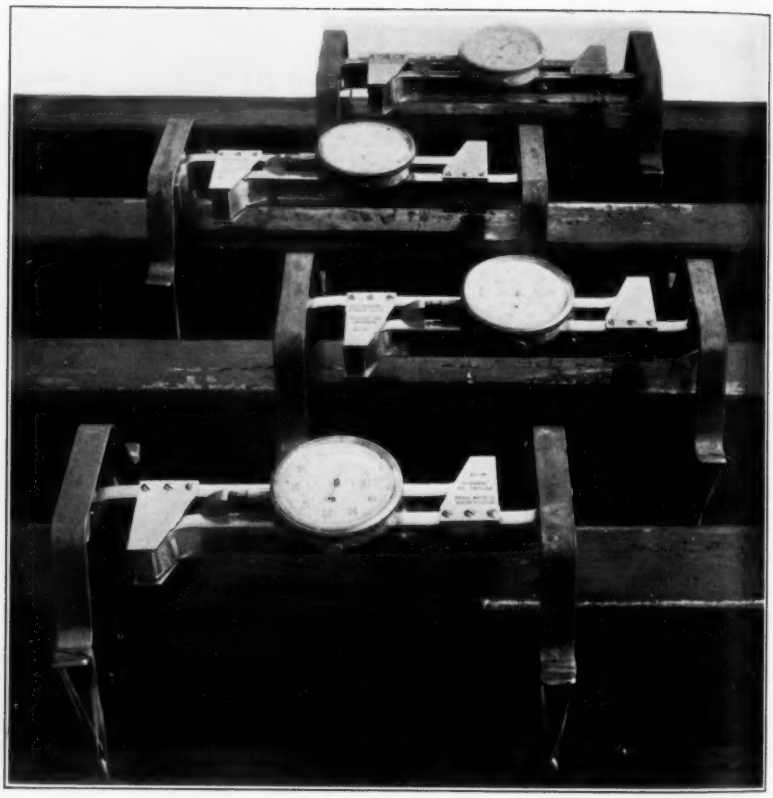

FIGURE 11.—*Bottom of a floor panel showing arrangement of strain gages*

kinematically nonredundant. This frame and its mounting is shown in Figures 9 and 10. Such a mounting assures the frame remaining unstrained during all portions of the test. The deflection was therefore measured unambiguously relative to a plane close to the neutral surface of the panel, this neutral surface being computed to lie seven-eighths to 1 inch below the web for specimens of types A and C, and 1½ inches below the web for type B specimens. The deflection was taken on the webs at mid-span at two points 6 inches on either side of the center line.

The strains on a 10-inch gage length in the top and bottom of each cell were measured, also at mid-span, by the use of Whittemore hand strain gages.[6] These gages read to a ten-thousandth of an inch and the readings can be estimated to a hundred-thousandth of an inch, which corresponds to a stress of about 30 lbs./in.^{2} The error in the strain gages is believed not to exceed two divisions (600 lbs./in.^{2} equivalent stress), this error being due for the most part to irregularities in the dial mechanism. The readings on the top of the panel, the compression side, were taken by the customary hand application of the gage as illustrated in Figure 10, while the readings on the bottom were taken with instruments attached to the specimen with rubber bands. Details of the method of attaching the bottom gages can be seen in Figure 11. The gage lengths on the bottom were staggered two inches alternately on either side of the mid-span for convenience in attaching the instruments.

According to the conventional engineering theory, the stresses in the extreme fibers should be constant between the loads, this being due to the constancy of bending moment and section modulus. The stresses were computed by multiplying the strain by the average value of Young's modulus (28,700,000 lbs./in.^{2}) found in the tensile tests of the material.

The height of each cell at the two ends of the specimen was measured to the nearest hundredth of an inch by means of internal calipers at each load for which the top strain gages were read.

The usual procedure in a test consisted of taking cell heights, top and bottom strain-gage readings, and deflection measurements with no load on the panel. These readings were repeated at 2,000-pound intervals. The deflection dials and bottom strain gages were read at each 1,000-pound interval. In the case of the heaviest panels, XIX, XX, and XXI, of the A12–12 type, readings were made every 1,500 pounds; for all other specimens readings were taken every 1,000 pounds. The first group of 12 panels contained three specimens of each type. One of these was loaded in 1,000-pound increments straight up to the point at which it would support no added load. Strain-gage readings were taken until the change in gage length indicated that the material was well beyond its elastic range. The deflection measurements were taken over the full range of the apparatus (about 1¾ inches), which sufficed to carry the readings nearly to the maximum load. A second specimen of the same type was loaded until a "limiting deflection" was reached approximately equal to one three hundred and sixtieth of the span plus 10 per cent. As previously mentioned, the loading in the tests should produce a deflection 10

[6] See Arch Dam Investigation, vol. 1, Am. Soc. Civil Engrs., p. 64, November, 1927.

per cent greater than the same load uniformly distributed. In order to avoid cracking plaster ceilings, floors are generally restricted to a maximum deflection when uniformly loaded of one three hundred and sixtieth of the span. The limiting deflection of the tests consequently corresponds to the deflection limits set on floors in practice. At this load the specimen was held for one hour to observe any creep that might occur. Following this halt, the test was continued to failure as before. The third panel of the group was loaded up to the limiting deflection with the same load increments as before, then unloaded in steps to zero, readings being taken at the same loads as in the first portion of the test. The rest of the test then continued as for the

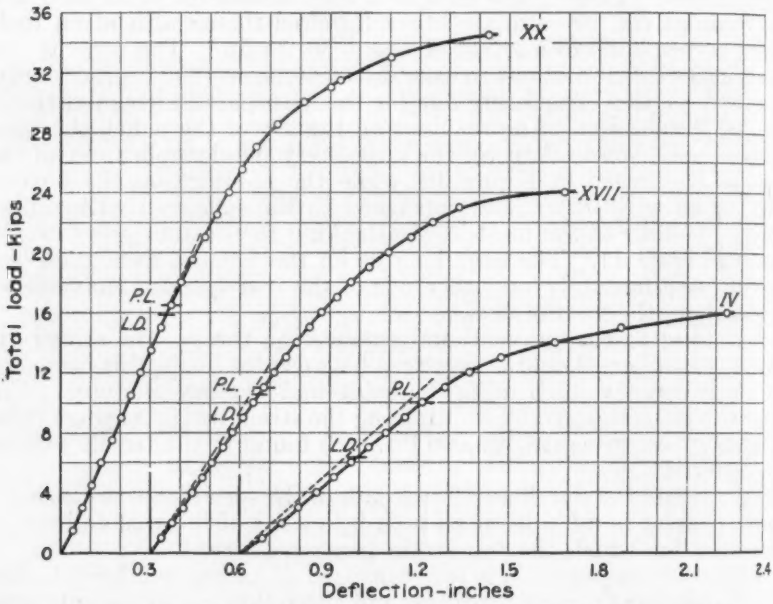

FIGURE 12.—*Load-deflection curves for panels IV, XVII, and XX*

first specimen. The object of this repeated loading was to observe hysteresis effects as well as permanent set on removing the load. Any effects of prestressing should show up on the second loading. Since secondary effects were found to obscure any real hysteresis that may have been present, the procedure followed for the last 12 specimens was to load to the limiting deflection, unload to zero to observe permanent set, no intermediate readings being taken during unloading, then reload to the limiting deflection and continue the test as before. To observe creep, one specimen of each group was held for an hour at the limiting deflection load before unloading.

Careful watch was maintained to observe the development of buckling failure in the various parts of the specimen, the principal points of interest being the cell tops at and between the loads and the side walls of the cells at the supports.

VII. RESULTS OF THE PANEL TESTS

The curves of Figures 12 and 13 show typical relations of load to average deflection at mid-span. It will be observed that up to a certain point on the curves, the deflection is proportional to the load within the experimental error. This was found to be true for all the specimens. The load at this point will be spoken of subsequently as the proportional limit of the floor panel. The proportional limit for the panel is indicated on the curves by P. L. and the limiting deflection load by L. D. A deviation of 0.002 inch from proportionality was taken as criterion for determining this limit. The proportional limit of the panel so defined and the load at the limiting deflection

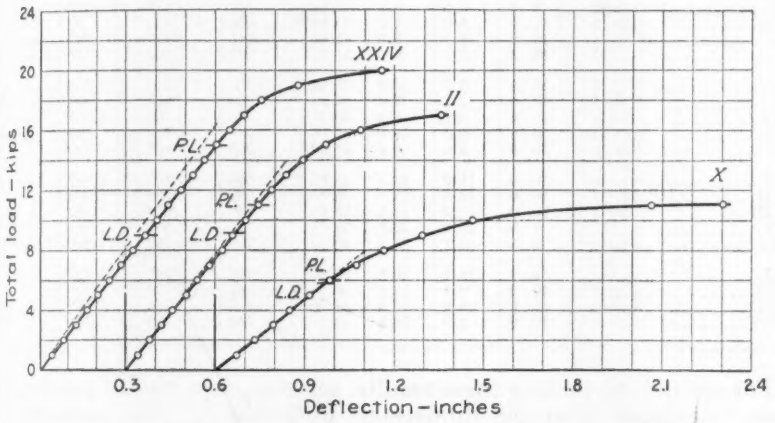

FIGURE 13.—*Load-deflection curves for panels II, X, and XXIV*

of the panels are used as a basis for discussing their behavior. For this reason these points are also marked on succeeding curves. Above the proportional limit the deflection increases more rapidly with successive increments of load, this being due to plastic yielding and to buckling. This yielding progresses until a point is reached where the panel will support no added load. Specimens remained intact, though deformed, after the test. Figures 14 to 17 show the appearance of some typical panels after testing.

Table 5 summarizes the strength properties of the specimens and gives also the spans on which they were tested and the permanent set indicated by the deflection dials when unloaded completely from the limiting deflection. The columns headed equivalent uniform loads per square foot give the distributed loads which were computed to give the same maximum bending moment on a 10-foot span as the observed loads.

TABLE 5.—*Strength properties of panels*

Panel No.	Description	Span	Limiting deflection load	Proportional limit	Maximum load	Equivalent uniform load on 10-foot span			Set after loading to limiting deflection
						Limiting deflection load	Proportional limit	Maximum load	
		Ft. in.	*Kips.*	*Kips.*	*Kips.*	*Lbs./ft.²*	*Lbs./ft.²*	*Lbs./ft.²*	*Inch*
I	A14–16	10 0	8.5	9.0	18.61	425	450	930	
II	A14–16	10 0	9.2	11.0	17.65	460	550	882	
III	A14–16	10 0	9.9	9.0	16.99	495	450	850	0.008
IV	A16–18	10 6	6.2	10.0	17.25	326	525	906	
V	A16–18	10 6	5.7	11.0	17.00	299	578	892	.010
VI	A16–18	10 6	6.5	6.5	15.77	341	341	828	
VII	C14–16	10 6	7.5	6.0	13.67	394	315	718	
VIII	C14–16	10 6	8.0	8.2	14.35	420	430	753	.016
IX	C14–16	10 6	8.4	3.8	15.30	441	200	803	
X	B16–16	10 0	5.7	6.0	11.54	285	300	577	
XI	B16–16	10 0	5.0	5.0	11.05	250	250	552	
XII	B16–16	10 0	5.2	7.4	13.32	260	370	666	.026
XIII	A14–16	10 0	9.7	8.0	20.45	485	400	1,022	.014
XIV	A16–18	10 6	6.5	10.0	18.05	341	525	948	.004
XV	B16–18	10 0	5.6	8.0	14 00	280	400	700	.002
XVI	A14–14	10 0	11.0	11.0	25.65	550	550	1,282	.006
XVII	A14–14	10 0	10.6	11.0	26.15	530	550	1,308	.011
XVIII	A14–14	10 0	11.0	11.0	25.65	550	550	1,282	.016
XIX	A12–12	9 8	15.3	19.5	38.15	739	942	1,844	.008
XX	A12–12	9 8	15.8	16.5	38.20	764	797	1,846	.003
XXI	A12–12	9 8	16.4	16.5	36.14	793	797	1,747	.008
XXII	A14–16	10 0	9.3	14.6	20.10	465	730	1,005	.003
XXIII	A14–16	10 0	9.9	14.8	21.80	495	740	1,090	.001
XXIV	A14–16	10 0	9.0	14.6	21.00	450	730	1,050	.005

For use in interpreting these results, section properties of the panels were calculated from the dimensions in Table 2. The moment of inertia, position of the neutral axis and section moduli were computed for each panel. In order to determine whether the use of average dimensions was justified in calculating these properties, the moment of inertia and position of the neutral axis was calculated cell by cell for some of the most irregular specimens. No appreciable differences, however, were found between the two methods of calculation. The dotted lines shown in the load-deflection and load-strain curves of the panels indicate the deflection calculated from these section properties.

The moment of inertia was also derived from the slope of the load-deflection curve below the proportional limit. The slope was determined by the method of least squares which takes here a particularly simple form on account of the equal increments of load.

Table 6 gives the computed values of the section properties and also the observed values of the moments of inertia taken from the load-deflection curves.

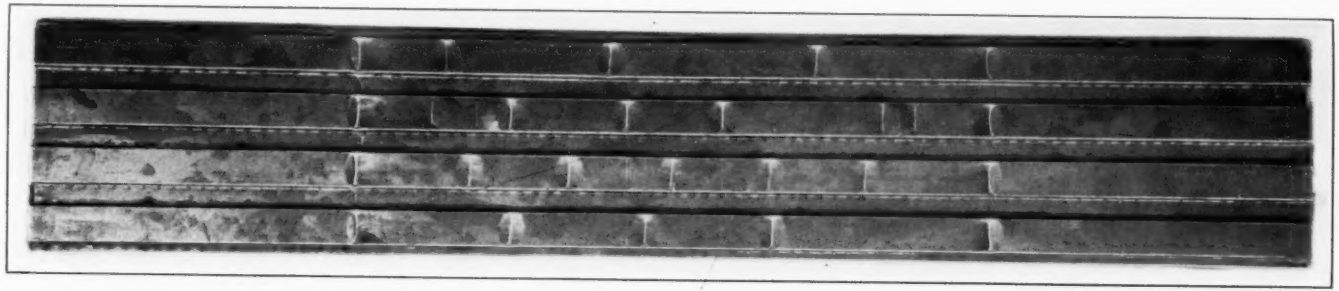

FIGURE 14.—*Top view of an A14–16 panel after testing*

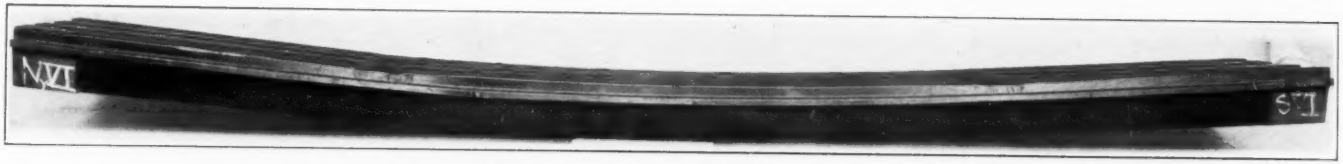

FIGURE 15.—*Side view of an A16–18 panel after testing*

UNIV OF MICH.

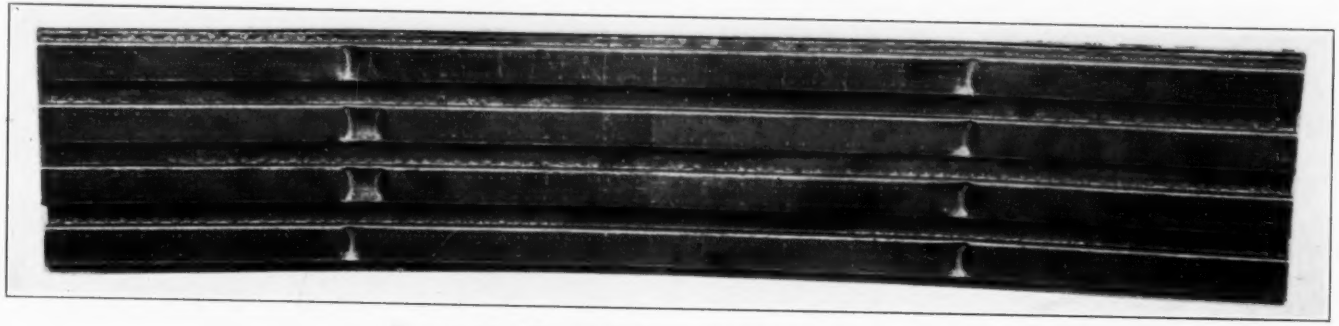

FIGURE 16.—*Top view of an A12–12 panel after testing*

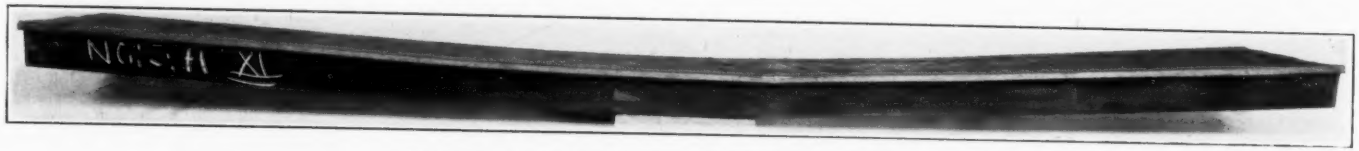

FIGURE 17.—*Side view of a B16–16 panel after testing*

TABLE 6.—*Section properties of panels*

S_c = compressive section modulus for panel.
S_t = tensile section modulus for panel.
v_c = distance from neutral axis to extreme compression fiber.
v_t = distance from neutral axis to extreme tension fiber.
$r_{calc.} = \frac{v_c}{v_c + v_t}$.
I = moment of inertia of panel.

Panel	Type	S_c	S_t	v_c	v_t	r (calc.)	I (calc.)	I (obs.)
		*In.*³	*In.*³	*Inches*	*Inches*		*In.*⁴	*In.*⁴
I	A14-16..	10.1	6.1	2.13	3.51	0.385	21.5	20.5
II	A14-16..	10.4	6.4	2.15	3.50	.381	22.4	21.5
III	A14-16..	10.3	6.3	2.17	3.52	.381	22.3	24.5
IV	A16-18..	8.4	5.1	2.11	3.52	.374	17.8	16.9
V	A16-18..	8.2	4.8	2.08	3.52	.371	17.0	16.2
VI	A16-18..	8.7	5.1	2.09	3.57	.369	18.1	17.4
VII	C14-16..	10.5	6.4	2.15	3.51	.380	22.5	20.4
VIII	C14-16..	10.4	6.4	2.20	3.54	.383	22.8	20.8
IX	C14-16..	10.6	6.5	2.16	3.52	.380	23.0	26.3
X	B16-16..	8.7	4.6	1.51	2.84	.347	13.2	13.9
XI	B16-16..	8.5	4.5	1.50	2.85	.345	12.7	13.4
XII	B16-16..	9.2	4.8	1.49	2.88	.341	13.7	13.8
XIII	A14-16..	10.8	6.6	2.17	3.53	.381	23.4	23.4
XIV	A16-18..	8.5	5.0	2.10	3.54	.372	17.8	17.1
XV	B16-16..	9.0	4.7	1.48	2.86	.341	13.4	13.4
XVI	A14-14..	12.0	8.1	2.30	3.41	.403	27.6	27.0
XVII	A14-14..	11.8	8.1	2.32	3.39	.406	27.3	25.4
XVIII	A14-14..	11.6	8.0	2.33	3.38	.405	27.1	26.2
XIX	A12-12..	15.9	10.6	2.22	3.31	.402	35.2	33.7
XX	A12-12..	16.5	10.4	2.15	3.42	.386	35.5	35.9
XXI	A12-12..	15.9	10.4	2.22	3.39	.396	35.4	36.1
XXII	A14-16..	11.1	6.6	2.11	3.53	.374	23.4	22.4
XXIII	A14-16..	11.1	6.6	2.11	3.55	.373	23.5	22.9
XXIV	A14-16..	11.0	6.6	2.12	3.54	.375	23.4	21.8

Figures 18 to 21 show some typical load-strain curves for the four cells of various panels. The curves for Panel III, Figure 18, show the strains in the panel on the second loading, the dashed lines showing the calculated values of the strains are drawn through the set obtained at zero load after loading to the limiting deflection.

From the compressive and tensile strain data the neutral axis could be located at different loads on the assumption that plane sections remain plane. It was found desirable to express the location of the neutral axis in terms of a proportion of the total height of the cell, thus minimizing the effect of irregularities in the heights of the cells. As will appear later, the relation to load of the apparent position of the neutral axis given by the strain data is of value in determining the way in which the specimen begins to fail at mid-span and also in judging whether the various parts of the section are acting integrally. The location of the neutral axis was expressed in terms of a variable defined as follows:

$$r = \frac{e_c}{e_c + e_t}$$

where e_c and e_t are the compressive and tensile strains respectively. This r is the ratio to the total height of the distance from the neutral axis to the top of the cell. Even when plastic deformation has occurred, r continues to represent quite closely the position of the neutral axis [7] provided that the upper and lower elements composing the

[7] Bach and Baumann, Elastizität und Festigkeit, 9th ed., p. 266. Eugen Meyer, Berechnung der Durchbiegung von Stäben, deren Material den Hookeschen Gesetz nicht folgt. Zeit. des Verein Deutscher Ingenieure, p. 167, 1908.

cell act integrally. Values of r are determined very simply by graphical methods and from these values plots of r against load were made

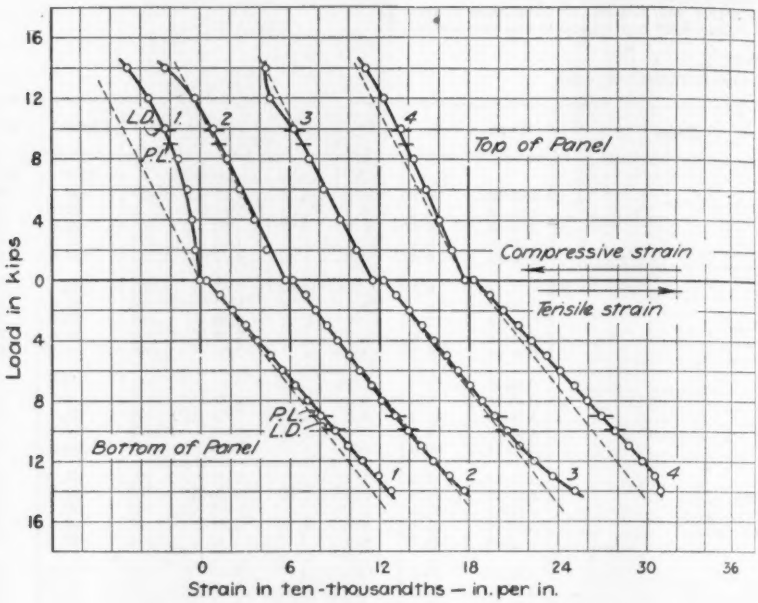

FIGURE 18.—*Load-strain curves for Panel III*

for each cell. For a sturdy beam acting according to the usual simple theory, these values of r should be identical with the values of $r_{calc.}$ given in Table 6.

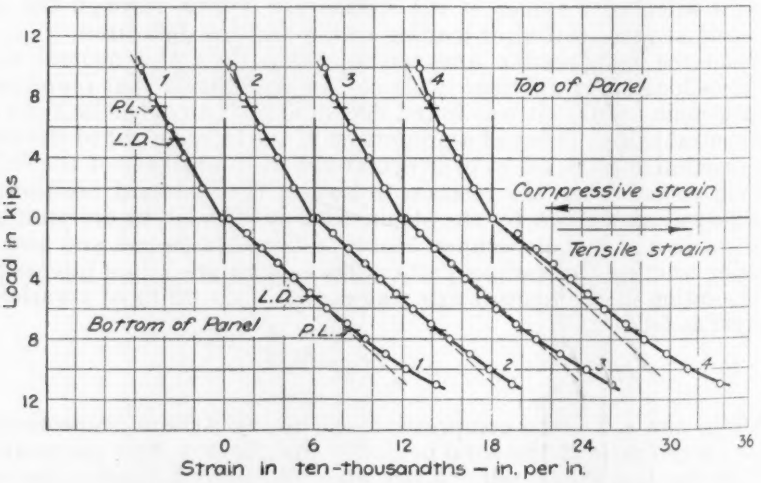

FIGURE 19.—*Load-strain curves for Panel XII*

Figures 22 to 24 give characteristic curves showing the values of r at the various loads. The values of $r_{calc.}$ are indicated by the dashed lines.

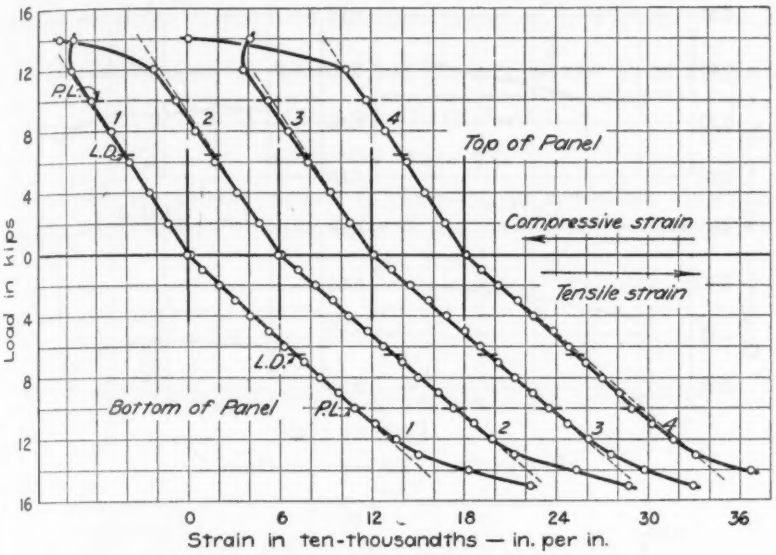

FIGURE 20.—*Load-strain curves for Panel XIV*

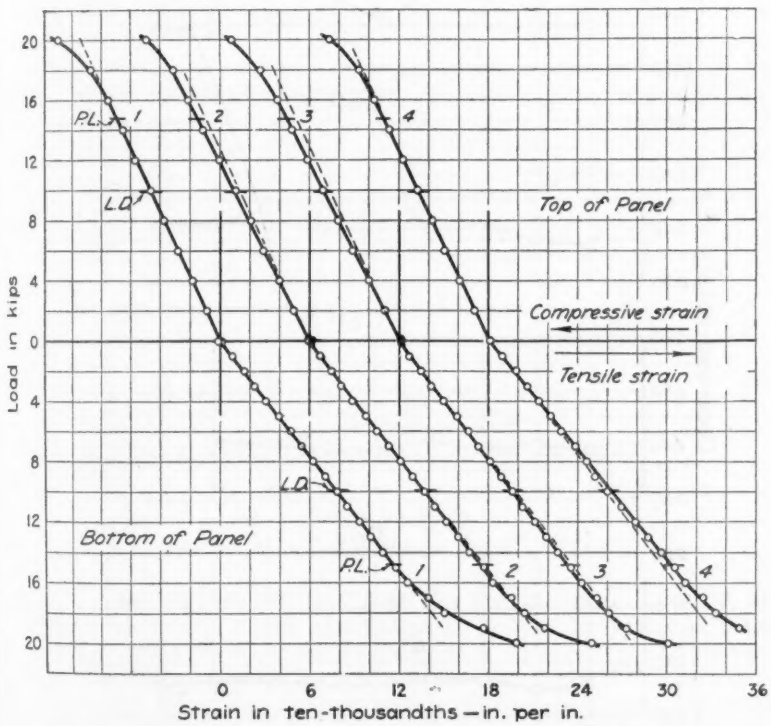

FIGURE 21.—*Load-strain curves for Panel XXIII*

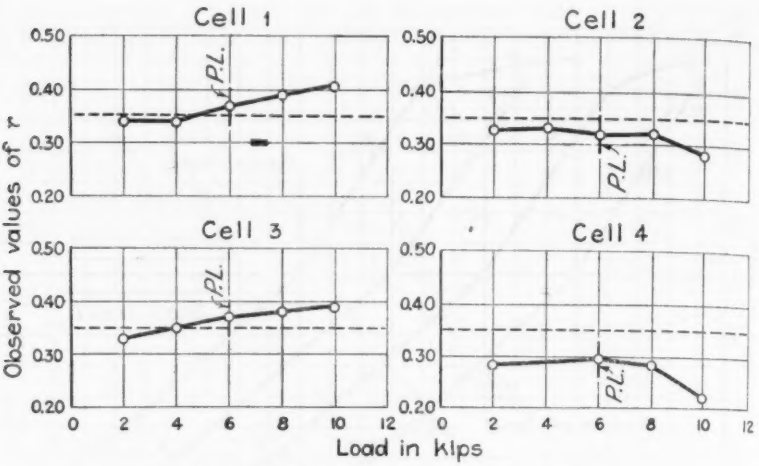

FIGURE 22.—*Values of r for Panel X*

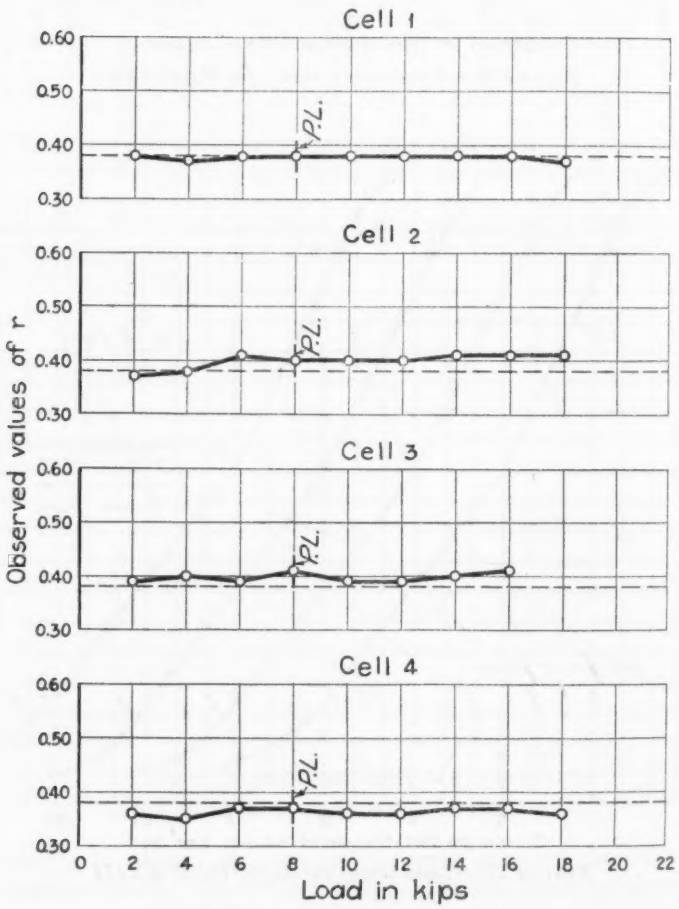

FIGURE 23.—*Values of r for Panel XIII*

Some typical curves showing the reduction in height of the cells over the supports as the load increases are given in Figures 25 to 27.

VIII. DISCUSSION OF THE TEST RESULTS OF THE PANELS

1. SPECIMENS OF TYPES A AND B

(a) ELASTIC BEHAVIOR

The close agreement shown in Table 6 between the calculated moment of inertia and that derived from the load-deflection data

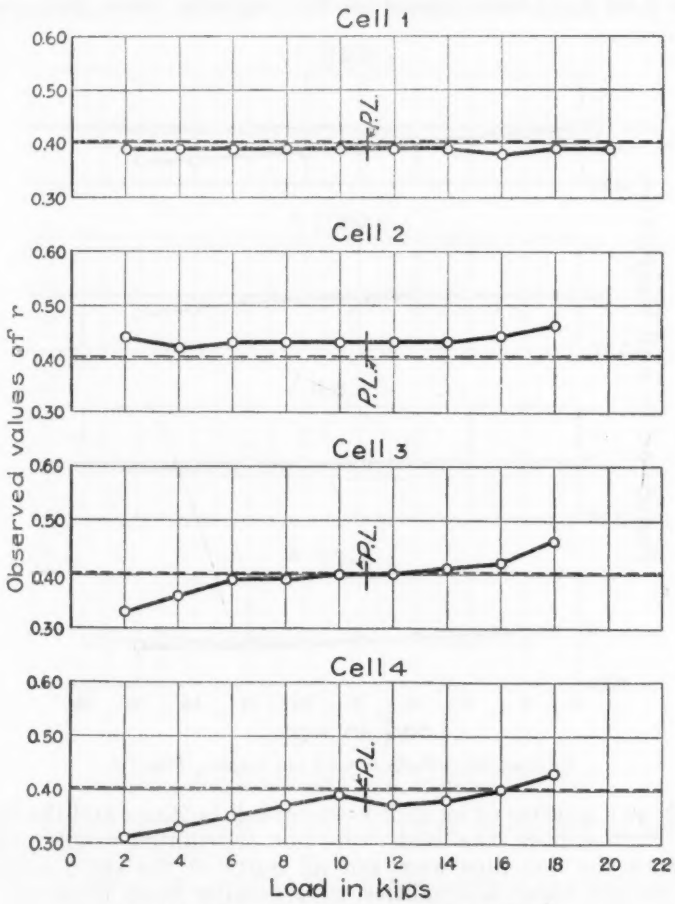

FIGURE 24.—*Values of r for Panel XVIII*

shows that for engineering purposes the specimens of types A and B behaved as purely elastic structures up to the proportional limit. The average ratio of observed to calculated moment of inertia is 98 per cent, the ratios ranging from 93 per cent for panel XVII to 110 per cent for Panel III. For three-quarters of the specimens the ratios were within 4 per cent of the average value. In the load-deflection curves of Figures 12 and 13, the calculated deflection will be seen to

be close to the observed value, the observed value for all the panels being in general a little greater. The sets in deflection after unloading from the limiting deflection, given in Table 5, were negligible. They were due to readjustment of the specimen near the loads and supports and to local yielding. It is believed that additional applications of load would produce only slight changes in the values of the set. The creep in deflection observed after holding at constant load for one hour at the limiting deflection was negligible, the maximum value being 0.002 inch for Panel XI.

When some of the specimens formed by hand setting of the brake (panels I to XII) were placed on the supports, there were gaps of

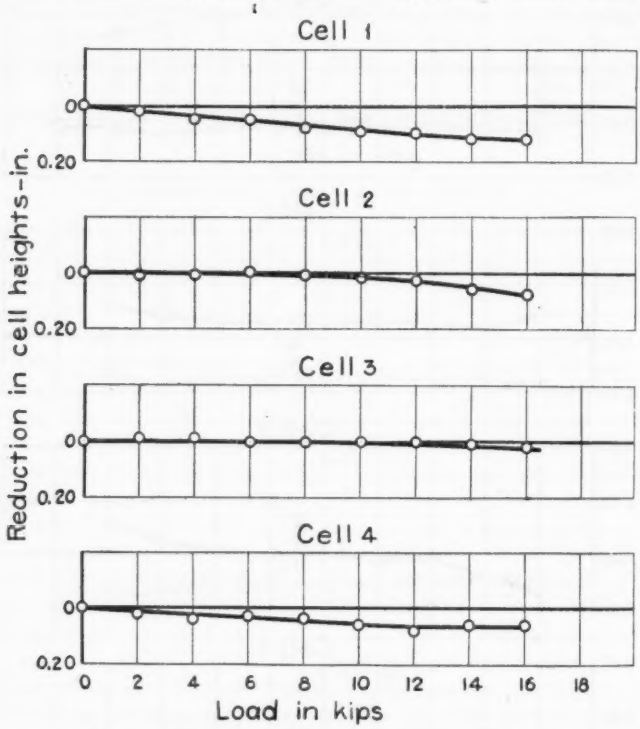

FIGURE 25.—*Reduction in cell heights, Panel I*

as much as a quarter of an inch between cell bottoms and the bearing pads. Furthermore, the loads were not distributed evenly over the cells, since the cell tops were not all quite in the same horizontal plane, though these inequalities were smaller than those observed for the cell bottoms at the supports. When the load was applied the horizontal webs bent, forcing the cell tops into the same plane under the load and tending to close up the gaps over the supports, but even at the limiting deflection the loads and reactions were not evenly distributed over the cells because of the differences in the heights of the cells. Because of this condition, the strain and deflection often increase more rapidly for the first increments of load than for succeeding increments. Examples of this may be seen in the load-deflection curves for Panels IV and X (figs. 12 and 13) and in the load-strain curves for Panel III (fig. 18).

On the other hand, the die-braked specimens (XII to XXIV) were much more uniform in dimensions and were flatter. For these panels the inequalities of the kind mentioned produced no appreciable effects on the deflections or strains.

The load-strain curves of typical panels given in Figures 18 to 21 show that the observed strain is in no case much greater than that computed by the conventional theory. The sets in the strain readings after loading to the limiting deflection were small, Panel III as a whole showing the largest values of these sets.

For all specimens of types A and B, except Panel III, Table 5 shows that the proportional limit was equal to or higher than the load

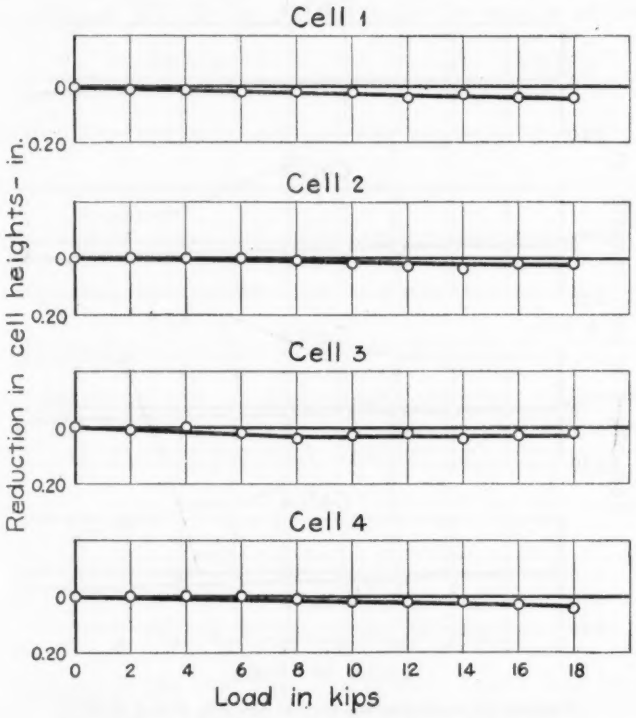

FIGURE 26.—*Reduction in cell heights, Panel XIII*

at the limiting deflection. Panel III was a product of the earlier manufacturing technique.

Buckling under the loading plates was present in all panels before the limiting deflection was reached and could be observed distinctly looking along the interior of the cell illuminated with a flash light. After removing the limiting deflection load, slight permanent buckles remained in about two-thirds of the panels which were examined for permanent buckles. In one case three of the eight areas of contact of the loading plates with the specimen were buckled, in another case two, and in the remaining five cases only one. It appeared that the uniformity of the die-braked panels resulted in less severe indentation under load and in fewer permanent buckles. For loads below the limiting deflection, the buckling under the loading plates

is almost entirely elastic. Under repeated loading the presence of slight permanent buckles did not produce any measurable change in the elastic properties.

(b) NEUTRAL AXIS

The position of the neutral axis as determined by the strain measurements at the middle of the specimens was usually in good agreement with the values calculated from the dimensions. The close agreement of the observed and calculated moments of inertia indicates also that the actual nuetral axis was close to its calculated position. For some cells, however, the observed values of r do not check well

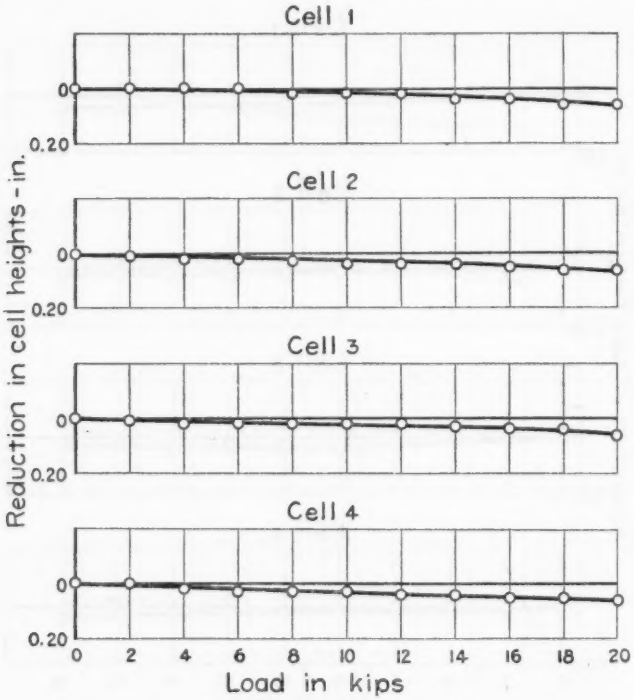

FIGURE 27.—*Reduction in cell heights, Panel XXIV*

with the calculated values. An extreme example of this may be seen in Figure 28, showing the values of r for Panel IV. This was due to the top and bottom of the cells not acting integrally in portions of the specimen near the gage lines.

The integral action of the upper and lower elements depends upon shearing forces being transmitted by the welds. When welds fail under load, or if the welding should fail to join portions of the web, there is a lack of integral action between the top and bottom of the panel. What happens then may best be visualized by considering the action of the top and bottom elements when placed together as in the panel, but unconnected by any welding. The bending moment then is distributed between the two elements in proportion to their respective moments of inertia. Since the moment of inertia of the bottom element is much greater than that of the top, most

of the bending moment will be carried by the lower element. It follows that for a given bending moment on a panel the compressive stress at the top of an unwelded panel is less, while the tensile stress at the bottom is greater than if the panel had been welded. Strain-gage readings on the upper and lower surfaces of such a panel would indicate the position of the neutral axis to be above that for a welded panel. The values of r observed in such a case would be less than those calculated on the assumption of integral action of the upper and lower elements of the panel.

Actual cases of incomplete integration in the webs are intermediate between the fully welded and the unwelded case described. The values of r in Figure 28 show an extreme effect of this kind. Cells 3 and 4 of Panel XVIII (fig. 24) illustrate the results of poorly inte-

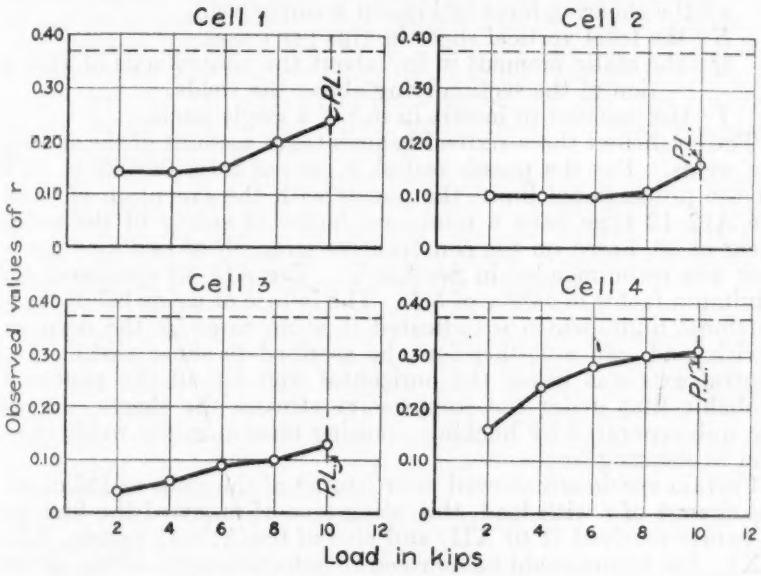

FIGURE 28.—*Values of* r *for Panel IV*

grated portions of the web near mid-span. As the load increased on the panel, the intact welds at the end of the defective portion began to take up the shearing forces that otherwise would have been transmitted by that portion. This tightening-up process brings the value of r nearer the calculated value as the load increases, as can be seen in the curves. The compressive-strain curve for the first cell of Panel III (fig. 18) illustrates the effect of defective integration on the strains. The tensile-strain curve for this cell shows an increase over the calculated value, but the percentage change is not as great as for the compressive strain. In general, it may be said that defective integration in the web reduced the compressive stresses in the upper cells to a greater degree than it increased the tensile stresses in the lower cells. For Panel IV the compressive stresses observed at the proportional limit were markedly lower than the computed values, while the tensile stresses observed were not much greater than the computed values, the maximum value of the observed stress being

33.6 kips/in.^{2} compared with a computed stress of 31.2 kips/in.^{2}. At the limiting deflection the maximum excess of observed over computed tensile stress amounted to 4.3 kips/in.^{2}, or 18 per cent, for the hand-set Panel III, as can be seen in Figure 18 (cell 4). For the more accurately dimensioned panels formed over dies and welded automatically, the maximum excess was 1.9 kips/in.^{2}, or 9 per cent for Panel XIX.

(c) WELDS

The shearing forces on the welds may be computed from the formula

$$s = \frac{3}{16}\frac{SQ}{I}$$

where

s = the shearing force in kips on a single weld,
S = the total vertical shear in kips per panel,
Q = the static moment in in.^{3} about the neutral axis of that portion of the section lying above the welds.
I = the moment of inertia in in.^{4} of a single panel.

The coefficient three-sixteenths inch takes account of the spacing of the welds. For the panels tested, s ranged from $0.032S$ to $0.036S$. At the proportional limit, the panels with the exception of those of the A12–12 type gave a minimum factor of safety of the welds in shear of 10, based on the conservative strength of two kips per weld that was recommended in Section V. The A12–12 specimens had a minimum factor of safety of 5.5. The failure of welds below the proportional limit, which is indicated in some cases by the decrease of r with load, can not, therefore, be ascribed to shear alone. As the neutral axis was below the horizontal web for all the panels, it is probable that under the compressive stresses the sheets composing the web separated by buckling, causing tension in the welds in addition to shearing forces.

Certain specimens showed poor joining of the webs as indicated by the change of r with load, this being true of many of the first group of panels received (I to XII) and also of the A12–12 panels, XIX to XXI. No failure could be ascribed to defective welds alone, although undoubtedly the increased tensile stress produced yielding in the panels at earlier loads. Any significant effects of poor or inadequate welding would be shown by a lowering of the proportional limit.

(d) CELL HEIGHTS AT THE SUPPORTS

The pressure of the reactions reduced the height of the cells over the supports as shown by Figures 25, 26, and 27. This reduction of the height was shown to be almost entirely elastic up to the limiting deflection load by the absence of appreciable permanent changes in the cell heights. Except for Panel III, the maximum observed permanent reduction, after applying the limiting deflection load, was 0.03 inch for one cell of Panel XXII. Two cells in Panel III decreased 0.05 inch in height, one cell 0.04 inch, and three cells 0.03 inch. This anomalous behavior of Panel III is due apparently to irregularity in sizes of the cells, this panel having been formed on a hand-set brake. The average permanent reduction in cell heights after unloading from the limiting deflection was 0.007 inch.

The maximum reductions in cell height observed at the limiting deflection were 0.08 inch for one cell of Panel I, 0.07 inch for one cell of Panel III, and 0.05 inch for one cell of Panel XVI. The high values for Panel I and III are due to the irregularity of dimensions characteristic of the panels formed on the hand-set brake. Values for the other panels were all less than 0.05 inch and averaged 0.02 inch. The reduction in cell height for die-braked panels is therefore negligible at the limiting deflection load.

(c) FAILURE OF THE PANELS

As the load was increased above the proportional limit, buckles appeared in the cell tops between the loads and increased in size and number up to the maximum load. At the same time the indentations in the cell tops under the loading plates increased slowly in depth and in a few panels buckles appeared in the upper portion of the side walls of the cells. Failure in the upper portion of the specimen appeared to take place entirely by buckling, though the A12–12 specimens (see fig. 16) showed strain lines on the cell tops running about 45° to the axis of the panel, which indicated that the yield point in compression had been reached.

In no cases did any crumpling or buckling start from irregularities of shape or from dents which had occurred in manufacture or shipment. Even in the panels having the thinnest bottom sheets (18 gage), the reinforcing at the ends of these panels inhibited completely any crumpling of the cell bottoms over the supports.

For most of the specimens sharp cracks were heard as the maximum load was approached and occasionally at loads below the proportional limit. It is believed that these sounds were due to the fracturing of welds. Many weld fractures, however, were undoubtedly inaudible.

Departure from elastic behavior in the specimens may be due to the following causes: (1) Yielding of the cell bottoms in tension, (2) buckling of the cell tops in compression, (3) failure of welds, and (4) effect of the concentrated loads.

The first three points will be discussed in the light of the observations at mid-span, 30 inches from the loads.

The stress at which compression failure by buckling began to occur is dependent on the yield point of the material, since the elastic buckling is negligible with respect to the inelastic. For 14 and 16 gage sheet having a yield point of 20 to 25 kips/in.^{2}, inelastic buckling seemed to set in at a stress of around 12 kips/in.^{2} for specimens of type A. The 14-gage material with a yield point of 41 to 46 kips/in.^{2} in type A buckled at a stress of about 22 kips/in.^{2} For type B, the buckling stress appeared to be a little lower with respect to the yield point, 16-gage material with a yield point of 21 kips/in.^{2} beginning to show marked buckling at stresses of 10 to 12 kips/in.^{2}

The dimensions of panels of the A14–16 and A16–18 types were such that simultaneous compression and tension failures occurred at mid-span provided that the observed values of r were in fair agreement with the computed values. The compression failures in the A16–18 panels, once they started, progressed more rapidly, however, than in the heavier top sheets of the A14–16 type. When the observed values of r agree with the computed values, the ratio of compressive to tensile stress in these two types is about 0.60. When this ratio

becomes a little greater, as the A14–14 and A12–12 types, for which it is about 0.67, failure tends to begin by buckling and then develops by combined buckling and yielding in tension.

In the type B panels the restraint offered to the buckling by the webs caused tensions in the welds which, in conjunction with the shearing forces, were sometimes enough to cause failure of the welds when buckling was well advanced. In Figure 29 is shown a B16–16 specimen in which the top sheet separated from the bottom sheet at a load near the maximum, thus permitting the buckles to spread from one cell top to another across the full width of the panel.

The effects of the welding on the failures have already been discussed.

The effect of the concentration of the loads on the proportional limits of the panels may best be judged by comparing the stresses at mid-span at the proportional limit with the yield point of the bottom sheets given either by the tensile tests or by the load-strain curves. On the average, the proportional limit occurs at a mid-span stress of around 0.7 of the yield point, though some specimens had proportional limits which develop the yield point stresses at the center (V, XXII, and XXIII). A closer examination of the results on this point is of little use, since in many cases materials of widely different yield points were used for the bottom sheets.

The local effects produced by the concentrated loads may be three, as follows: (1) Indentation and buckling of the cell tops under the loading plates; (2) buckling of the web producing weld failures near the loads and consequently increased tensile stress in the cell bottom; and (3) possibly an increase in stress under the concentrated loads considerably above that calculated from the conventional theory. Such stresses have been predicted by Schnadel.[8] For box girders with a length of 6.3 times the width and loaded at the quarter points, he has calculated the maximum longitudinal stress in the top and bottom plates at the quarter points to be 70 per cent in excess of that at mid-span.

The disappearance of buckles under the loading plates on unloading from the limiting deflection and the fact that there was no evidence of reduction in the proportional limit on repeated loading justifies the conclusion that indentation of the cell tops by the concentrated loads is of small importance up to the proportional limit. It would be reasonable to expect, however, that the indentations would lower the compressive resistance of the panel at these points. The effect predicted by Schnadel should be verified by some independent means, but must be accepted as a possibility. In any case, it may be concluded that under uniform loading and on similar spans the panels will behave satisfactorily over a range at least equal to that given by the proportional limit of the present tests.

Had the dimensions of the first 12 specimens been uniform and had the material and welding been likewise more uniform, the results would, undoubtedly, have not shown so much scatter. The tests have shown that the three stages of manufacturing technique have resulted in panels progressively better in strength properties and in uniformity of dimensions.

[8] Georg Schnadel, Die mittragende Breite in Kastenträgern und in Doppelboden, Werft-Reederei-Hafen, Mar. 7, 1928, Heft 5, p. 92.

FIGURE 29.—*Top view of a B16–16 panel after testing*

B. S. Journal of Research, RP463

UNIV. OF MICH.

2. SPECIMENS OF TYPE C

The agreement between the observed and computed moments of inertia in Table 6 is poor for the specimens of type C. No reason was found for the high moment of inertia observed for Panel IX. The proportional limits (Table 5) were low with respect to the limiting deflection loads and the maximum loads were lower than for any specimens of the A14–16 type. The panels failed from an inherent defect in design, the sheets composing the webs splitting apart at the ends due to combined tension and shear on the welds. The tension on the welds was produced by the panel being supported at the ends only by the projecting top element.

IX. CONCLUSIONS

The loading tests on sheet steel floor panels having longitudinal stiffening cells and either flat or corrugated top surfaces justify the following conclusions for types A and B (fig. 1).

1. The elastic range of the panels was equal to or in some cases in excess of the maximum working range set by the usual deflection requirements (deflection less than one three hundred and sixtieth of the span) in 10-foot floor panels. This elastic range is the fundamental criterion of the usefulness of the panels.

2. The maximum load carried by these panels showed a considerable and satisfactory margin of safety against overloading.

3. The method in common use for designing beams affords a satisfactory basis for predicting the elastic behavior of these floor sections. The stiffness of the panels calculated from average dimensions was in excellent agreement with that calculated from the deflection. The distribution of longitudinal stress in the die-braked panels can be satisfactorily predicted by the usual methods of design if an allowance of 10 per cent is made to cover the possible irregularities in the distribution of tensile stress.

4. The spot welds used in joining the sheets were amply strong in shear, but some may have failed by buckling apart of the two sheets in the web between the welds. These failures, however, had no appreciable effect on the behavior of the panels within the elastic range.

5. The location of the neutral axis is in accord with the calculated location except where imperfect integration by the welds of the top and bottom elements of the section may lead to a displacement. It is therefore desirable that controlled automatic welding be used in the manufacture of such panels.

6. The thin-walled sections showed a considerable stability against secondary failure, even under concentrated loads.

Panels of type C (fig. 1) showed an inherent defect in design, failure being due to tension on the end welds of the web, there being no provision to strengthen the ends of the webs to withstand these forces.

WASHINGTON, June 4, 1932.

127984—32——4

THE INFLUENCE OF TEMPERATURE ON THE EVOLUTION OF HYDROGEN SULPHIDE FROM VULCANIZED RUBBER

By A. D. Cummings

ABSTRACT

Evolution of hydrogen sulphide from vulcanized rubber containing 8 to 32 per cent sulphur has been measured when the temperature of the specimens was raised step by step from 105° to 265° C., and the time intervals kept equal. The same sample of each compound was employed throughout the whole temperature range. The rate of decomposition increases as the temperature is raised, except in the case of the compounds containing the higher percentages of sulphur, when it passes through a maximum.

The loss of hydrogen sulphide has also been determined for four different compounds containing 4, 10, 18, and 32 per cent sulphur when samples were heated for 200 hours at 136° C., and also when other samples of these compounds were maintained for the same length of time at 220° C. In each case, the rate of decomposition decreases rapidly at first, but after several days' heating, the decrease becomes relatively slow. In general, the rate increases with temperature and with increasing sulphur content. Other products evolved are moisture and organic compounds.

The data presented in this paper supplement and confirm previous results on the evolution of hydrogen sulphide from vulcanized rubber and indicate at what temperatures direct thermal decomposition of different rubber-sulphur compounds will become significant. No mechanism to explain the chemical changes involved is suggested. This question is worthy of further investigation.

CONTENTS

	Page
I. Introduction	163
II. Preparation of specimens	165
III. Apparatus and procedure for determining the hydrogen sulphide evolved	165
1. Measurement of the evolution of hydrogen sulphide during step-by-step heating	166
2. Measurement of the evolution of hydrogen sulphide at constant temperature	166
IV. Results of decomposition during step-by-step heating	167
V. Results of decomposition at constant temperature	167
1. Rate of loss of hydrogen sulphide	168
(*a*) Effect of time	168
(*b*) Effect of temperature	168
(*c*) Effect of composition of samples	170
2. Other decomposition products and moisture	170
VI. Characteristics of the rubber after heating	171
VII. Discussion	172

I. INTRODUCTION

This paper presents the results of measurements of the evolution of hydrogen sulphide from rubber-sulphur compounds heated at various temperatures. Determination of the amount of hydrogen sulphide produced under different conditions was used to measure

the degree of decomposition of the rubber. Two types of experiments were carried out: (1) Samples of vulcanized rubber containing 8 to 32 per cent sulphur were heated for 8-hour intervals at 13 temperatures between 105° and 265° C., and (2) samples having sulphur contents of 4, 10, 18, and 32 per cent were maintained for about 200 hours at constant temperature, one set of specimens at 136° and another group at 220° C.

These measurements of deterioration were undertaken in connection with an investigation on the electrical properties of vulcanized rubber at relatively high temperatures. During these experiments, samples of rubber-sulphur compounds had been subjected to a wide range of temperatures. Time of exposure to each temperature had been about eight hours. The purpose of the present work was to determine when the sulphur content of a specimen had changed sufficiently to affect its dielectric constant and power factor by a measurable amount. In order to approximate the conditions under which the electrical tests were made, it was necessary to determine the amount of decomposition when rubber vulcanized with 8 to 32 per cent sulphur was heated for successive intervals of eight hours each at temperatures changed in unequal steps from 105° to 265° C. To make this information more complete and to obtain additional data which could be compared with previous investigations, the work was extended to include determinations of the loss of hydrogen sulphide from vulcanized rubber heated for a long time at constant temperature. The electrical properties of the whole series of rubber-sulphur compounds is the subject of a separate investigation at this bureau, and will be reported in another paper.

Many investigators have shown that hydrogen sulphide is associated with the vulcanization of rubber and with its subsequent deterioration during aging. Stevens and Stevens have noted the evolution of hydrogen sulphide during the vulcanization of ebonite at temperatures above 70° C. Webster, Fry, and Porritt have shown that ebonite evolves hydrogen sulphide at ordinary temperatures as well as when heated and have measured the rate of decomposition at several temperatures. Wolesensky has found that both soft and hard rubber lose hydrogen sulphide at all temperatures above 25° C. For more details of previous investigations on this problem during the last few years, the reader is referred to the papers by the authors mentioned.[1] A review of the literature up to 1929 is given in the paper by Wolesensky.

The results described in this paper represent a single set of measurements of the evolution of hydrogen sulphide when compounds of purified rubber and sulphur were heated under different conditions of time and temperature. Possible effects or variations which might be encountered with rubber samples made at different times or prepared in different forms for exposure to the heat, or with other changes in experimental conditions were not investigated. The results show the loss of hydrogen sulphide when rubber-sulphur compounds representative of the whole series from soft to hard rubber were heated step by step from 105° to 265° C., and also when heated for 200 hours at 136° and at 220° C.

[1] Edward Wolesensky, B. S. Jour. Research, vol. 4, p. 501, 1930; Rubber Chem. Tech., vol. 3, p. 386, 1930. J. D. Fry and B. D. Porritt, India Rubber J., vol. 78, p. 307, 1929. D. M. Webster and B. D. Porritt, India Rubber J., vol. 79, p. 239, 1930; Rubber Chem. Tech., vol. 3, p. 618, 1930. H. P. Stevens and W. H. Stevens, J. Soc. Chem. Ind., vol. 50, p. 397T, 1931.

II. PREPARATION OF SPECIMENS

The rubber specimens were prepared from protein-free rubber hydrocarbon and sulphur. The rubber hydrocarbon was obtained from latex by digestion with hot water and extraction with water and alcohol, in accordance with the method described by McPherson,[2] which gives a purified material containing about 99.5 per cent hydrocarbon. A master batch of rubber and sulphur was made and portions of this were blended with fresh rubber hydrocarbon to give any sulphur content desired. The specimens were prepared by pressing samples of these rubber-sulphur mixtures between thin aluminum plates separated by a spacer 1.25 mm in thickness. The specimens were then placed in an autoclave and vulcanized for 40 hours at 141° C. under pressure of carbon dioxide. The long period of vulcanization

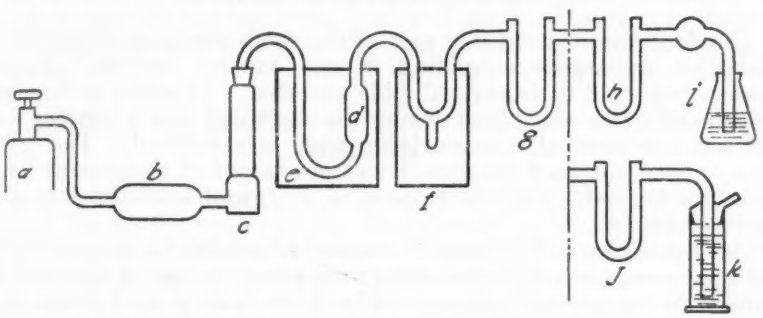

FIGURE 1.—*Apparatus used for measurement of decomposition of vulcanized rubber*

a, cylinder of commercial hydrogen to provide an inert atmosphere and sweep out products evolved while the rubber is heated.
b, concentrated alkaline pyrogallol solution on glass wool to absorb traces of oxygen.
c, tower containing calcium chloride and magnesium perchlorate to dry the gas stream.
d, glass tube containing the rubber sample cut into strips.
e, oil bath, electrically heated and thermostatically controlled.
f, trap in ice-salt freezing mixture to collect any volatile liquids.
g, U tube containing magnesium perchlorate to absorb moisture given off from the rubber.
h, U tube containing saturated potassium hydroxide solution on glass wool to absorb hydrogen sulphide, protected at each end by drying agent to prevent loss of moisture from the tube.
i, protective drying tube and bubble counter.
NOTE.—In some cases lead acetate solution was used as an absorber for hydrogen sulphide. This is indicated by the gas-washing bottle, *k*, preceded by the drying tube, *j*, to prevent back diffusion of moisture into the weighed drying tube, *g*.

resulted in a product which contained practically no free sulphur in the soft and medium hard rubber ranges. In the case of pure hard rubber, analyses on different samples of stock containing 32 per cent sulphur showed from 0.5 to 0.8 per cent free sulphur. In the present experiments, the 32 per cent sample was the only one to show a deposit of sublimed sulphur.

III. APPARATUS AND PROCEDURE FOR DETERMINING THE HYDROGEN SULPHIDE DISSOLVED

The essential features of the apparatus were a supply of inert gas, a tube to hold the rubber sample, a constant temperature bath, and an absorber for the hydrogen sulphide. The individual parts of the apparatus are indicated and described in Figure 1.

[2] A. T. McPherson, A Method for the Purification of Rubber and Properties of the Purified Rubber B. S. Jour. Research, vol. 8 (RP449), p. 751, 1932.

The general method chosen for measuring the deterioration of vulcanized rubber when heated was determination of the amount of hydrogen sulphide evolved. This determination was carried out in two ways: (1) the hydrogen sulphide was absorbed in lead acetate solution and the lead sulphide collected and weighed, and (2) the hydrogen sulphide was absorbed by saturated potassium hydroxide solution contained in a tube which could be weighed directly. Both methods were equally satisfactory under appropriate conditions. Absorption in lead acetate is preferable when a very small amount of hydrogen sulphide is to be measured, but when much lead sulphide is formed this method becomes exceedingly time-consuming on account of slow filtration.

1. MEASUREMENT OF THE EVOLUTION OF HYDROGEN SULPHIDE DURING STEP-BY-STEP HEATING

The decomposition in this part of the work was carried out with a simplified apparatus consisting of gas supply, sample tube and heater, trap, and hydrogen sulphide absorber. In order to duplicate more nearly the conditions during the electrical test when the inert gas was not purified, the purifying train was omitted. The drying tube, *g*, was not used because it was not intended to account for all products formed. Only sections *a*, *d*, *e*, *f*, and *k* of the apparatus were employed.

The tubes containing 5-gram samples of rubber in strips cut from the specimens previously described were placed in the oil bath and the stream of hydrogen [3] started. The bath was heated from room temperature up to 105° C. where it was held for eight hours. The absorber containing lead acetate solution was then changed, provided any precipitated lead sulphide was visible, and the temperature was raised to 115°. The lead sulphide formed was collected by filtration through a Gooch crucible, washed, dried, and weighed. This procedure was repeated step by step every eight hours at 13 temperatures between 105° and 265°, with samples containing from 8 to 32 per cent sulphur. All samples were heated for eight hours at each temperature before being raised to the next higher temperature. It was already known that the electrical properties of rubber containing less than 8 per cent sulphur were not changed a significant amount by loss of sulphur when heated under these conditions, consequently the experiments were begun with the 8 per cent compound. Temperatures below 100° did not cause a change in sulphur content sufficient to be detected in the electrical measurements on a specimen containing the maximum amount, 32 per cent, of sulphur, therefore 105° was selected as the initial temperature.

2. MEASUREMENT OF THE EVOLUTION OF HYDROGEN SULPHIDE AT CONSTANT TEMPERATURE

The apparatus was used complete as described for this part of the investigation, and both methods for the absorption of the hydrogen sulphide were employed. The specimen tubes containing 20 to 50 g

[3] No significant error was introduced by reaction of the hydrogen with any small amount of free sulphur in the rubber. The rate of reaction of hydrogen with sulphur is relatively slow at the highest temperature used in the present experiments. (See J. W. Mellor, A Comprehensive Treatise on Inorganic and Theoretical Chemistry, vol 10, pp. 117 ff., 1930.) Furthermore, an experiment in which steam was used as the inert gas gave substantially the same rate of evolution of hydrogen sulphide as was obtained with hydrogen (unpublished work of A. T. McPherson).

of rubber were set up at room temperature outside the oil bath. While the bath was being heated to the temperature desired, the apparatus was swept with hydrogen to displace air. The tubes for absorption of moisture and of hydrogen sulphide, when potassium hydroxide was used, were removed, weighed, and then replaced. The tubes containing the rubber samples were next immersed in the hot oil, and the hydrogen stream was adjusted to about one bubble per second. The hydrogen sulphide was measured at intervals by weighing the U-tube absorbers directly or by determining the amount of lead sulphide formed. The amount of moisture and volatile oils was determined only at the end of the experiment. This served to account for the entire loss in weight of the samples. The loss of hydrogen sulphide was determined for four rubber compounds containing 4, 10, 18, and 32 per cent sulphur when samples were heated for about 200 hours at 136° C., and also when other samples were heated at 220° C. for the same length of time. The temperature of the oil bath was held within ± 1° at the former temperature and ± 3° at the latter.

IV. RESULTS OF DECOMPOSITION DURING STEP-BY-STEP HEATING

The evolution of hydrogen sulphide from vulcanized rubber containing 8 to 32 per cent sulphur when heated in the 8-hour stepwise manner increases with rising temperature, with the exception that the loss from the compounds containing the higher percentages of sulphur passes through a maximum. In view of the large change in sulphur content during heating, this is not surprising. The amount of hydrogen sulphide evolved in an 8-hour interval at each temperature is shown in Figure 2.

The change in sulphur content calculated from the loss of sulphur as hydrogen sulphide between 105° and each higher temperature is given in Figure 3. These values for the sulphur content are not identical with those which would be determined by analysis of a sample of rubber taken at each temperature, because there was some loss in weight of the sample due to distillation of volatile liquids. However, the error is not great. This is indicated by the agreement between the final sulphur content calculated from the data of the present experiments and that obtained by analysis of samples used in the electrical measurements mentioned previously. This comparison, printed in Table 1, shows that the heating in the present investigation had satisfactorily paralleled the conditions during the electrical test and that the procedure and calculations were adequate to furnish the information desired.

V. RESULTS OF DECOMPOSITION AT CONSTANT TEMPERATURE

In addition to determination of hydrogen sulphide, measurements were made of the amounts of other decomposition products and moisture which resulted from heating vulcanized rubber containing 4, 10, 18, and 32 per cent sulphur at 136° and 220° C. for 200 hours.

1. RATE OF LOSS OF HYDROGEN SULPHIDE

The results show the effects of time, temperature, and composition of samples on the rate of evolution of hydrogen sulphide.

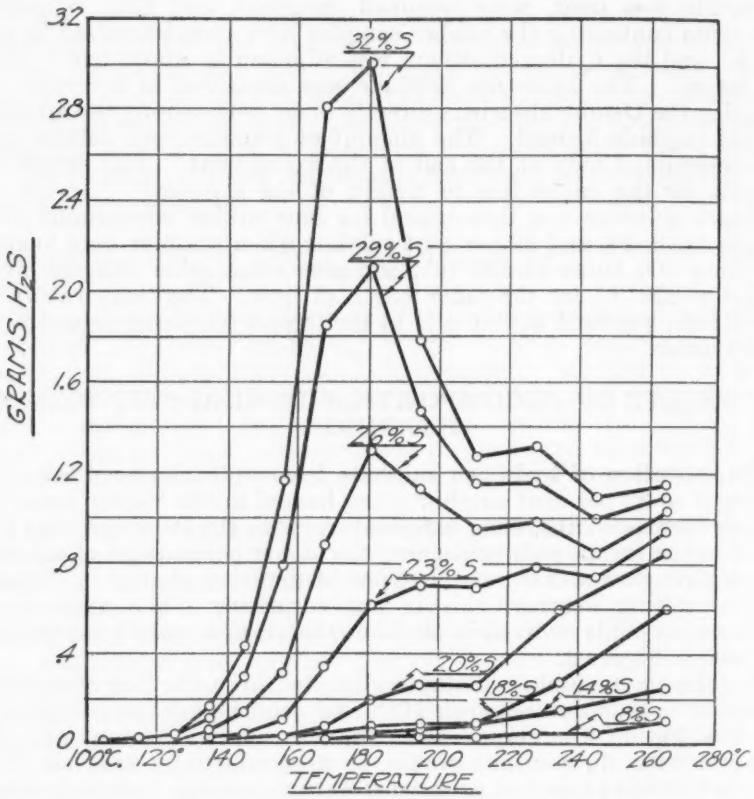

FIGURE 2.—*Evolution of hydrogen sulphide from vulcanized rubber during step-by-step heating*

Grams of hydrogen sulphide liberated from 100 g vulcanized rubber heated for eight hours at each temperature indicated. Every sample was started at 105° and the same sample was carried through to 265°.

(a) EFFECT OF TIME

For a given composition at each temperature, the rate of loss of hydrogen sulphide, high at first, decreases rapidly during the first few days' heating, but subsequently the decrease becomes slow.

(b) EFFECT OF TEMPERATURE

For a given composition and period of time, the rate increases with rising temperature.

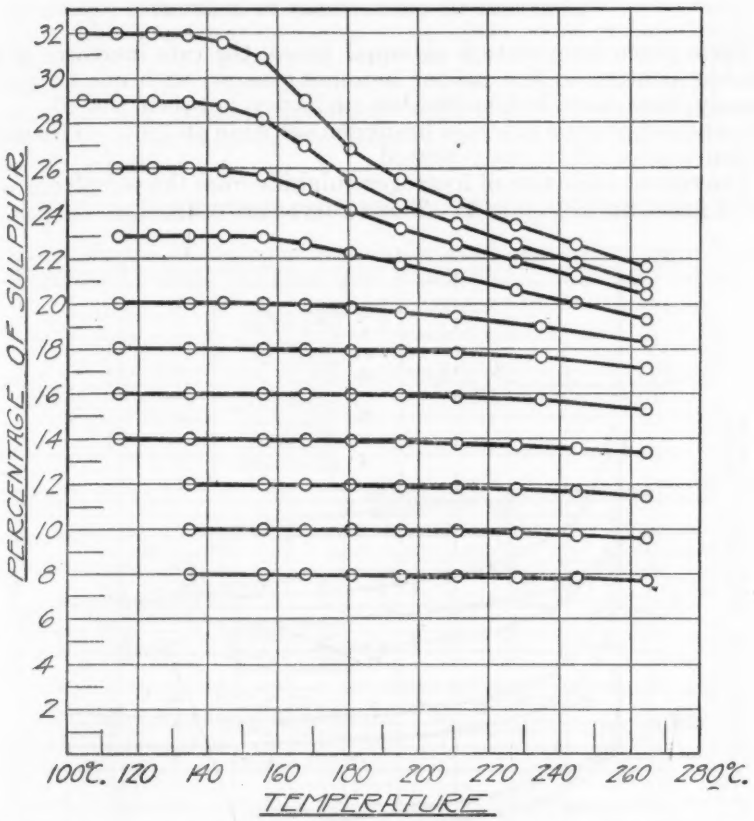

FIGURE 3.—*Change in sulphur content of vulcanized rubber during step-by-step heating*

Samples were heated for 8 hours at each temperature indicated by the various points. Every sample was started at 105° and the same sample was carried through to 265°.

TABLE 1.—*Analysis of electrical test specimens for sulphur compared with sulphur content calculated from the present experiments*

Original sulphur	Sulphur after heating calculated from present measurements	Total sulphur in specimens after high temperature electrical test
Per cent	*Per cent*	*Per cent*
32	21.6	22.0
29	20.9	21.5
26	20.4	20.5
23	19.3	19.6
20	18.3	18.1
18	17.0	16.8
16	15.4	15.2
14	13.4	13.4
12	11.4	11.1
10	9.6	9.5
8	7.7	7.8

(c) EFFECT OF COMPOSITION OF SAMPLES

For a given temperature at equal times, the rate increases as the sulphur content of the rubber becomes greater, with one exception, namely, that there is a noticeable similarity between the 10 and 18 per cent compounds in loss of hydrogen sulphide at 136°. This observation was satisfactorily repeated.

The rate of evolution of hydrogen sulphide from the samples investigated is shown in Figure 4. These curves are started at the point of

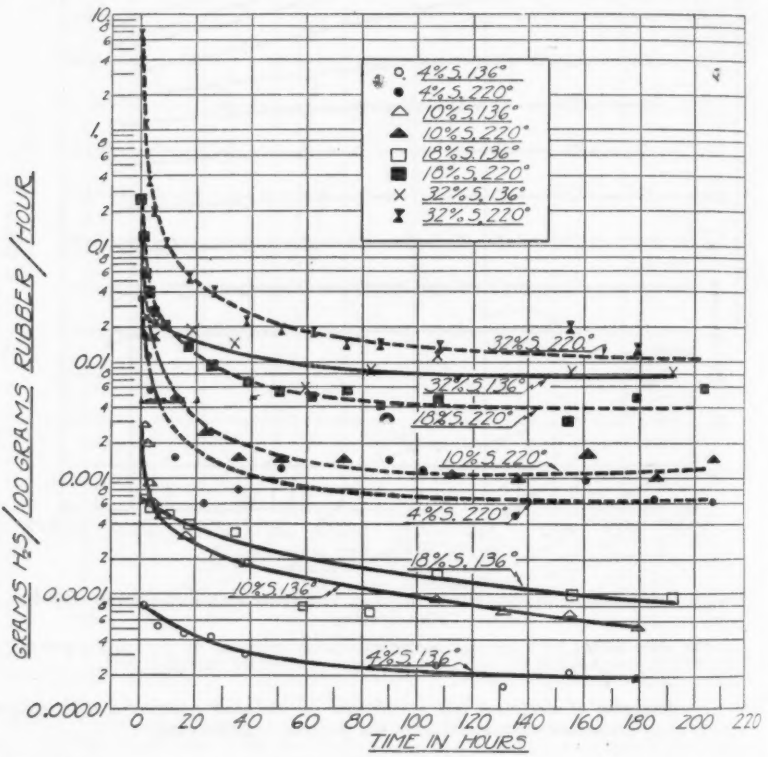

FIGURE 4.—*Rate of evolution of hydrogen sulphide from vulcanized rubber heated at 136° and 220° C., plotted on a semilogarithmic scale*

maximum evolution, an initial increase in rate being disregarded because it must be due only to the heating up of the sample and the approach to a quasi-steady state throughout the apparatus. The percentage of the original weight lost as hydrogen sulphide plotted against the time is given in Figure 5.

2. OTHER DECOMPOSITION PRODUCTS AND MOISTURE

Along with the hydrogen sulphide, volatile oils having slight terpenelike odors were formed. At 220°, these oils made up 10 to 40 per cent of the total loss in weight of the samples during 200 hours' heating. There was also a trace of some compound having a faint onionlike odor which was never condensed or absorbed by potassium hydroxide or lead acetate. No attempt was made to identify this

or any of the other organic products. Some moisture[4] was evolved from the rubber and was measured at the end of each group of experiments in order to be able to account for the entire loss in weight of the samples. The percentage of the original weight obtained in the products from a typical experiment with a 32 per cent compound at 136° is given in Table 2, which shows that the total loss was satisfactorily accounted for.

VI. CHARACTERISTICS OF THE RUBBER AFTER HEATING

The specimens all changed materially in physical properties during the exposure to heat. Compounds which had initially contained up

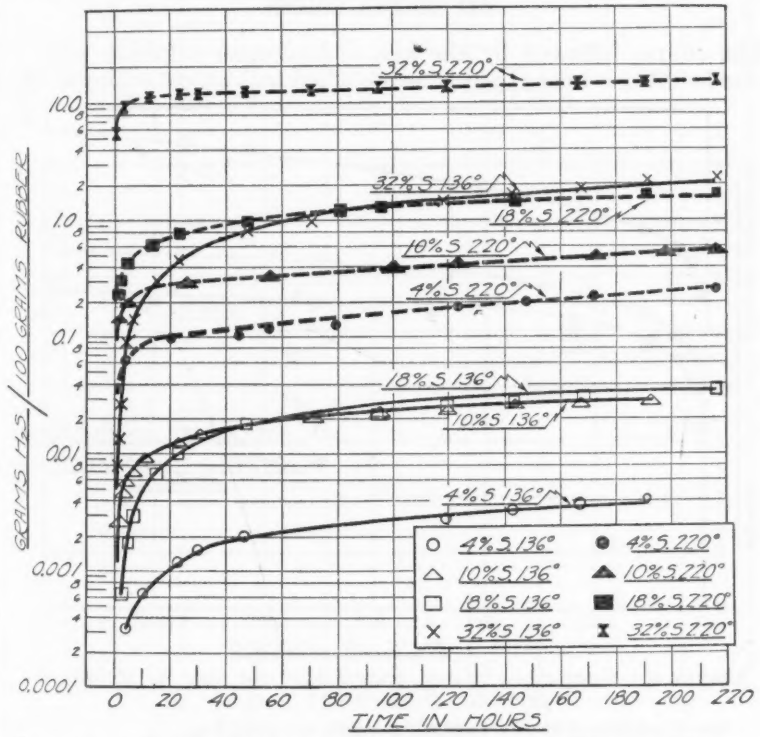

FIGURE 5.—*Percentage loss of hydrogen sulphide at 136° and 220° C., plotted on a semilogarithmic scale*

to 26 per cent sulphur became translucent and showed a reddish color when samples 1 mm in thickness were examined in sunlight, whereas all above 12 per cent of sulphur were originally opaque. At the end of the heating, the intermediate and hard rubbers were brittle at room temperature, but became flexible and tacky when warmed. A similar change in properties, less in degree, was evident in the samples of soft rubber. The conversion of vulcanized rubber into thermoplastic materials has been noted by Kemp,[5] who heated rubber mixed with

[4] The moisture may have been an impurity or may have come from the thermal decomposition of a small amount of oxidized material in the rubber. For a discussion of the products formed by oxidation of rubber, see Oxidation Studies of Rubber, Gutta-Percha, and Balata Hydrocarbons by A. R. Kemp, W. S. Bishop, and P. A. Lasselle, Ind. Eng. Chem., vol. 23, p. 1444, 1931.

[5] A. R. Kemp, U. S. Patent 1638535, Aug. 9, 1927. For a general review of the field of thermoplastic products made from rubber, including patent references, the reader is directed to the Chemistry of Rubber, by Harry L. Fisher, Chem. Rev., vol. 7, No. 1, pp. 94, 112–123, March, 1930.

8 to 16 per cent sulphur to 200° to 280° C., and the manufacture of such products from raw rubber is now a commercial process.

TABLE 2.—*Percentage of original sample accounted for after a 32 per cent compound was heated 200 hours at 136° C.*

	Per cent
Residual rubber	95. 55
Oils	. 01
Sulphur	. 02
Moisture	. 18
Hydrogen sulphide	2. 17
Total	99. 93

VII. DISCUSSION

The course followed by the loss of hydrogen sulphide when vulcanized rubber is heated is well established and agrees with the results

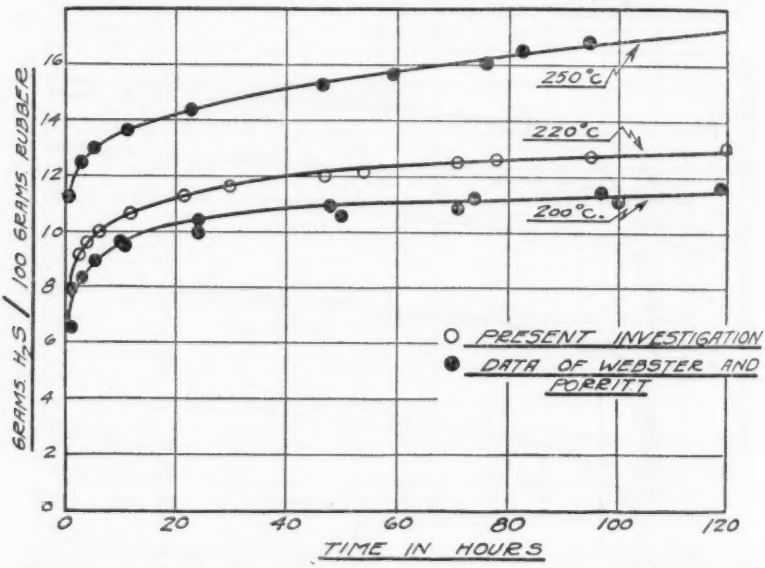

FIGURE 6.—*Comparison between present data and those of Webster and Porritt.* (*See footnote 1, p. 164.*)

Loss of hydrogen sulphide from hard rubber at 200°, 220°, and 250° C.

of previous investigations so far as can be told from consideration of the data taken under different conditions. The curve for evolution of hydrogen sulphide from the 32 per cent compound at 220° lies between similar curves published by Webster and Porritt [6] for ebonite heated at 200° and 250° C. This comparison is shown in Figure 6.

Calculation of the ratio of sulphur lost at the end of 190 hours to the initial sulphur content shows that the percentage of the original sulphur lost at 136° is greater for the compound containing 10 per cent sulphur than for that containing 18 per cent, and at 220° is greater for the compound containing 4 per cent sulphur than for that having 10 per cent. On the other hand, the weight of sulphur actually lost per gram of rubber compound was nearly equal for the

[6] See footnote 1, p. 164.

10 and 18 per cent compounds at 136°, and was less for the 4 per cent sample than for that containing 10 per cent sulphur at 220°. These calculations are given in Table 3 and the proportionate loss of sulphur is plotted in Figure 7. The similarity in rate and in total percentage of loss at 136° for the samples containing 10 and 18 per cent sulphur led to a repetition of this experiment over the first 80 hours using

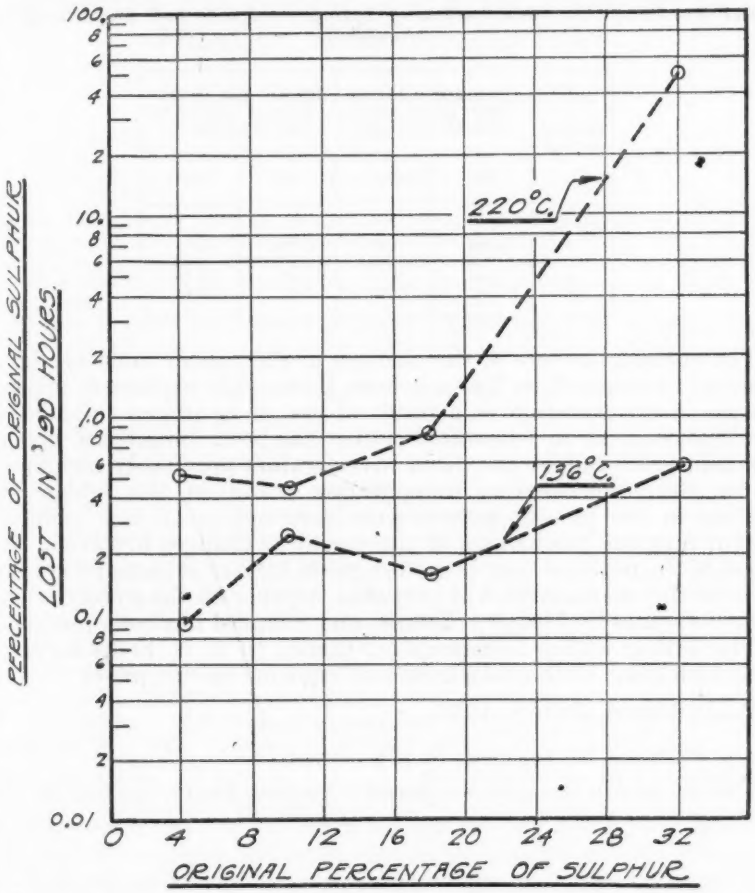

FIGURE 7.—*Percentage of original sulphur lost in 190 hours at 136° and 220° C., plotted on a semilogarithmic scale as a function of initial sulphur content*

other specimens containing the same percentages of sulphur. This determination checked the original observations satisfactorily. Also, an inspection of the data from the earlier experiments showed a distinct similarity in rate of evolution from compounds containing 10 to 18 per cent sulphur at the lower end of the temperature range. These observations can be interpreted as indicating that there may be a range of compositions, varying with the temperature, where rates of decomposition are similar, and where the proportionate loss of sulphur may grow less while the original sulphur content of the

specimens increases. There may be a fairly sharp break at the end of this range, above which the loss of hydrogen sulphide may become much more rapid and follow the course expected for the order of ascending sulphur content. The data of the present experiments do not show whether the cases at hand are part of a general phenomenon or only isolated instances.

TABLE 3.—*Comparison between loss of hydrogen sulphide and proportionate loss of sulphur*

Original sulphur	H_2S lost at end of 190 hours as per cent of original compound		Sulphur lost in 190 hours as per cent of original sulphur	
	136°	220°	136°	220°
Per cent				
4	0.004	0.23	0.094	5.29
10	.029	.51	.26	4.58
18	.033	1.56	.17	8.15
32	1.96	13.92	5.77	40.93

The chemical nature of the changes in the rubber molecule during thermal decomposition has not been thoroughly explained, although change in unsaturation as a result of loss of hydrogen sulphide and the effect of heat on vulcanized rubber has been commented upon by Winkelmann,[7] and by the other investigators previously mentioned.[8] A few determinations of unsaturation made on the rubber after heating in the present experiments have not given any additional insight into the mechanism of the chemical changes involved. This phase of the problem may be investigated further at some future time.

Since this manuscript was prepared, a paper on the pyrolysis products of ebonite by Midgley, Henne, and Shepard has been published.[9]

The author wishes to express his thanks to A. H. Scott for assistance with some of the measurements reported in this paper.

WASHINGTON, June 1, 1932.

[7] H. A. Winkelmann, Ind. Eng. Chem., vol. 18, p. 1163, 1926.
[8] See footnote 1, p. 164, and footnote 5, p. 171.
[9] T. Midgley, jr., A. L. Henne, and A. F. Shepard, J. Am. Chem. Soc., vol. 54, p. 2953, 1932.

SOME OF THE FACTORS WHICH AFFECT THE MEASUREMENT OF SOUND ABSORPTION

By V. L. Chrisler and Catherine E. Miller

ABSTRACT

It has been found that air has an appreciable absorption for sound at frequencies as low as 512 cycles per second. This absorption varies with the temperature, the moisture content, and the barometric pressure. Curves are given showing such changes in absorption in the reverberation room at the Bureau of Standards.

Attention is called to the fact that when a highly absorbent sample is placed in a very reverberant room the decay curve may not be logarithmic.

Measurements of sound absorption on the same samples made by different observers in different reverberation rooms have in the past shown variations difficult to explain. Some of the factors responsible for these variations are now beginning to be recognized and understood. Humidity, temperature, and even barometric pressure have been found to cause quite perceptible changes in sound absorption measurements. P. E. Sabine [1] first called attention to the fact that decreased humidity materially increased the absorption of an empty reverberation room for frequencies above 2,000 cycles. Later Knudsen [2] described some pioneer work on this effect and determined coefficients for the sound absorption of air containing varying amounts of water vapor. Additional experimental work shows that not only humidity, but also temperature and pressure cause changes in the sound absorption of air.

For the most part the effect of these factors (in rooms of 10,000 to 20,000 cubic feet) is perceptible only at the higher frequencies of 1,000 cycles or more, but under favorable conditions this effect can be measured at 512 cycles. In large rooms of 1,000,000 cubic feet or more this effect should be noticeable at all frequencies.

These hitherto unexplained changes were noticed by us over two years ago and records of temperature, humidity, and pressure have been kept for the last year in the hope that a correlation would become evident. Knudsen's paper gave the first suggestion as to how the data might be interpreted. He determined the reverberation time of two rooms which had the same lining material but different volumes. The temperature in these two rooms was maintained approximately constant, but the relative humidity varied.

[1] P. E. Sabine, The Measurement of Sound Absorption Coefficients, J. Franklin Inst., vol. 207, p. 347.
[2] V. O. Knudsen, The Effect of Humidity upon the Absorption of Sound in a Room, and a Determination of the Coefficients of Absorption of Sound in Air, J. Acoustical Soc. Am., July, 1931.

As a result of his investigation, Knudsen proposed that the customary formula for the reverberation time be written with a corrective term depending upon humidity, as follows:

$$T=\frac{0.05V}{-S\log_e(1-\alpha)+4mV} \tag{1}$$

where

T = reverberation time,
V = volume of room in cubic feet,
S = surface in square feet,
α = average coefficient of sound absorption, and
m is an attenuation constant, measuring the decay of the sound intensity with the distance traveled. The observed values of T, S, and V were substituted in equation (1) thus obtaining two equations from which α and m were calculated.

In this way Knudsen determined m for different relative humidities and at four different frequencies for temperatures between 21° and 22° C. It was found that α was a constant within the limits of experimental error, but that m varied with the humidity.

To fit Knudsen's results to the present work, the assumption was made that the effect of water vapor on sound absorption of air depended solely upon vapor pressure and was independent of temperature and barometric pressure. On this basis Knudsen's curves for m, given in terms of relative humidity, were replotted in terms of vapor pressure and the corresponding values of $4mV$ subtracted from the measured total absorption of our reverberation room. The residual absorption was then plotted against temperature. The scatter of these points suggested that Knudsen's values of m did not adequately represent the effect of water vapor in our experiments. In addition, Knudsen's figures did not cover the full range of our vapor pressures. His curves were, therefore, modified by successive trial and error until the curves for residual absorption showed a minimum scatter of points from a smooth curve, the average variation being less than 1 per cent of the initial measured absorption and the maximum variation being only a little over 2 per cent.

The resulting empirical curves for m at 2,048 and 4,096 cycles are shown in Figure 1 and the residual absorption-temperature curves in Figures 2 and 3.

The question of sound absorption of air has been considered theoretically by Rayleigh [3] and others, and the conclusion was reached that the sound absorption should be proportional to the square of the frequency. This relation appears to hold good in the empirical curves for m shown in Figure 1, as the value for m at 4,096 cycles is four times that at 2,048 cycles. An exception to this is found when the vapor pressure is about 0.15 inch of mercury or less. Here the ratio seems to be about 3.9.

In drawing the curves in Figures 2 and 3 the term $4mV$ was calculated from the curves in Figure 1 and subtracted from the measured total absorption. The remainder has hitherto been assumed to depend only on the absorption of the surface of the room, as indicated by its form $-S\log(1-\alpha)$. But after correction has thus been made

[3] Rayleigh, Theory of Sound, vol. 2, pp. 315-316.

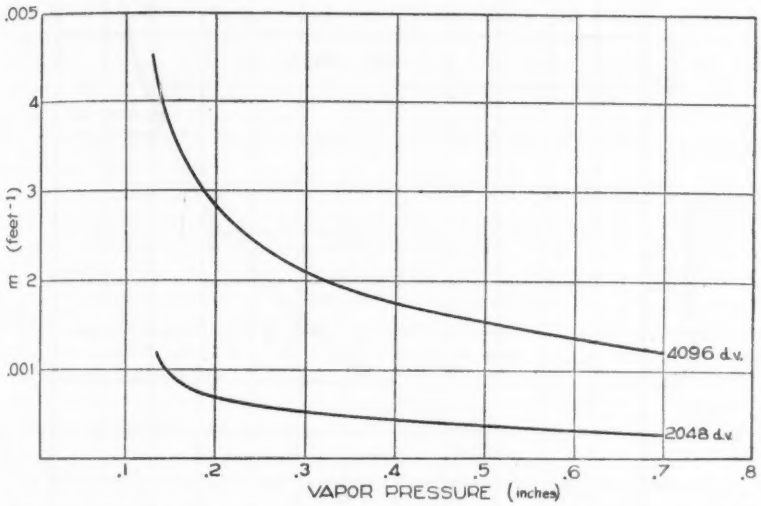

FIGURE 1.—*Values of m for air for different vapor pressures, at frequencies of 2,048 and 4,096 cycles*

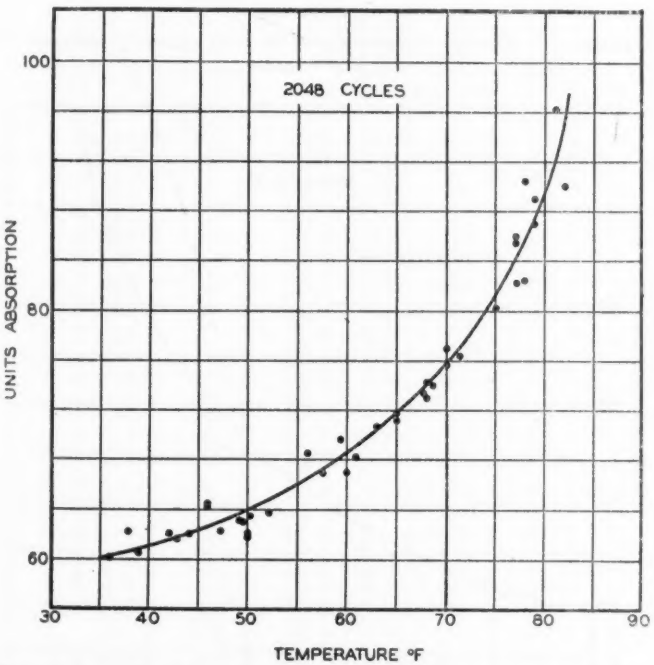

FIGURE 2.—*Change of absorption of air with change of temperature at 2,048 cycles*

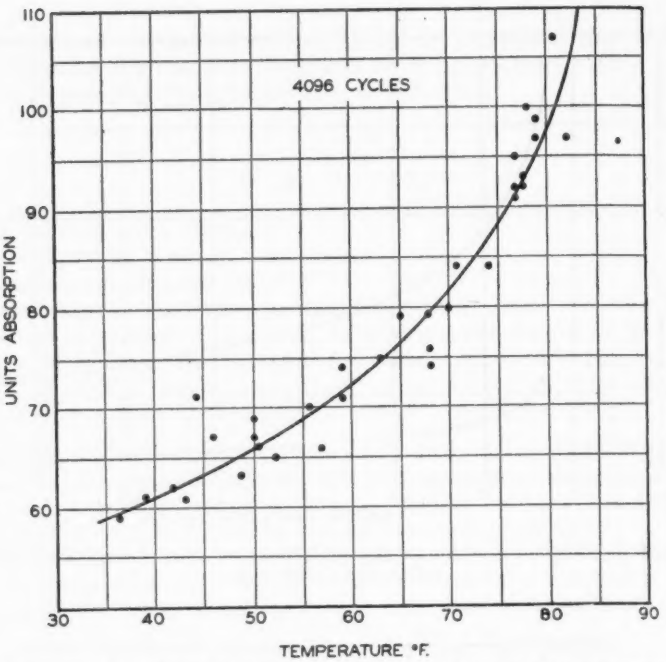

FIGURE 3.—*Change of absorption of air with change of temperature at 4,096 cycles*

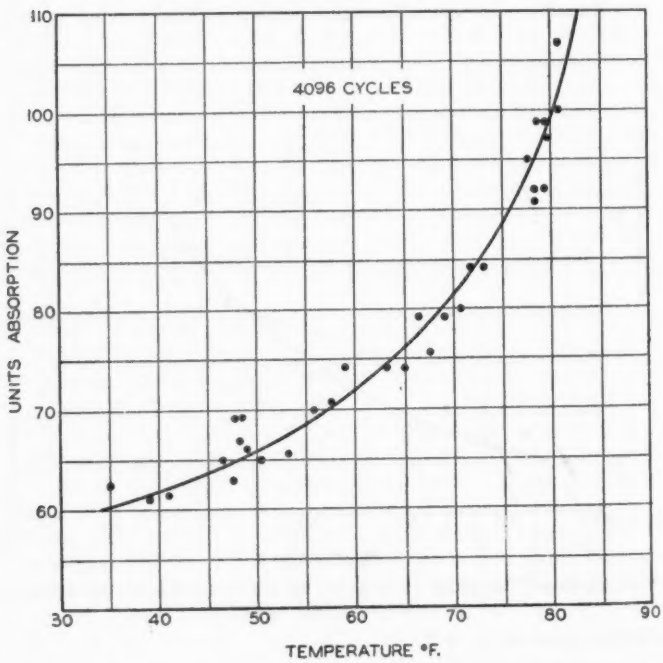

FIGURE 4.—*Curve of Figure 3 corrected for changes in barometric pressure*

for water vapor, the absorption shows a very large variation with temperature, much more than can reasonably be ascribed to any change in absorption of the wall surfaces. It appears, then, that an additional correction must be made for the absorption of air as a function of temperature if a constant absorption coefficient for the walls of the room is assumed. That this surface absorption is practically independent of temperature is indicated by all measurements on absorbing materials.

On examining these curves, drawn so as to represent as fairly as possible the mean of the experimental observations, it was noticed that, in general, those points which departed from the curve on one side corresponded to higher barometric pressures than those on the other side of the curve. No theoretical explanation has been found for this fact, but it is possible to deduce from these deviations an empirical correction. For instance, at 4,096 cycles it was found that a decrease of 0.1 inch in barometric pressure has an effect on the sound absorption equivalent to that of an increase in temperature of 0.8° F. Replotting the curve with this empirical correction the experimental points fit much more closely to a smooth curve. (Fig. 4.)

At 2,048 cycles it is found that the same change in barometric pressure is equivalent to a change in temperature only one-fourth that with 4,096 cycles. For lower frequencies this correction becomes practically unimportant.

TABLE 1.—*Corrections for water vapor at 2,048 cycles*

Total absorption	Vapor pressure	$m \times 10^6$	Correction for water vapor	Total absorption minus correction	Temperature
	Inches Hg				° *F*
102.1	0.54	365	21.7	80.4	75
101.7	.69	303	18.0	83.7	77
108.6	.68	307	18.2	90.4	78
105.2	.62	331	19.6	85.6	77
107.6	.67	312	18.5	89.1	79
113.4	.68	307	18.2	95.2	81
107.5	.72	295	17.5	90.0	82
101.8	.62	331	19.6	82.2	77
95.0	.52	375	22.2	72.8	68
99.4	.47	400	23.7	75.7	70
100.2	.46	403	23.9	76.3	71
104.4	.71	295	17.5	86.9	79
105.0	.65	320	19.0	86.0	78
104.7	.66	315	18.7	86.0	77
102.4	.65	320	19.0	83.4	78
96.3	.52	375	22.2	74.1	68
102.0	.62	331	19.6	82.4	74
97.9	.56	356	21.1	76.8	70
98.7	.44	415	24.6	74.1	68
101.3	.46	403	23.9	77.4	65
97.1	.36	467	27.7	69.4	59
96.6	.40	440	26.1	70.5	63
97.5	.32	504	29.9	68.6	56
96.2	.39	447	26.6	69.6	59
94.4	.314	510	30.6	63.8	52
94.0	.298	540	32.1	61.9	50
94.9	.278	552	32.8	62.1	50
98.3	.251	593	35.3	63.0	49
102.6	.200	690	41.0	61.6	43
102.9	.228	630	37.4	65.5	44.5
103.2	.213	660	39.2	64.0	45
96.6	.273	560	33.3	63.3	50.5
102.2	.223	640	38.0	64.2	46
106.3	.173	705	41.9	62.2	44
102.5	.204	680	40.4	62.1	42
129.5	.134	1,160	68.9	60.6	39
113.6	.153	905	53.8	59.8	36.3
114.6	.159	880	52.3	62.3	37.5

TABLE 2.—*Corrections for water vapor at 4,096 cycles*

Total absorption	Vapor pressure	$m \times 10^5$	Correction for water vapor	Total absorption minus correction	Observed temperature	Corrected temperature
	Inches Hg				° *F.*	° *F.*
163	0.69	121	72	91	77	78.3
173	.68	122	73	100	78	81
173	.62	132	78	95	77	77.5
173	.67	124	74	99	79	79.6
179	.69	121	72	107	81	80.7
167	.71	118	70	97	82	79.8
170	.62	132	78	92	77	78.4
168	.52	150	89	79	68	68.7
176	.47	161	96	80	70	70.8
180	.46	162	96	84	71	71.8
168	.71	118	70	98	79	79
167	.65	127	75	92	78	78.9
165	.66	125	74	91	77	
168	.65	127	75	93	78	
165	.52	150	89	76	68	67.
162	.62	132	78	84	74	73.1
168	.56	143	85	83	70	68.4
172	.45	165	98	74	68	65.4
174	.46	162	96	78	65	66.4
182	.36	186	111	71	59	57.7
179	.40	176	105	74	63	63
189	.32	200	119	70	56	56.2
180	.39	178	106	74	59	58.7
185	.314	202	120	65	52	50.4
172	.387	179	106	66	56.8	53.3
195	.289	216	128	67	50	49.1
201	.278	222	132	69	50	47.9
205	.251	239	142	63	49	48.1
228	.200	281	167	61	43	38.7
221	.228	256	152	69	44.5	48.1
225	.213	269	160	65	45	46.6
200	.273	226	134	66	50.5	53
222	.223	260	155	67	46	48.4
227	.204	273	165	62	42	40.9
313	.134	424	250	63	39	
269	.159	346	206	63	37.5	35.1

The original measurements at 2,048 and 4,096 cycles, and the corrections made for the moisture content of the air are shown in Tables 1 and 2. In Table 2 the corrected temperature in the last column is obtained from the observed temperature by applying the above-mentioned change of temperature empirically equivalent to the variation in barometric pressure. This correction at 2,048 cycles is quite small and has been neglected in Table 1.

Figure 5 shows the relation between m and vapor pressure for 1,024 and 512 cycles and Figures 6 and 7 show the corresponding absorption-temperature curves. These curves were calculated from the curves for 2,048 and 4,096 cycles by Rayleigh's law and fitted the data so well that no further empirical adjustment was made

One of the most striking illustrations of the use of these curves occurred on a day of cold, windy weather in Washington in March, 1932. It has been our custom to measure the absorption of the empty room either immediately before or immediately after the measurements on the sample of the material. On this particular day the measurements were made on the sample first. As soon as the sample was removed from the room, measurements were made of the

absorption of the empty room at 2,048 and 4,096 cycles. Much to our surprise it was found that at 4,096 cycles the empty room had more absorption than when it contained the sample.

By referring to the wet and dry bulb thermometer measurements made before and after the sample was removed it was found that there had been a considerable change in the humidity and a very small change in temperature, caused by the high wind changing the air in the room while the door was opened for removing the sample. When corrections taken from the curves of Figures 1, 2, and 3 were made for the changes in humidity and temperature, the sample was found to have a reasonable degree of absorption. On a later day when conditions (in respect to humidity and temperature) were approximately the same inside and outside the reverberation room, measurements were repeated on this same sample, and the coefficients

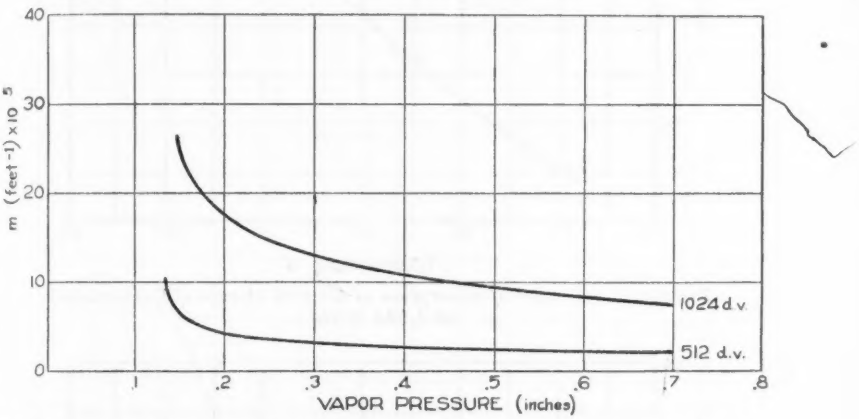

FIGURE 5.—*Values of m for different conditions of vapor pressure, for frequencies of 512 and 1,024 cycles*

of absorption which were obtained were found to agree almost exactly with those previously found.

The fact that air may have considerable absorption for sound is of interest in other fields. For instance, the distance that sound signals can be heard is of vital importance to shipping. Until quite recently it was thought that wind direction and velocity, layers of air of different densities which might cause reflection and refraction, and noise due to a storm were the principal factors which affected the distance at which a sound signal could be heard. More recent work shows that both temperature and humidity are important factors. Horner [4] gives some of the results of a study in which it was found that the distance at which a sound signal might be heard depends upon the humidity and the temperature of the air. He states that when the humidity is high, distant sounds can be heard with abnormal loudness, while under very low humidity these same sounds may become completely inaudible. He also stated "the worst acoustical conditions were almost invariably found in the type of weather commonly known as oppressive." Here the temperatures were high and evidently the increased absorption due to the high temperature was the predominating factor.

[4] Horner, Effect of Meteorological Condition on Sound Transmission at Sea, Nautical J., 1927.

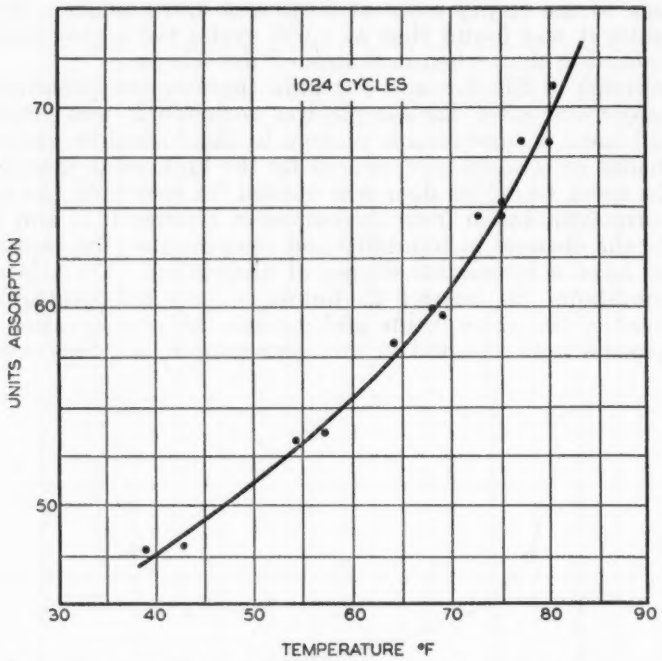

FIGURE 6.—*Change of absorption of air with change of temperature at 1,024 cycles*

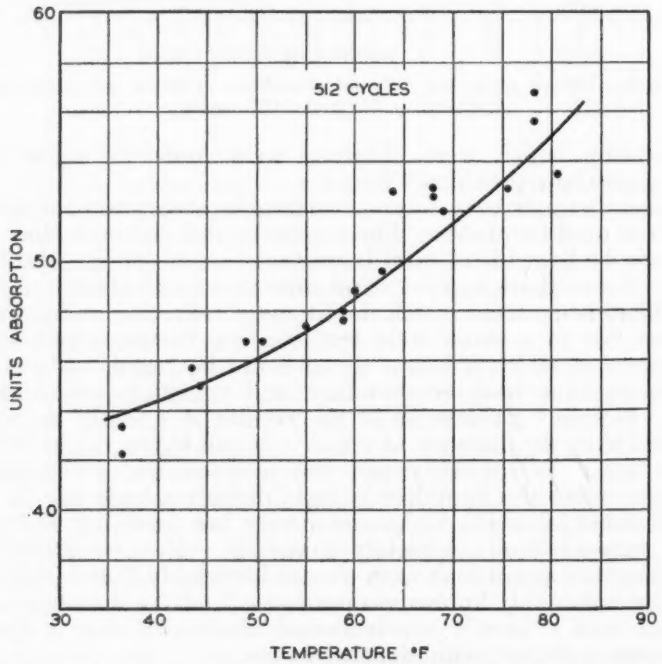

FIGURE 7.—*Change of absorption of air with change of temperature at 512 cycles*

Recent measurements made near Boston by the Lighthouse Service also show some interesting facts. A comparison was being made between a siren and an electric oscillator. In both cases the fundamental note was about 180 cycles per second. A considerable percentage of the energy of the siren was in overtones while the electric oscillator gave practically a pure note. When the observer was close the siren sounded the louder, but at a distance of 2 or 3 miles the oscillator was the louder, showing that the air has considerably less absorption for low-pitched notes.

In all sound-absorption measurements the assumption has heretofore been made that the decay of sound energy in a reverberation

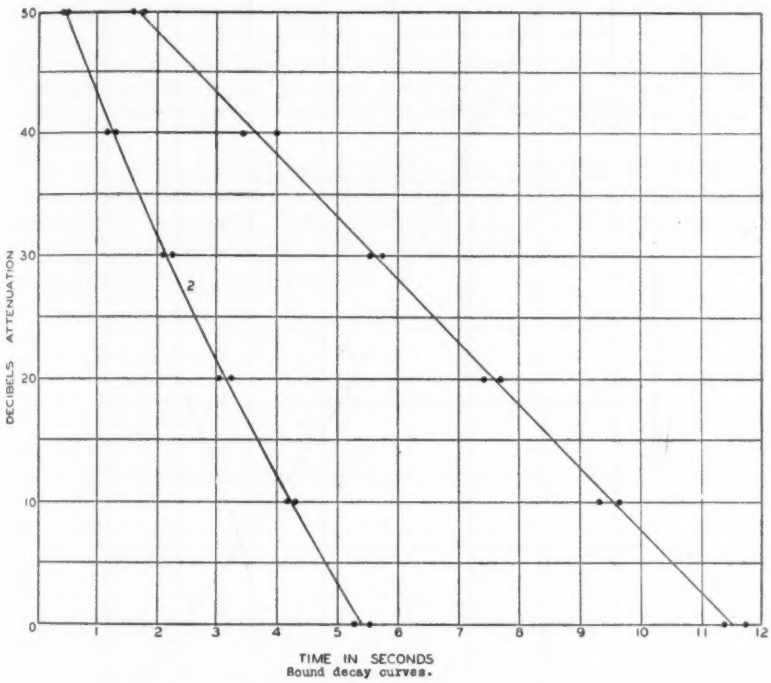

FIGURE 8.—*Sound-decay curves*

1, empty room.
2, highly absorbent sample in room.

room is logarithmic. With improved methods of measurement now available it is possible to determine the form of the decay curve with considerable accuracy. Figure 8 shows the decay curve at 1,024 cycles plotted logarithmically, for an empty reverberation room and for the same room containing a highly absorbent sample of material. With the sample in the room it will be noticed that the rate of decay is not uniform.

In the case of curve 2 of Figure 8, while the rate of decay is variable it shows no sudden change. In another case, illustrated in Figure 9, the distribution of the observed points is fitted more closely by a broken line than by a smooth curve.

Since the slope of the decay curve is dependent in part upon the absorption of the sample, it might be supposed from the form of

curve 2 (fig. 8) and of the curve in Figure 9 that the coefficient of absorption of the sample varied with the intensity of the sound; but by repeating the experiment of Figure 9, starting from an initial level of sound intensity some 20 or 30 db lower, it is found that the knee is not fixed in position, but suffers a corresponding shift downward. We must, therefore, conclude that the change in slope is not due to change in coefficient with the intensity of the sound, but is rather to be ascribed to nonuniform distribution of the sound energy. Considerations of conditions in the reverberation room indicate that

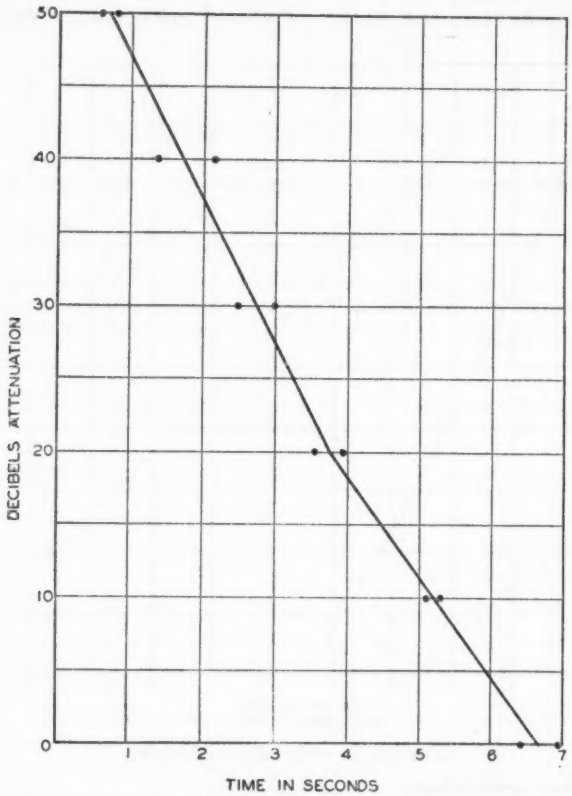

FIGURE 9.—*Sound-decay curve with a sample of highly absorbent material in the reverberation room*

this is the probable explanation. In the empty room the absorption coefficient of the walls, etc., is only about 1 per cent, and is approximately uniform over the whole interior, but when a sample of highly absorbent material is placed in the room the rate of absorption over the surface of this sample may be 60 or more times as great as over the wall surfaces. Moreover, this sample is usually of an area which is not negligible as compared to the boundaries of the room.

The source of sound is designed so as to give as nearly as possible a a uniform initial distribution of sound energy in the room, but after the source has been stopped the extreme heterogeneity of absorption present makes it probable that the distribution of sound energy does not remain uniform as it decays.

The question then arises as to how the absorption should be calculated, as in all reverberation methods a straight line decay has been assumed. If the reason advanced above for the change of slope is correct, the slope of the initial portion of the curve would give the better value for the absorption. With a curve of varying slope the ear method, necessarily involving the whole curve, is incapable of giving correct results, as it measures only the average slope of the whole curve.

SUMMARY

The total absorption of a room appears to depend upon the amount of water vapor present and upon the temperature. The calibration of the room is therefore not definite unless these factors are kept constant.

The coefficient of absorption of a sample of material will depend upon whether the initial, average, or final slope of the decay curve is used in the calculation. The ear method necessarily employs an average.

It may now be recognized that the determination of the sound-absorption coefficient of a material is not as simple a matter as has been hitherto supposed, but appears to depend upon a number of factors which are now beginning to be understood.

WASHINGTON, May 20, 1932.

THE RECIPROCAL SPHERICAL ABERRATION OF AN OPTICAL SYSTEM INCLUDING HIGHER ORDERS

By Harold F. Bennett

ABSTRACT

The aberration present when an axial point is imaged by a centered system of spherical optical surfaces may be expressed by any one of a number of power series. In this paper the reciprocal of the distance between the intersection of a ray with the axis and a fixed point on the axis is expressed as a series in h, where h is the perpendicular distance from the ray to the fixed point.

Formulas are derived by which the constant coefficients of the series expressing the aberration in the image space of a single spherical surface may be computed if the corresponding coefficients for the object space are known, the fixed point of reference being the center of curvature of the surface. These formulas can not be used in the case of a plane surface since there is no center of curvature. Accordingly, after developing transfer formulas by which the aberration may be referred to a new point of reference, a second set of formulas is derived in which the point of reference is taken as the vertex of the surface. A final set of formulas expresses the longitudinal in terms of the reciprocal aberration.

As a numerical example, the computation of the aberration of the third, fifth, and seventh orders of an ordinary photographic "landscape" lens is given in full. Its results compare favorably with those of a trigonometric tracing of rays in which seven place tables were used.

In conclusion the convergence of these series is briefly discussed and some relations to diffraction theory are pointed out.

CONTENTS

	Page
I. Introduction	188
1. Spherical aberration	188
2. Series expressions of longitudinal spherical aberration	189
3. Methods of evaluating the constants	190
4. Reciprocal spherical aberration	191
5. Historical sketch and bibliography	191
6. Notation and sign convention	192
II. The reciprocal aberration of a single spherical surface referred to the center of curvature	193
1. Preliminary statement of problem	193
2. Derivation of the formulas	195
3. Discussion	201
(*a*) Inherent and propagated aberration	201
(*b*) Notes on numerical applications	201
(*c*) Roots, anomalous points, and specific examples	202
III. Transfer formulas	205
1. Derivation	205
2. Notes on generality	208
3. Transfer formulas involving powers of n	209
IV. The reciprocal aberration of a single surface referred to the vertex	210
1. Derivation of the formulas	210
2. Discussion	213
V. Inversion to longitudinal spherical	215

		Page
VI.	Numerical example	217
	1. Details of construction of the lens	217
	2. First surface; infinite object distance	217
	3. Transfer from center of curvature to center of curvature; first surface to second	218
	4. Second surface and transfer to third; center of curvature to vertex	218
	5. Third surface and inversion to longitudinal aberration	220
	6. Comparison with ray tracing	221
VII.	Discussion	223
	1. Convergence of aberration series	223
	2. Relation to path difference equations	225
	3. Conclusion	225

I. INTRODUCTION

1. SPHERICAL ABERRATION

Rays of monochromatic light proceeding from a luminous point and passing through a lens are generally focussed not in a single image

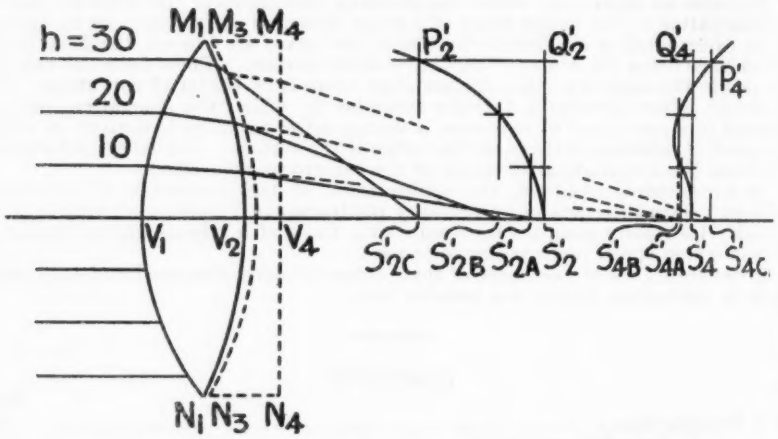

FIGURE 1.—*Spherical aberration of a single lens and of a doublet*

The paths of three rays when the concave lens is not present are shown in full lines. The concave lens and the paths of the rays if both lenses are present are shown in dotted lines. All parts of this figure are drawn in proportion to values obtained by an actual calculation. ($n_{1,3}=1.54$; $n_{2,4}=1.63$.)

point, but at varying distances from the lens according to the zone of the lens traversed. In the case of an object point on the axis of a centered system of spherical surfaces (the plane being considered a sphere of infinite radius) this defect in imagery is called "spherical aberration." Points off the axis are affected by the same aberration, but they are also affected by other aberrations, the presence of which makes analysis more difficult. The term "spherical aberration" is sometimes used more broadly to include these extra-axial aberrations and sometimes rather loosely in referring to the axial aberration where nonspherical surfaces are involved. In the present paper "spherical aberration" in the stricter sense of the word is discussed and a method is given for computing and expressing it quantitatively.

As an example of spherical aberration consider the portion of Figure 1 drawn in full lines. Light from an infinitely distant object point is

incident upon the lens M_1N_1, and the three rays shown are refracted at the two surfaces so as to intersect the axis at S'_{2A}, S'_{2B}, and S'_{2C}, which are the foci for these respective zones. If perpendiculars to the axis are drawn at these points, their intersections with lines parallel to the axis through the points of incidence on the first surface form the locus of the curve $S'_2P'_2$ which may be considered as representing both in direction and magnitude the spherical aberration in the image. For example, the distance $Q'_2P'_2$ is the measure of the longitudinal spherical aberration of the ray at $h_1=30$. The dotted lines illustrate the method of correcting the spherical aberration by the insertion of a negative component, M_3. N_4, of suitable design.

2. SERIES EXPRESSIONS OF LONGITUDINAL SPHERICAL ABERRATION

The aberration of a lens may be expressed quantitatively by giving the location of one or more points on the curve or by an equation for the curve. Such an equation is customarily written as an infinite series in which the terms beyond a certain order are neglected; thus the aberration represented by the curve $S'_4P'_4$ (fig. 1) may be expressed as follows:

$$\text{Long. spher.} = S' - s' = A'h^2 + B'h^4 + C'h^6 + \quad . \quad . \quad . \qquad (1)$$

where $S'-s'$ represents the abscissa and h the ordinate, and where s', A', B', C', . . . , are constants. The odd powers of h are absent because of axial symmetry.

The number of terms of the series which it is necessary to retain depends upon the conditions of the problem in hand. The straight line, $S'_4Q'_4$, given by the equation $S'=s'$ is a first approximation which is exact only for infinitesimal apertures. A value of the constant A' may then be found such that the parabola $S'=s'+A'h^2$ gives a sufficiently close approximation to the curve up to some aperture depending upon the accuracy required. Each of the terms of higher order has the property of remaining quite small for small apertures and then beginning to increase rapidly at some finite value of h. Accordingly, if the accuracy is not to diminish as larger and larger apertures are considered, the fifth order [1] term and then the seventh order [1] term must be taken into account, and so on.

In the present example A' is negative while B' and C' are positive, causing the upper portion of the curve to turn in the positive direction.

The same aberration, it is evident, could quite as legitimately be represented by one of a number of other curves and its corresponding

[1] The longitudinal spherical aberration which varies as the ith power of the aperture ($i=2, 4, 6$ . . .) corresponds to an angular aberration (see equation (3), p. 194) which varies as the $(i+1)$th power of the aperture and also to a path difference which varies as the $(i+2)$th power of the aperture. The corresponding reciprocal spherical aberration (see Sec. I, 4) varies also as the ith power of the aperture, but the lateral aberration varies as the $(i+1)$th power. These differences of order of the expressions which refer in different manners to the same aberration give rise to a difficulty in nomenclature. To avoid this the use of the terms primary, secondary, tertiary, etc., has been proposed. These designations not only become somewhat awkward for the higher-order aberrations treated in this paper, but some confusion might occur because primary and secondary already have special meanings in connection with astigmatism and curvature of field.

In the original papers of L. Seidel the aberrations are measured by their lateral value so that the terms for spherical aberration assume the orders 3, 5, 7, etc. In view of this and the general acceptance of Seidel's work it has been considered as desirable to designate a particular term of spherical aberration by the order which the corresponding lateral geometric aberration assumes. The expression "the third order longitudinal (or reciprocal) aberration" may then be interpreted as referring to "the longitudinal (or reciprocal) aberration which corresponds to the third order lateral aberration," and similarly for the terms of higher order.

It is to be noted that the constant coefficient $\beta^{(i+1)}$ of reciprocal aberration has the dimensions $L^{-(i+1)}$ and thus corresponds exactly to the above designation of order $(i+1)$.

equation, for instance by a curve the ordinates of which are equal to the heights of incidence on the last surface instead of the first. For any particular ray the total aberration would necessarily be the same according to either equation but, since the two values of h are not directly proportional, different portions of the total aberration would be attributed to the different orders. It can be shown that the various orders differ, even if only a single surface is considered, according as the ordinate is defined as the height of incidence upon the surface, as the height of intersection with a plane tangent at the vertex, as the distance from the vertex or from the center of curvature of the surface measured along a perpendicular to the ray, as the arc, tangent, or sine of the angle of inclination of the ray with the axis, or as one of a number of other functions of the aperture. Upon investigation it is found that the third order coefficient, A', is identical in each group in which (as for the first three cases mentioned) the ordinate reduces to the same infinitesimal for very small apertures. For large apertures, however, the third order for a particular ray differs in the several equations insofar as h^2 is slightly different. Thus it may be seen that, if the expressions "third order," "fifth order," etc., are to have exact significance, the exact definition of the aperture must be indicated. Moreover, direct comparisons between different lenses can be made only when the aberrations of both are expressed in exactly the same manner.

3. METHODS OF EVALUATING THE CONSTANTS

It has been pointed out that successively closer approximations to the aberration curve can be obtained by evaluating additional terms of the series (equation (1)). The usual methods of evaluating these coefficients are of three general types. First, if the lens has actually been constructed, a number of narrow beams of light may be singled out, as in the Hartmann test, by a diaphragm with several small holes, and their positions after traversing the lens may be determined photographically or otherwise. Second, from the specifications of the lens system the theoretical position of several rays may be found by trigonometric ray tracing. In either case an empirical curve or equation is fitted to the discrete points thus obtained. Third, trigonometric relations, such as those used in ray tracing, are expanded as Taylor's or similar series in ascending powers of whatever function of the aperture is chosen as the parameter. The aberration coefficients are thereby expressed as functions of the object distance and of the constants of the lens system. The present investigation is of this third type, which is usually called the algebraic or analytical method.

Ray tracing gives directly the total longitudinal aberration of one or more individual rays for any given lens. The algebraic method, however, is often more useful to the lens designer in that it reveals more fully the portion of the final aberration which is contributed by each surface of the lens and suggests in what manner the design should be altered. Moreover, very often when the design is altered only a small part of the computation need be repeated. The algebraic method has been considered objectionable because the third order equations are not sufficiently exact while if higher order terms are included the computation becomes too laborious. It is believed, however, that frequently the additional information is worth the labor

involved, and, accordingly, formulas are given for enough orders so that sufficient accuracy may be attained in practically all cases.

4. RECIPROCAL SPHERICAL ABERRATION

The frequent occurrence of reciprocal distances in optical equations has suggested that the spherical aberration formulas might be simplified in form if the aberration instead of being expressed as a difference between the focal lengths of different zones were expressed as a difference between the powers of the reciprocals of the focal lengths.

An idea of the relation of the reciprocal aberration to the longitudinal may be gained as follows: Take for a moment the back image distance $V_4S'_4 = s'_4$ (fig. 1) as the unit of length. Plot a curve with the same ordinates as $S'_4P'_4$, but with abscissas equal to the reciprocals of those of this curve when measured from the vertex, V_4, as the origin. Where the abscissa of the old curve is slightly less than one that of the new is slightly more than one. Thus it is easily seen that the new curve will be very similar to $S'_4P'_4$ but reversed with with respect to $S'_4Q'_4$. Since the aberration is measured by the departure from the vertical straight line, the reciprocal aberration in any case is opposite in sign to the longitudinal aberration. The statements regarding equations expressing aberration, which were made in the two preceding sections (2 and 3), apply directly to the new curve except that other symbols, to be introduced later (see equations (2) and (2′)) should replace the ones in equation (1). If a different unit of length is used the reciprocal aberration curve will merely be changed in scale in the horizontal direction. If, however, a different origin be selected, the curve will also be changed in shape.

5. HISTORICAL SKETCH AND BIBLIOGRAPHY

The theory of third-order aberrations is treated in the majority of books on geometrical optics. Among these Conrady [2] is unexcelled from a practical standpoint, while Von Rohr [3] gives a more elegant mathematical development and also includes an extensive bibliography.

Fifth-order terms for rays in the axial plane were published by Keller [4] and by Bauer.[5] Their expressions are not strictly accurate, however, in that h is not exactly defined. Kerber [6] derived the fifth order reciprocal aberration of a single surface defining h as the height of incidence. Schupmann [7] used a fifth order term which he credited to Kerber. Von Rohr [8] and König derived the fifth order term by Abbe's method of invariants with the angle of inclination of the ray as the variable. Risco [9] extended these equations to apply to aspherical surfaces. Smart [10] published terms of the fifth order, but unfortunately a number of his equations appear to be in error.

---

[2] A. E. Conrady, Applied Optics and Optical Design, pt. 1, 518 pp., Oxford Univ. Press, 1929.
[3] M. Von Rohr, editor, Die Bilderzeugung in optischen Instrumenten, J. Springer, Berlin, 1904. Also translation by R. Kanthack, His Majesty's Stationery Office, London, 1920.
[4] G. A. Keller, Zur Dioptrik, Entwicklung der Glieder fünfter Ordnung. 24 pp., C. R. Schurich, Munich, 1866.
[5] K. L. Bauer, Carl's Reportorium f. Phys. Tech., vol. 1, pp. 219-241, 1886.
[6] A. Kerber, Centr. Z. f. Opt. u. Mech., vol. 7, pp. 217-218, 1886.
[7] L. Schupmann, Die Medial-Fernrohre. B. G. Teubner, Leipzig, 1899.
[8] M. Von Rohr, pp. 238-244. See footnote 3.
[9] M. Martinez Risco, Estudios Generales sobre Aberración Esferica de Orden Superior, Anales Soc. Espanola Fis. y Quim vol. 25 pt. 1, pp. 100-136, 1927.
[10] E. H. Smart, Phil. Mag., vol. 20, pp. 82-91, 1910.

Early investigators, notably Petzval, may have been in possession of formulas of higher orders than the fifth,[11] but it is not known that any of these have been published. It is true, however, that investigations of aberrations from somewhat different standpoints have been extended to fifth and higher orders. Most of these are based upon the eikonal function, which depends upon the variation of path length through the lens.

6. NOTATION AND SIGN CONVENTION

A thoroughly consistent and complete system of notation for optical equations is, unfortunately, not available. In the present paper the aims have been to follow, in general, one of the systems already in use and to use as small a number of symbols as is compatible with clarity and brevity in presentation. In particular may be mentioned the use of the Greek characters β and ζ with superscripts ($\beta^{(3)}$, $\beta^{(5)}$, etc.) as constant coefficients of the various orders of reciprocal spherical aberration. (See equation (2) and footnote 1, p. 189.)

The original direction of the light is assumed to be from left to right. The refracting and reflecting surfaces are numbered in the order in which they are encountered by the light and are indicated by numerical subscripts. The well-known idea of regarding reflection as a special case of refraction in which the index ratio is -1 has been extended to include absolute indices (and indices relative to air), the index of any medium being considered as negative in sign if the light travels through it in a negative direction.[12] Nevertheless, any other self-consistent sign convention may be used if preferred.

A list of the characters with their meanings is given herewith. Unprimed letters denote magnitudes in the object space, primed letters the corresponding magnitude in the image space. If the two are identical, as in the case of r or ϕ, the character is always written unprimed. In the following summary the primed character is omitted in most cases, it being assumed that its meaning is easily deduced from the definition of the corresponding unprimed character.

ENGLISH LETTERS

$A, B, C, \ldots$ = the third order, fifth order, seventh order, ..., coefficients of longitudinal spherical aberration, positive if the aberration tends to make the rim ray cross the axis to the right of the paraxial focus.

c = a subscript meaning "referred to the center of curvature" of the appropriate surface.

d = the distance from the old point of reference to the new one to which the transfer is made, positive if to the right.

h = (in Introduction) linear aperture, subject to a variety of definitions.

---

[11] See, for instance, Trans. Opt. Soc. London, vol. 22, p. 214; 1920-21. Also Berek, Grundlagen der praktischen Optik, p. 43. Walter de Gruyter Co., Berlin, 1930.

[12] This convention is also applicable in path length equations as may be seen from the following simple example. Suppose a ray from some point A is reflected back to A from a mirror at B. The first distance, A to B or AB, being positive, the distance B to A or BA, after reflection must be negative. Adding the distances together would give zero for the path length. However, if the index be considered negative after an odd number of reflections and, as is universally done, the distance in each medium be multiplied by the index of refraction to get the equivalent path length in air the result is:

$$\begin{aligned}\text{Equiv. path length} &= n\mathrm{AB}+n'\mathrm{BA}\\ &= n\mathrm{AB}+(-n)(-\mathrm{AB})\\ &= 2n\mathrm{AB}\end{aligned}$$

which is obviously correct.

An alternative sign convention in which some of the angles are considered as obtuse after reflection has been proposed by T. Smith in Trans. Opt. Soc. London, vol. 27, pp. 312-316, 1925-26.

h=the distance from the point of reference or origin of coordinates to a ray, measured along a perpendicular to the ray and positive if upward.

i, j=generalized integers.

n=the index of refraction of a medium, usually taken relative to air, to be given a negative sign if the light traverses it from right to left.

r=the radius of curvature of a spherical surface, positive if the surface is concave to the right.

s=the distance from the vertex of a surface to the paraxial object point for that surface, positive if to the right.

$t=s-r$=the distance from the center of curvature of a surface to the paraxial object point for that surface, positive if to the right.

S=the distance from the vertex of a surface to the intersection of a ray in the object pencil with the axis; reduces to s as the aperture approaches zero.

$T=S-r$=the distance from the center of curvature of a surface to the intersection of a ray in the object pencil with the axis; reduces to t as the aperture approaches zero.

v=a subscript meaning "referred to the vertex" of the appropriate surface.

GREEK LETTERS

α=the acute angle between a ray and the axis, positive if the ray lies above the axis to the left of the point of intersection.

$\beta^{(i)}$=the coefficient of reciprocal spherical aberration of the ith order, in the series referred to the center of curvature, usually of the sign opposite that of the corresponding longitudinal aberration coefficient.

$\zeta^{(i)}$=the coefficient of reciprocal spherical aberration of the ith order in the series referred to the vertex of the lens surface, usually of the sign opposite that of the corresponding longitudinal aberration coefficient.

Θ=the reciprocal of T (*q. v.*).

ϑ, ϑ'=the angle of incidence, the angle of emergence; that is, the acute angle between a ray and the normal to the surface at the point of incidence, positive if the ray lies above the normal to the right of the surface.

κ=the constant of transfer to a new point of reference.
=the ratio of the new paraxial reciprocal object (or image) distance to the old paraxial reciprocal image distance.

κ, κ' in Part IV take on the special meaning that the transfer is made from the vertex to the center of curvature of a single surface, κ applying to the object pencil and κ' to the image pencil.

μ=relative index=n/n'.

μ'=relative index=n'/n.

ρ, σ, τ=the reciprocals of r, s, and t.

Σ=the reciprocal of S.

ϕ=the central angle or the angle between the radius drawn to the point of incidence and the axis, positive if the radius lies above the axis to the left of the center of curvature.

Ψ=reciprocal object distance from any point of reference on the axis.

II. THE RECIPROCAL ABERRATION OF A SINGLE SPHERICAL SURFACE REFERRED TO THE CENTER OF CURVATURE

1. PRELIMINARY STATEMENT OF PROBLEM

A set of formulas will first be derived which express the reciprocal aberration coefficients of the refracted or image pencil of any spherical surface when the corresponding constants of the incident or object pencil for that surface are known, the point of reference being chosen at the center of curvature of the surface.

In Figure 2, VS represents the axis of symmetry of a lens system of which one surface, with vertex at V and center of curvature at C, is shown in cross section. In a symmetrical pencil of rays incident upon this surface, consider the ray QP, incident at the point P. Let this ray (extended if necessary) intersect the axis at the point S, removed from the center of curvature by a distance T, positive if to the right. Let h_c denote the perpendicular distance from the center of curvature to the ray, positive if upward, and r the radius of curvature of the surface, positive if the surface is concave toward the right.

Let $\beta^{(3)}$, $\beta^{(5)}$, $\beta^{(7)}$, etc., be constants, such that if h_c is given, T is determined to as close an approximation as may be desired by retaining enough terms of the series:

$$\frac{1}{T}=\frac{1}{t}+\beta^{(3)}h_c^2+\beta^{(5)}h_c^4+\beta^{(7)}h_c^6+\ \ldots \tag{1}$$

Here t is the limiting value of T as h_c approaches zero; that is, the paraxial value of T, $\beta^{(3)}h_c^2$ is the third order term of reciprocal aberra-

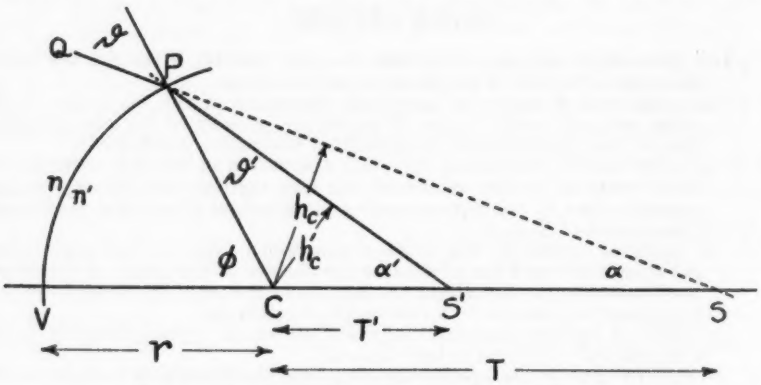

FIGURE 2.—*Refraction of a ray at a single surface*

tion, $\beta^{(5)}h_c^4$ is the fifth order, etc. For convenience in writing the equation, let $\frac{1}{T}=\Theta$ and $\frac{1}{t}=\tau$, then

$$\Theta=\tau+\beta^{(3)}h_c^2+\beta^{(5)}h_c^4+\beta^{(7)}h_c^6+\beta^{(9)}h_c^8+\ \ldots \tag{2}$$

The angles α, ϑ, and ϕ are shown in Figure 2. They are defined by the following equations, apparent from the geometry of the figure

$$\sin\alpha=\frac{h_c}{T}=\Theta h_c$$

$$=\tau h_c+\beta^{(3)}h_c^3+\beta^{(5)}h_c^5+\ \ldots \tag{3}$$

$$\sin\vartheta=\frac{h_c}{r}=\rho h_c \tag{4}$$

$$\phi=\alpha+\vartheta$$

where ρ is written for $\frac{1}{r}$.

Let the ray pass from a medium of index n into one of index n' and write for convenience $\frac{n'}{n}=\mu'$.[13] Denote the various functions of the refracted ray, PS', by priming those symbols which when unprimed represent the corresponding functions of the incident ray. Then:

$$\Theta'=\tau'+\beta'^{(3)}h'_c{}^2+\beta'^{(5)}h'_c{}^4+\ \ldots \tag{2'}$$

$$\sin\alpha'=\tau'h'_c+\beta'^{(3)}h'_c{}^3+\beta'^{(5)}h'_c{}^5+\ \ldots \tag{3'}$$

$$\sin\vartheta'=\rho h'_c \tag{4'}$$

and

$$\alpha'+\vartheta'=\phi=\alpha+\vartheta \tag{5}$$

2. DERIVATION OF THE FORMULAS

By Snell's law and equations (4) and (4')

$$\sin\vartheta=\rho h_c=\mu'\rho h'_c \tag{6}$$

From this $h_c=\mu'h'_c$; then substituting in equation (3):

$$\sin\alpha=\mu'\tau h'_c+\mu'^3\beta^{(3)}h'_c{}^3+\mu'^5\beta^{(5)}h'_c{}^5+\mu'^7\beta^{(7)}h'_c{}^7+\mu'^9\beta^{(9)}h'_c{}^9+\mu'^{11}\beta^{(11)}h'_c{}^{11} \tag{7}$$

The sines of α, ϑ, and ϑ' have now been expressed as functions of the same variable, h'_c. Of the possible methods of combining these to give $\sin\alpha'$, the unknown angle of equation (5), the following one using trigonometrical addition formulas and series expansions has been thought the most convenient:[14]

$$\cos\vartheta=1-\frac{1}{2}\sin^2\vartheta-\frac{1}{8}\sin^4\vartheta-\ \ldots$$

by equation (6)

$$=1-\frac{1}{2}\mu'^2\rho^2h'_c{}^2-\frac{1}{8}\mu'^4\rho^4h'_c{}^4-\frac{1}{16}\mu'^6\rho^6h'_c{}^6-\frac{5}{128}\mu'^8\rho^8h'_c{}^8-\frac{7}{256}\mu'^{10}\rho^{10}h'_c{}^{10}$$

$$\cos\vartheta'=1-\frac{1}{2}\rho^2h'_c{}^2-\frac{1}{8}\rho^4h'_c{}^4-\frac{1}{16}\rho^6h'_c{}^6-\ \ldots$$

$$\sin(\vartheta-\vartheta')=\sin\vartheta\cos\vartheta'-\cos\vartheta\sin\vartheta'$$

$$=(\mu'-1)\rho h'_c-\frac{1}{2}(\mu'-\mu'^2)\rho^3h'_c{}^3-\frac{1}{8}(\mu'-\mu'^4)\rho^5h'_c{}^5-\frac{1}{16}(\mu'-\mu'^6)\rho^7h'_c{}^7-\frac{5}{128}(\mu'-\mu'^8)\rho^9h'_c{}^9-\frac{7}{256}(\mu'-\mu'^{10})\rho^{11}h'_c{}^{11}$$

[13] The sense of the index ratio and the direction of the ray are thus mutually defined. If the ray passes through the refracting surface from left to right, then the index n pertains to the medium on the left and vice versa. The sign convention for distances and angles is independent of the direction of propagation of light along the ray. The index is considered as negative if the light travels from right to left. (See footnote 12, p. 192.)

[14] It is to be remembered, of course, if one is interested only in the third order or the third and fifth orders, that the higher orders may be ignored entirely. Moreover, it will doubtless be found that the method of derivation of the formulas is more easily followed if only the first one or two terms of each equation are taken into consideration.

TABLE 1.—*Cos ϑ cos ϑ'*

1	$h'_c{}^2$	$h'_c{}^4$	$h'_c{}^6$	$h'_c{}^8$	$h'_c{}^{10}$
1	$-\frac{1}{2}\mu'^2\rho^2$	$-\frac{1}{8}\mu'^6\rho^4$	$-\frac{1}{16}\mu'^6\rho^6$	$-\frac{5}{128}\mu'^8\rho^8$	$-\frac{7}{256}\mu'^{10}\rho^{10}$
	$-\frac{1}{2}\rho^2$	$+\frac{1}{4}\mu'^2\rho^4$	$+\frac{1}{16}\mu'^4\rho^6$	$+\frac{1}{32}\mu'^6\rho^8$	$+\frac{5}{256}\mu'^8\rho^{10}$
		$-\frac{1}{8}\rho^4$	$+\frac{1}{16}\mu'^2\rho^6$	$+\frac{1}{64}\mu'^4\rho^8$	$+\frac{1}{128}\mu'^6\rho^{10}$
			$-\frac{1}{16}\rho^6$	$+\frac{1}{32}\mu'^2\rho^8$	$+\frac{1}{128}\mu'^4\rho^{10}$
				$-\frac{5}{128}\rho^8$	$+\frac{5}{256}\mu'^2\rho^{10}$
					$-\frac{7}{256}\rho^{10}$

$$\cos(\vartheta-\vartheta') = \cos\vartheta\cos\vartheta' + \sin\vartheta\sin\vartheta'$$
$$= \text{the expansion}^{15} \text{ in Table } 1 + \mu'\rho^2 h'_c{}^2$$
$$= 1 - \frac{1}{2}(\mu'-1)^2\rho^2 h'_c{}^2 - \frac{1}{8}(\mu'^2-1)^2\rho^4 h'_c{}^4$$
$$- \frac{1}{16}(\mu'^2-1)^2(\mu'^2+1)\rho^6 h'_c{}^6$$
$$- \frac{1}{128}(\mu'^2-1)^2(5\mu'^4+6\mu'^2+5)\rho^8 h'_c{}^8$$
$$- \frac{1}{256}(\mu'^2-1)^2(7\mu'^6+9\mu'^4+9\mu'^2+7)\rho^{10} h'_c{}^{10}$$
$$\cos\alpha = 1 - \frac{1}{2}\sin^2\alpha - \frac{1}{8}\sin^4\alpha - \quad . \quad . \quad .$$
$$= \text{the expansion}^{15} \text{ in Table } 2$$

TABLE 2.—*Expansion of cos α*

[The coefficient of each power of h'_c is the sum of all the quantities below it in the same column]

1	$h'_c{}^2$	$h'_c{}^4$	$h'_c{}^6$	$h'_c{}^8$	$h'_c{}^{10}$
1	$-\frac{1}{2}\mu'^2\tau'^2$	$-\mu'^4\tau'\beta'^{(1)}$	$-\mu'^6\tau'\beta'^{(1)} - \frac{1}{2}\mu'^4\beta'^{(1)2}$	$-\mu'^8\tau'\beta'^{(7)} - \mu'^4\beta'^{(3)}\beta'^{(1)}$	$-\mu'^{10}\tau'\beta'^{(9)} - \mu'^{10}\beta'^{(3)}\beta'^{(7)}$
					$-\frac{1}{2}\mu'^{10}\beta'^{(5)2}$
		$-\frac{1}{8}\mu'^4\tau'^4$	$-\frac{1}{2}\mu'^6\tau'^3\beta'^{(1)}$	$-\frac{1}{2}\mu'^8\tau'^3\beta'^{(5)} - \frac{3}{4}\mu'^8\tau'^2\beta'^{(1)2}$	$-\frac{1}{2}\mu'^{10}\tau'^3\beta'^{(7)} - \frac{3}{2}\mu'^{10}\tau'^2\beta'^{(3)}\beta'^{(1)} - \frac{1}{2}\mu'^{10}\tau'\beta'^{(3)2}$
			$-\frac{1}{16}\mu'^6\tau'^6$	$-\frac{3}{8}\mu'^8\tau'^4\beta'^{(3)}$	$-\frac{3}{8}\mu'^{10}\tau'^4\beta'^{(5)} - \frac{15}{16}\mu'^{10}\tau'^4\beta'^{(3)1}$
				$-\frac{5}{128}\mu'^8\tau'^8$	$-\frac{5}{16}\mu'^{10}\tau'^7\beta'^{(3)}$
					$-\frac{7}{256}\mu'^{10}\tau'^{10}$

$$\sin\alpha' = \sin[\alpha + (\vartheta-\vartheta')]$$
$$= \sin\alpha\cos(\vartheta-\vartheta') + \cos\alpha\sin(\vartheta-\vartheta')$$
$$= \text{the expansion}^{15} \text{ in Table } 3$$
$$= \tau' h'_c + \beta'^{(3)} h'_c{}^3 + \beta'^{(5)} h'_c{}^5 + \beta'^{(7)} h'_c{}^7 + \ldots \qquad (8)$$

the last term being obtained from equation (3′).

[15] This member of the equation has been written in tabular form for clearness and convenience. In Tables 1 and 2 the quantities in a single column are to be considered as inclosed in brackets and multiplied by the power of h at the top. In Tables 3 and 4 the quantity in each small rectangle in the body of the table is to be multiplied by the power of h at the top of the column and also by the β—coefficient at the left end of the row. The quantity represented by the whole table is the sum of all these products. The products may be grouped either by row or by column (in this case the latter is more convenient) and the common factors taken out.

TABLE 3.—*Expansion of sin [$\alpha + (\vartheta - \vartheta')$]*

TABLE 3.—*Expansion of* $\sin[\alpha+(\vartheta-\vartheta')]$

[Each quantity in the body of the table is to be multiplied both by the power of h'_a at the top and by the β-coefficient at the left]

	h'_a	$h'_a{}^3$	$h'_a{}^5$	$h'_a{}^7$	$h'_a{}^9$	$h'_a{}^{11}$
1	$\mu'\tau$	$-\frac{1}{2}\mu'(\mu'-1)^2\rho^2\tau$	$-\frac{1}{8}\mu'(\mu'^2-1)^2\rho^4\tau$	$-\frac{1}{16}\mu'(\mu'^2-1)^2\cdot(\mu'^2+1)\rho^6\tau$	$-\frac{1}{128}\mu'(\mu'^2-1)^2\cdot(5\mu'^4+6\mu'^2+5)\rho^8\tau$	$-\frac{1}{256}\mu'(\mu'-1)^2\cdot(7\mu'^6+9\mu'^4+9\mu'^2+7)\rho^{10}\tau$
	$+(\mu'-1)\rho$	$-\frac{1}{2}(\mu'-\mu'^2)\rho^3$	$-\frac{1}{8}(\mu'-\mu'^4)\rho^5$	$-\frac{1}{16}(\mu'-\mu'^6)\rho^7$	$-\frac{5}{128}(\mu'-\mu'^8)\rho^9$	$-\frac{7}{256}(\mu'-\mu'^{10})\rho^{11}$
		$-\frac{1}{2}(\mu'^2-\mu'^2)\rho\tau^2$	$+\frac{1}{4}(\mu'^2-\mu'^4)\rho^3\tau^2$	$+\frac{1}{16}(\mu'^2-\mu'^6)\rho^5\tau^2$	$+\frac{1}{32}(\mu'^2-\mu'^8)\rho^7\tau^2$	$+\frac{5}{256}(\mu'^2-\mu'^{10})\rho^9\tau^2$
			$-\frac{1}{8}(\mu'^3-\mu'^4)\rho\tau^4$	$+\frac{1}{16}(\mu'^3-\mu'^6)\rho^3\tau^4$	$+\frac{1}{64}(\mu'^3-\mu'^8))\rho^5\tau^4$	$+\frac{1}{128}(\mu'^3-\mu'^{10})\rho^7\tau^4$
				$-\frac{1}{16}(\mu'^7-\mu'^6)\rho\tau^6$	$+\frac{1}{32}(\mu'^7-\mu'^8)\rho^3\tau^6$	$+\frac{1}{128}(\mu'^7-\mu'^{10})\rho^5\tau^6$
					$-\frac{5}{128}(\mu'^9-\mu'^8)\rho\tau^8$	$+\frac{5}{256}(\mu'^9-\mu'^{10})\rho^3\tau^8$
						$-\frac{7}{256}(\mu'^{11}-\mu'^{10})\rho\tau^{10}$
$\beta^{(2)}$	$+\mu'^2$	$-\frac{1}{2}\mu'^2(\mu'-1)^2\rho^2$	$-\frac{1}{8}\mu'^2(\mu'^2-1)^2\rho^4$	$-\frac{1}{16}\mu'^2(\mu'^2-1)^2\cdot(\mu'^2+1)\rho^6$	$-\frac{1}{128}\mu'^2(\mu'^2-1)^2\cdot(5\mu'^4+6\mu'^2+5)\rho^8$
		$-(\mu'^2-\mu'^4)\rho\tau$	$+\frac{1}{2}(\mu'^2-\mu'^6)\rho^3\tau$	$+\frac{1}{8}(\mu'^2-\mu'^8)\rho^5\tau$	$+\frac{1}{16}(\mu'^2-\mu'^{10})\rho^7\tau$
			$-\frac{1}{2}(\mu'^7-\mu'^6)\rho\tau^3$	$+\frac{1}{4}(\mu'^7-\mu'^6)\rho^3\tau^3$	$+\frac{1}{16}(\mu'^7-\mu'^{10})\rho^5\tau^3$
				$-\frac{3}{8}(\mu'^9-\mu'^8)\rho\tau^5$	$+\frac{3}{16}(\mu'^9-\mu'^{10})\rho^3\tau^5$
					$-\frac{5}{16}(\mu'^{11}-\mu'^{10})\rho\tau^7$

TABLE 3.—*Expansion of sin* $[\alpha+(\vartheta-\vartheta')]$—Continued

	h'_o	h'^3_o	h'^5_o	h'^7_o	h'^9_o	h'^{11}_o
$\beta^{(1)}$			$+\mu'^5$	$-\frac{1}{2}\mu'^3(\mu'-1)^2\rho^2$	$-\frac{1}{8}\mu'^3(\mu'^2-1)^2\rho^4$	$-\frac{1}{16}\mu'^3(\mu'^2-1)^2(\mu'^2+1)\rho^6$
				$-(\mu'^7-\mu'^5)\rho\tau$	$+\frac{1}{2}(\mu'^7-\mu'^5)\rho^3\tau$	$+\frac{1}{8}(\mu'^7-\mu'^{13})\rho^5\tau$
					$-\frac{1}{2}(\mu'^9-\mu'^5)\rho\tau^2$	$+\frac{1}{4}(\mu'^9-\mu'^{13})\rho^3\tau^2$
						$-\frac{3}{8}(\mu'^{11}-\mu'^{13})\rho\tau^3$
$\beta^{(3)}$				$-\frac{1}{2}(\mu'^7-\mu'^5)\rho$	$+\frac{1}{4}(\mu'^7-\mu'^5)$	$+\frac{1}{16}(\mu'^7-\mu'^{13})\rho^3$
					$-\frac{3}{4}(\mu'^9-\mu'^5)\rho\tau^2$	$+\frac{3}{8}(\mu'^9-\mu'^{13})\rho^3\tau^2$
						$-\frac{15}{16}(\mu'^{11}-\mu'^{13})\rho\tau^4$
$\beta^{(7)}$				$+\mu'^7$	$-\frac{1}{2}\mu'^7(\mu'-1)^2\rho^3$	$-\frac{1}{8}\mu'^7(\mu'^2-1)^2\rho^4$
					$-(\mu'^9-\mu'^5)\rho\tau$	$+\frac{1}{2}(\mu'^9-\mu'^{13})\rho^3\tau$
						$-\frac{1}{2}(\mu'^{11}-\mu'^{13})\rho\tau^2$
$\beta^{(5)}\beta^{(1)}$					$-(\mu'^9-\mu'^5)\rho$	$+\frac{1}{2}(\mu'^9-\mu'^{13})\rho^3$
						$-\frac{3}{2}(\mu'^{11}-\mu'^{13})\rho\tau^2$
$\beta^{(9)}$					$+\mu'^9$	$-\frac{1}{2}\mu'^9(\mu'-1)^2\rho^3$
						$-(\mu'^{11}-\mu'^{13})\rho\tau$
$\beta^{(5)}\beta^{(3)}$						$-\frac{1}{2}(\mu'^{11}-\mu'^{13})\rho\tau$
$\beta^{(9)}\beta^{(7)}$						$-(\mu'^{11}-\mu'^{13})\rho$
$\beta^{(5)2}$						$-\frac{1}{2}(\mu'^{11}-\mu'^{13})\rho$
$\beta^{(11)}$						$+\mu'^{11}$

Since, to the order of approximation attained, this is true for any value of h'_c, the coefficients of like powers of h'_c may be equated and are readily reduced to the following form:

$$\tau' = \mu'\tau + (\mu' - 1)\rho \tag{9a}$$

$$\beta'^{(3)} = \mu'^3\beta^{(3)} - \tfrac{1}{2}\mu'\rho[(\mu'-1)^2\rho\tau + (\rho^2 + \mu'^2\tau^2) - \mu'(\rho^2+\tau^2)] \tag{9b}$$

$$\begin{aligned}\beta'^{(5)} = {} & \mu'^5\beta^{(5)} - \tfrac{1}{2}\mu'^3\beta^{(3)}(\mu'-1)\rho[(\mu'-1)\rho + 2\mu'\tau] \\ & - \tfrac{1}{8}\mu'\rho[(\mu'^2-1)^2\rho^3\tau + (\rho^2 - \mu'^2\tau^2)^2 - \mu'^3(\rho^2-\tau^2)^2]\end{aligned} \tag{9c}$$

$$\begin{aligned}\beta'^{(7)} = {} & \mu'^7\beta^{(7)} - \tfrac{1}{2}\mu'^6\beta^{(3)2}(\mu'-1)\rho - \tfrac{1}{2}\mu'^5\beta^{(5)}(\mu'-1)\rho[(\mu'-1)\rho + 2\mu'\tau] \\ & - \tfrac{1}{2}\mu'^3\beta^{(3)}\rho[\tfrac{1}{4}(\mu'^2-1)^2\rho^3 - \mu'^2\tau(\rho^2 - \mu'^2\tau^2) + \mu'^3\tau(\rho^2-\tau^2)] \\ & - \tfrac{1}{16}\mu'\rho[(\mu'^2-1)^2(\mu'^2+1)\rho^5\tau + (\rho^2 - \mu'^2\tau^2)^2(\rho^2 + \mu'^2\tau^2) \\ & \quad - \mu'^5(\rho^2-\tau^2)^2(\rho^2+\tau^2)]\end{aligned} \tag{9d}$$

$$\begin{aligned}\beta'^{(9)} = {} & \mu'^9\beta^{(9)} - \mu'^8\beta^{(3)}\beta^{(5)}(\mu'-1)\rho - \tfrac{1}{2}\mu'^7\beta^{(7)}(\mu'-1)\rho[(\mu'-1)\rho + 2\mu'\tau] \\ & + \tfrac{1}{4}\mu'^7\beta^{(3)2}\rho[(\rho^2 - 3\mu'^2\tau^2) - \mu'(\rho^2 - 3\tau^2)] \\ & - \tfrac{1}{2}\mu'^5\beta^{(5)}\rho[\tfrac{1}{4}(\mu'^2-1)^2\rho^3 - \mu'^2\tau(\rho^2 - \mu'^2\tau^2) + \mu'^3\tau(\rho^2-\tau^2)] \\ & - \tfrac{1}{8}\mu'^3\beta^{(3)}\rho[\tfrac{1}{2}(\mu'^2-1)^2(\mu'^2+1)\rho^5 - \mu'^2\tau(\rho^2 - \mu'^2\tau^2)(\rho^2 + 3\mu'^2\tau^2) \\ & \quad + \mu'^5\tau(\rho^2-\tau^2)(\rho^2+3\tau^2)] \\ & - \tfrac{1}{128}\mu'\rho[(\mu'^2-1)^2(5\mu'^4 + 6\mu'^2 + 5)\rho^7\tau + (\rho^2 - \mu'^2\tau^2)^2 \cdot \\ & \quad \cdot(5\rho^4 + 6\mu'^2\rho^2\tau^2 + 5\mu'^4\tau^4) - \mu'^7(\rho^2-\tau^2)(5\rho^4 + 6\rho^2\tau^2 + 5\tau^4)]\end{aligned} \tag{9e}$$

$$\begin{aligned}\beta'^{(11)} = {} & \mu'^{11}\beta^{(11)} - \tfrac{1}{2}\mu'^{10}[\beta^{(5)2} + 2\beta^{(3)}\beta^{(7)} + \tau\beta^{(3)3}](\mu'-1)\rho \\ & - \tfrac{1}{2}\mu'^9\beta^{(9)}(\mu'-1)\rho[(\mu'-1)\rho + 2\mu'\tau] \\ & + \tfrac{1}{2}\mu'^9\beta^{(3)}\beta^{(5)}\rho[(\rho^2 - 3\mu'^2\tau^2) - \mu'(\rho^2 - 3\tau^2)] \\ & - \tfrac{1}{2}\mu'^7\beta^{(7)}\rho[\tfrac{1}{4}(\mu'^2-1)^2\rho^3 - \mu'^2\tau(\rho^2 - \mu'^2\tau^2) + \mu'^3\tau(\rho^2-\tau^2)] \\ & - \tfrac{1}{16}\mu'^7\beta^{(3)2}\rho[(\rho^4 + 6\mu'^2\rho^2\tau^2 - 15\mu'^4\tau^4) - \mu'^3(\rho^4 + 6\rho^2\tau^2 - 15\tau^4)] \\ & - \tfrac{1}{8}\mu'^5\beta^{(5)}\rho[\tfrac{1}{2}(\mu'^2-1)^2(\mu'^2+1)\rho^5 - \mu'^2\tau(\rho^2 - \mu'^2\tau^2)(\rho^2 + 3\mu'^2\tau^2) \\ & \quad + \mu'^5\tau(\rho^2-\tau^2)(\rho^2+3\tau^2)] \\ & - \tfrac{1}{16}\mu'^3\beta^{(3)}\rho[\tfrac{1}{8}(\mu'^2-1)(5\mu'^4 + 6\mu'^2 + 5)\rho^7 - \mu'^2\tau(\rho^2 - \mu'^2\tau^2) \cdot \\ & \quad \cdot(\rho^4 + 2\mu'^2\rho^2\tau^2 + 5\mu'^4\tau^4) + \mu'^7\tau(\rho^2-\tau^2)(\rho^4 + 2\rho^2\tau^2 + 5\tau^4)] \\ & - \tfrac{1}{256}\mu'\rho[(\mu'^2-1)^2(7\mu'^6 + 9\mu'^4 + 9\mu'^2 + 7)\rho^9\tau \\ & \quad + (\rho^2 - \mu'^2\tau^2)^2(7\rho^6 + 9\mu'^2\rho^4\tau^2 + 9\mu'^4\rho^2\tau^4 + 7\mu'^6\tau^6) \\ & \quad - \mu'^9(\rho^2-\tau^2)^2(7\rho^6 + 9\rho^4\tau^2 + 9\rho^2\tau^4 + 7\tau^6)]\end{aligned} \tag{9f}$$

If, instead, the quantities in Table 3 be factored the following equations (written only to the ninth order) result:

$$\tau' = \mu'(\tau + \rho) - \rho \text{ or } (\tau' + \rho) = \mu'(\tau + \rho) \tag{10a}$$

$$\beta'^{(3)} = \mu'^3\beta^{(3)} + \frac{1}{2}\mu'(\mu'-1)\ \rho\ (\rho+\tau)\ (\rho - \mu'\tau) \tag{10b}$$

$$\begin{aligned}\beta'^{(5)} = {} & \mu'^5\beta^{(5)} - \frac{1}{2}\mu'^3\beta^{(3)}(\mu'-1)\rho[(\mu'-1)\rho + 2\mu'\tau] + \frac{1}{8}\mu'(\mu'-1)\rho(\rho+\tau) \\ & (\rho - \mu'\tau)\ [(\mu'^2 + \mu' + 1)\ \rho^2 - \mu'(\mu-1)\ \rho\tau + \mu'^2\tau^2]\end{aligned} \tag{10c}$$

$$\begin{aligned}\beta'^{(7)} = {} & \mu'^7\beta^{(7)} - \frac{1}{2}\mu'^6\beta^{(3)2}(\mu'-1)\rho - \frac{1}{2}\mu'^5\beta^{(5)}(\mu'-1)\rho[(\mu'-1)\rho + 2\mu'\tau] \\ & - \frac{1}{8}\mu'^3\beta^{(3)}(\mu'-1)\rho[(\mu'+1)(\mu'^2\quad 1)\rho^3 + 4\mu'^2\tau(\rho^2 + \mu'\tau^2)] \\ & + \frac{1}{16}\mu'(\mu'-1)\ \rho(\rho+\tau)(\rho-\mu'\tau)[(\mu'^4 + \mu'^3 + \mu'^2 + \mu' + 1)\rho^4 \\ & - \mu'(\mu'^3 - 1)\rho^3\tau + \mu'^2(\mu'^2+1)\rho^2\tau^2 - \mu'^3(\mu'-1)\rho\tau^3 + \mu'^4\tau^4]\end{aligned} \tag{10d}$$

$$\beta'^{(9)}=\mu'^{9}\beta^{(9)}-\mu'^{8}\beta^{(3)}\beta^{(5)}(\mu'-1)\rho-\frac{1}{2}\mu'^{7}\beta^{(7)}(\mu'-1)\rho[(\mu'-1)\rho+2\mu'\tau]$$
$$-\frac{1}{4}\mu'^{7}\beta^{(3)2}(\mu'-1)\rho[\rho^2+3\mu'\tau^2]-\frac{1}{8}\mu'^{5}\beta^{(5)}(\mu'-1)\rho\cdot$$
$$\cdot[(\mu'+1)(\mu'^{2}-1)\rho^3+4\mu'^{2}\tau(\rho^2+\mu'\tau^2)]-\frac{1}{16}\mu'^{3}\beta^{(3)}(\mu'-1)\rho\cdot$$
$$\cdot[(\mu'+1)(\mu'^{4}-1)\rho^5+2\mu^2(\mu'^{2}+\mu'+1)\rho^2\tau+4\mu'^{4}\rho^2\tau^3+6\mu'^{5}\tau^5]$$
$$+\frac{1}{128}\mu'(\mu'-1)\rho(\rho+\tau)(\rho-\mu'\tau)[5(\mu'^{6}+\mu'^{5}+\mu'^{4}+\mu'^{3}+\mu'^{2}+\mu'+1)\rho^4$$
$$-\mu'(\mu'-1)(5\mu'^{4}+6\mu'^{3}+7\mu'^{2}+6\mu'+5)\rho^3\tau$$
$$+\mu'^{2}(5\mu'^{4}+\mu'^{3}+3\mu'^{2}+\mu'+5)\rho^2\tau^2-\mu'^{3}(\mu'-1)(5\mu'^{2}+4\mu'+5)\rho\tau^3$$
$$+\mu'^{4}(5\mu'^{2}-\mu'+5)\rho^2\tau^4-5\mu'^{5}(\mu'-1)\rho\tau^5+5\mu'^{6}\tau^6] \tag{10e}$$

If preferred, $(\tau'+\mu'\tau)$ may be substitued for $[(\mu'-1)\rho+2\mu'\tau]$ throughout these equations. In most numerical applications the computing of the higher powers of μ' may be avoided by dividing each equation by the appropriate power of n', remembering that $\mu'=\frac{n'}{n}$. Equations (9) then take the following form:

$$\frac{\tau'}{n'}=\frac{\tau}{n}+\left(\frac{1}{n}-\frac{1}{n'}\right)\rho \tag{11a}$$

$$\frac{\beta'^{(3)}}{n'^3}=\frac{\beta^{(3)}}{n^3}-\frac{1}{2}\rho\left[\left(\frac{1}{n}-\frac{1}{n'}\right)^2\frac{\tau}{n}\rho+\frac{1}{n}\left(\frac{\rho^2}{n'^2}+\frac{\tau^2}{n^2}\right)-\frac{1}{n'}\left(\frac{\rho^2}{n^2}+\frac{\tau^2}{n^2}\right)\right] \tag{11b}$$

$$\frac{\beta'^{(5)}}{n'^5}=\frac{\beta^{(5)}}{n^5}-\frac{1}{2}\frac{\beta^{(3)}}{n^3}\left(\frac{1}{n}-\frac{1}{n'}\right)\rho\left[\left(\frac{1}{n}-\frac{1}{n'}\right)\rho+2\frac{\tau}{n}\right]-\frac{1}{8}\rho\left[\left(\frac{1}{n^2}-\frac{1}{n'^2}\right)^2\frac{\tau}{n}\rho^3\right.$$
$$\left.+\frac{1}{n}\left(\frac{\rho^2}{n'^2}-\frac{\tau^2}{n^2}\right)^2-\frac{1}{n'}\left(\frac{\rho^2}{n^2}-\frac{\tau^2}{n^2}\right)^2\right] \tag{11c}$$

$$\frac{\beta'^{(7)}}{n'^7}=\frac{\beta^{(7)}}{n^7}-\frac{1}{2}\frac{\beta^{(3)2}}{n^6}\left(\frac{1}{n}-\frac{1}{n'}\right)\rho-\frac{1}{2}\frac{\beta^{(5)}}{n^5}\left(\frac{1}{n}-\frac{1}{n'}\right)\rho\left[\left(\frac{1}{n}-\frac{1}{n'}\right)\rho+2\frac{\tau}{n}\right]$$
$$-\frac{1}{2}\frac{\beta^{(3)}}{n^3}\rho\left[\frac{1}{4}\left(\frac{1}{n^2}-\frac{1}{n'^2}\right)^2\rho^3-\frac{1}{n}\frac{\tau}{n}\left(\frac{\rho^2}{n'^2}-\frac{\tau^2}{n^2}\right)+\frac{1}{n'}\frac{\tau}{n}\left(\frac{\rho^2}{n^2}-\frac{\tau^2}{n^2}\right)\right]$$
$$-\frac{1}{16}\rho\left[\left(\frac{1}{n^2}-\frac{1}{n'^2}\right)^2\left(\frac{1}{n^2}+\frac{1}{n'^2}\right)\frac{\tau}{n}\rho^5+\frac{1}{n}\left(\frac{\rho^2}{n'^2}-\frac{\tau^2}{n^2}\right)^2\left(\frac{\rho^2}{n'^2}+\frac{\tau^2}{n^2}\right)\right.$$
$$\left.-\frac{1}{n'}\left(\frac{\rho^2}{n^2}-\frac{\tau^2}{n^2}\right)^2\left(\frac{\rho^2}{n^2}+\frac{\tau^2}{n^2}\right)\right] \tag{11d}$$

If parallel light is incident upon a lens surface, $\tau=\beta^{(3)}=\beta^{(5)}=\ldots=0$. If also $n=1$ then equations (11) are greatly simplified, as follows:

$$\frac{\tau'}{n'}=\left(1-\frac{1}{n'}\right)\rho \tag{12a}$$

$$\frac{\beta'^{(3)}}{n'^3}=\frac{1}{2}\left(1-\frac{1}{n'}\right)\rho\frac{\rho^2}{n'} \tag{12b}$$

$$\frac{\beta'^{(5)}}{n'^5}=\frac{1}{8}\left(1-\frac{1}{n'^3}\right)\rho^3\frac{\rho^2}{n'} \tag{12c}$$

$$\frac{\beta'^{(7)}}{n'^7}=\frac{1}{16}\left(1-\frac{1}{n'^5}\right)\rho^5\frac{\rho^2}{n'} \tag{12d}$$

The higher-order equations in these last two sets may be written in a similar manner.

3. DISCUSSION

(a) INHERENT AND PROPAGATED ABERRATION

If the incident pencil is free from aberration, as is the case when it arises from a point on a material object, then $\beta^{(3)}=\beta^{(5)}=\ \ldots\ .=0$ and all terms in the aberration of the refracted pencil vanish except those in the upper row of Table 3; that is, all except the last term in each of the equations of (9), (10), or (11). This remaining term in each order will be referred to as the inherent aberration of that order, since it is independent of the aberration due to the other surfaces of the system and is entirely due to the surface in question. It is, of course, affected by a change of object distance.

If aberration is present in the incident pencil, then the terms of the image aberration which have a β coefficient do not, in general, vanish. These terms are to be considered as representing the aberration due to the preceding surfaces of the system after its propagation through the surface under consideration, and will be designated in the following manner:

The term in the fifth order equation ((9c), (10c), or (11c)) which contains the factor $\beta^{(3)}$ will be referred to as the third order term of the fifth order or the $\beta'^{(5)}$ ($\beta^{(3)}$) term. Similarly, the third order squared term of the seventh order denotes the $\beta'^{(7)}$ ($\beta^{(3)2}$) term, and the third-fifth order term of the ninth order denotes the $\beta'^{(9)}$ ($\beta^{(3)}\beta^{(5)}$) term, etc. These distinctions will apply directly to the system of equations to be developed later (Pt. III) except that the symbol ζ will replace β.

(b) NOTES ON NUMERICAL APPLICATIONS

There are a number of similarities among different terms of these equations which make the computation easier than would appear at first sight. The $\beta'^{(i)}(\beta^{(j)})$ term is identical with the $\beta'^{(i+2)}(\beta^{(j+2)})$ term, the $\beta'^{(i+4)}(\beta^{(j+4)})$ term, etc., except for factors in μ'^2. Moreover, the $\beta'^{(i)}(\beta^{(3)2})$, $\beta'^{(i+2)}(\beta^{(3)}\beta^{(5)})$, $\beta'^{(i+4)}(\beta^{(3)}\beta^{(7)})$, $\beta'^{(i+4)}(\beta^{(5)2})$, and the $\beta'^{(i+4)}(\beta^{(3)3})$ terms differ only by factors in μ'^2, $\frac{1}{2}$, and in one case τ. (i and j may be 3, 5, 7, or 9; $i\geqq j$.)

It is, of course, optional which form of the equations is to be used in computing. The third order of (10b) is doubtless simpler than that of (9b). However, if orders higher than the third are also to be computed, the equations (9) have their advantages, notably in the marked similarities among the following bracketed quantities:

$$[(\mu'-1)^2\rho\tau+(\rho^2+\mu'^2\tau^2)-\mu'(\rho^2+\tau^2)]$$

$$[(\mu'^2-1)^2\rho^3\tau+(\rho^2-\mu'^2\tau^2)^2-\mu'^3(\rho^2-\tau^2)^2]$$

$$\left[\frac{1}{4}(\mu'^2-1)^2\rho^3-\mu'^2\tau(\rho^2-\mu'^2\tau^2)+\mu'^3\tau(\rho^2-\tau^2)\right]$$

$$[(\mu'^2-1)^2(\mu'^2+1)\rho^5\tau+(\rho^2-\mu'^2\tau^2)^2(\rho^2+\mu'^2\tau^2)-\mu'^5(\rho^2-\tau^2)^2(\rho^2+\tau^2)]$$

Each of these quantities is the sum of three terms. Each term in the last bracket (seventh order) contains as factors the corresponding terms in the first two brackets, except for (μ'^2+1) instead of $(\mu'-1)^2$. Also the terms in the third bracket contain factors of the terms in the second bracket. All this reduces considerably the labor involved in

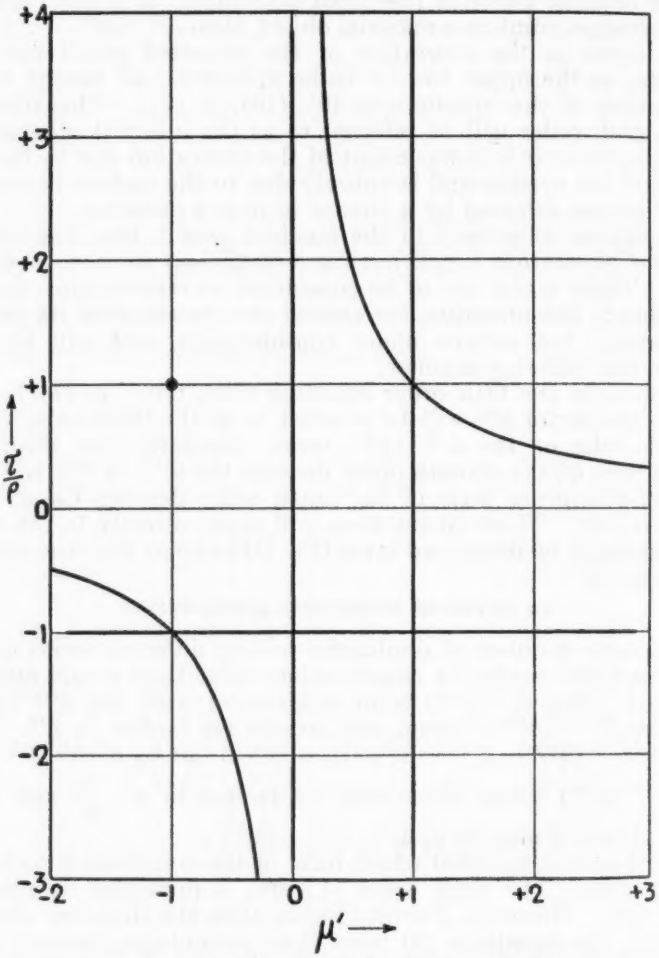

FIGURE 3.—*Zero reciprocal spherical aberration contour*

The point at $\mu'=-1$, $\frac{\tau}{\rho}=+1$ pertains only to orders higher than the third.

computing. Either of these sets may be written in the reduced form, as equations (11).

(c) ROOTS, ANOMALOUS POINTS, AND SPECIFIC EXAMPLES

It is interesting to note the conditions under which the aberration of a surface vanishes; that is, to find the root of the inherent terms

f the equations (9) or (10) when set equal to zero. In equations (10) he factors common to all orders may be written thus:

$$\rho^3\left[\mu'(\mu'-1)\left(1+\frac{\tau}{\rho}\right)\left(1-\mu'\frac{\tau}{\rho}\right)\right]=0$$

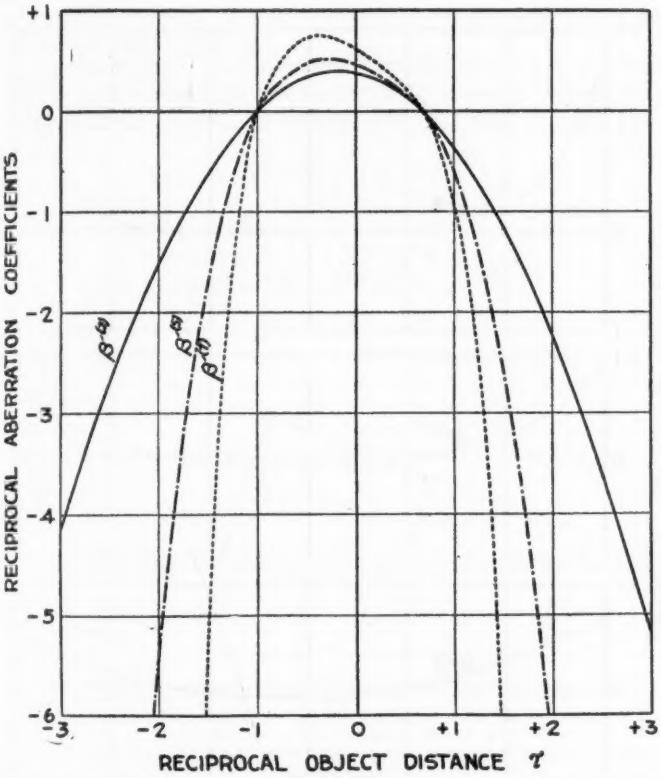

FIGURE 4.—*Reciprocal aberration coefficients for surface of unit radius, $\mu'=1.5$*

hen ρ has a finite value not zero the roots of this are as follows:

$\mu'=0$ Physically impossible.
$\mu'=1$ Same index on both sides; no refraction.
$\tau/\rho=-1$, $\tau=-\rho$ } Object and image coincide at the vertex.
$\mu'\frac{\tau}{\rho}=1$, $\tau=\rho/\mu'$ } The well-known aplanatic point.

hese roots are shown in Figure 3. If $\rho=0$, the surface is a plane nd there is no center of curvature from which to measure the dis- ances. If the object coincides with the center of curvature then

$\tau = \infty$ and the series is nonconvergent. (See Part VII, sec. 1.) Another set of formulas will be derived which may be used in these cases.

The orders higher than the third have the additional roots given by equating to zero the quantities in brackets in the inherent terms of equations (10). The only root yet found for these is the isolated point

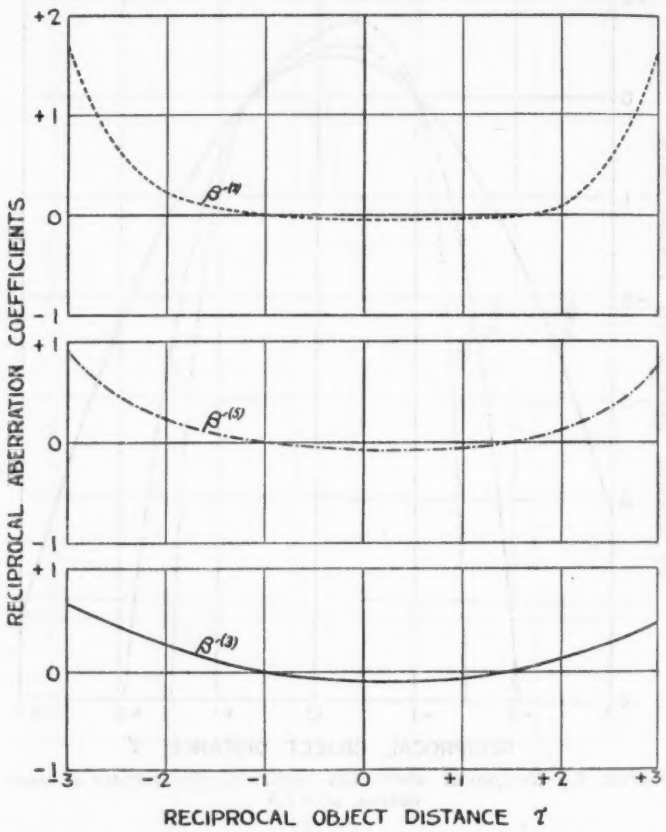

FIGURE 5.—*Reciprocal aberration coefficients for surface of unit radius, $\mu' = 1/1.5$*

$\left(\frac{\tau}{\rho} = +1,\ \mu' = -1\right)$ indicated in Figure 3. Since the value $\mu' = -1$ indicates a reflection, it may be noted that in the image formed by a spherical mirror the reciprocal aberration of all orders higher than the third vanishes when the object is at a distance $2r$ from the vertex.

The advisability of computing and tabulating the values of these coefficients for different values of μ' and τ is being considered. Figures 4 and 5 show, for the values $\mu' = 1.5$ and $\mu' = 1/1.5$, the form of the functions which would result. These values would have to be multiplied by the power of ρ corresponding to the order of the aberration to obtain the actual value of any particular coefficient.

III. TRANSFER FORMULAS

1. DERIVATION

The refracted or image pencil from one surface is, of course, identical with the incident or object pencil of the succeeding surface. However, when the point of reference is changed, the aberration coefficients are also altered. Formulas will now be developed for computing the new coefficients.

Let the subscripts i and j refer, respectively, to a surface whose aberration is known and to the succeeding surface, whose aberration is to be computed. Then, as before, see (2′) and (3′) for the known surface,

$$\Theta'_i = \tau'_i + \beta'_i{}^{(3)} h'^2_i + \beta'_i{}^{(5)} h'^4_i + \ldots$$
$$\sin \alpha'_i = \Theta'_i h'_i = \tau'_i h'_i + \beta'_i{}^{(3)} h'^3_i + \ldots . \tag{13}$$

and for the succeeding surface,

$$\Theta_j = \tau_j + \beta_j{}^{(3)} h_j^2 + \beta_j{}^{(5)} h_j^4 + \ldots \tag{14}$$
$$\sin \alpha_j = \Theta_j h_j = \tau_j h_j + \beta^{(3)}{}_j h^3{}_j + \ldots \tag{15}$$

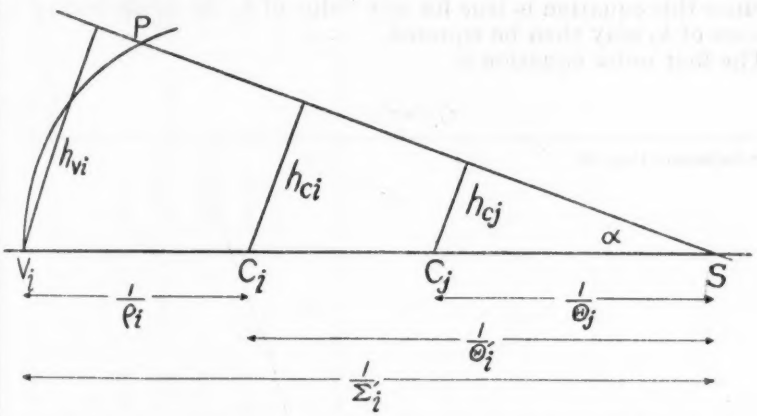

FIGURE 6.—*Diagram showing aperture, h, as measured from different points on the axis*

Let C_i and C_j (fig. 6) be the respective centers of curvature, and let the distance from C_i to C_j be d, positive if to the right. Then, for any ray, as PS, the adding of axial distances gives:

$$\frac{1}{\Theta'_i} = \frac{1}{\Theta_j} + d \tag{16}$$

Similarly, for a paraxial ray

$$\frac{1}{\tau'_i} = \frac{1}{\tau_j} + d, \text{ or } \frac{1}{\tau_j} = \frac{1}{\tau'_i} - d \tag{17}$$

then:

$$\frac{\tau_j}{\tau'_i} = 1 + d\tau_j = \frac{1}{1 - d\tau'_i} = \kappa \tag{18}$$

where κ is a new symbol introduced for convenience.

Manifestly

$$\sin \alpha'_i = \sin \alpha_j$$

or, by equations (13) and (15):

$$h'_i = \frac{1}{\Theta'_i}\Theta_j h_j$$

Then, substituting in turn from equations (16), (14), and (18):

$$\begin{aligned} h'_i &= (1+d\Theta_j)h_j \\ &= (1+d\tau_j)h_j + d\beta_j^{(3)}h^3_j + \ldots \\ &= \kappa h_j + d\beta_j^{(3)}h^3_j + d\beta_j^{(5)}h^5_j + \ldots \end{aligned}$$

This last expression for h'_i may be substituted in the right-hand member of equation (13), and then since the latter is equal to equation (15)

$$\begin{aligned} \sin \alpha_j &= \tau_j h_j + \beta_j^{(3)}h^3_j + \beta_j^{(5)}h^5_j + \ldots \\ &= \text{the series expanded [16] in Table 4.} \end{aligned}$$

Since this equation is true for any value of h_j the coefficients of like powers of h_j may then be equated.

The first order equation is

$$\tau_j = \kappa\tau'_i \qquad (18a)$$

[16] See footnote 15, p. 196.

TABLE 4.—*sin* α_j

TABLE 4.—$\sin \alpha_i$

[Each term in the body of the table is to be multiplied both by the power of h_i at the top of the column and by the β'_i—coefficient at the left]

	h_i	h_i^2	h_i^4	h_i^7	h_i^9	h_i^{11}
τ'_i	κ	$+d\beta_i$ (1)	$+d\beta_i$ (1)	$+d\beta_i$ (7)	$+d\beta_i$ (9)	$+d\beta_i$ (11)
β'_i (3)	$+\kappa^3$	$+3\kappa^2 d\beta_i$ (3)	$+3\kappa^2 d\beta_i$ (3)	$+3\kappa^2 d\beta_i$ (7) $+ 3cd^2\beta_i$ (3) β_i (7) $+ 3cd^2\beta_i$ (3) $^2\beta_i$ (3)	$+3\kappa^2 d\beta_i$ (9) $+ 6cd^2\beta_i$ (3) β_i (9) $+ 3cd^2\beta_i$ (3) $^2\beta_i$ (3)	$+3\kappa^2 d\beta_i$ (11) $+ 6cd^2\beta_i$ (3) β_i (11) $+ 3cd^2\beta_i$ (3) $^2\beta_i$ (3)
β'_i (5)		$+\kappa^5$	$+\kappa^5$	$+5\kappa^4 d\beta_i$ (5)	$+5\kappa^4 d\beta_i$ (9) $+ 10\kappa^3 d^2\beta_i$ (3) ^{2}	$+5\kappa^4 d\beta_i$ (11) $+ 20\kappa^3 d^2\beta_i$ (3) β_i (11) $+ 10\kappa^3 d^2\beta_i$ (3) ^{2}
β'_i (7)				$+\kappa^7$	$+7\kappa^6 d\beta_i$ (9)	$+7\kappa^6 d\beta_i$ (11) $+ 21\kappa^5 d^2\beta$ (3) ^{2}
β'_i (9)					$+\kappa^9$	$+9\kappa^8 d\beta$ (3)
β'_i (11)						$+\kappa^{11}$

The third order, after combining terms, is

$$(1-d\tau'_t)\beta_j^{(3)}=\kappa^3\beta'^{(3)}_t$$

or, substituting from equation (18)

$$\beta_j^{(3)}=\kappa^4\beta'^{(3)}_t \tag{18b}$$

The fifth order, likewise, is

$$(1-d\tau_t')\beta_j^{(5)}=3\kappa^2 d\beta_j^{(3)}\beta_t'^{(3)}+\kappa^5\beta'^{(5)}_t$$

Substituting for $(1-d\tau_t')$ and $\beta_j^{(3)}$ from equations (18) and (18*b*):

$$\beta_j^{(5)}=\kappa^6(\beta'^{(5)}_t+3\kappa d\beta'^{(3)2}_t) \tag{18c}$$

The higher orders may be reduced in a similar manner and the transfer formulas summarized as follows:

$$\kappa=\frac{1}{1-d\tau'_t} \tag{18}$$

$$\tau_j=\kappa\tau'_t \tag{18a}$$

$$\beta_j^{(3)}=\kappa^4\beta'^{(3)}_t \tag{18b}$$

$$\beta_j^{(5)}=\kappa^6(\beta'^{(5)}_t+3\kappa d\beta'^{(3)2}_t) \tag{18c}$$

$$\beta_j^{(7)}=\kappa^8(\beta'^{(7)}_t+8\kappa d\beta'^{(3)}_t\beta'^{(5)}+12\kappa^2 d^2\beta'^{(3)3}_t) \tag{18d}$$

$$\beta_j^{(9)}=\kappa^{10}(\beta'^{(9)}_t+10\kappa d\beta'^{(3)}_t\beta'^{(7)}+5\kappa d\beta'^{(5)2}_t+55\kappa^2 d^2\beta'^{(3)2}_t\beta'^{(5)}_t+55\kappa^3 d^3\beta'^{(3)4}_t) \tag{18e}$$

$$\beta_j^{(11)}=\kappa^{12}[\beta'^{(11)}_t+12\kappa d(\beta'^{(3)}_t\beta'^{(9)}_t+\beta'^{(5)}_t\beta'^{(7)}_t)+78\kappa^2 d^2(\beta'^{(3)2}_t\beta'^{(7)}_t+\beta'^{(3)}_t\beta'^{(5)2}_t)+364\kappa^3 d^3\beta'^{(3)3}_t\beta'^{(5)}_t+273\kappa^4 d^4\beta'^{(3)5}_t] \tag{18f}$$

2. NOTES ON GENERALITY

These transfer formulas are more general than has been indicated. By definition, the series

$$\Theta=\tau+\beta^{(3)}h_c^2+\beta^{(5)}h_c^4+\ \ldots$$

refers exclusively to the center of curvature of a lens surface. It is evident, however, that a similar series may be written referring to any point on the axis and that the transfer formulas will apply in transferring to any other point on the axis if Θ, τ, β, and h_c are replaced by the corresponding symbols from the new series. Moreover, these formulas apply as well to some of the series with different definitions of h mentioned in the introduction, the condition for their validity being

$$\Psi h=f(\alpha)$$

where Ψ corresponds to Θ above, but may refer to any point on the axis and $f(\alpha)$ is any function of α the use of which results in a convergent series throughout the required range of h for each case in question.

3. TRANSFER FORMULAS INVOLVING POWERS OF n

If the reduced form of the aberration equations (equations (11) or (12)) is used, then the transfer formulas must also be divided by the corresponding powers of n. They are then as follows:

$$\kappa = \frac{1}{1 - n_i' d \frac{\tau_i}{n_i}} \tag{19}$$

$$\frac{\tau_j}{n_j} = \kappa \frac{\tau_i'}{n_i'} \tag{19a}$$

$$\frac{\beta_j^{(3)}}{n_j^3} = \kappa^4 \frac{\beta_i'^{(3)}}{n_i'^3} \tag{19b}$$

$$\frac{\beta_j^{(5)}}{n_j^5} = \kappa^6 \left(\frac{\beta_i'^{(5)}}{n_i'^5} + 3\kappa n_i' d \frac{\beta_i'^{(3)2}}{n_i'^6} \right) \tag{19c}$$

$$\frac{\beta_j^{(7)}}{n_j^7} = \kappa^8 \left(\frac{\beta_i'^{(7)}}{n_i'^7} + 8\kappa n_i' d \frac{\beta'_i{}^{(3)} \beta'_i{}^{(5)}}{n_i'^8} + 12\kappa^2 n_i'^2 d^2 \frac{\beta_i'^{(3)3}}{n_i'^9} \right) \tag{19d}$$

Other reduced forms of aberration equations are to be given later. The various forms of the transfer formulas are collected here for convenience in reference.

Center of curvature to vertex:

$$n\kappa = \frac{1}{\frac{1}{n} - d \frac{\tau_i'}{n_i'}} \tag{20}$$

$$n_j \sigma_j = n (n\kappa) \frac{\tau_i'}{n_i'} \tag{20a}$$

$$n_j \zeta_j^{(3)} = (n\kappa)^4 \frac{\beta_i'^{(3)}}{n_i'^3} \tag{20b}$$

$$n_j \zeta_j^{(5)} = (n\kappa)^6 \left[\frac{\beta_i'^{(5)}}{n_i'^5} + 3 (n\kappa) d \frac{\beta_i'^{(3)2}}{n_i'^6} \right] \tag{20c}$$

$$n_j \zeta_j^{(7)} = (n\kappa)^8 \left[\frac{\beta_i'^{(7)}}{n_i'^7} + 8 (n\kappa) d \frac{\beta'_i{}^{(3)} \beta_i'^{(5)}}{n_i'^8} + 12 (n\kappa d)^2 \frac{\beta_i'^{(3)3}}{n_i'^9} \right] \tag{20d}$$

Vertex to center of curvature:

$$\frac{\kappa}{n} = \frac{1}{n - d n_i' \sigma_i'} \tag{21}$$

$$\frac{\tau_j}{n_j} = \frac{1}{n} \frac{\kappa}{n} n_i' \sigma_i' \tag{21a}$$

$$\frac{\beta_j^{(3)}}{n_j^3} = \left(\frac{\kappa}{n} \right)^4 n_i' \zeta_i'^{(3)} \tag{21b}$$

$$\frac{\beta_j^{(5)}}{n_j^5} = \left(\frac{\kappa}{n} \right)^6 \left[n_i' \zeta_i'^{(5)} + 3 \frac{\kappa}{n} d (n_i' \zeta_i'^{(3)})^2 \right] \tag{21c}$$

$$\frac{\beta_j^{(7)}}{n_j^7} = \left(\frac{\kappa}{n} \right)^8 \left[n_i' \zeta_i'^{(7)} + 8 \frac{\kappa}{n} d (n_i' \zeta_i'^{(3)}) (n_i' \zeta_i'^{(5)}) + 12 \left(\frac{\kappa}{n} d \right)^2 (n_i' \zeta_i'^{(3)})^3 \right] \tag{21d}$$

Vertex to vertex:

$$\kappa = \frac{1}{1 - \frac{d}{n} n_i' \sigma_i'} \tag{22}$$

$$n_j \sigma_j = \kappa n_i' \sigma_i' \tag{22a}$$

$$n_j \zeta_j'^{(3)} = \kappa^4 n_i' \zeta_i'^{(3)} \tag{22b}$$

$$n_j \zeta_j^{(5)} = \kappa^6 \left[n_i' \zeta_i'^{(5)} + 3\kappa \frac{d}{n} (n_i' \zeta_i'^{(3)})^2 \right] \tag{22c}$$

$$n_j \zeta_j^{(7)} = \kappa^8 \left[n_i' \zeta_i'^{(7)} + 8\kappa \frac{d}{n} (n_i' \zeta_i'^{(3)}) (n_i' \zeta_i'^{(5)}) + 12 \left(\kappa \frac{d}{n} \right)^2 (n_i' \zeta_i'^{(3)})^3 \right] \tag{22d}$$

Higher orders are derived from equations (18*e*) and (18*f*) in a similar manner.

IV. THE RECIPROCAL ABERRATION OF A SINGLE SURFACE REFERRED TO THE VERTEX

A second set of formulas will now be investigated in which the point of reference is chosen at the vertex of the surface. These are to be used in the cases where the formulas referred to the center of curvature are not applicable (see p. 203), although in many cases either set may be used.

1. DERIVATION OF THE FORMULAS

As has been stated, aberration series of the form (2) or (2′) may be written referring to any point on the axis. Let the two which refer to the vertex of a surface (as V_i, fig. 6) be

$$\Sigma = \sigma + \zeta^{(3)} h_v^2 + \zeta^{(5)} h_v^4 + \zeta^{(7)} h_v^6 + \ldots \tag{23}$$

for the incident pencil and

$$\Sigma' = \sigma' + \zeta'^{(3)} h'^2_v + \zeta'^{(5)} h'^4_v + \zeta'^{(7)} h'^6_v + \ldots \tag{23'}$$

for the refracted pencil. Probably the easiest way to establish a relation between these two series is to transfer the aberration to the center of curvature by means of equations (18) so that the resulting coefficients are identical with those of series (2) and (2′) and then to substitute these coefficients in equations (10).

Let κ and κ' be the constants of transfer in the object and image spaces, respectively. Then substituting the appropriate values for

the object space in the formulas (18), the following relations are derived:

$$\kappa=\frac{1}{1-r\sigma}=1+r\tau=\frac{\rho}{\rho-\sigma}=\frac{\rho+\tau}{\rho} \tag{24}$$

$$\tau=\kappa\sigma \tag{24a}$$

$$\beta^{(3)}=\kappa^4\zeta^{(3)} \tag{24b}$$

$$\beta^{(5)}=\kappa^6(\zeta^{(5)}+3\kappa r\zeta^{(3)2}) \tag{24c}$$

$$\beta^{(7)}=\kappa^8(\zeta^{(7)}+8\kappa r\zeta^{(3)}\zeta^{(5)}+12\kappa^2r^2\zeta^{(3)3}) \tag{24d}$$

$$\beta^{(9)}=\kappa^{10}(\zeta^{(9)}+10\kappa r\zeta^{(3)}\zeta^{(7)}+5\kappa r\zeta^{(5)2}+55\kappa^2r^2\zeta^{(3)2}\zeta^{(5)}+55\kappa^3r^3\zeta^{(3)4}) \tag{24e}$$

By a similar substitution and also by reason of equations (10*a*) and (24)

$$\kappa'=\frac{\rho}{\rho-\sigma}=\frac{\rho+\tau}{\rho}=\frac{\mu'(\rho+\tau)}{\rho}=\mu'\kappa \tag{25}$$

in the case of the refracted pencil. Continuing the substitution

$$\tau'=\kappa'\sigma'=\mu'\kappa\sigma' \tag{25a}$$

$$\beta'^{(3)}=\mu'^4\kappa^4\zeta'^{(3)} \tag{25b}$$

and similarly the higher orders differ in form from (24*c* to 24*e*) only by the use of $\mu'\kappa$ instead of κ.

Substituting these values throughout equations (10), dividing each equation by the power of $\mu'\kappa$ appearing as a factor of the left member, and writing $\frac{1}{\mu'}=\frac{n}{n'}=\mu$

$$\sigma'=\left(\sigma+\frac{\rho}{\kappa}\right)-\mu\frac{\rho}{\kappa} \tag{26a}$$

$$\zeta'^{(3)}=\mu\zeta^{(3)}+\frac{1}{2}\mu(1-\mu)\frac{\rho}{\kappa^2}\left(\frac{\rho}{\kappa}+\sigma\right)\left(\mu\frac{\rho}{\kappa}-\sigma\right) \tag{26b}$$

$$\begin{aligned}(\zeta'^{(5)}&+3\mu'\kappa r\zeta'^{(3)2})\\&=\mu(\zeta^{(5)}+3\kappa r\zeta^{(3)2})-\frac{1}{2}\mu\zeta^{(3)}(1-\mu)\frac{\rho}{\kappa}\cdot\\&\quad\cdot[(1-\mu)\frac{\rho}{\kappa}+2\sigma]+\frac{1}{8}\mu(1-\mu)\frac{\rho}{\kappa^2}\left(\frac{\rho}{\kappa}+\sigma\right)\left(\mu\frac{\rho}{\kappa}-\sigma\right)\cdot\\&\quad\cdot[(1+\mu+\mu^2)\frac{\rho^2}{\kappa^2}-(1-\mu)\frac{\rho}{\kappa}\sigma+\sigma^2]\end{aligned} \tag{26c}$$

$$\begin{aligned}(\zeta'^{(7)}&+8\mu'\kappa r\zeta'^{(3)}\zeta'^{(5)}+12\mu'^2\kappa^2r^2\zeta'^{(3)3})\\&=\mu(\zeta^{(7)}+8\kappa r\zeta^{(3)}\zeta^{(5)}+12\kappa^2r^2\zeta^{(3)3})-\frac{1}{2}\mu\zeta^{(3)2}(1-\mu)\rho\\&-\frac{1}{2}\mu(\zeta^{(5)}+3\kappa r\zeta^{(3)2})(1-\mu)\frac{\rho}{\kappa}[(1-\mu)\frac{\rho}{\kappa}+2\sigma]\\&-\frac{1}{8}\mu\zeta^{(3)}(1-\mu)\frac{\rho}{\kappa}[(1+\mu+\mu^2+\mu^3)\frac{\rho^3}{\kappa^3}+4\mu\frac{\rho^2}{\kappa^2}\sigma+4\sigma^3]\\&+\frac{1}{16}\mu(1-\mu)\frac{\rho}{\kappa^2}\left(\frac{\rho}{\kappa}+\sigma\right)\left(\mu\frac{\rho}{\kappa}-\sigma\right)[(1+\mu+\mu^2+\mu^3+\mu^4)\frac{\rho^4}{\kappa^4}\\&-(1-\mu^3)\frac{\rho^3}{\kappa^3}\sigma+(1+\mu^2)\frac{\rho^2}{\kappa^2}\sigma^2-(1-\mu)\frac{\rho}{\kappa}\sigma^3+\sigma^4]\end{aligned} \tag{26d}$$

$$(\zeta'^{(9)}+10\mu'\kappa r\zeta'^{(3)}\zeta'^{(7)}+5\mu'\kappa r\zeta'^{(5)2}$$
$$+55\mu'^{2}\kappa^{2}r^{2}\zeta^{(3)2}\zeta'^{(5)}+55\mu'^{3}\kappa^{3}r^{3}\zeta'^{(3)4})$$
$$=\mu(\zeta^{(9)}+10\kappa r\zeta^{(3)}\zeta^{(7)}+5\kappa r\zeta^{(5)2}+55\kappa^{2}r^{2}\zeta^{(3)2}\zeta^{(5)}$$
$$+55\kappa^{3}r^{3}\zeta^{(3)4})-\mu(\zeta^{(3)}\zeta^{(5)}+3\kappa r\zeta^{(3)3})(1-\mu)-\frac{1}{2}\mu\cdot$$
$$\cdot(\zeta^{(7)}+8\kappa r\zeta^{(3)}\zeta^{(5)}+12\kappa^{2}r^{2}\zeta^{(3)3})(1-\mu)\frac{\rho}{\kappa}\left[(1-\mu)\frac{\rho}{\kappa}+2\sigma\right]$$
$$-\frac{1}{4}\mu\zeta^{(3)2}(1-\mu)\rho\left[\mu\frac{\rho^{2}}{\kappa^{2}}+3\sigma^{2}\right]-\frac{1}{8}\mu(\zeta^{(5)}+3\kappa r\zeta^{(3)2})(1-\mu)\frac{\rho}{\kappa}\cdot$$
$$\cdot\left[(1+\mu-\mu^{2}-\mu^{3})\frac{\rho^{3}}{\kappa^{3}}+4\mu\frac{\rho^{2}}{\kappa^{2}}\sigma+4\sigma^{3}\right]-\frac{1}{16}\mu\zeta^{(3)}(1-\mu)\frac{\rho}{\kappa}\cdot$$
$$\cdot\left[(1+\mu-\mu^{4}-\mu^{5})\frac{\rho^{5}}{\kappa^{5}}+2(\mu+\mu^{2}+\mu^{3})\frac{\rho^{4}}{\kappa^{4}}\sigma+4\mu\frac{\rho^{2}}{\kappa^{2}}\sigma^{3}+6\sigma^{5}\right]$$
$$+\frac{1}{128}\mu(1-\mu)\frac{\rho}{\kappa^{2}}\left(\frac{\rho}{\kappa}+\sigma\right)\left(\mu\frac{\rho}{\kappa}-\sigma\right)\left[5(1+\mu+\mu^{2}+\mu^{3}+\mu^{4}+\mu^{5}+\mu^{6})\frac{\rho^{6}}{\kappa^{6}}\right.$$
$$-(5+\mu+\mu^{2}-\mu^{3}-\mu^{4}-\mu^{5})\frac{\rho^{5}}{\kappa^{5}}\sigma+(5+\mu+3\mu^{2}+\mu^{3}+5\mu^{4})\frac{\rho^{4}}{\kappa^{4}}\sigma^{2}$$
$$\left.-(5-\mu+\mu^{2}-5\mu^{3})\frac{\rho^{3}}{\kappa^{3}}\sigma^{3}+(5-\mu+5\mu^{2})\frac{\rho^{2}}{\kappa^{2}}\sigma^{4}-(5-5\mu)\frac{\rho}{\kappa}\sigma^{5}+5\sigma^{6}\right] \tag{26e}$$

Equation (26*b*) is used in eliminating $\zeta'^{(3)}$ from equations (26*c*) to (26*e*). Following this step, the resulting form of equation (26*c*) is used in eliminating $\zeta'^{(5)}$ from the higher order equations, and so on. Remembering at the same time that, from equation (24), $\frac{\rho}{\kappa}=(\rho-\sigma)$ and $\left(\frac{\rho}{\kappa}+\sigma\right)=\rho$. The equations may be brought into the following form:

$$\sigma'=\rho-\mu\,(\rho-\sigma)=\mu\sigma-(\mu-1)\,\rho \tag{27a}$$

$$\zeta'^{(3)}=\mu\zeta^{(3)}-\frac{1}{2}\mu(\mu-1)(\rho-\sigma)^{2}[\mu(\rho-\sigma)-\sigma] \tag{27b}$$

$$\zeta'^{(5)}=\mu\zeta^{(5)}+\frac{1}{2}\mu\zeta^{(3)}(\mu-1)(\rho-\sigma)[(5\mu+1)(\rho-\sigma)-4\sigma]-\frac{1}{8}\mu(\mu-1)\cdot$$
$$\cdot(\rho-\sigma)^{2}[\mu(\rho-\sigma)-\sigma]\,[(7\mu^{2}-5\mu+1)\,(\rho-\sigma)^{2}-(5\mu-5)\,(\rho-\sigma)\sigma+\sigma^{2}] \tag{27c}$$

$$\zeta'^{(7)}=\mu\zeta^{(7)}-\frac{1}{2}\mu\zeta^{(3)2}(\mu-1)[(7\mu+4)(\rho-\sigma)-3\sigma]$$
$$+\frac{1}{2}\mu\zeta^{(5)}(\mu-1)(\rho-\sigma)[(7\mu+1)(\rho-\sigma)-6\sigma]$$
$$+\frac{1}{8}\mu\zeta^{(3)}(\mu-1)(\rho-\sigma)[(63\mu^{3}-33\mu^{2}-7\mu+1)(\rho-\sigma)^{3}$$
$$-(96\mu^{2}-68\mu-8)(\rho-\sigma)^{2}\sigma+(40\mu-32)(\rho-\sigma)\sigma^{2}-4\sigma^{3}]$$
$$-\frac{1}{16}\mu(\mu-1)(\rho-\sigma)^{2}[\mu(\rho-\sigma)-\sigma(33][\mu^{4}-47\mu^{3}+25\mu^{2}-7\mu+1)(\rho+-\sigma)^{4}$$
$$-(47\mu^{3}-80\mu^{2}+40\mu-7)(\rho-\sigma)^{3}\sigma+(25\mu^{2}-40\mu+17)(\rho-\sigma)^{2}\sigma^{2}$$
$$-(7\mu-7)(\rho-\sigma)\sigma^{3}+\sigma^{4}] \tag{27d}$$

$$\zeta'^{(9)}=\mu\zeta^{(9)}-\mu\frac{1}{\rho-\sigma}\zeta^{(3)3}(\mu-1)[(411\ \mu\ +81)(\rho-\sigma)-330\sigma]-\mu\zeta^{(3)}\zeta^{(5)}\cdot$$
$$\cdot(\mu-1)[(9\mu+5)(\rho-\sigma)-4\sigma]+\frac{1}{2}\mu\zeta^{(7)}(\mu-1)(\rho-\sigma)[(9\mu+1)(\rho-\sigma)$$
$$-8\sigma]-\frac{1}{8}\mu\zeta^{(3)2}(\mu-1)[(198\mu^3-42\mu^2-80\mu-3)(\rho-\sigma)^3$$
$$-(240\mu^2-116\mu-75)(\rho-\sigma)^2\sigma+(70\mu-51)(\rho-\sigma)\sigma^2+41\sigma^3]$$
$$+\frac{1}{8}\mu\zeta^{(5)}(\mu-1)(\rho-\sigma)[(99\mu^3-61\mu^2-9\mu+1)(\rho-\sigma)^3-(160\mu^2-124\mu$$
$$-10)\cdot$$
$$\cdot(\rho-\sigma)^2\sigma+(70\mu-60)(\rho-\sigma)\sigma^2-6\sigma^3]+\frac{1}{16}\mu\zeta^{(3)}(\mu-1)(\rho-\sigma)\cdot$$
$$\cdot[(429\mu^5-531\mu^4+140\mu^3+20\mu^2-9\mu+1)(\rho-\sigma)^5$$
$$-(960\mu^4-1{,}372\mu^3+428\mu^2+38\mu-10)(\rho-\sigma)^4\sigma$$
$$+(770\mu^3-1{,}190\mu^2+1{,}320\mu+20)(\rho-\sigma)^3\sigma^2-(280\mu^2-394\mu+130)\cdot$$
$$\cdot(\rho-\sigma)^2\sigma^3+(50\mu-40)(\rho-\sigma)\sigma^4-4\sigma^5]-\frac{1}{128}\mu(\mu-1)(\rho-\sigma)^2\cdot$$
$$\cdot[\mu(\rho-\sigma)-\sigma][(715\mu^6-1{,}525\mu^5+1{,}335\mu^4-665\mu^3+215\mu^2-35\mu+5)\cdot$$
$$\cdot(\rho-\sigma)^6-(1{,}525\mu^5-3{,}671\mu^4+2{,}709\mu^3-1{,}489\mu^2+371\mu-35)(\rho-\sigma)^5\sigma$$
$$+(1{,}265\mu^4-3{,}189\mu^3+2{,}873\mu^2-1{,}099\mu+165)(\rho-\sigma)^4\sigma^2$$
$$-575\mu^3-1{,}369\mu^2+1{,}049\mu-275)(\rho-\sigma)^3\sigma^3+(215\mu^2-371\mu+165)\cdot$$
$$\cdot(\rho-\sigma)^2\sigma^4-(35\mu-35)(\rho-\sigma)\sigma^5+5\sigma^6] \qquad (27e)$$

It may, at times, be preferable to multiply these equations by n' and write them in the following reduced form

$$n'\sigma'=n\sigma-(n-n')\rho \qquad (28a)$$

$$n'\zeta'^{(3)}=n\zeta^{(3)}-\frac{1}{2}n(\mu-1)(\rho-\sigma)^2[\mu(\rho-\sigma)-\sigma] \qquad (28b)$$

$$n'\zeta'^{(5)}=n\zeta^{(5)}+\frac{1}{2}n\zeta^{(3)}(\mu-1)(\rho-\sigma)[(5\mu+1)(\rho-\sigma)-4\sigma]$$
$$-\frac{1}{8}n(\mu-1)\ (\rho-\sigma)^2[\mu(\rho-\sigma)-\sigma][(7\mu^2-5\mu \qquad (28c)$$
$$+1)(\rho-\sigma)^2-(5\mu-5)(\rho-\sigma)\sigma+\sigma^2]$$

and similarly for higher orders. In computations by means of these equations it is not necessary to find the ζ coefficients explicitly, but only the "reduced coefficients," $n\zeta^{(3)}$, $n\zeta^{(5)}$, etc.

2. DISCUSSION

It is evident that these formulas are considerably more complex in form than those which refer to the center of curvature. They are included here as supplementary formulas to be applied where the other system is unsuitable. The eleventh order has not been included partly because of its unwieldiness and partly because in the cases where these equations will be most frequently applied, namely, surfaces of small or zero curvature or where the object is near the center of curvature, the inherent aberration will be small and fewer orders will, in general, be required than for the other surfaces of the system.

The zero points common to all orders of inherent aberration are given by

$$\mu(\mu-1)\left(\frac{\sigma}{\rho}-1\right)^2\left[\mu\left(\frac{\sigma}{\rho}-1\right)+\frac{\sigma}{\rho}\right]\rho^2=0$$

$\mu=0$, physically impossible.

$(\mu-1)=0$, the same root as in the other system.

$\left(\frac{\sigma}{\rho}-1\right)^2=0$, a double root at the center of curvature.

$(\mu+1)\left(\frac{\sigma}{\rho}-1\right)=-1$, the aplanatic point again.

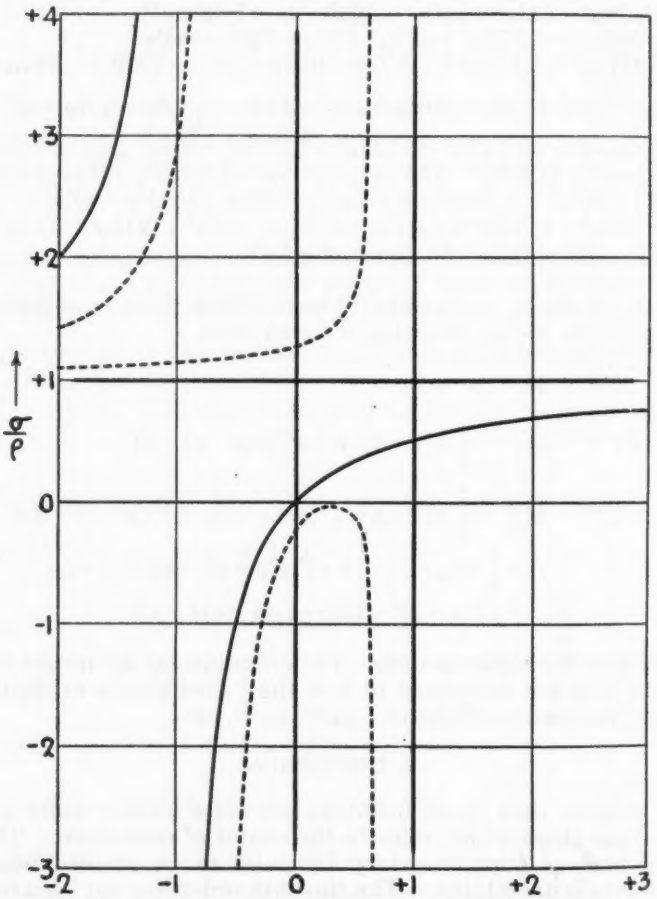

FIGURE 7.—*Zero reciprocal spherical aberration contour*

The solid lines indicate zero values of all orders. The dotted curve indicates an additional root of the fifth order. Additional roots of higher orders are not shown.

These roots are shown for $\rho=1$ in Figure 7, as is also an additional root of the fifth order. The additional roots of the higher orders have not been investigated.

Figures 8 and 9, corresponding to Figures 4 and 5, show the values of the inherent aberration coefficients for $\mu=1/1.5$ and $\mu=1.5$ when $\rho=1$. It is to be remembered that $\mu=1/1.5$ corresponds to $\mu'=1.5$ in Figure 4.

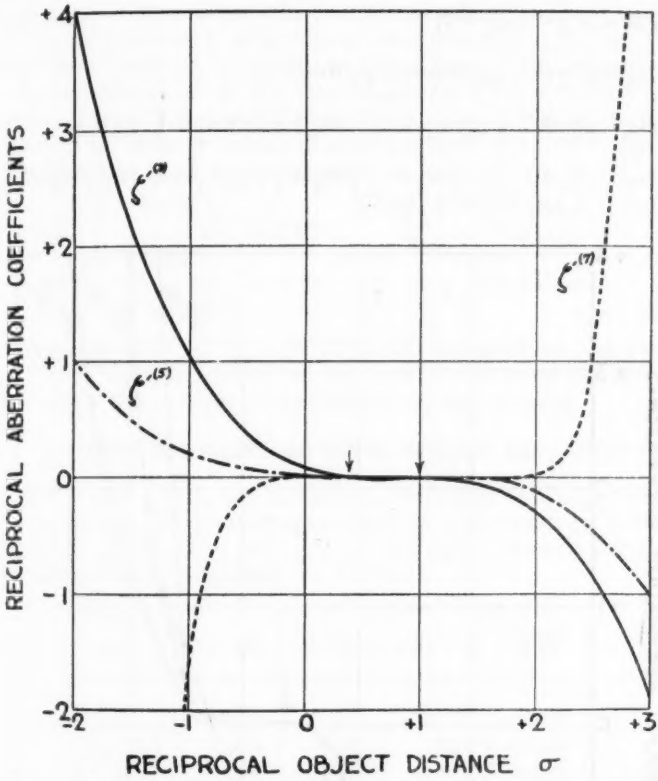

FIGURE 8.—*Reciprocal aberration coefficients for single surface of unit radius, $\mu=1/1.5$*

V. INVERSION TO LONGITUDINAL SPHERICAL ABERRATION

Given the reciprocal aberration of a pencil of rays, the longitudinal aberration may be derived by expanding the brackets in the following equation

$$S=\frac{1}{\Sigma}=\frac{1}{\sigma+\zeta^{(3)}h^2v+\zeta^{(5)}h^4v+\ \ldots}$$

$$=\frac{1}{\sigma\left(1+\frac{1}{\sigma}\zeta^{(3)}h^2{}_v+\frac{1}{\sigma}\zeta^{(5)}h^4v+\ \ldots\right)}$$

$$=s[1+(s\zeta^{(3)}h^2{}_v+s\zeta^{(5)}h^4{}_v+s\zeta^{(7)}h^6{}_v+s\zeta^{(9)}h^8{}_v+s\zeta^{(11)}h^{10}{}_v)]^{-1}$$

according to the formula $(1+x)^{-1}=1-x+x^2-x^3+\ \ldots$ If the longitudinal aberration be expressed as before. (See Introduction.)

$$S=s+Ah^2+Bh^4+Ch^6+Dh^8+Eh^{10} \qquad (1)$$

the following formulas are found for converting reciprocal into longitudinal aberration:

$$A = -s^2\zeta^{(3)} \tag{29a}$$

$$B = -s^2(\zeta^{(5)} - s\zeta^{(3)2}) \tag{29b}$$

$$C = -s^2(\zeta^{(7)} - 2s\zeta^{(3)}\zeta^{(5)} + s^2\zeta^{(3)3}) \tag{29c}$$

$$D = -s^2[\zeta^{(9)} - s(2\zeta^{(3)}\zeta^{(7)} + \zeta^{(5)2}) + 3s^2\zeta^{(3)2}\zeta^{(5)} - s^3\zeta^{(3)4}] \tag{29d}$$

$$E = -s^2[\zeta^{(11)} - 2s(\zeta^{(3)}\zeta^{(9)} + \zeta^{(5)}\zeta^{(7)}) + 3s^2(\zeta^{(3)2}\zeta^{(7)} + \zeta^{(3)}\zeta^{(5)2}) - 4s^3\zeta^{(3)3}\zeta^{(5)} + s^4\zeta^{(3)4}] \tag{29e}$$

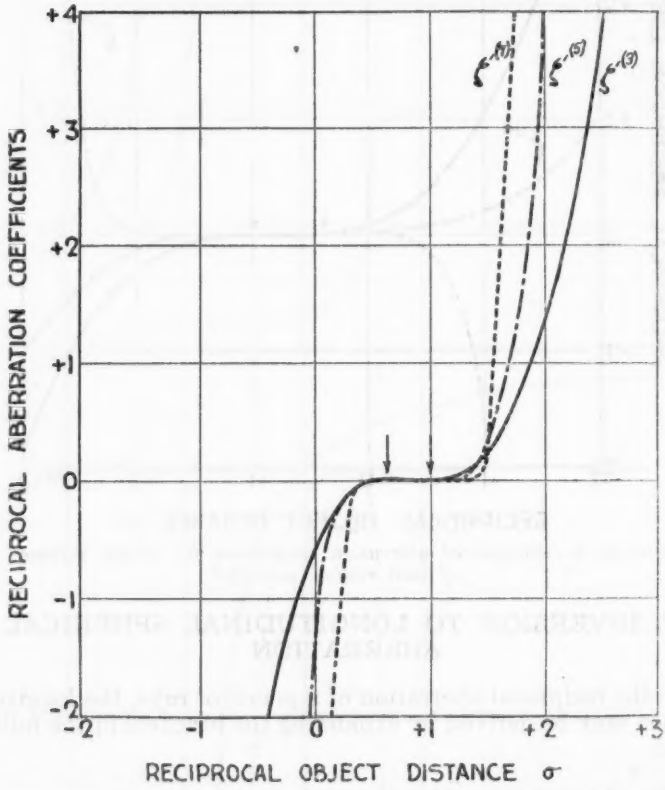

FIGURE 9.—*Reciprocal aberration coefficients for single surface of unit radius, $\mu = 1.5$*

These formulas are quite general. If the aberration refers to some point other than the vertex of a surface, it is necessary only to replace these symbols by the corresponding ones in the new series. The parameter may be taken as any function of the aperture and of any constants (as, for instance, the constants of a surface of the lens) so long as a convergent series result both for the reciprocal and for the longitudinal aberrations.

VI. NUMERICAL EXAMPLE

1. DETAILS OF CONSTRUCTION OF THE LENS

As an illustration of the application of the formulas derived in the preceding parts of the paper, the reciprocal spherical aberration of the third, fifth, and seventh orders has been computed for an ordinary landscape lens such as is found in most low-priced cameras. The details of construction of the lens as given by Conrady [17] and the necessary reciprocals are as follows, except that the decimal point has been changed in order to bring it near the first significant figure both in the lengths and in their reciprocals:

$$r_1 = -0.5556 \qquad \rho_1 = -1.7999$$
$$n_{1,2} = 1.63487 \qquad d_{1,2} = 0.01 \qquad n^{-1}{}_{1,2} = 0.61167$$
$$r_2 = +1.492 \qquad \rho_2 = +0.67024$$
$$n_{2,3} = 1.54712 \qquad d_{2,3} = 0.03 \qquad n^{-1}{}_{2,3} = 0.64636$$
$$r_3 = -0.2506 \qquad \rho_3 = -3.9904$$

The formulas (12), (11), and (28) will be used at the respective surfaces. The final longitudinal aberration will then be derived and compared with the results of trigonometric ray tracing.

2. FIRST SURFACE; INFINITE OBJECT DISTANCE

Since $\tau_1 = 0$ and $n_1 = 1$, the simplified formulas (12) may be used at the first surface. The numerical work is conveniently arranged in four columns, one for the paraxial values and one each for the three orders of aberration computed, as follows:

	Paraxial	Third order	Fifth order	Seventh order
$\frac{1}{n'^j}$	0.61167	0.61167	0.22885	0.08562
$\left(1-\frac{1}{n'^j}\right)$	.38833	.38833	.77115	.91438
$\rho^{j}{}_{2}$	−1.7999	−1.7999	−5.8310	−18.890
$\frac{\rho}{n'}$	----------	1.9816	1.9816	1.9816
		½	⅛	1/16
$\frac{\tau}{n'}; \frac{\beta'^{(i)}}{n'^i}$	−0.69896	−0.69253	−1.11381	−2.1392

where $j = 1, 1, 3$, and 5 in the respective columns.

The first line in this computation need not be written down if the computer so prefers. The next four lines contain the factors of the coefficients of the respective orders. The reciprocal of the intersection distance measured from the center of curvature could now be found for a ray at any height h'_{c1} from the center of curvature after refraction at this surface, this quantity being given by the series

$$\theta'_1 = \left(\frac{\tau_1}{n'_1}\right)n'_1 + \left(\frac{\beta'_1{}^{(3)}}{n'_1{}^3}\right)n'_1{}^3 h'_{c1}{}^2 + \left(\frac{\beta'_1{}^{(5)}}{n'_1{}^5}\right)n'_1{}^5 h'_{c1}{}^4 + \left(\frac{\beta'_1{}^{(7)}}{n'_1{}^7}\right)n'_1{}^7 h'_{c1}{}^6 - \cdots$$
$$= -0.69896\, n'_1 - 0.69253\, n'_1{}^3 h'_{c1}{}^2 - 1.11381\, n'_1{}^5 h'_{c1}{}^4$$
$$-2.1392\, n'_1{}^7 h'_{c1}{}^6 - \cdots$$

[17] Conrady, Applied Optics, p. 316. See footnote 2, p. 191.

3. TRANSFER FROM CENTER OF CURVATURE TO CENTER OF CURVATURE; FIRST SURFACE TO SECOND

Formulas (19), Section III, 3, are used in transferring the point of reference to the center of curvature of the second surface. The numerical work is most conveniently carried out in two parts, first computing the various terms and factors in the formulas, and second combining them to find the new coefficients, as follows:

1	d	+2.0576	κ	+0.29640	$\frac{\beta'^{(3)}}{n'^6}$	+0.47960
2	$n'd$	+3.3639	κ^2	.089043		
3	$\kappa n'd$	+1.00379	κ^4	$.79287 \cdot 10^{-2}$	$\frac{\beta'^{(4)}\beta'^{(5)}}{n'^9}$	+.77135
4			κ^6	$.70600 \cdot 10^{-3}$		
5	$(\kappa n'd)^2$	+1.00759	κ^8	$.62864 \cdot 10^{-4}$	$\frac{\beta'^{(2)}}{n'^6}$	−.33214

		Paraxial	Third order	Fifth order	Seventh order
6	$\frac{\tau'_1}{n'_1}; \frac{\beta'_1{}^{(1)}}{n'_1{}^2}$	−0.69896	−0.69253	−1.11381	−2.1392
7	κ−term			+1.44425	+6.1942
8	κ^3−term				−4.0159
9	Sum			+.33044	+.0391
10	$\frac{\tau_2}{n_2}; \frac{\beta_2{}^{(1)}}{n_2{}^2}$	−.20857	$-.54909 \cdot 10^{-2}$	$+.23329 \cdot 10^{-3}$	$+.0246 \cdot 10^{-4}$

In this computation the value of d is found from the original data ($d_{c1c2} = d_{v1v2} - r_1 + r_2$), then κ and its powers and multiples are computed, $n'd$ being found incidentally to the computation of κ. Line 6 is copied from the last line of the computation in the preceding section. The "sums" in line 9 are the numerical values of the quantities in brackets in the formulas, which, when multiplied by the proper power of κ give the coefficients for the object pencil at the second surface.

4. SECOND SURFACE AND TRANSFER TO THIRD; CENTER OF CURVATURE TO VERTEX

The aberration at the second surface is computed by means of formulas (11). As may be seen below, the computation falls readily into three parts. In lines 1 to 10 the various monomial and binomial quantities and their powers which appear in the formulas are computed. In lines 11 to 14 are computed the four bracketed quantities which appear in the $\frac{\beta'^{(3)}}{n'^3}$−inherent, the $\frac{\beta'^{(5)}}{n'^5}$−inherent, the $\frac{\beta'^{(7)}}{n'^7}\left(\frac{\beta^{(3)}}{n^3}\right)$, and the $\frac{\beta'^{(7)}}{n'^7}$−inherent terms respectively.[18] In each case the three products composing the quantity are written in the first three columns and their sum is written in the last column. In lines 15 to 20 the various terms in the formulas are evaluated and added together to find the constants of the refracted pencil. The inherent aberration appears in line 16, the terms containing the factor $\frac{\beta^{(3)}}{n^3}$ are in line 17, and so on.

[18] These designations are explained in Sec. II, 3; p. 201.

In the transfer to the vertex of the third surface, the first part of the computation, lines 25 to 29, has been written below the second part, lines 20 to 24 in order to eliminate the recopying of line 20. Moreover, the computation differs slightly from that in the preceding section in the use of formulas (20) instead of (19).

The numerical work, then, is as follows:

	i	ρ^i	$\frac{1}{n^i}$	$\frac{1}{n'^i}$	$\left(\frac{1}{n^i}-\frac{1}{n'^i}\right)$
1	1	+0. 67024	0. 61167	0. 64636	−0. 03469
2	2	+. 44922	. 37414	. 41778	−. 04364
3	3	+. 30109			
4	5	+. 13525			
		$\left(\frac{\tau}{n}\right)^i$	$\left(\frac{\rho}{n'}\right)^i$	$\left(\frac{\rho}{n}\right)^i$	$\left(\frac{\rho}{n}-\frac{\rho}{n'}\right)+(i-1)\frac{\tau}{n}$
5	1	−0. 20857	+0. 43322	+0. 40997	−0. 02325
6	2	+. 043501	+. 18768	+. 16808	−. 23182
7	3				−. 44039
		$\left(\frac{1}{n^i}-\frac{1}{n'^i}\right)^2$	$\left(\frac{\rho^2}{n'^2}-\frac{\tau^2}{n^2}\right)$	$\left(\frac{\rho^2}{n^2}-\frac{\tau^2}{n^2}\right)$	
8	1	+0. 001203	+0. 14418	+0. 12458	
9	2	+. 001904	+. 020788	+. 015520	
		$\left(\frac{1}{n^2}+\frac{1}{n'^2}\right)$	$\left(\frac{\rho^2}{n'^2}+\frac{\tau^2}{n^2}\right)$	$\left(\frac{\rho^2}{n^2}-\frac{\tau^2}{n^2}\right)$	
10	1	+0. 79192	+0. 23118	+0. 21158	
		Bracketed quantities			Sum
11	$\beta'^{(3)}$	−0. 00017	+0. 14141	−0. 13676	+0. 00448
12	$\beta'^{(5)}$	−. 000120	+. 012715	−. 010031	+. 002564
13	$\beta'^{(7)}(\beta^{(3)})$	+. 000143	+. 018394	−. 016795	+. 001742
14	$\beta'^{(7)}$	−. 0000425	+. 0029395	−. 0021225	+. 0007745

		Paraxial	Third order	Fifth order	Seventh order
15	$\frac{\tau_2}{n_2}$; $\frac{\beta_2{}^{(i)}}{n_2{}^i}$	−0. 20857	−0. 54909·10⁻²	+0. 23329·10⁻³	+0. 0246·10⁻⁴
16	Inher.	−. 02325	−. 1501 ·10⁻²	−. 2148 ·10⁻³	−. 3244·10⁻⁴
17	$(\beta^{(3)})$			+. 0281 ·10⁻³	+. 0321·10⁻⁴
18	$(\beta^{(5)})$				−. 0119·10⁻⁴
19	$(\beta^{(3)2})$				+. 0035·10⁻⁴
20	$\frac{\tau'_2}{n'_2}$; $\frac{\beta'_2{}^{(i)}}{n'_2{}^i}$	−. 23182	−. 6992 ·10⁻²	+. 0466 ·10⁻³	−. 2761·10⁻⁴
21	(κ)			−. 6975 ·10⁻³	+. 1239·10⁻⁴
22	(κ^2)				−. 9275·10⁻⁴
23	Sum			−. 6509 ·10⁻³	−1. 0797·10⁻⁴
24	$n\sigma_3$; $n\zeta$	−1. 16660	−. 7827	−. 7709	−1. 3529

25	d	−1. 462	$n\kappa$	+3. 2527	$\frac{\beta^{(3)2}}{n^5}$	+0. 48888·10⁻⁴
26	$1/n'$	. 64636	$(n\kappa)^2$	10. 5801		
27	$n'\kappa d$	−4. 7554	$(n\kappa)^4$	1. 11939·10²	$\frac{\beta^{(3)}\beta^{(5)}}{n^9}$	−. 03258·10⁻³
28	$(n'\kappa d)^2$	+22. 614	$(n\kappa)^6$	1. 18433·10³		
29	σ	−. 75404	$(n\kappa)^8$	1. 25303·10⁴	$\frac{\beta^{(3)3}}{n^{13}}$	−. 3418 ·10⁻³

5. THIRD SURFACE AND INVERSION TO LONGITUDINAL ABERRATION

The aberration due to the third surface of the lens might also be computed by the same method as was used at the second surface. However, it is desired to illustrate the use of formulas (28), and moreover it is preferable to have the final aberration referred to the back vertex without the additional transfer from the center of curvature to the vertex. Since the image is in air, then n' is unity, $\mu = n$, equations (28) are identical with equations (27), and the "reduced" coefficients, $n'\sigma'$, $n'\zeta'^{(3)}$, . . ., are equal to the actual coefficients, σ', $\zeta'^{(3)}$, . . .

In lines 1 to 4 of the computation the preliminary data are prepared. The bracketed quantities computed in lines 5 to 22 are given the designation of the term in which they appear. The various sums of the powers of n appear in the first column of numbers. These are multiplied by the appropriate powers of $(\rho - \sigma)$ and σ, and the products are written in the next column. Finally, these products are added together to give the total value appearing in the last column.

The coefficients of longitudinal spherical aberration are computed in lines 28 to 34 by formulas (29), Part V, in much the same manner as a transfer is made to a new point of reference.

These computations are as follows:

	i	n^i	$(\rho-\sigma)^i$	σ^i		
(1)	1	1.54712	−3.2364	−0.75404		
(2)	2	2.39358	+10.4743	+.56858		
(3)	3	3.70316	−33.899	−.42873		
(4)	4	5.7292	+109.711	+.32328		
	Bracketed quantities					Sum
(5)	$\zeta'^{(3)}(\zeta^{(3)})$	$(5n+1)$	8.7356	$\cdot(\rho-\sigma)$	−28.272	
(6)				-4σ	+3.016	−25.256
(7)	$\zeta'^{(3)}(Inh.)$	$(7n^2-\ .\ .)$	10.0195	$\cdot(\rho-\sigma)^2$	+104.947	
(8)		$-(5n-5)$	−2.7356	$\cdot(\rho)\sigma$	−6.6759	
(9)				$+\sigma^2$	+.5086	+98.840
(10)	$\zeta'^{(7)}(\zeta^{(3)2})$	$(7n+4)$	14.8298	$\cdot(\rho-\sigma)$	−47.995	
(11)				-3σ	+2.2621	−45.733
(12)	$\zeta'^{(7)}(\zeta^{(3)})$	$(7n+1)$	11.8298	$\cdot(\rho-\sigma)$	−38.286	
(13)				-6σ	+4.524	−33.762
(14)	$\zeta'^{(7)}(\zeta^{(3)})$	$(63n^3-\ .\ .)$	144.481	$\cdot(\rho-\sigma)^3$	−4,897.8	
(15)		$-(96n^2-\ .\ .)$	−116.579	$\cdot(\rho)^2\sigma$	+920.75	
(16)		$(40n-32)$	29.8848	$\cdot(\rho)\sigma^2$	−54.99	
(17)				$-4\sigma^3$	+1.71	−4,030.3

(18)	$\xi'^{(1)}$ (*Inh.*)	$(33n^4-\ldots)$	65.0247	$\cdot(\rho-\sigma)^4$	+7,133.92	
(19)		$-(47n^3-\ldots)$	−37.446	$\cdot(\rho)^3\sigma$	−957.16	
(20)		$(25n^2-\ldots)$	14.9547	$\cdot(\rho)^2\sigma^2$	+89.06	
(21)		$-(7n-7)$	−3.8298	$\cdot(\rho)\,\sigma^3$	−5.31	
(22)				$+\rho^4$	+.32	+6,260.8

		Paraxial	Third order	Fifth order	Seventh order
(23)	$n\sigma_3;\ n\xi'_3{}^{(1)}$	−1.16660	−0.7827	−0.7709	−1.3529
(24)	Inher:	+2.1832	+18.854	+465.88	+14,755.
(25)	$(\xi'^{(3)})$			−27.08	−1,080.2
(26)	$(\xi'^{(5)})$				−35.7
(27)	$(\xi'^{(3)}i^2)$				+11.9
(28)	$\sigma'_3;\xi'_3{}^{(1)}$	+1.0166	+18.071	+438.03	+13,650
(29)	s-term			−321.23	−15,573
(30)	s^2-term				+5,710
(31)	Sum			+116.80	+3,787
(32)	s', A', B', C'	+.98367	−17.486	−113.02	−3,664

(33)	s^2	0.96761	$\xi'^{(3)}\,\xi'^{(5)}$	+7,915.6
(34)	$\xi'^{(3)2}$	+326.56	$\xi'^{(5)2}$	+5,901.3

It is more or less customary to change the dimensions of a lens proportionately so that the focal length is 1,000 mm when plotting the aberrations. This is done to a satisfactory approximation in the present case by merely changing the decimal point. The intersection distance measured from the back vertex for an image ray at height h'_3 is then given by the series

$$S'_3 = s'_3 + A'h'_3{}^2 + B'h'_3{}^4 + C'h'_3{}^6$$

$$= 983.67 - 0.017486\ h'_3{}^2 - 0.00011302\ h'_3{}^4 - 0.000003664\ h'_3{}^6$$

6. COMPARISON WITH RAY TRACING

In comparing the results of algebraic and trigonometric computations it is well to keep in mind the following essential difference between the two: In the trigonometric work the longitudinal spherical aberration is found as the difference between the intersection lengths of a paraxial and another ray. If either length is determined with an uncertainty of 0.01 mm, the uncertainty in the aberration thus determined is at least as large as that. In the algebraic series, on the other hand, the spherical aberration is expressed as one or more correction terms to be applied to the paraxial focal length, and accordingly the aberration may sometimes be found with an uncertainty of 0.001 mm or less when the intersection lengths are not known to within 0.1 mm.

For the lens in our example Conrady gives the following values obtained by tracing a ray with the use of five place tables:

$$h_1 = \quad 30.0 \qquad \alpha'_3 = \quad 1.8253°$$

$$s'_3 = +983.67 \qquad S'_3 = 967.13$$

$$\text{Long. Spher.} = -16.54$$

For purposes of comparison, the algebraic aberration must be determined for the same ray, that is

$$h'_3 = S'_3 \sin \alpha'_3 = 967.13 \sin 1.8253° = 30.805$$

This value substituted into the final series in section 5, above, gives:

$A'h'^2_3 =$	-16.593	$s'_3 =$	$+983.67$
$B'h'^4_3 =$	$-.1018$	Long. Spher. =	-16.698
$C'h'^6_3 =$	$-.0031$	$S'_3 =$	$+966.972$
Total =	-16.698		

These results are shown in Figure 10.

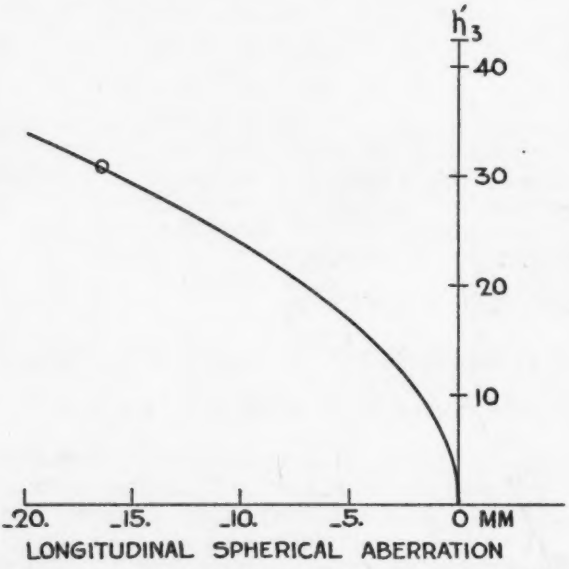

FIGURE 10.—*Spherical aberration of "landscape" lens*

The curve shows the aberration of this lens as given by the accompanying calculation. The circle indicates a value obtained by trigonometric ray tracing using 5 place tables. The curve as shown corresponds to a back focal length of 983.6 mm. The horizontal scale, however, is twice the vertical.

In order to determine whether the discrepancy of 0.158 mm between the two values of Long. Spher. is due more largely to the trigonometric or to the algebraic computation, a seven-figure trigonometric computation has been carried out. Its results are as follows:

$s'_3 =$	983.591	$\alpha'_3 =$	$1.82576°$
$S'_3 =$	966.888	Long. Spher. =	-16.703

When this more precise value is taken as a standard of comparison, it may be seen that the algebraic computation, even if only the third spherical order term be considered, gives a better value for the spherical aberration than does the five-figure trigonometric computation. Moreover, if the fifth order term is included the resulting aberration differs but little from that given by the seven-place work. The sev-

enth order term is negligible in the present case, but with larger relative apertures it would become more prominent.

It is interesting to note that Conrady computes the third order spherical aberration to be −16.702, which is virtually identical with the total aberration given by the 7-place computation, and then states that this value "agrees very well with the more exact trigonometric amount, −16.54, showing that the higher spherical aberration is small." The difference between the two values of the third order aberration may be considered as due to the causes mentioned in Part I, section 2. On the other hand, the close agreement between the first two paraxial image distances mentioned above appears to be largely fortuitous.

Although a final appraisal of the values of algebraic *v.* trigonometric computations should not be based upon one numerical example alone, still the following estimate, based upon this computation along with others which the author has made, may well be given here. The algebraic method is believed to be capable of giving as dependable results as the trigonometric in all practical cases. As a general rule, an exactness comparable to that given by 5-figure ray tracing may be obtained for apertures up to approximately $f/10$ by computing the third order only, and for apertures up to approximately $f/6$ by computing the third and fifth orders. These stated apertures will vary widely, tending to be smaller for meniscus than for symmetrical lenses. The labor involved in computing the paraxial and third order quantities by the method described in this paper is about the same as that of tracing one paraxial and one rim ray, that involved in computing also the fifth order is about the same as that of tracing one paraxial and two other rays. However, the possibility exists of compiling tables of the series aberrations, for instance as functions of the index of refraction and the reciprocal object distance, and thus of reducing the work to a minimum.

VII. DISCUSSION

1. CONVERGENCE OF ABERRATION SERIES

The validity of series expressions of aberration has been questioned on the ground that the magnitude of the terms which are neglected is not known. In fact Baker and Filon[19] have pointed out two cases in which these series actually become nonconvergent. There are analogous cases in the system of equations developed in the foregoing paragraphs, and these will be briefly discussed here.

In one case of nonconvergence the image distance for rays at some finite distance from the axis is infinite and, accordingly, the longitudinal aberration is infinite and can be expressed by no convergent series. In reciprocal aberration this case can be seen merely to be one of a zero value of the series. Nevertheless, analagous difficulty arises in the reciprocal series when a ray passes through the point of reference so that the reciprocal distance, and hence the reciprocal aberration, becomes infinite. This difficulty, however, can easily be avoided by a proper choice of the point of reference.

The second case mentioned by Baker and Filon concerns aberration series which are written in terms of the inclination of the ray in the

[19] Baker and Filon, On an Empirical Formula for the Longitudinal Spherical Aberration of a Thick Lens; Trans. Opt. Soc. London, vol. 20, pp. 67–92, 1918–19. See particularly pp. 74–76.

image space and involves longitudinal and reciprocal series alike. It was shown that two rays in the image pencil may have equal inclinations but unequal aberrations so that the aberration is a double-valued function of the independent variable. Manifestly no series can be convergent for both values.

In the present system of equations there is the following analagous case: Let ST (fig. 11) be the caustic curve of a pencil of rays. If the origin be chosen as at O so that a normal, N, to the caustic curve passes through it, then for every ray, R_BS_B, tangent to the curve beyond N, there is another ray, R_AS_A, such that the normals, OQ and OP, of the two rays are equal. There are, then two values of the aberration for a single value of the variable, h, and consequently no series can be convergent throughout this interval.

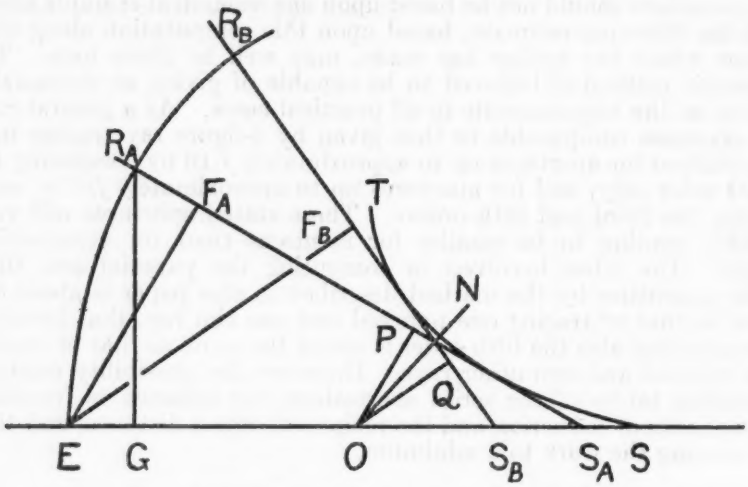

FIGURE 11.—*Diagram illustrating nonconvergence of aberration series*

However, by choosing a suitable point of reference, this difficulty is avoided, or at least the interval of convergence may be sufficiently extended for practical purposes.

Without stopping for the proof for other types of series, it may be stated as a more or less general rule that, if any aberration series be written using as a variable a length measured from a point on the axis to a point on the ray in some specified manner, than an absolute limit to the interval of convergence of the series is reached when the specified point on the ray coincides with the point of tangency of the ray with the caustic curve. In practice, however, long before this limit is reached the series will become so slowly convergent as to be of no practical value. It is to be observed, however, that nonconvergence can be avoided in the proposed system by a proper choice of the point of reference, while Baker and Filon found it necessary to use a function of the incident ray rather than of the refracted ray as the variable.

This is objectionable on account of the indefiniteness inherent in using a function of the incident ray. For example, if h is given in S_4P_4 (fig. 1), S'_4 may be found from equation (1). However, this determines only one point on the ray since the ray might traverse the lens by a different path and still intersect the axis at the same point. Even if the height of incidence on the last surface is used as the ordi-

nate and the axial point determined as before, the exact direction of the ray is not known unless the radius of the surface is given also. On the other hand, in the proposed system when the axial point is found by equation (1), the position of the ray is competely determined by a simple geometrical construction. Moreover, the ratio (or in the case of reciprocal aberration, the product) of these two quantities equals the sine of the angle of inclination of the ray while in the two systems just mentioned there is no direct relation.

2. RELATION TO PATH DIFFERENCE EQUATIONS

If it is desired to find the path difference between the two rays at some point on the axis, in order to work out the diffraction effects according to formulas such as those published by L. C. Martin,[20] a further advantage is gained in measuring the aperture along a line perpendicular to the ray rather than to the axis. In Martin's formula the independent variable is the height of intersection of the ray with a wave front through a fixed axial point. If ER_AR_B (fig. 11) is a wave front, then R_AG is such a height. Plainly an axial aberration series could not easily be written using this variable since the shape of the wave front is not usually known. If the wave front were exactly spherical then it is evident that R_AG would be exactly equal to EF which is the variable used in the present paper. Now, since wave fronts do not ordinarily depart from sphericity by more than one or two wave lengths, or 0.001 mm, when h equals, say, 20 mm, the two lengths could be considered equal in most cases without appreciable error, so that the coefficients of the series derived in this paper could be substituted directly into Martin's equations.

A further investigation of the relation between reciprocal aberration and path length differences has been begun, and exact equations have been derived. It is expected that these will be published soon.

3. CONCLUSION

Besides the theoretical interest which attaches to the equations derived in this paper, there also is believed to be a considerable possibility of their practical application. No optical computer to-day questions the value of the third order aberrations developed by Seidel, and yet Berek [21] states that "L. Seidel himself did not consider the aberration formulas of the third order which he published between 1853–1856 suitable for practical purposes and, therefore, furnished trigonometrical tracing formulas to the C. A. Steinheil Optical Co. (1866)." Further, it may be stated that the mathematical tools furnished by Seidel lay idle for about 60 years, and only recently their usefulness, in spite of their restrictions, has been recognized. Although the fifth order, up to the present time, has been considered too unwieldy to be useful, still it is not impossible that it, like the third order, will in time be brought into a simpler form adaptable to numerical work. In addition to this there is the possibility of the compilation of tables of these aberrations which would shorten considerably the work of computing.

WASHINGTON, June 16, 1932.

[20] L. C. Martin, A Physical Study of Spherical Aberration, Trans. Opt. Soc., London, vol. 23, pp. 63–92 1921–22.

[21] Berek, p. 41, see footnote 11, p. 192.

AN ATTACHMENT FOR TURNING APPROXIMATELY SPHERICAL SURFACES OF SMALL CURVATURE ON A LATHE

By I. C. Gardner

ABSTRACT

This device replaces the compound rest on a lathe and was particularly designed for the production of the convex or concave surfaces of lens-grinding tools although it is well adapted for the production of such surfaces for any purpose. It is intended to be used only for the production of surfaces of which the radius of curvature is too great to permit the use of a tool mounted on the end of a radius rod. The mathematical theory underlying the design and a detailed description of the instrument as built are given in detail. The attachment, as constructed, permits disks under 300 mm in diameter to be faced and any radius of curvature, greater than 500 mm may be obtained.

The surfaces produced are not accurately spherical, but for many purposes the approximation is entirely satisfactory. The approximation becomes poorer as either the curvature or diameter of the surface is increased. For a surface 200 mm in diameter with a radius of curvature of 1,000 mm the maximum departure from sphericity is 0.02 mm. If the diameter of the tool is 300 mm and the radius of curvature is 500 mm, the departure from sphericity is approximately 0.3 mm. This last value is the maximum departure for any surface lying within the working range of the instrument.

CONTENTS

		Page
I.	Introduction	227
II.	General description of the attachment	228
III.	Derivation of the equation of the curve generated by the linkage	230
IV.	Dimensions and performance characteristics of linkage adopted for construction	232
V.	Mechanical details of the completed instrument	235

I. INTRODUCTION

In the construction of machines or tools it is often necessary to form a small portion of a spherical surface of which the radius of curvature is very long. This is particularly the case when making lens-grinding tools. The tool employed for grinding or polishing the surface of a lens may be described as a circular disk, usually of brass or cast iron, with a hub at the center of one face by which it can be mounted on a spindle and with the other face, in special cases plane, but generally convex or concave, the radius of curvature being the same in magnitude but opposite in sense to that of the surface desired on the finished lens.

When the radius of curvature is not too great such surfaces can be conveniently generated by mounting the cutting tool of a lathe on the end of a radius rod of the desired length. However, if the radius of curvature is much greater than 2,000 mm such a method is not

suitable, and convenient methods for producing such surfaces are not commonly available in the machine shop. There is a machine tool by which spherical surfaces of small curvature can be generated, but its method of operation requires the use of a milling cutter with its diameter at least as great as that of the lens tool to be made. It follows that a machine of this type must be large and strongly built. It is necessarily expensive and can not be used economically unless the demand for spherical surfaces is such that it can be kept in operation for long periods of time.

There are other devices on the market for producing tools for the manufacture of ophthalmic lenses. Some of these are not fitted for making a surface with the radius of curvature greater than 2 or 3 m. Others, which permit surfaces of less curvature to be made, employ templates, and hence do not permit any desired curvature to be obtained except by the construction of a special template.

Accordingly, when the radius of curvature is large, the difficulty of readily producing such a surface, by methods hitherto available, is so great that, in some instances, the lens designer actually avoids the use of surfaces of small curvature although this course is not satisfactory except for certain types of optical systems. In other cases, arcs are described on sheet metal by a marker on the end of the required length of piano wire. Two templates are filed from the metal—the one convex, the other concave—and these are ground together to eliminate the smaller irregularities. These templates are used to control the form of the tool which is turned by hand on a lathe. Hand turning would not be sufficiently precise except that lens tools are usually required in pairs, convex and concave, and the two tools can be ground together before use. The turning of tools by such a method is not only costly and tedious, but the cost is often further increased by the excessive amount of grinding which is required to prepare hand-turned tools for use.

Because of these difficulties a new method of producing approximately spherical surfaces of small curvature has been developed. By this method the surfaces may be produced on a lathe by substituting a relatively simple attachment for the compound rest. An adjustment can be readily made to give any radius of curvature within the range of the attachment. The sharper curvatures can not be generated by this device, but this offers no serious disadvantages as simple and satisfactory methods are already available for such curves. The surfaces generated are not truly spherical but in many cases, particularly for the larger radii of curvature, or for tools of small diameter, the departure from sphericity is so small that the tools may be used as turned. For the sharper curvatures falling within the range of the instrument it may be necessary to grind the members of a pair of tools together, but the time of grinding will be small as compared with that required for tools turned by hand.

II. GENERAL DESCRIPTION OF THE ATTACHMENT

According to this method the spherical surface to be produced is turned on a lathe by a single-tooth tool mounted in a special tool holder which is guided to generate the desired surface by a simple linkage system. A plan view of the fundamental parts is shown diagrammatically in Figure 1. The line *KN* is the axis of the lathe

spindle and the arc KL is a meridian section of the curved surface which is turned by the cutting tool indicated at K. At A and B are two pins which are fixed to the lathe carriage. The triangle CDE, on which the cutting tool is rigidly mounted, is pushed across the lathe by a cross-feed and, as it advances, the two sides remain in contact with the pins A and B, thereby causing the triangle to rotate

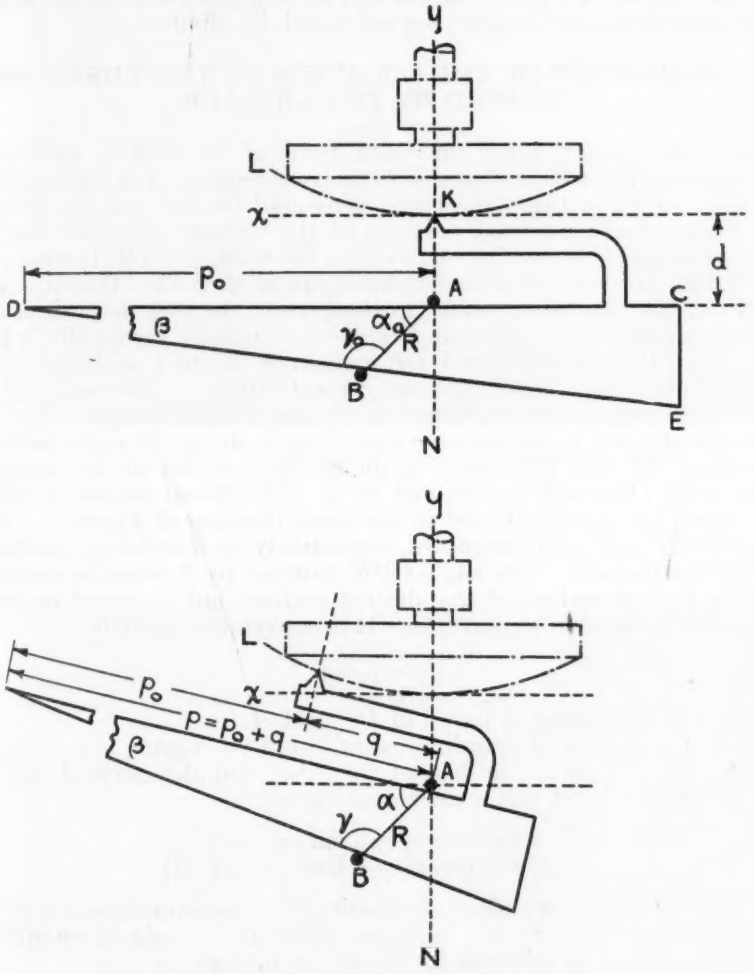

FIGURE 1.—*Diagrammatic sketch of linkage*

in such a manner that the cutting tool generates the arc KL. When the lathe spindle is revolving, therefore, a surface of revolution with the arc KL as a meridian section is produced.

Under the guidance of this linkage, the tool generates an arc which is not truly circular, but the approximation is satisfactory over the entire range of curvatures for which the use of a radius bar is unsatisfactory. Therefore the two methods supplement each other and, together, provide for the production of any curvature. The amount

of curvature is determined by the magnitude of the angle between lines DE and DC and by the length AB. It is convenient to hold AB constant and provide means for varying the angle. The instrument may be calibrated to permit a setting to be readily made for any desired curvature. It is an advantage of this linkage that the constraints at A and B do not change their directions of action during the production of a given surface and accordingly inaccuracies, which may arise from lost motion, are substantially eliminated.

III. DERIVATION OF THE EQUATION OF THE CURVE GENERATED BY THE LINKAGE

In order to determine the exact form of the surface generated by this attachment it is desirable to derive the equation of the meridian section, which is the plane curve generated by the linkage system. In Figure 1 the essential portions of the linkage are illustrated in two positions. In the upper drawing the triangle CDE is shown in its initial position with DC at right angles to the bed of the lathe and with K, the generating point, in the prolongation of the axis of the spindle of the lathe. As this triangle is advanced across the bed of the lathe the sides DC and DE remain in contact with the fixed constraints A and B, thus causing the triangle in the course of its motion to assume the position shown in the lower drawing of Figure 1. Two parameters, p, the distance from D to A, and α, the angle between the lines AB and CD, serve to define the position of the triangle. The angle DBA will be denoted by γ. The initial values of these are p_0, α_0, and γ_0 as indicated in the upper drawing of Figure 1. The lengths AB and AK, designated, respectively, as R and d are constants of the instrument. The angle CDE, denoted by β, remains constant during the generation of any desired surface, but is varied in order to produce different curvatures. It is convenient to write

$$p - p_0 = q \tag{1}$$

where q is the extent of travel of DC past A.

The x y system of coordinates indicated on Figure 1 is assumed fixed with respect to the bed of the lathe and the parts A and B. Then, for any point on the generated curve,

$$\begin{aligned} x &= q \cos(\alpha - \alpha_0) - d \sin(\alpha - \alpha_0) \\ y &= q \sin(\alpha - \alpha_0) + d[\cos(\alpha - \alpha_0) - 1] \end{aligned} \tag{2}$$

but for the more convenient application of these equations it is desirable that the trigonometric functions of $(\alpha - \alpha_0)$ be replaced by equivalent expressions in terms of β. If, by definition

$$\begin{aligned} P &= \frac{p}{R} \sin \beta \\ Q &= (1 - P^2)^{1/2} \end{aligned} \tag{3}$$

then

$$\begin{aligned} \sin \gamma &= P \\ \cos \gamma &= -Q \end{aligned} \tag{4}$$

Since

$$\alpha = 180° - (\beta + \gamma)$$

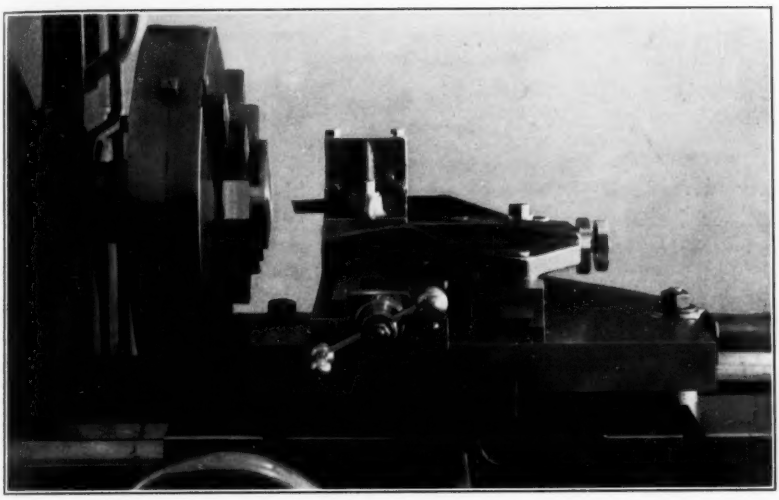

FIGURE 3.—*Front view of attachment mounted on a lathe*

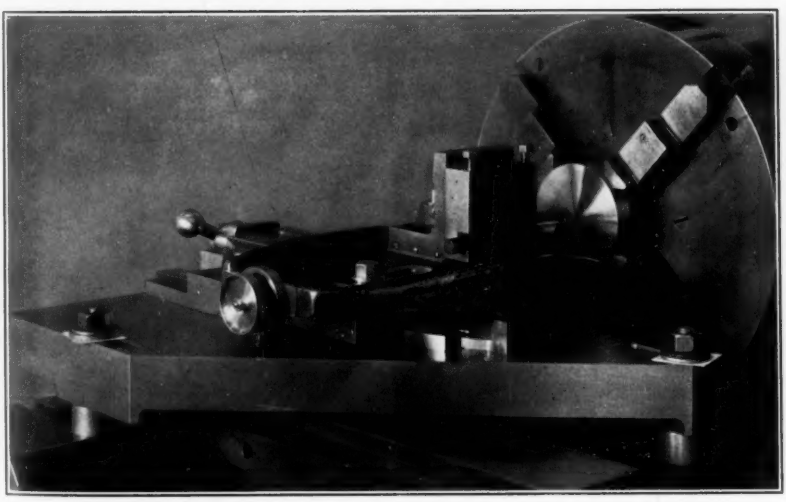

FIGURE 4.—*Back view of attachment mounted on a lathe*

UNIV OF

$$\sin \alpha = \sin (\beta + \gamma) = P \cos \beta - Q \sin \beta \quad \text{and} \tag{5}$$
$$\cos \alpha = -\cos (\beta + \gamma) = Q \cos \beta + P \sin \beta.$$

Similarly

$$\sin \alpha_0 = P_0 \cos \beta - Q_0 \sin \beta \tag{6}$$
$$\cos \alpha_0 = Q_0 \cos \beta + P_0 \sin \beta$$

where

$$P_0 = \frac{p_0}{R} \sin \beta \tag{7}$$
$$Q_0 = (1 - P_0^2)^{1/2}$$

By an evident trigonometric transformation

$$\sin (\alpha - \alpha_0) = PQ_0 - P_0 Q \tag{8}$$
$$\cos (\alpha - \alpha_0) = PP_0 + QQ_0$$

Substituting the values from equation (8) in equation (2)

$$x = (PP_0 + QQ_0)\, q - (PQ_0 - P_0 Q)\, d \tag{9}$$
$$y = (PQ_0 - P_0 Q)\, q + (PP_0 + QQ_0 - 1)\, d$$

Equations (9) enable the coordinates of any desired point on the curve to be obtained, but the form remains an inconvenient one for the present purpose. If x_1, y_1 be the coordinates of a given point on the curve, r may be defined by the equation

$$r = \frac{x_1^2 + y_1^2}{2\, y_1} \tag{10}$$

where r is the radius of curvature of a circle which cuts the axis of the lathe at right angles at the origin and passes through the point x_1, y_1. If the generated curve were truly circular the value of r would be independent of the particular point x_1 y_1 selected. As has been mentioned, however, the generated curve is only approximately circular and r is a function of x_1 y_1.

Substitution from equations (9) may be made directly in equation (10). However, a more convenient form is obtained by a series development. Two auxiliary quantities are defined by the equations

$$\rho = \frac{Q_0 R}{2 \sin \beta} \tag{11}$$
$$n = q/d$$

From equations (1), (3), (7), and (11) one may write

$$P = P_0 + \frac{n\, d\, Q_0}{2\, \rho} \tag{12}$$

and; by substitution in equation (3), Q may be expressed as an infinite series and P_0 and Q_0.

By making these substitutions for P and Q in equations (9) and substituting these values of x and y for x_1 and y_1 in equation (10), a series development for r may be obtained of which the first few terms are given in equation (13).

$$r = \rho - \left(\frac{3}{4} + \frac{1}{4}\frac{P_0}{Q_0} n\right) d + \frac{1}{16}\left[1 - \left(\frac{P_0}{Q_0}\right)^2 n^2\right]\frac{d^2}{\rho} - \frac{1}{64}\left(n\frac{P_0}{Q_0} - 1\right)\left[2\frac{P_0^2}{Q_0^2} n^2 + 2\frac{P_0}{Q_0} n + n^2 + 1\right]\frac{d^3}{\rho^2} \tag{13}$$

The right-hand member is an implicit function of β as will be noted by reference to equations (7) and (11). In the applications which have

been made this series is so rapidly convergent that it is necessary to retain only the first three terms and $\frac{P_0}{Q_0}$ changes so slowly for changes in r that the value of β corresponding to any value of r may be readily obtained. The angle β, as indicated in Figure 1, is considered positive, r and ρ of equation (16), for this case, are positive and a convex surface is produced. If the slope of the line DE changes sign, β, r and ρ are negative and a concave surface is produced.

IV. DIMENSIONS AND PERFORMANCE CHARACTERISTICS OF LINKAGE ADOPTED FOR CONSTRUCTION

The instrument which has been built enables tools 300 mm in diameter to be produced and permits the turning of either convex or concave surfaces with the radius of curvature greater than 500 mm. This range of curvatures is considered entirely satisfactory as more sharply curved surfaces may be readily and conveniently produced by mounting the tool on the end of a radius rod.

The constants which were adopted for the instrument are

$$\alpha_0 = 45°$$

$$R = 150\sqrt{2} \text{ mm}$$

$$d = 50 \text{ mm}$$

and the maximum value of n is 3. Reference to Figure 1 indicates that

$$p_0 = 150 \cot \beta + 150 \tag{14}$$

From equation (7)

$$\begin{aligned} P_0 &= \frac{\cos \beta}{\sqrt{2}} + \frac{\sin \beta}{\sqrt{2}} = \sin (45 + \beta) \\ Q_0 &= \qquad\qquad \cos (45 + \beta) \end{aligned} \tag{15}$$

and equation (13), with the last term omitted, becomes

$$r = \rho - \frac{3}{4}d - \frac{1}{4}nd \tan (45° + \beta) + \frac{1}{16}\frac{d^2}{\rho} - \frac{1}{16}\frac{n^2 d^2}{\rho} \tan^2 (45° + \beta) \tag{16}$$

As has been already mentioned, the surfaces which are generated by this apparatus are approximately but not strictly spherical. In equation (16) this is evidenced by the presence of n and n^2 in the right-hand member. In investigating this departure from sphericity several assumptions will be made in order to simplify the work without any important lessening of the accuracy.

1. The last two terms in equation (16) will be neglected.
2. It will be assumed that x of the coordinate system indicated in Figure 1 is equal to nd. Reference to the first of equations (2) will indicate the approximation involved.[1]
3. The sagitta of the approximately circular arc, KL, shown in Figure 2 will be assumed equal to $\frac{x^2}{2r}$.
4. In the quantity $(4\rho + 3d)$, which will occur, it will be assumed that ρ can be replaced by $r + 60$.

[1] The approximation of assumption 2 is applied successively to two nearly equal quantities, and only the difference between these two quantities is of importance in the following discussion. The approximation is therefore much closer than may at first appear. This is also true of the approximation of assumption 3.

If $n_1 d$ is the radius of the tool to be turned, the radius of curvature of the edge zone, as it has been defined, will be approximately given by the equation

$$r_1 = \rho - \frac{3}{4} d - \frac{1}{4} n_1 d \tan (45° + \beta)$$

The sagitta of a sperical surface, having this radius of curvature, at a distance nd from the center, will be

$$\frac{2n^2 d^2}{4\rho - 3d}\left[1 + \frac{n_1 d \tan (45° + \beta)}{4\rho - 3d}\right]$$

and, similarly, the sagitta of the actual surface, at the same distance from the center, will be

$$\frac{2n^2 d^2}{(4\rho - 3d)}\left[1 + \frac{nd \tan (45° + \beta)}{4\rho - 3d}\right]$$

The distance between these two surfaces, which will be/termed the departure from sphericity, for the zone nd will be

$$\frac{2\ n^2\ d^3\ (n_1 - n)}{(4\rho - 3\ d)^2} \tan\ (45° + \beta)$$

Applying assumption 4 one may write
Departure from sphericity

$$= \frac{2\ (n_1\ n^2 - n^3)\ d}{(4\ r + 90)^2} \tan\ (45° + \beta) \qquad (17)$$

For given values of r and n_1, this expression will assume a maximum value when $n = \frac{2}{3}\ n_1$ and, substituting this value
Maximum departure from sphericity

$$= \frac{8}{27} \frac{n^3_1\ d^3}{(4\ r + 90)^2} \tan\ (45° + \beta) \qquad (18)$$

This expression gives the maximum distance, measured parallel to the axis of the tool, between the actual surface as turned and a spherical surface with a radius of curvature corresponding to the zone of radius $n_1\ d$ and is a measure of the thickness of metal which must be removed to obtain a rigorously spherical surface. For a given radius of curvature it is evident that this departure varies as the cube of the diameter of the tool and inversely, approximately as the square of the radius of curvature. Consequently, within the working range of the instrument, the greatest values of the departure from sphericity will be obtained when the diameter of the tool is 300 mm ($n_1 = 3$) and when r equals $+500$ or -500 mm. For r equals $+500$ (convex surface) and r equals -500 (concave surface), β assumes the values $+6.7°$ and $-11.4°$, respectively, and tangent $(45° + \beta)$ assumes the values 1.27 and 0.55. This indicates that a

concave surface generated by this attachment will, in general, be more nearly spherical than a convex surface although, as the absolute value of r increases, β approaches zero as a limit and the values of tan $(45°+\beta)$ approach equality for the two types of surfaces. For $n_0=3$ and $r=+500$ or -500, the maximum departures from sphericity are

	mm
For convex surface	0.3
For concave surface	.15

In considering these values of the departure from sphericity it should be remembered that these are the extreme values for the most unfavorable conditions and that the departures are very much less for the greater part of the working range of the instrument. For example, for tools 200 mm in diameter and r equals $+1{,}000$ or $-1{,}000$ mm the departures from sphericity are

	mm
For convex surface	0.02
For concave surface	.01

In equation (16) for all values of β and ρ lying within the range of the instrument, the third term of the right-hand member is the term which determines the sense in which the surface departs from true sphericity. This term does not change sign, and, accordingly, for a convex surface, the absolute value of the radius of curvature decreases from the center outward and for a concave surface the change is in the opposite direction. Consequently the marginal portions of a convex surface and the central portions of a concave surface are the more strongly curved.

In Table 1, the values of β corresponding to different values of r are tabulated. These values are determined for $n=1.8$ and the values of β, as tabulated, may be used for tools 200 mm or less in diameter. For convex surfaces approaching 300 mm in diameter it is well to increase the desired value of r by 15 and to use this new value when entering the table.[2] Similarly, for a concave surface the absolute value of the desired r should be decreased by 10 before entering the table. For values of r greater than 10,000 mm, the value of β can be computed to a satisfactory approximation by the formula

$$\tan \beta=\frac{75}{r+135} \tag{19}$$

where r and β are positive for convex, negative for concave surfaces.

[2] As has been noted, Table 1 is computed for $n=1.8$. For a tool approaching 300 mm in diameter it is desirable that the surface actually turned and the desired spherical surface coincide for a zone further from the center than that corresponding to $n=1.8$. For a convex surface, this result will be attained if the value of r for $n=1.8$ is made 15 mm greater than the nominal value desired for the complete surface. Similarly, for the concave surface, the value of r for $n=1.8$ is less than the value corresponding to the complete surface.

TABLE 1.—*Values of β corresponding to r*

r	Convex surface β	Concave surface β
mm	°	°
500	6.66	−11.38
600	5.78	−9.04
700	5.10	−7.49
800	4.56	−6.39
900	4.13	−5.57
1,000	3.77	−4.93
2,000	2.01	−2.30
3,000	1.37	−1.50
4,000	1.04	−1.11
5,000	.84	−.88
6,000	.70	−.73
7,000	.60	−.63
8,000	.53	−.55
9,000	.47	−.48
10,000	.42	−.44

V. MECHANICAL DETAILS OF THE COMPLETED INSTRUMENT

The attachment has been built in such form that it replaces the usual compound slide rest on the lathe. No other alterations are necessary and the lathe may be used interchangeably for ordinary turning or the facing of spherical surfaces. In Figure 1 the constraints have been represented as pins against which the sides of the triangle bear. In the mechanical realization of this linkage the pins are necessarily replaced by pivoted slides of sufficient strength to oppose the forces on the cutting tool. The detailed design, as completed at the Bureau of Standards, is shown in Figure 2. The tool, indicated at *L*, is carried on a cross slide pivoted at *A*. The pivot at *A* corresponds to the similarly lettered constraint in Figure 1 and the line *CD* corresponds to the line *CD* of the triangle. The member which carries the tool is extended to the right of the slide and carries a sector *FGB*, pivoted at *B*. This sector is rotated about *B* and may be set in any desired position by means of the worm which is rotated by the handle at *I*. The angular setting of the sector can be read by an arc graduated in degrees and by a graduated drum which is mounted on the shaft of the worm. On the lower surface of the sector there is a male dovetailed member, indicated by the dotted lines parallel to the line DE of Figure 1. This dovetailed member corresponds to the side *DE* of the triangle of Figure 1 and it can be set in the required position for any desired radius of curvature by rotating the sector. The arc, carried by the sector, is graduated to permit the value of β to be read directly. In Figure 2 the setting illustrated corresponds to $\beta=0$, *CD* and *DE* are parallel and the instrument will produce a plane surface. The dovetailed member which has been mentioned slides in a short dovetailed slide pivoted in the base at *B*. The small section in Figure 3 indicates the details of this arrangement. The pivots at *A* and *B*, corresponding to the constraints *A* and *B*, respectively, of Figure 1, are carried by the base of the attachment and remain invariant in position with respect to each other. It will be noted that the pivot about which the sector rotates is directly over the pivot at *B* when the main slide is at right

angles to the axis of the lathe and the point of the tool is on the axis of the lathe. Consequently, when in this position, the sector can be rotated through any desired angle without causing any rotation of the line *DC* about *A*.

As has been mentioned, this attachment is mounted on the carriage of the lathe in place of the compound slide rest. Reference to a table, such as Table 1, gives the required value of β for the desired radius

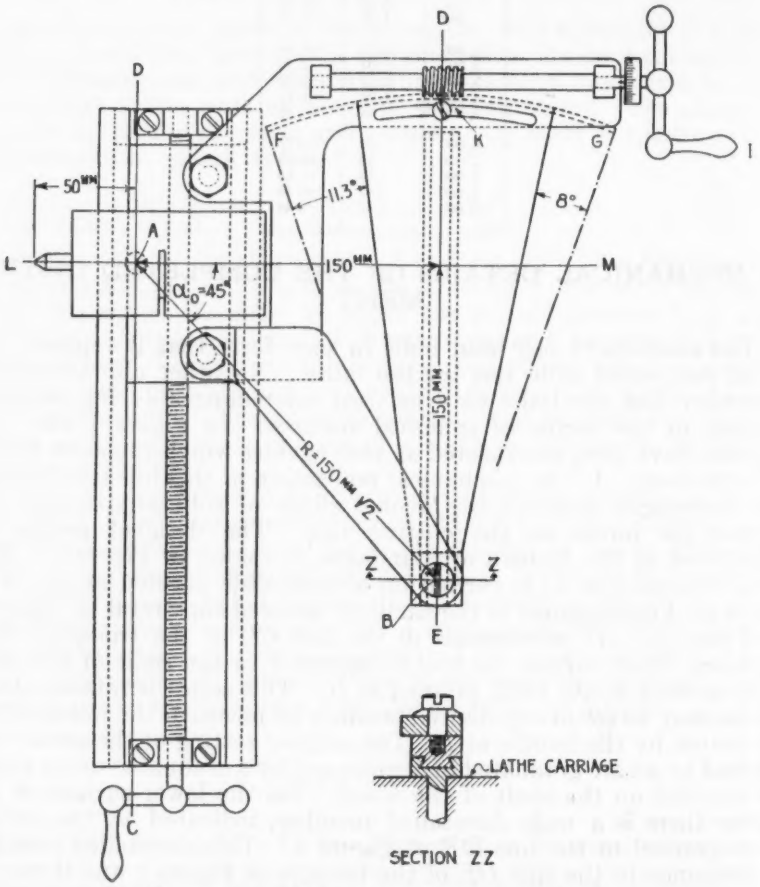

FIGURE 2.—*Mechanical realization of linkage*

and the setting is made by turning the handle *I*, after which the sector is clamped in position by the nut at *K*. The cut is then made in the uaual manner by turning the handle at *I*. To advance the tool for a second cut, the entire attachment is advanced toward the work by traversing the carriage along the bed of the lathe. The operation of facing a spherical surface with this attachment is quite as simple as facing a plane surface with a compound slide rest except that no automatic cross-feed is provided. This could be easily added if it were considered essential.

One of these attachments has been built by the Mann Instrument Company, Cambridge, Mass. Although the details of the design shown in Figure 2 have been modified to correspond to their practice in instrument design, the fundamental dimensions and elements of design were retained unaltered Figures 3 and 4 give two views of the completed attachment mounted on a lathe in position for operation. In the two views the different details of construction to which reference has been made are clearly recognizable. The attachment has proved quite satisfactory for the production of surfaces for lens, tools, and similar purposes.

WASHINGTON, June 2, 1932.

WAVE LENGTHS AND ZEEMAN EFFECTS IN LANTHANUM SPECTRA

By William F. Meggers

ABSTRACT

The wave lengths corresponding to more than 1,500 lines photographed in the arc and spark spectra of lanthanum were measured relative to standards in the iron spectrum. The values extend from 2,142.81 A in the ultra-violet to 10,954.6 A in the infra-red. Data on the furnace spectra of 695 lanthanum lines studied by King and Carter in the interval 2,798 to 8,346 A are quoted. Measurements of Zeeman effects for 476 lines ranging in wave length from 2,791 to 7,483 A are also presented. Comparison of relative intensities and other characteristics of lines in the different sources permitted a sharp discrimination between three classes of lines; about 700 are ascribed to neutral atoms (constituting the La I spectrum), 800 originate with singly ionized atoms (La II spectrum), and 10 belong to doubly ionized atoms (La III spectrum). These data form a complete and accurate description of atomic lanthanum spectra, suitable for chemical indentification and for analysis of the spectral structures. A new infra-red sequence of La O bands is appended.

CONTENTS

	Page
I. Introduction	239
II. Experimental	240
1. Wave lengths	240
2. Zeeman effects	240
III. Results	242

I. INTRODUCTION

Lanthanum (La = 138.90; Z = 57) is the third element in the sixth period of the periodic classification, and is analogous to scandium and yttrium which appear in similar positions in the fourth and fifth periods. The emission spectra of scandium [1] and yttrium [2] have been described with satisfactory thoroughness and precision, but lanthanum data of the same quality have been lacking up to the present.

Attempts to analyze the structures of lanthanum spectra,[3] when based upon the published wave lengths and Zeeman effects, were only partially successful and it was evident that more extensive and accurate descriptive material was required before the structural analyses could be completed. Such data are now presented in this paper; they comprise wave-length measurements from 2,100 to 11,000 A, estimated relative intensities for 1,535 lines, and Zeeman effect observations for 476 lines in the interval 2,800 to 7,500 A.

[1] W. F. Meggers, B. S. Sci. Paper No. 549, vol. 22, p. 61, 1927.
[2] W. F. Meggers, B. S. Jour. Research, vol. 1 (RP12), p. 319, 1928.
[3] W. F. Meggers, La I, J. Wash. Acad. Sci., vol. 17, p. 25, 1927. W. F. Meggers, La II, J. Opt. Soc. Am., vol. 14, p. 191, 1927.

Analysis of the structures of lanthanum spectra and details concerning the hyperfine structure of lanthanum lines will be given in other papers.

The only remaining spectra of this type are those associated with actinium, the optical spectra of which have never been investigated.

II. EXPERIMENTAL

1. WAVE LENGTHS

The lanthanum salts used in this investigation consisted of $LaCl_3$ purified by Auer v. Welsbach, pure La_2O_3 kindly supplied by Prof. B. S. Hopkins of the University of Illinois, and commercial $LaCl_3$ purchased from Eimer and Amend. The latter material contained a considerable amount of cerium, and its use was confined mainly to the observation of Zeeman effects.

Arc spectrograms were made with electric arcs between electrodes of graphite, silver, or copper, a small portion of lanthanum salt being placed on the lower electrode before striking the arc. The arc was fed by 5 to 6 amperes direct current from a circuit with 220 volts potential difference. Some of the spark spectrograms were made with the same metal electrodes which had been used previously for arc spectra, the salt fused on the rods in the arc sufficed to give well-developed spark spectra. Additional spark spectrograms were obtained with graphite electrodes upon which a solution of $LaCl_3$ was allowed to drip during the exposure. For excitation of spark spectra a 40,000-volt transformer consuming about a kilowatt was used, with condensers of 0.006Hμf capacity in parallel with the spark in the secondary circuit. Comparison arc and spark spectra of graphite, silver, and copper were photographed adjacent to those of the electrodes plus lanthanum salt so that lines due to the electrodes or to atmospheric gases could be recognized and avoided during measurement. Finally, the arc spectrum of iron was recorded alongside each lanthanum spectrogram to supply the scale of standard wave lengths from which the values for lanthanum lines were derived.

The wave-length interval from 2,500 A in the ultra-violet to 11,000 A in the infra-red was investigated with concave gratings, while the shorter wave portion to 2,000 A was photographed with a quartz spectrograph. Since these spectrographs have already been described in connection with their use in the study of yttrium spectra [4] further details concerning them can be dispensed with here.

Most of the spectrograms were made on photographic plates of thin glass coated with Eastman 33 emulsion, the plates being sensitized with pinaverdol, pinacyanol, dicyanin, and neocyanin to photograph the longer wave portions. The longest wave length photographed in lanthanum spectra with neocyanin-stained plates was 9,737 A, but the infra-red limit was easily extended to 10,955 A during the past winter by employing Eastman "Q" type plates sensitized with xenocyanine.

2. ZEEMAN EFFECTS

Spectrograms for the study of lanthanum lines in a magnetic field were made with one of the stigmatic concave-grating spectographs

[4] W. F. Meggers, B.S. Jour. Research, vol. 1 (RP12), p. 320, 1928.

referred to above. The spectral range investigated extended from 2,500 A to 8,000 A, the first half of which was photographed in the second-order spectrum with a scale of 1.8 A per millimeter and the remainder in the first order. Photographic plates and procedure were the same as for wave-length measurements described above. The exposures ranged from 30 minutes in the violet to 5 hours in the red, the source being a spark between graphite electrodes upon which $LaCl_2$ solution was allowed to drip from a burette during the exposure.

The magnetic resolution was obtained with a water-cooled Weiss electromagnet operated with a speed-regulated motor-generator set supplying 150 amperes at 98 volts to the magnet windings. With a pole gap of 6 mm, the field strength was about 33,000 gausses. The actual field strength obtaining for each exposure was derived from the measured resolutions of standard lines. The following lines served as field standards:

Element	Wave length	Zeeman pattern
Ca	3,933.670	(1) 3, 5 / 3
	3,968.475	(2) 4 / 3
Al	3,944.025	(2) 4 / 3
	3,961.537	(1) 3, 5 / 3
Zn	4,680.140	(0) 4 / 2
	4,722.163	(1) 3, 4 / 2
	4,810.534	(0, 1) 2, 3, 4 / 2
Na	5,889.965	(1) 3, 5 / 3
	5,895.932	(2) 4 / 3
K	7,664.94	(1) 3, 5 / 3
	7,699.01	(2) 4 / 3

The Ca, Na, and K lines arose naturally from impurities in the La Cl_2 solution, and to these a 2-minute exposure of Al or Zn was added at the end of the La exposure. Thus either four or five lines were always present to reveal the intensity of the magnetic field and the average probable error of such a determination was about one-fourth per cent.

In making the Zeeman-effect spectrograms light from the source was projected onto the slit of the spectrograph by means of a fused quartz lens after passing through a quartz Wollaston prism. A double image was thus obtained which gave a complete separation of light polarized parallel and perpendicular to the lines of force, thus permitting the two polarizations to be photographed simultaneously without overlap.

III. RESULTS

Limited portions of the arc and spark spectra of La have already been described by different observers. The early observations up to 1910 are quoted by Kayser[5]; the only ones worth mentioning here are measurements in arc spectra by Rowland and Harrison (3,104.702 to 5,930.330 A), and by Wolff (2,610.428 to 5,762.040 A).[6]

A list of arc lines (2,610.43 to 6,774.52 A) and another of spark lines (2,216.20 to 6,643.10 A) was published by Exner and Haschek.[7] The arc spectrum of La was investigated in the region of longer wave lengths (5,501.349 to 9,078.99 A) by Kiess,[8] and in the ultra-violet (2,200 to 3,100 A) by Piña de Rubies.[9]

The above-mentioned descriptions refer mainly to arc spectra, they contain little or no information as to which lines belong to ionized atoms, and they cover their respective intervals with different scales of wave lengths and of intensities.

Altogether, their inadequacy as standard descriptions of the successive spectra characteristic of La atoms justifies the preparation and publication of the following results, appearing in Table 1. No mention is made in any of the earlier descriptions of La spectra of hyperfine structure; it was first noted by King[10] and studied by Meggers and Burns.[11] It now appears that a considerable number of the La lines are complex. (Indicated in Table 1 by the letter "c" following the wave length.) Since hyperfine structure of La lines has no particular importance in a general description, and is furthermore the subject of a special investigation, no further discussion of it will be made here; the results in Table 1, either for wave-length values or for Zeeman effects, apply to the center of gravity of a line whether it is narrow or appears widened due to partial resolution of the hyperfine components.

The probable errors of wave-length measurements reported in Table 1 are usually less than 0.01 A for the stronger lines between 3,100 and 6,000, but the errors for the remaining lines are somewhat larger since they were measured for the most part with smaller dispersion. Many lines appearing enhanced or only on the spark spectrograms are hazy and unsymmetrical; such lines are not susceptible of precise measurement and may be in error by several hundredths of an angstrom unit.

Any attempt to describe the atomic spectra of La must contend with the nuisance of bands due to molecular compounds. In an investigation of the band spectra of LaO, Meggers and Wheeler[12] measured more than 300 band heads in the ordinary arc spectrum and classified the bands in possibly nine systems. The bands appear with considerable intensity throughout almost the entire range from 4,300 to 9,800 A, causing difficulty and uncertainty in the detection

[5] H. Kayser, Handbuch der Spectroscopie, vol. 5, p. 655, S. Hirzel, Leipzig, 1910.
[6] A. Rowland and C. N. Harrison, Astrophys. J., vol. 7, p. 373, 1898; E. Wolff, Zeitschr. f. wis. Phot., vol. 3, p. 395, 1905.
[7] F. Exner and E. Haschek, Die Spektren der Elemente bei Normalem Druck, vol. 2, p. 114, 1911; vol. 3, p. 105; 1912. F. Deuticke, Wien.
[8] C. C. Kiess, B. S. Sci. Paper No. 421, vol. 17, p. 318, 1921.
[9] S. Piña de Rubies, Anales Soc. Esp. Fis. Quim., vol. 23, p. 444, 1925.
[10] A. S. King and E. Carter, Astrophys. J., vol. 65, p. 86, 1927.
[11] W. F. Meggers and K. Burns, J. Opt. Soc. Am., vol. 14, p. 449, 1927.
[12] W. F. Meggers and J. A. Wheeler, B. S. Jour. Research, vol. 6 (RP273), p. 239, 1931.

of the weaker atomic lines. Since the data for LaO band heads (3,565 to 9,150 A) have already been published, they will be omitted here, and no reference to bands will be found in Table 1 except when coincident or unresolved from lines belonging to the atomic spectra. Observations of the arc spectrum of La in the infra-red with xenocyanine plates revealed another long sequence of band heads extending from 9,111 to 9,729 A. These constitute the 0–2 sequence of System VII, and are presented here as Table 2.

The only published Zeeman effects of lanthanum lines are those observed by Rybar[13] in 1911; they extend over the range 2,791 A to 5,188 A and include about 215 lines. These observations are fairly satisfactory, and it was at first my intention only to supplement them with data for the longer waves. However, a trial exposure in the ultra-violet indicated that Rybar's results might be improved and extended by reobservation, and the desirability of having the magnetic resolutions of La lines strictly comparable over a wide range of spectrum finally persuaded me to extend measurements to the same ultra-violet limit. In column 5 of Table 1, the observed Zeeman effects are given for 460 La lines ranging in wave length from 2,798 A to 7,483 A. A few lines observed by Rybar, but not measurable on my spectrograms, are quoted and followed by the letter R. The patterns are presented in the standard notation for Zeeman effects; that is, the separations are expressed in decimal parts of a, the separation of a normal triplet, components polarized parallel to the magnetic field being inclosed in parentheses followed by the perpendicular components. In resolved complex patterns the strongest components are printed in bold-face type. For unresolved patterns a conscious effort was made to measure the strongest components when the type could be easily recognized and a symbol added to indicate the intensity distribution among the fused components. For this purpose, the notation used by Back[14] for distinguishing various types of intensity gradients was employed. The letters A or B after a Zeeman effect mean that the pattern is complex but unresolved, and A indicates that the maximum intensity for perpendicular components is at the edge of a group, while B signifies that it is in the middle. The distinction between strongest component inside or outside of the group is shown by A^1 and A^2, respectively. The interpretation of these Zeeman effects will be given in another paper dealing with the spectral series classification of La lines.

An important contribution to the description of the atomic spectra of La is found in the temperature classification of La lines by King and Carter.[15] From an examination of the furnace, arc, and spark spectra in the interval 2,800 A to 8,400 A data were obtained for a classification of 695 La lines according to the temperature required for initial appearance and the rate of change of line intensity as the temperature is increased. These lines were divided into five classes. Lines in Classes I and II appear at low temperature (2,000° C.), but those of Class I show a slower change from low to high temperature

[13] S. Rybar, Math. es Phys. Lapok, vols. 20–21, p. 198, 1911–12; Phys. Zeitschr. vol. 12, p. 889, 1911, a partial list.
[14] E. Back, Zeitschr. f. Phys., vol. 15, p. 212, 1923.
[15] A. S. King and E. Carter, Astrophys. J. 65, p. 86; 1927.

than those of Class II, and as a rule are less conspicuous in the arc. Lines of Class III are usually well developed at medium temperature (2,200° to 2,300° C.), while lines clearly associated with high temperatures (2,600° to 2,800° C.) are placed in Classes IV and V, those of Class V being absent or very faint in the furnace spectrum. A large number (230) of the lines thus classified are enhanced in the spark and more than half of these appear in the furnace. This indicates that La atoms are ionized with relative ease, which accounts for the great prominence of spark lines in the ordinary arc. In fact, a majority of the La atoms appear to be ionized in the 220-volt arc, and there can be no doubt that the best method of developing the spectrum of neutral atoms is by means of a temperature-controlled vacuum furnace which restricts ionization and also eliminates confusion with molecular spectra. A few lines not detected on my spectrograms were measured on furnace spectrograms by Professor Russell; they are marked H. N. R. in Table 1.

In the last column of Table 1 an attempt is made to assign each observed wave length to its proper atomic origin. This separation of lines into La I, La II, La III spectra is based primarily upon the relative intensities and other characteristics appearing in column 2. It is supported by the temperature classification and further description in column 3 and by Zeeman effects (column 5) describing combinations of spectral terms having even multiplicity for La I and La III lines, but odd multiplicity for La II lines. In the infra-red where data on spark intensities, temperature classes, and Zeeman effects are lacking, the lines are assumed to belong to the La I spectrum unless they are accounted for as combinations of the La II spectral terms. The significance of the symbols and abbreviations used in Table 1 is summarized as follows:

h=hazy (n for King and Carter).
l=shaded to long wave lengths.
M=molecular spectrum, La O band head.
p=part of band structure.
d=double.
c=complex.
E=enhanced line.
A=stronger in furnace than in arc.
A^1=strongest *s*-components of Zeeman effect inside.
A^2=strongest *s*-components of Zeeman effect outside.
B=strongest *s*-components of Zeeman effect in center.
w=wide.
W=very wide.
us=unsymmetrical.
ur=unresolved.
R=Zeeman effect by Rybar.
H. N. R.=wave length by Henry Norris Russell.
e=appearing only at negative electrode.

TABLE 1.—*Wave lengths and Zeeman effects in lanthanum spectra*

λ (air) I. A.	Intensity arc spark B. S.	Arc intensity and temperature class K and C	ν (vac.) cm^{-1}	Zeeman effect	Spectrum
10,954.6	3		9,126.09		II
10,952.0	1		9,128.25		I
10,739.66	5		9,308.73		I
10,612.56	10		9,420.21		I
10,552.41	6		9,473.91		I
10,522.09	10		9,501.21		I
10,483.0	2		36.6		I
61.69	15		56.07		I
50.82	20		66.01		I
23.4	1		9,591.2		I
10,409.55	3		9,603.93		I
10,372.4	1		38.4		I
57.70	20		52.01		I
49.08	40		60.05		I
37.20	3		71.15		I
32.40	2		75.64		I
30.3	1		77.6		I
10,318.2	2		9,689.0		I
10,294.68	10d		9,711.09		I
85.64	3		21.52		I
81.34	10		23.69		I
78.52	3		26.37		I
74.85	10		29.84		I
34.78	2		67.93		I
23.76	1		78.46		I
19.83	3		82.22		I
10,209.85	2		9,791.78		I
10,186.5	2		9,814.2		II
84.60	20		16.06		I
77.74	6h		22.67		I
54.74	40		44.92		I
43.38	2		55.95		I
41.20	10		58.06		I
30.82	5		68.17		I
10,111.9	2h		9,886.6		I
10,093.54	1		9,904.62		II
83.96	2		14.03		I
66.77	6		30.95		I
58.79	2		34.84		I
54.82	2		42.76		I
29.74	2		67.62		I
14.45	4		82.84		I
10,005.73	50		9,991.54		I
9,988.47	10		10,008.80		I
81.24	6		016.05		I
80.38	10		016.91		I
65.70	3		031.67		I
32.72	2		064.98		I
20.82	150		077.06		I
9,911.08	3		086.95		I
9,893.82	4		104.55		II
81.24	100		117.42		I
62.60	3		136.54		I
52.58	6		146.85		I
48.70	4		150.84		I
42.0	2		157.8		I
33.30	3h		166.74		I
05.2	1h		195.9		I
9,894.20	2		196.92		I
9,775.09	8		227.28		I
72.24	20		230.26		I
68.82	3h		233.85		I
37.09	100		267.20		I
13.52	3		292.11		I
9,709.45	10		10,296.42		

TABLE 1.—*Wave lengths and Zeeman effects in lanthanum spectra*—Continued

λ (air) I. A.	Intensity arc spark B. S.	Arc intensity and temperature class K and C	ν (vac.) cm⁻¹	Zeeman effect	Spectrum
9,706.48	20		10,299.57		I
9,699.64	20		306.84		I
96.7	1		310.0		I
92.6	2		314.3		I
72.94	3		335.29		II
72.04	8		336.25		I
57.00	20		352.35		II
46.47	3		363.65		I
40.81	30		369.73		I
33.72	40		377.36		I
9,631.84	2		379.38		I
9,570.38	5		446.04		I
63.60	4		453.45		II
60.69	10		456.63		I
42.06	50		477.05		I
41.23	20		477.96		I
9,528.0	1h		492.5		I
9,485.15	15		539.91		I
84.2	1		541.0		I
76.98	3		548.99		I
74.45	5		551.81		I
67.25	2		559.84		I
61.82	60		565.89		I
57.62	2		570.59		I
41.7	1		588.4		I
38.30	100		592.23		I
15.64	3		617.71		I
9,412.65	100		621.08		I
9,398.2	1		637.4		I
90.56	4		646.07		I
77.71	3		660.66		I
76.10	3		662.49		I
72.57	30		661.51		I
46.69	15		696.04		II
28.87	2		716.47		I
24.5	1		721.5		I
9,312.9	1h		724.5		I
9,293.3	2h		757.5		I
87.5	1h		764.2		I
60.42	3		795.69		II
54.70	10		802.36		I
50.06	20		807.78		I
26.63	30		835.22		I
9,219.64	10		843.44		I
9,172.88	5		898.71		I
72.39	10		899.30		I
57.13	10		917.46		I
51.62	6		924.03		I
46.75	2		929.85		II
43.78	5		933.40		I
42.24	6		935.24		I
27.5	1		952.9		II
19.18	20		962.89		I
09.25	2		974.84		I
9,101.10	2		984.67		II
9,096.71	3		10,989.97		II
79.10	50		11,011.29		I
58.63	2		036.17		I
56.53	5		038.73		I
46.97	2		050.39		I
25.05	4		077.23		I
16.80	2		087.37		II
9,008.26	6		097.88		I
8,977.39	2		136.04		I
8,970.07	3		11,145.13		I

TABLE 1.—*Wave lengths and Zeeman effects in lanthanum spectra*—Continued

λ (air) I. A.	Intensity arc spark B. S.	Arc intensity and temperature class K and C	ν (vac.) cm⁻¹	Zeeman effect	Spectrum
8,965.41	2		11,150.92		I
63.63	10		153.13		I
57.74	50		160.47		I
48.89	2		171.50		I
47.95	1		172.68		I
8,917.70	1h		210.58		I
8,891.06	1		244.17		I
84.24	2		252.80		I
79.56	3		258.73		I
75.05	2		264.45		I
71.00	4		269.60		I
67.35	3		274.24		I
39.64	20		309.57		I
25.86	50		327.23		I
21.66	1h		332.62		I
18.96	20		336.10		I
8,810.57	3		346.89		II
8,797.6	2h		363.6		I
81.98	2		383.83		II
72.02	1		396.76		I
67.92	4		402.07		I
60.4	1		411.9		I
48.42	50		427.50		I
24.12	1		459.33		I
20.42	20		464.19		I
8,703.13	5		486.97		I
8,674.40	60		525.01		I
72.10	30		528.07		I
50.82	2		556.43		II
24.22	6		592.07		I
8,621.55	2		595.66		I
8,590.97	6		636.94		I
58.9	1		680.5		I
45.44	50		698.94		I
43.46	20		701.65		I
29.68	3		720.55		I
14.65	3		741.24		II
13.55	15		742.76		I
8,507.37	10		751.29		I
8,484.01	2		783.65		II
76.48	30		794.12		I
67.62	15		806.45		I
8,440.06	3		845.01		I
8,379.80	20		930.18		I
58.50	2h		960.59		I
46.60	100	12 III	977.64		I
34.44	3		11,995.11		I
24.72	100	15 III	12,009.12		I
24.59	H. N. R.	1 III A	009.30		I
23.35	1		011.10		II
16.05	10	2 IV A	021.64		I
8,302.82	4		040.80		I
8,247.46	60	10 III	121.62		I
37.90	3		135.68		I
11.65	2		174.48		I
8,203.38	3		186.75		I
8,159.05	10 M(?)		252.96		II(?)
8,086.10	20+M4	15 III	363.50		I
84.53	3		365.92		I
59.5	3h 3h		404.3		II
51.38c	10 2	10 III	416.82		I
8,001.91	4 1	4 III A	493.58		I
7,964.86	5 2	6 III	551.70		I
48.30	H. N. R.	10 III	577.85		I+*M*
7,931.18	1 —		12,605.00		I

TABLE 1.—*Wave lengths and Zeeman effects in lanthanum spectra*—Continued

λ (air) I. A.	Intensity arc	Intensity spark B. S.	Arc intensity and temperature class K and C	ν (vac.) cm^{-1}	Zeeman effect	Spectrum
7,927.83	1	2		12,610.33		II
7,891.69	1	2		668.08		II
79.93	2	4		686.98		II
64.98	1	—		711.10		I
41.76	3	1	2 III A	748.74		I
7,838.83	1	1		753.50		II
7,740.54	(?)	2h		915.45		II+M
7,737.74	1h	(?)		12,920.12		I+M
7,664.38	4	2	? III	13,043.78		I
7,612.94	3	3		131.92		II
7,539.24	10	3	15 II	260.29		I+M
33.64	2	(?)		270.14		I
7,501.78	1	(?)		326.50		I
7,498.82	2	2	5 III A	331.76		I
89.15	(?)	1		348.98		II
83.48c	15	30	20 IV E	359.10	(0.00) 1.12	II
7,463.08c	5	2	10 III	395.61		I
7,382.73	6	2	5 III A	541.40		I
79.71			10 III A	546.94		I+M
45.36c	25	7	20 III A	610.30	(0.42) 1.18	I
44.42	H. N. R.		2 III A	612.03		I
40.08	—	2		620.08		II
34.18c	50	10	60 II	631.04	(0.00 w) 1.30 w	I
20.90	2	1		655.77		I
7,308.46	2h	(?)		679.01		I+M
7,297.99	—	2		698.63		II
85.83	1	(?)		721.50		I
82.36	100	150	100 III E	728.03	(0.00 w) 1.26	II
70.30	H. N. R.		5 II A	750.81		I
70.07	H. N. R.		10 III	751.24		I
66.13	2	5		758.70		II
63.68	2	(?)		763.34		I
62.83	2	(?)		764.95		I
50.38	1	—		788.59		I
19.92	15	2	15 II A	846.76		I
17.16	2	(?)		852.06		I
7,213.95	1	2		858.22		II
7,161.25	40	10	50 III	960.20	(0.00) 0.91	I
58.11c	30	10	50 II A	966.32	(0.00) 1.27	I
51.92	H. N. R.		1 III A	978.42		I
49.76	2	1	2 III	13,982.63		I
18.6	(?)	2		14,043.8		II
16.8	(?)	3		047.4		II
7,104.7	(?)	3h		071.3		II
7,098.18	2	(?)		084.24		I
92.40	H. N. R		2 I A	095.72		I
79.74	—	4		120.92		II
76.36	3	2	3 III	127.67		I
68.37	60	10	100 II	143.64	(0.69) (?)	I
66.24c	200	300	400 III E	147.90	(0.00) 0.70	II
62.4	1h	(?)		155.6		I
45.96c	200	30	300 II	188.62	(**0.21,** 0.65) 1.04, **1.47**	I
32.07	25	5	15 III	216.65	(0.60) 1.27	I
23.67c	150	20	150 III	233.66	(0.00) 1.16	I+M
7,013.15	2	1		255.00		I
6,978.09	2	1		326.62		I
76.87	2	1	3 III	329.13		I
68.78	2	25	tr V E	345.76	(0.00) 0.81	II
58.11	30	100	20 IV E	367.76	(0.21) 0.96	II
54.54c	20	20	8 IV	375.14		II
52.52c	10	10	2 IV	379.31	(0.00) 1.10	II
35.03	50	8	50 III	415.58	(0.48) 1.14	I
25.27	80	15	100 III	435.90	(0.00w) 1.58 A^2	I
18.33	8	2	8 III A	450.38		I
6,917.26	10	3	10 III A	14,452.61		I

TABLE 1.—*Wave lengths and Zeeman effects in lanthanum spectra*—Continued

λ (air) I. A.	Intensity arc	Intensity spark B. S.	Arc intensity and temperature class K and C	ν (vac.) cm⁻¹	Zeeman effect	Spectrum
6,903.08	2	1	1 III A	14,482.30		I
6,902.08	3	3	1 III	484.40		I(?) II
6,899.63	2h	1	tr V	489.54		
98.41			tr V	492.10		I
59.03	4	5	tr V	575.31		II
37.91	15	15	3 IV(?) E	620.32		II
34.07	20	20	4 IV(?) E	628.54	(1.05) (?)	II
30.83	1	6	tr V E	635.48	(0.00) 0.98	II
23.80	40	10	15 II A	650.56	(0.00) 1.15	I
21.51	5d	2	3n V	655.47		I
19.14	1	—		660.57		I
16.29			1n V(?)	666.70		
13.68	5	50	1 V(?) E	672.32	(1.04) 1.29 B	II
08.88c	30	30	6 IV	682.65	(0.00h) 1.56h	II
6,801.38	1	5		698.85	(0.00) 1.10	II
6,796.73	4	1	4 II A	708.90		I
83.55	1	—	tr IV A	737.48		I
78.19	1	—	tr V	749.14		I
76.69	1	—	1 III A	752.40		I
74.28c	80	100	30 III E	757.65	(6.00w) 1.10	II
60.73	H. N. R.		1 III A	787.23		I
60.23	1	1		788.32		I
53.05	40	10	50 I A	804.04	(0.00W) 1.51 A²	I
50.47	1	1		809.70		II
48.12c	10	3	10 II A	814.86		I
41.20	2	1		830.07		I
37.29	1	—		838.67		I
32.80c	2	40	1 V E	848.57	(0.00) 0.99	II
18.68	2	60	tr V E	879.78	(0.69) 1.12 B	II
15.96	1	—	1 IV A(?)	885.80		I
14.08	5	80	2 V E	889.97	(0.00) 1.38	II
6,709.49	150	30	200 I	900.15	(0.00) 1.13	I
6,699.86	3	1	4 III A	921.57		I
99.26	2	2	2 III(?)	922.91		I
92.86c	20	4	30 I A	937.18	(0.00) 1.06	I
76.14	1	3		974.59		II
71.41c	15	40	6 IV(?) E	14,985.20	(0.63) 1.17	II
64.45	1	—		15,000.85		I
61.40c	60	15	80 I A	007.72	(0.65) 1.23 B(?)	I
58.06	1	—		015.25		I
50.81c	80	20	100 I A	031.62	(0.00w) 0.88	I
45.15	7	3	8 IV	044.42		I
44.40c	30	5	40 I A	046.12		I
42.79	10	100	3 V E	049.77	(0.33) 0.82	II
36.53	3	5	1 V	063.96		II
31.20	3	3	3 V(?)	076.07		I(?)
28.4	1	1	1 IV A	082.4		I
19.10	—	2		103.63		II
16.59c	60	10	80 I	109.36	(0.59) 1.12 B	I
12.48	3	1		118.75		I
08.25c	40	5	40 II	128.43	(0.00) 1.01	I
07.7	1	—	3 IV	129.7		I+M
6,660.17c	25	5	50 II A	146.95	(0.35) 1.12	I
6,599.48			tr IV A	148.53		
93.45c	40	5	60 I	162.39	(0.00w) 1.30 A²	I
90.59	1	—		168.97		I
82.18	4	2	6 IV	188.35	(0.00h) 1.41	I
78.51c	200	100	400 I	196.82	(0.00) 1.00	I
70.96	2	(?)	2n III	214.28		II
68.54	1	(?)		219.89		I
65.45	40	(?)	40 I A	227.05		I
55.95			3 III A	249.12		I
55.11	2	(?)	1 V	251.07		I
54.18	2	(?)	1 V	253.23		II
6,551.78	1	(?)		15,258.82		I

TABLE 1.—*Wave lengths and Zeeman effects in lanthanum spectra*—Continued

λ (air) I. A.	Intensity arc	Intensity spark B. S.	Arc intensity and temperature class K and C	ν (vac.) cm^{-1}	Zeeman effect	Spectrum
6, 549. 16	2	(?)	2n III(?)	15, 264. 92		I
43. 17c	300	100	500 I	278. 90	(**0.33,** 0.99) 0.00, 0.74, 1.41, **2.07**	I
29. 72c	4	4h	4 III(?)	310. 37		II
26. 99c	100	200	100 III E	316. 77	(**0.00,** 0.22) 0.94 A^2	II
23. 86	2	1	2 III A(?)	324. 12		
						I
20. 70	15	3	20 IV	331. 55	(0.00h) 1.10h	I
19. 30	3	1	4 IV	334. 84		I
17. 35	1	—		339. 43		I
6, 506. 25	4	2	6 IV	365. 59		I
6, 498. 19	30	250	7 IV(?) E	384. 66	(0.00) 0.81	II
92. 86	4	2	5 V	397. 29		I
85. 54c	20	5	20 II A	414. 66	(0.00) 1.10	I
80. 20	1	—		427. 37		I
68. 44c	10	3	8 II A	455. 42		I
55. 99	250	100	300 I	485. 22	(0.00) 1.18	I
54. 50c	150	50	200 I	488. 80	(**0.38,** 1.11) 0.80, 1.54, **2.26**	I
50. 34	6	3	8 II A	498. 78	(0.00) 1.29	I
49. 94	3	—		499. 74		I
48. 25	4	2	10(?) II A	503. 81		I
48. 10	20	10	50(?) II A	504. 17		I
46. 62	15	200	5 V E	507. 73	(0.00w) 1.43 A^2	II
43. 05	3	50h	1 V	516. 32	(0.00w) 0.76 A^1	II
26. 60	2	1		556. 04		I
20. 90	1	—		569. 85		I+M
17. 23	2	1	3 III(?) A	578. 75		I+M
15. 39	1	1		583. 22		II
6, 410. 98	200	60	300 I	593. 94	(0.00) 1.09	I
6, 399. 04	20	400	10 V(?) E	623. 04	(0.00) 1.04	II
94. 23c	400	100	600 I	634. 79	(0.00 w) 1.02 A^1	I
90. 48	100	200	80 III	643. 96	(0.00) 1.03	II
80. 48	1	1	1 V	664. 48		I
75. 50	2	—		780. 72		I
75. 11	2	—	2 V	681. 68		I
74. 08	3	30	1 V	684. 21	(0.00 W) 1.67 A^2	II
60. 20c	30	10	30 II	718. 44	(0.00) 0.89	I
58. 12	20	30	5 IV	723. 58	(0.99) 0.49, 1.52	II
56. 38	3	1	4 III A	727. 88		I
53. 63	1	—		734. 69		I
39. 16	2	1	2 III A	770. 61		I
37. 88	2	3	1 V	773. 79		II
33. 74	3	2	2 IV(?)	784. 10		I
33 24	2	1	2 III(?)	785. 35		I+*M*
30. 42	3	1	2 III A	792. 38		I
25. 90	100	20	150 I	803. 67	(0.63, **0.99**) 0.25, 0.63, **1.01,** 1.38, 1.76	I
20. 39c	100	200	80 III	817. 44	(0.44) 0.87 B	II
18. 26	5	2	12 III A	822. 78		I
15. 79	3	50	1 V	828. 96	(0.95) 0.49, 1.43	II
10. 91	8	200	4 V E	841. 20	(0.27) 1.10 B	II
10. 13	8	5	12 IV	843. 16		I
08. 87	2	?	2 III	846. 32		I
08. 21	2	?	3 III	847. 98		I
07. 25	1	20h	tr IV	850. 40	(0.00) 0.51	II
6, 305. 46	10	10	5 IV	854. 90		II
6, 296. 08c	100	300	50 IV E	878. 52	(0.00 W) 1.20 A^2	II
93. 57c	60	10	80 II A	884. 85	(0.00) 1.33	I
88. 56	6	3	7 III A	897. 50		I
87. 73	7	3	8 III A	899. 60		I
78. 31	1	1		923. 46		I
73. 76	4	100	2n III(?)	935. 01	(0.00) 1.04	II
66. 00c	40	20	60 III	954. 74	(0.00) 1.06	I
62. 30	100	300	{30(?) 50(?)} III	964. 17	(0.00 w) 1.10 A^1	II
49. 92c	300	100	500 I	15, 995. 79	(0.00) 1.13	I
38. 58	12	3	15 III A	16, 024. 86		I
36. 76c	7	2	10 III A	029. 54		I
6, 236. 17	8	3	12 IV	16, 031. 06		I

TABLE 1.—*Wave lengths and Zeeman effects in lanthanum spectra*—Continued

λ (air) I. A.	Intensity arc	Intensity spark B. S.	Arc intensity and temperature class K and C	ν (vac.) cm⁻¹	Zeeman effect	Spectrum
6,234.85c	10	3	15 III A	16,034.45	(0.00) 1.26	I
33.51	10	3	15 III A	037.90		I
32.56	1	1		040.34		I
25.33	2h	1		058.97		I
24.24	1	1		061.78		I
19.46	2	1	2 V	074.13		I
18.19	5	2	7 III	077.41		I
14.35	2	1		087.34		I+M
06.76	2	1		107.02		I
6,203.51	3	50l	2 V	115.46	(0.17) 1.14h	II
6188.09	5	100l	1 V	155.61	(0.00 W) 1.02 A^1	II
74.15	4	6	1 V	192.09	(0.00) 0.63	II
73.74			1 IV A	193.17		I
72.72	10	10	5 V	195.84	**(0.00,** 0.32, 0.63) 1.69 A^2	II
67.69	2	1		209.05		I
65.69c	30	10	40 II	214.31	(0.88) 0.87, **1.43,** 1.99	I
65.02	3	1	2 IV	216.07		I
54.55	1	—		243.66		I
46.53	10	15	5 IV	264.85	(0.00 W) 1.69 A^2	II
45.29	3	2	3 III	268.13		I
42.98c	10	5	10 III	274.25	(0.00) 1.15	I
41.71	3	—		277.61		I
36.48	2	1	2 II A	291.49		I
34.39c	20	8	30 III	297.34	(1.34) 1.37	I
31.92	1	1		303.60		II
29.57c	30	50	15 IV(?)	309.85	(0.00 W) 0.99 A^1	II
27.04	8	5	12 III A	316.59		I
26.09	20	50	10 V(?)	319.12	(0.34) 0.92 B	II
23.75	2	1	2 IV	325.36		I
21.27			1 IV	331.97		I
20.34			1 IV	334.45		I II
11.71c	20	7	30 II	357.52	(0.00) 1.17	I
08.47c	40	10	60 II	366.19	(0.53) 1.34 B	I
07.26	4	2	12 II A	369.43		I
6,100.37	10	30	10 V	387.92	**(0.00,** 0.34) **0.84,** 1.16	II
6,092.22	2	1	1 III A	409.85		I
88.00	2	1	1n IV	421.22		I+M
85.43	2	10	1n V	428.15	**(0.00,** 0.74) 1.20, **1.90**	II
84.86	5	3	8 III	429.69		I
75.24			1 III A	455.71		I
74.01	3	5	1 III A	459.04	(0.21) **1.12**	I II
72.04	3	2	4 III A	464.38		I
68.70c	20	6	30 III	473.44	(0.75) **0.40,** 1.90	I
67.13	2	6	1 V(?)	477.71	(0.00) 1.49	II
61.42	2	2	2 V(?)	493.23		II(?)
46.07	2p(?)	2	1 IV(?)	535.10		II(?)
44.8	2	2	2 III A	538.6		I
41.6	2	2	2 III	547.3		I
38.57c	20	5	25 III A	555.64		I
37.98	1	2		557.25		II
35.12			2 V	565.11		
34.5	2h	2	3 V	566.8		I+M
32.38	5	2		572.63		I
31.46	5	2	3n IV(?)	575.15		I+M
25.09	2p(?)	1	1 IV(?)	592.68		I
17.16	3	2	1 III A	614.54		I
6,007.34c	50	10	50 III A	641.70	(0.00 W) 1.77 A^2	I
5,992.35c	3	2	2 III A	683.33		I
91.98	1	4h		684.36		II
82.34	10	4	5 III A	711.25		I
75.75c	10	6	3 III A	729.68		I+M
73.52c	15	120l	5 V E	735.92	(0.00) 1.20	II
71.09	3	8		742.73	(0.00) 1.18	II
70.58	H. N. R.		1 III A	744.16		I
5,965.30	3	2	1 III	16,758.98		I

TABLE 1.—*Wave lengths and Zeeman effects in lanthanum spectra*—Continued

λ (air) I. A.	Intensity arc	Intensity spark B. S.	Arc intensity and temperature class K and C	ν (vac.) cm⁻¹	Zeeman effect	Spectrum
5,962.59	4	2	1 III A	16,766.60		I
61.43	2	3		769.86		II
60.59	4	3	3 III A	772.23		I
57.90	—	4		779.80		II
48.30c	10	20		806.9	(0.52) 0.86 h	II+M
40.83c	3	1	1 III A	828.01		I
36.22c	15	20	12 V E	841.08	(0.00) 1.21	II
35.29c	20	5	15 II A	843.72	(0.00 W) 1.72 A²	I
30.68	100	20	400 I	856.81		I
30.61	200	40		857.01	(0.00) 0.87	I
28.48	5	4	4 III A	863.07		I
27.71	5	30		865.26	(0.00) 1.30	II
18.26	—	4		892.19		II
17.64c	20	6	15 II A	893.96	(0.27) 1.10 h	I
04.28	4	3	2 III A	932.20	(0.00) 1.25	I
01.95	5	401	2 IV E	938.87	(0.00 W) 1.60 A²	II
5,900.75c	3	2	1 III A	942.31		I
5,894.84c	20	10	8 III A	959.30		I
92.66	3	4	1 V	965.58	(0.00) 1.54	II
85.23	—	1		16,986.99		II
80.63c	40	50	30 III E(?)	17,000.28	(**0.00**, 0.42) 0.54, 0.96, 1.38	II
77.96	3	2	1 III A	008.00		I
77.62	4	2	2 III A	008.98		I
74.72c	8	4	8 III A	017.38		I
74.00	5	6	3 IV	019.47	(0.00) 1.49	II
69.93	2	2	1 III A	031.27		I
63.70	30	80	20 V E	049.36	(0.00) 0.96	II
57.44	2	—		067.58		I
55.57c	20	8	15 II A	073.03	(0.00 W) 1.42 A²	I
52.26c	6	4	2 III A	082.69		I
48.95	3	20		092.36	(0.00) 0.54	II
48.37c	15	5	8 III A	094.05	(0.00) 0.90	I
45.02c	10	5	6 II A	103.85	(0.00) 1.18	I
39.77	3	2	2 II A	119.23		I
29.71c	20	10	10 III A	148.77	(0.00) 1.75	I
28.44	2	2		152.51		II
27.56c	8	3	3 III A	155.10	(0.59) 1.50(?)	I
23.82c	15	10	10 III A	166.11	(0.00 w) 0.96 h	I
21.98c	30	20	30 III	171.54	(0.00) 0.93	I
13.44	2	1	1 III A	196.76		I
08.63	4	8		211.00		II
03.31	40	60	15 IV(?)	211.95	(0.00) 0.75	II
06.56	3	8		217.14		II
05.77	80	120	50 III E	219.48	(0.00) 1.09	II
5,802.10c	2	1	1 III A	230.37		I
5,797.57	100	150	50 III E	243.84	(0.00) 1.24	II
91.32c	200	60	400 I	252.45	(0.00 W) 1.31 B	I
89.22c	150	40	250 I	258.71	(0.15) 1.21	I
81.02	2	3		293.20		II
79.91	2	4		296.52	(0.00) 1,38 h	II
69.97c	25	20	25 III A	326.32		I
69.32	80	30	80 I	328.27	(0.00) 1.01	I
69.06c	40	60	50 VE	329.05	(0.00) 1.09	II
61.83c	50	20	60 I	350.80	(0.94) **0.00**, 0.68, 1.34	I
49.59	—	2		387.73		II
44.41c	60	20	80 III	403.41	(0.00 w) 1.24	I
42.93c	4	3	2 IIIA	407.90		I
40.65c	80	20	100 I	414.81	(0.47) 0.59 B	I
34.93c	6	4	5 IIIA	432.18	(0.00) 0.92	I
27.29	5	20	4 VE	455.43	(0.00) 1.45	II
20.01c	10	4	10 IIIA	477.65	(**0.16**, 0.48, 0.81) 1.93A²	I
14.55c			1 IIIA	494.35		I
14.01	4	3	5 IIIA	496.00	(0.62) (?)	I
12.39c	20	20	20 IIIE(?)	500.96	(0.00) 0.98	II
10.85	2p(?)	(?)	2 III	505.68		I
5,703.32	20	20	10 III	17,528.80	(0.00) 1.48	I II

TABLE 1.—*Wave lengths and Zeeman effects in lanthanum spectra*—Continued

λ (air) I. A.	Intensity arc	Intensity spark B. S.	Arc intensity and temperature class K and C	ν (vac.) cm⁻¹	Zeeman effect	Spectrum
5,702.57			2 III	17,531.10		I
01.15			1 III	535.47		I
5,700.25			3 III	538.24		Cu. (?)
5,699.32	3	2	5 III	541.10		I
96.18	30	15	40 I	550.77	(0.00w) 0.80A[1]	I
71.54	10	100	8 VE	627.02	(0.00) 0.79	II
69.97			1 IV	631.90		Ce (?)
61.34c	2	2	1 IIIA	658.78		I
57.71c	30	15	50 II	670.10	**(0.29,** 0.88) 0.73, 1.33, **1.94**	I
56.54	2	2	1 IIIA	673.76		I
54.8c	20	10	3 IIIA	679.2		I+*M*
52.3	5	10h		687.0		II+M
48.24c	50	30	80 III	699.73	(00.0) 1.12	I
39.31c	8	5	5 IIIA	727.76		I
32.02	15	6	25 II	750.70	(0.00) 0.93	I
31.22	60	10	100 I	753.22	(0.00W) 1.45 A[3]	I
5,610.53	2	20		818.69		II
5,598.52	3	—		856.92	(0.00) 0.49	I
91.51	1	1		879.30		II
88.33c	100	20	80 II	889.48		I
70.37	3	2	5 IIA	947.16		I
68.45c	30	10	50 II	953.35	(0.44) 1.16	I
66.92	5	40	2 VE	958.28	(0.37) 1.24	II
65.70	10	5	20 II	962.22		I
65.43c	10	5	20 III	963.09	(0.00) 1.52	I
62.54	2	1	2 III(?)	17,972.42		I
47.56	2p(?)	3h		18,020.95	(0.00) 1.13	II
44.90	3	2	6 III	029.60	(0.28) 1.47	I
41.25c	15	10	20 III	041.47	(0.00) 1.25	I
35.66c	20	80	15 VE	059.69	(0.00W) 0.80 A[1]	II
32.17	4	10	3 III	071.08	(0.00W) 0.61h	I II
29.86	2	2	3 III	078.63		I
26.51			2 V	089.59		I
24.40			1 V	096.50		
17.34c	20	7	30 III	119.66	(0.00) 1.10	I
15.28c	5	4	10 III	126.42	(0.25) 1.42	I
07.33			2 III	152.59		I
06.00c	20	5	40 II	156.97	(0.00w) 1.54h	I
03.80c	40	10	80 III	164.23	(0.70) 1.22 B	I
02.66	5	2	10 III	168.00		I
02.24	3	2	4 III	169.38		I
5,501.34	200	70	300 I	172.35	(0.00) 0.80	I
5,498.70	2	1	2n III	181.08		I
93.45	10	20	20 VE	198.45	(0.00w) 1.57 A[3]	II
91.07	5	2	8 III	206.34		I
86.86	3	5	3 V	220.31		II
82.27c	20	40	50 VE	235.57	(0.00W) 1.89 A[3]	II
80.72	4	25	1 VE	240.72	(0.00) 1.03h	II
75.17c	10	6	15 III	259.21	(0.00) 1.08	I
66.91	2	2	3 III	286.80		I
64.37	10	25	25 VE	295.30	(**0.00,** 0.49, 0.97) **0.60**d, 0.49, 0.97	II
58.68c	10	50	20 VE	314.37	(0.00) 1.00	II
55.14	200	40	400 I	326.25	(0.00) 1.20	I
47.59	2	10		351.65	(0.22) 1.14	II
37.55	2	2	5 III	385.54	(0.00) 2.54	I
29.86c	6	5	15 III	411.57	(0.49) 1.04	I
23.82	4	4		432.08		II
22.10			3 IIIA	437.93		I
5,415.67	4	3	8 III	459.82	(0.36) 1.56w	I
5,390.63	(?)	1		545.56		I
81.91	15	100	15 VE	575.61	(0.00) 0.74	II
81.77	5	50		576.10		II
80.97	40	100	80 VE	578.86	(0.00) 0.77	II
80.00	3	1	5 III	582.21		I
5,377.08	20	200	2 VE	18,592.30	(0.00w) 0.82 A[1]	II

TABLE 1.—*Wave lengths and Zeeman effects in lanthanum spectra*—Continued

λ (air) I. A.	Intensity arc	Intensity spark B. S.	Arc intensity and temperature class K and C	ν (vac.) cm^{-1}	Zeeman effect	Spectrum
5, 365. 87	4	2	8 III	18, 631. 14		I
59. 70	2	1	2 III A	652. 59		I
57. 85c	25	10	60 III	659. 03	(0.00) 1.53	I
40. 66	20	100	40 III E	719. 09	(0.00) 1.07	II
33. 42	1	2		744. 50		II
30. 64	1	2		754. 27		I(?)
23. 56	3	2	3 III	779. 22		I
21. 34	1	1		787. 04		I
20. 14	3	2	3 III	791. 28		I
07. 52	3	2	3 III	835. 96		I
04. 01c	20	5	30 III	848. 43		I
03. 54	50	100	100 III E	850. 10	(**0.00,** 0.61) 0.57, 1.17, **1.78**	II
02. 62	30	150	40 V E	853. 37	(0.00) 1.16	II
5, 301. 97c	80	200	200 III E	855. 68	(0.00 w) 1.50 w	II
5, 290. 83	30	50	60 III E	895. 38	(0.34) 0.82 B	II
87. 45	1	1	1 V	907. 46		I
79. 11	6	40	2 V E	937. 33	(0.00) 1.20	II
76. 40	5	4	10 III	947. 06	(0.00) 0.90	I
71. 18	100	30	150 I	18, 965. 82	(0.00) 1.39 A^2	I
59. 38c	30	50	40 III E	19, 008. 37	(0.00 W) 0.46 A^1	II
57. 83	4	3	3 III	013. 98	(0.00) 1.07	I
57. 28	—	2		015. 96		II
53. 45	100	30	100 I	029. 83	(**0.23,** 0.69) 0.57, 1.03, 1.49, **1.95**	I
40. 81	4	3	2 III	075. 72		I
39. 54	4	3	4 III	080. 35		I
34. 27c	150	40	300 II	099. 56	(0.00 W) 2.10 A^2	I
26. 20	2	40l	1 V E	129. 05	(0.00 W) 0.32 W	II
22. 48	—	3h		142. 68	(0.00) 1.15	II
21. 32	—	3h		146. 93		II
17. 83	—	10h		159. 74		II
11. 85c	150	40	300 II	181. 72	(0.00 W) 1.73 A^2	I
5, 204. 14	25	300	12 V E	210. 14	(0.00) 0.86 A^1 (?)	II
5, 191. 50	1	3h		256. 91	(0.00) 1.05	II
90. 34	8	4		261. 21		I
88. 21	40	500	25 V E	269. 12	(0.00) 1.09	II
83. 91	10	10(?)	20 II	285. 10		I
83. 42c	200	400	400 III E	286. 93	(0.00) 1.31	II
79. 11	2	2	2 III	302. 98		I
77. 30c	150	50	300 II	309. 72	(0.00) 1.07	I
73. 83	10	25l	10 IV (?) E	322. 67	(0.00) 1.06	II
72. 89	5	20l	1 V E	326. 19	(0.20) 1.03	II
68. 95	2	2		340. 92		I
67. 79	20	10	20 III	345. 26		I
67. 28	4	10		347. 17		II
64. 03			1 V (?)	359. 34		I
63. 61	20	40	20 V (?) E	360. 92	(0.74) 1.18 B	II
62. 68	2	3		364. 41		II
61. 54	2	1		368. 68		I
58. 68	40	20	80 I	379. 42	(**0.19,** 0.57) 1.05, 1.45, **1.85**	I
57. 43	15	150	15 V E	384. 12	(0.00) 0.66	II
56. 74	20	40	30 V E	386. 71		II
52. 31	1	1		403. 38		I II
45. 42	100	40	200 II	429. 36	(0.00) 0.89	I
39. 16	3	2		453. 03		I
35. 42	3	2	2 V	467. 20		I
34. 37	2	1		471. 18		1
29. 81	3	2		488. 48		I
22. 99	100	200	150 III E	514. 43	(0.00) 1.16	II
20. 87	10	4	10 III	522. 51	(0.00) 0.92	I
14. 55c	100	200	150 III (?) E	546. 63	(0.00) 0.54	II
12. 37	1	2		554. 97		II
09. 12	3	2	2 III A	567. 40		I
07. 54	—	6h		573. 46	(0.00) 1.19	II
06. 23c	100	40	150 II	578. 48	(0.19) 0.62 A^2 (?)	I
5, 103. 11	3	2	2 III	19, 590. 45		I

TABLE 1.—*Wave lengths and Zeeman effects in lanthanum spectra*—Continued

λ (air) I. A.	Intensity arc	Intensity spark B. S.	Arc intensity and temperature class K and C	ν (vac.) cm⁻¹	Zeeman effect	Spectrum
5,096.59	2	1	1 IV (?)	19,615.51		I
90.56	2	20l	tr V E	638.74	(0.00 W) 1.33 A^2	II
86.71	—	3hl		653.61		II
86.22	2	1		655.50		I
80.21	10	40	1 V E	678.76	(0.38) 0.98 w	II
79.37	4	3	5 IV	682.01		I
78.92	3	2	2 V (?)	683.76		I
72.10	3	1	1 III A	710.22		I
67.90c	15	10	15 III	726.56		I
66.99	1	20h		730.10	(0.00) 1.10 h	II
63.76	2	3		742.68		II
62.91	10	20	4 V E	746.00	**(0.00,** 0.66) 0.90, 1.56, **2.32**	II
60.85	2	3		754.04		II
58.56	—	1h		762.97		II
56.46c	60	20	80 II	771.18	(1.20) **0.00,** 0.79, 1.57	I
52.10	1	1		788.25		I
50.57	60	20	80 II	794.24	(0.80) 1.18 B	I
48.04	4	30l	1 V E	804.16	(0.00) 1.16	II
46.87c	30	15	60 III	808.75	(0.00 w) 1.24	I
37.60	2	2		845.20		I
33.24	2	1		862.40		I
19.50	10	5	8 III	916.76		I
14.45	5	30hl		936.82		II
02.12	10	40	3 V E	985.96	(0.00) 1.09	II
5,001.78c	20	6	10 III A	987.32		I
4,999.46c	100	200	200 III E	19,996.60	(0.00 w) 1.28 A^2	II
96.82	6	50	2 V E	20,007.16		II
95.95	1	1		010.64		I
95.17	1	1		013.77		II
94.64	2	1	1 III A	015.90		I
93.87	15	5	20 II	018.98		I
91.27c	40	80	20 IV E	029.41	(0.00) 0.85	II
86.82c	60	100	100 III E	047.28	**(0.00,** 0.43) 0.57, 1.00, **1.43**	II
84.92	3	2	2 IV(?)	054.92		I
84.63	1	1		056.09		I
83.56	2	1		060.40		I
77.95	8	4	8 II A	083.01		I
74.20	—	4h		098.14		II
70.39	50	100	100 III E	113.55	**(0.00,** 0.29) **0.83,** 1.12 us	II
68.59	4d	3	2{III, V} A	120.84		I
64.84	3	2	4 III A	136.03		I
57.77	4	3		164.75		I
56.04	2	2	1 V	171.79		II(?)
52.06	10	40	5 V E	188.00	(0.00) 1.17	II
49.76	50	20	200 I	197.38	(0.00) 0.84	I
46.47c	20	50	20 IV(?) E	210.81	**(0.00,** 0.67) 1.05, **1.82**	II
45.84	3	2	5 III A	213.39		I
35.61	5	10	2 V E	255.28		II
34.83	40	100	20 V E	258.48	(0.00) 0.97	II
25.40	3	2	2 IV	297.27		I(?)
21.80	200	300	400 III E	312.12	(0.00) 1.11	II
20.98	200	300	400 III E	315.50	(0.00) 1.00	II
16.62	3	2	1 III(?) A	333.52		I
11.34	4	10		355.38		II
05.13	4	3	4 III A	381.15		I
04.43	1	2h		384.05		II
4,901.87	15	10	25 I	394.70	(0.00) 0.94	I
4,899.92	150	200	300 III E	402.82	(0.00) 0.80	II
94.24	2	2	1 III	426.49		I
91.43	4	10		438.23		II
87.60	4	3	5 III	454.24		I
86.82	3	2	2 IV	457.51		I
81.94	1	1		477.96		I
80.22	1	10h		485.17		II
4,878.86	10	10	15 III	20,490.89	(0.00) 1.10 R	I

TABLE 1.—*Wave lengths and Zeeman effects in lanthanum spectra*—Continued

λ (air) I. A.	Intensity arc	Intensity spark B. S.	Arc intensity and temperature class K and C	ν (vac.) cm^{-1}	Zeeman effect	Spectrum
4,874.99	1	1		20,507.15		II
70.56	5	2	5 III	525.81		I
68.90	3	1	2 IV(?)	532.80		I
67.37	3	1		539.26		I
60.90	60	80	100 III E	566.59	(0.00) 1.19	II
59.18	2	5h		573.87		II
54.95c	8	6	8 III	591.80	(0.00) 1.21 R	I
50.81	20	10	20 I	609.37		I
50.58	20	30	5 V E	610.35	(0.00) 1.03	II
43.29	4	5	1 V	641.37		II
40.02	20	30	10 V E	655.32	(0.67) 1.30(?)	II
39.51	20	10	25 II	657.49	(0.00) 0.89	I
30.51	5	10	1 V E	695.98	(0.00) 0.76 R	II
26.87c	10	20	4 V E	711.59	(0.33) 1.08 R	II
24.05	80	100	80 III E	723.70	(0.00) 0.79	II
17.55	3	2		751.66		I
17.17	10	6	4 IV(?)	753.29		I
09.00c	60	100	80 V E	788.55	(0.00) 0.51	II
04.04c	50	80	50 V E	810.02	(0.95) 0.49, **1.43**	II
4,800.24	9	6	8 III	826.49		I
4,799.99	8	5	8 III	827.57		I
96.67	10	25	4 V E	841.99		II
94.55	3	3	2 V E	851.20		II
92.46	1	1	tr III A	860.30		I
91.77	1	—		863.30		I
91.39	5	3	5 II	864.96		I
80.55c	2	2	1 V	912.27		II(?)
79.89c	4	3	4 II	915.16		I
75.14c	3	3	2 V	935.96		I(?)
70.43	10	8	15 II	956.63	(0.00) 0.93 R	I
67.80	1h	1h		968.19		I
66.89	60	30	100 I	20,972.19	(0.00) 0.99	I
59.71c	2	2	2 IV(?)	21,003.83		I
58.40	2	3		009.61		II
57.14c	3	2	2 IV	015.18		I
56.97			1 V	015.93		I
53.11c	2	1	1 IV	032.99		I
52.41c	3	2	3 III	036.09		I
50.41c	10	8	15 III	044.95	(0.00) 1.04 R	I
48.73	80	150	100 V E	052.39	(0.00) 1.00	II
43.08c	100	250	100 V E	077.47	(0.52 w) 0.95 B	II
40.27	100	120	150 III E	089.96	(0.00 w) 0.97 A^1	II
39.80	6	15	2 V E	092.06		II
33.82c	8	5	4 V(?)	118.70		I
30.73	2	3h		132.50		II
29.09	1	—	1 V	139.82		I(?)
28.41c	80	100	80 V(?) E	142.86	(**0.00**, 0.32) 1.31, 1.61, **1.91**	II
24.42	20	40	6 V E	160.72	(0.65) 0.95 us	II
23.72	2	1	3 II	163.85		I
22.14	1	2h		170.94		II
19.93c	40	150	15 V E	180.85	(0.00) 1.06	II
17.58	10	50	4 V E	191.40	(0.50) 1.2	II
16.44c	40	80	25 V E	196.52	(**0.00**, 0.60) 0.92, 1.52, **2.12**	II
14.14	4	2	5 I	206.86		I
12.92c	20	40	12 V E	212.35	(**0.00**, 0.47, 0.92) 1.83, **2.26** R	II
08.18c	8	8	8 III (?)	233.71	(0.00) 0.97 R	I
03.27c	30	150	20 V E	255.87	(0.00 W) 1.70 A^2	II
02.64	8	6	10 I	258.72		I
4,700.26c	8	8	8 III (?)	269.48		I
4,699.62c	20	50	20 V E	272.38		II
95.30	3	3		291.95		I
92.50c	50	200	50 V E	304.66	(0.00 W) 1.21 A^2	II
91.17c	25	50	30 V E	310.70	(0.00, 0.46) 0.46 us	II
88.65	8	40	2 V E	322.15	(0.00) 0.96	II
4,684.39	1	2h		21,341.54		II

TABLE 1.—*Wave lengths and Zeeman effects in lanthanum spectra*—Continued

λ (air) I. A.	Intensity arc	Intensity spark B. S.	Arc intensity and temperature-class K and C	ν (vac.) Cm^{-1}	Zeeman effect	Spectrum
4,682.12	4	5		21,351.89		II
73.53	—	1h		391.14		II
71.82c	30	200	40 V E	398.96	(0.00 w) 1.29h	II
68.91c	40	250	50 V E	412.30	(**0.00** 0.34, 0.68) 0.77, 1.12, **1.47,** 1.81 us	II
63.76c	50	300	50 V E	435.94	(0.20) 0.99	II
62.51	100	200	200 III E	441.69	(0.00 W) 0.89 A^2	II
60.70	8	8	8 III	450.02	(0.00) 0.92 R	I
55.49c	80	400	150 V E	474.02	(0.43) 1.20 B	II
53.90c	4	3		481.36		I
52.07	15	30hl	20 I	489.81		I II(?)
50.32	12	8	15 I	497.90	(0.30) 1.13 R	I
48.64	30	20	40 I	505.67	(0.48) ?	I
47.50c	25	100	8 V E	510.94	(**0.00,** 0.31, 0.61) 1.98 A^2	II
46.33	10	10	12 III	516.36	(0.00) 0.89 R	I
45.28	40	100	40 V E	521.22	(0.60) 1.26 B	II
43.11c	5	5	5 III	531.28		I
41.40	—	2h		539.21		II
36.42	10	80	4 V E	562.35	(0.21) 1.00	II
34.95	2	2hl		569.19	(0.00) 1.43	II
33.4	1	10hl		576.4		II
27.35	2	2		604.61		I
23.99	1	2h		620.31		II
19.87c	100	300	150 V E	639.59	(0.00) 0.70	II
15.06c	8	7	15 III	662.14	(1.31) 1.37 R	I
13.38	100	200	200 V E	670.03	(**0.00,** 0.33) **0.83,** 1.16, 1.49	II
05.78	50	100	50 V E	705.79	(0.63) 0.89, 1.52	II
05.08	6	3	10 III	709.09		I
04.24	6	4	10 III	713.05		I
02.04c	10	10	20 III	723.43		I
01.65	—	3		725.27		II
4,600.59	1	5h		730.27		II
4,596.19	6	6	10 I	751.08		I
95.06	1	2h		756.42		II
89.89	5	5		780.93		I
87.14	—	2h		793.99		II
81.20c	10	10	12 III	822.25		I
80.05	50	150	100 V E	827.73	(0.00) 1.51	II
74.87c	150	200	300 III E	852.44	(0.49, **0.98**) 0.49, **0.98, 1.46,** 1.94	II
70.97	6	10	8 V E	871.08	(0.43) 1.00 R	II
70.02	60	50	250 I	875.63	(0.00) 1.34	I
67.90	50	40	200 I	885.78	(0.00) 1.24	I
64.85c	6	4	12 III	900.41	(0.00) 1.42 R	I
62.5	1	5h		911.7		II
59.28	30	100	50 V E	927.16	(**0.00,** 0.18) 1.62	II
58.46	100	200	250 III E	931.10	(0.00 W) 0.88 A^1	II
52.47	8	8	8 II A	959.96	(0.00) 0.87	I
50.76c	8	6	10 III A	968.21	(0.78) 0.38 R	I
50.16	4	3	5 III A	971.11		I
49.50	40	30	50 I	21,974.30	(0.00) 1.08	I
41.78c	10	8	15 III	22,011.65		I
40.71	3	10		016.84	(0.00) 1.27	II
38.87	1	8hl		025.76		II
37.57	2	2		032.07		I
30.54	4	15	2 V E	066.26		II
28.88	3	2		074.34		I
26.12	100	200	200 III E	087.81	(0.00 W) 1.01 A^1	II
25.31c	40	100	20 V E	091.76	(0.46) 1.19 B	II
22.37	200	400	500 III E	106.12	(0.00) 1.02	II
16.38	2	5hl		135.44		II
08.48	3	10		174.22	(0.00) 0.90	II
07.4	2	2		179.5		I
05.82	1	3hl		187.32		II
02.16	1	10hl		205.35	(0.00) 1.47	II
01.57	6	4	10 II A	208.26		I
4,500.21	30	30	40 II	22,214.97	(0.00 W) 1.10 A^1	I

TABLE 1.—*Wave lengths and Zeeman effects in lanthanum spectra*—Continued

λ (air) I. A.	Intensity arc	Intensity spark B. S.	Arc intensity and temperature class K and C	ν (vac.) cm⁻¹	Zeeman effect	Spectrum
4,499.04c	10	10	10 III	22,220.75	(0.00) 1.02	I
98.76	2	10		222.13	(0.00) 1.14	II
97.00	2	2		230.83		II
94.71c	20	15	30 I	242.16	(0.51) 0.27, **0.58,** 0.91 us	I
93.81	5	3	10 IA	246.61	(0.00) 0.72 R	I
93.11	15	10	25 I	250.08	(0.00) 1.16	I
91.76c	10	8	15 III	256.76	(0.00) 1.52	I
86.06	10	10	20 III	285.04		I
84.48	—	1h		292.90		II
81.21	3	25hl		309.16	(0.40) **0.50,** 0.87	II
79.82c	6	5	15 II A	316.08		I
74.54	4	3	5 III A	342.42		I
74.03	2	10		344.96	(**0.00,** 0.66) 0.50, 1.17, **1.83**	II
68.97	10	6	25 II	370.26		I
59.10	—	3		419.78		II
55.79	20	50	25 V E	436.43	(0.24) 1.41	II
55.21	3	2	10 II A	439.35		I
53.85			2 IV A	446.20		I
52.15	15	15	30 II	449.78	(0.00) 0.98	I
45.12	2	1	2 III A	490.79		I
43.94c	5	20hl	10 I	496.26	(0.00) 1.18 h	I II?
42.68	6	3	12 II	502.64		I
35.84	6	10	6 IV E	537.34	(**0.00,** 0.60, 1.19) 1.28, 1.86, **2.44**	II
32.95	10(?)	20(?)		552.03		II+M
29.90c	200	400	500 III E	567.56	(**0.00,** 0.40) 0.51, 0.91, **1.31**	II
27.52c	30	100	40 V E	579.69	(0.00w) 1.06	II
23.90	20	15	30 II	598.16	(0.00) 1.09	I
19.16	20	30	6 V E	622.41	(0.28) 1.04	II
17.14	2	2h	6n III	632.75		I II
13.45			2 III A	651.67		I
12.22	—	2h		657.98		II
11.21	1	25hl	2 V E	663.17	(0.00h) 1.13h	II
03.02c	2	2	8 III A;	705.33		I II?
4,402.64	5	4	15 III	707.29	(0.00) 0.86	I
4,397.04			2 IV A	736.21		I
96.79c			4 IV A	737.50		I
96.31			2 IV	739.98		I
93.52c	2	1	4 III	754.42		I
89.87	6	4	15 III	773.34	(0.00) 1.07	I
85.20c	10	40	20 V E	797.59	(0.00) 1.24	II
83.44	20(?)	100	25 V E	806.75	(**0.00,** 0.40, 0.80) 0.28, 0.68, 1.08, 1.48, **1.88**	II+M
80.55	4	2	12 II A	821.79		I
78.10c	15	50	15 IV E	834.56	(0.30w) 0.95	II
64.66c	25	100	30 IV E	904.88	(0.00) 1.28	II
63.05	5	50l	4 V E	913.33	(00.0h) 1.32h	II
60.86	2	?	2 III A	924.84		I
60.49	2	2	2 III A	926.78		I
57.88	2	1	2 III A	940.51		I
56.18	—	1		949.46		II
54.79	20	?	25 III	956.79		I
54.40	60	200	80 IV E	22,958.84	(0.00) 1.08	II
40.72c	10	6	15 III	23,031.20	(0.00) 0.90	I
39.93	5	3	6 III A	035.39		I
37.78	2	10l		046.81	(0.00) 1.08h	II
34.96c	50	100	60 V E	061.80	(**0.00,** 0.29, 0.57) 0.69, 0.97, 1.26, **1.54**	II
33.76c	300	500	600 III E	068.19	(0.17) 0.94	II
26.19	2	2		108.55		I
22.51c	60	100	130 III E	128.22	(0.00) 1.10	II
15.90c	10	30	12 V E	163.65	(**0.00,** 0.50, 1.00) 0.86, 1.36, 1.86, **2.36**	II
11.73c	5	4	4 III A	186.05	(0.59) 0.96 R	I
4,306.00	6	5	6 II A	23,216.90	(0.14) 1.49	I

TABLE 1.—*Wave lengths and Zeeman effects in lanthanum spectra*—Continued

λ (air) I. A.	Intensity arc	Intensity spark B. S.	Arc intensity and temperature class K and C	ν (vac.) cm⁻¹	Zeeman effect	Spectrum
4,304.11	1	10hl		23,227.10	(0.00h) 1.24h	II
00.62	H. N. R.		3	245.94		I
4,300.44	40	60	30 IV E	246.92	(0.73, **1.48**) 0.00, **0.72, 1.45,** 2.18	II
4,296.05c	100	300	200 IV E	270.67	(0.00) 1.48	II
91.00	2	2		298.06		I
89.65	H. N. R.		1	305.39		I
89.01	H. N. R.		2	308.87		I
86.97c	80	300	150 V E	319.96	(0.00) 1.08	II
80.27	60	40	100 I	356.46	(0.00) 1.14	I
75.64	50	100	60 IV E	381.75	(**0.00,** 0.35) 0.82, 1.17, **1.52**	II
71.14	4	3		406.39		I
69.50c	80	300	150 V E	415.38	(0.00) 1.20	II
67.74	2	2		425.04		I
63.59c	60	200	100 V E	447.83	(0.00) 1.12	II
62.35	10	5	15 II A	454.66	(0.00w) 1.19	I
59.51	—	2h		470.30		II
56.92c	6	5	6 III A	484.58	(0.00) 1.29 R	I
56.50	—	3		486.89		II
52.93	3	4		506.61		II
49.99c	20	100	25 V E	522.87	(0.74) 0.50, 0.76, **1.02, 1.27,** 1.53, 1.76	II
48.32	—	2		532.11		II
41.20	1	15hl		571.62		II
38.59	4	(?)	10 III A	586.13		I
38.38c	200	400	400 III E	587.30	(0.74) 0.56, 0.82, **1.08, 1.34,** 1.60, 1.86	II
30.95c	20	150	30 V E	628.72	(0.80) 0.65, 0.85, **1.06, 1.26,** 1.47, 1.67 ur	II
17.56c	40	200	80 V E	703.74	(0.00) 1.22	II
16.54	4	3		709.47		I
10.22	4	50hl		745.06	(0.00h) 1.02h	II
07.61	2	10l		759.79	(0.27) 0.68h	II
04.03	40	100	100 V E	780.02	(0.00) 1.48	II
4,201.50		6h		794.34		II
4,196.55c	150	250	300 III E	822.41	(0.32, **0.64**) 0.51, **0.82, 1.13,** 1.44	II
94.36	4	30h		834.85	(0.00h) (1.06h)	II
93.34	1	5		840.64	(0.25) 0.64	II
92.72	H. N. R.		2	844.17		I
92.35c	40	100	80 V E	846.27	(0.00) 1.06	II
87.31	50	30	125 I	874.98	(0.00w) 1.16 A[2]	I
80.97	2	12l		911.18		II
77.48	15	10	30 I	931.15	(0.00) 1.50	I
72.32	6	4	10 III A	960.75		I
71.13	5	4	8 III A	23,967.58		I
63.31	5	4	8 III A	24,012.60		I
61.94	2	8h		020.51	(0.00h) 1.02	II
60.26	20	10	30 I	030.21	(0.00W) 1.65 w	I
57.52	6	5	10 II A	046.04		I
54.59	—	2h		063.00		II
52.78	40	100	40 IV(?) E	073.49	(0.43, **0.84**) 0.27, **0.67, 1.08,** 1.48	II
51.98c	100	250	300 III E	078.13	(0.29) 0.50, **0.77**	II
50.24	2	2		088.22		I
48.2	—	4h		100.1		II
44.36	4	2		122.40		I
43.92	5	(?)	12 III A	124.96		I
43.77	6	15		125.83		II
41.73c	80	200	{40 / 50} IV E	137.72	(0.00W) 1.50w	II
37.91	—	2		160.00		II
37.05	20	10	40 I	165.02	(0.00) 1.22	I
33.33	—	6hl		186.77	(0.00) 0.97	II
32.50	1	10hl		191.63	(0.00h) 0.83h	II
31.74	—	5h		196.08	(0.00h) 1.13h	II
4,123.23	200	400	600 III E	24,246.01	(0.00) 1.05	II

TABLE 1.—*Wave lengths and Zeeman effects in lanthanum spectra*—Continued

λ (air) I. A.	Intensity arc B. S.	Intensity spark B. S.	Arc intensity and temperature class K and C	ν (vac.) cm⁻¹	Zeeman effect	Spectrum
4,117.67	8	5	20 III	24,278.75	(0.00) 0.93	I
15.35	—	1h		292.44		II
13.28	2	40l		304.66	(0.00h) 1.09h	II
09.80	10	6	20 I A	325.24	(0.00) 1.04	I
09.48	6	3	15 II A	327.14	(0.00) 1.26	I
04.87	30	20	60 I	354.46	(**0.08,** 0.25) 0.53, 0.69, **0.85** ur	I
4,101.01	—	3h		377.38		II
4,099.54c	40	150	60 V E	386.12	(0.00) 0.77	II
98.73	1	5		390.94		II
90.40	2	1		440.61		I
89.61	25	12	50 I	445.33	(0.00) 0.93	I
86.72	200	300	400 III E	462.62	(0.32) 0.79 w	II
79.17	20	10	40 I	507.90		I
77.35c	200	300	400 III E	518.84	(**0.00,** 0.32) 0.57, 0.89, **1.20**	II
76.71	10	40	30 IV E	522.68	(**0.00,** 0.31, 0.62) 0.79, 1.08, 1.38, **1.69**	II
67.39c	60	100	125 IV E	578.88	(0.00w) 1.14 A[2]	II
65.58	15	6	30 II	589.82		I
64.79	25	15	50 II	594.60	(0.00w) 1.03 A[1]	I
60.33	30	20	60 II	621.61	(0.00w) 1.10 A[1]	I
58.08	2	5l		635.26	(0.45) 1.06, 1.47us	II
50.08c	50	200	60 V E	683.92	(0.00) 1.02	II
42.91	150	300	300 IV E	727.70	(0.00) 0.99	II
40.97	2	1		739.57		I
37.21	25	10	50 I	762.61	(0.00) 0.86	I
36.59c	7	15d	8 V E	766.41	(0.00) 1.54	II
31.68	100	300	300 III E	793.57	(0.00) 1.15	II
25.87	20	50	40 IV E	832.36	(0.00W) 1.37 A[2]	II
23.58c	10	40	15 IV E	846.49	(0.00) 1.07	II
20.19	—	2h		867.44		II
15.39	25	15	50 I	897.17	(**0.10,** 0.31) **0.90,** 1.10, 1.30, 1.48ur	I
07.64	1	7h		945.32	(0.00W) 1.01h	II
4,001.38	2	2		24,984.34		I
3,995.74c	200	400	600 III E	25,019.61	(0.30) 0.90w	II
94.50c	4	10		027.37	(0.57h) 1.25h	II
88.51c	300	500	800 III E	064.96	(0.00) 1.32	II
81.36	2	10l		109.97	(0.38) 0.98 h us	II
79.08	1	8l		124.35	(0.00) 1.26	II
63.04	1	5l		226.04	(0.00w) 0.82h	II
62.03	1	10l		232.47	(0.00) 1.10h	II
58.53	—	2		254.78		II
57.25	—	2		262.95		II
56.07	1	4		270.48	(0.00h) 1.29h	II
55.21	—	3h		275.98	(0.00) 1.15	II
53.67	10	5	40 II	285.83		I
53.36	—	2		287.81	(0.00) 1.06	II
51.43	1	3h		300.16		II
49.10c	400	600	1000 III E	315.09	(0.00) 1.13w	II
44.15	2	3		346.86	(0.00) 1.18h	II
39.85	2	20l		374.52	(0.21) 1.27h	II
36.22	20	50	60 IV E	397.92	(**0.00,** 0.25, 0.48) 0.86, 1.10, 1.34, **1.58**	II
32.53	3	10l		421.75	(0.44) 1.06 B	II
30.47	—	3		435.07	(0.00) 0.92	II
29.22c	100	300	500 III E	443.17	(0.00) 1.20	II
27.56	30	10	80 I	453.92	(**0.00**) **0.76**	I
25.09	1	5		469.94		II
24.69	—	3		472.53	(0.00h) 0.72h	II
21.54c	70	200	300 III E	492.99	(**0.00,** 0.66) 0.52, 1.18, **1.34**	II
16.05c	80	300	400 III E	528.73	(0.38) **0.51,** 0.88	II
10.81	4	10l	15 IV (?) E	562.94	(0.00) 1.04	II
3,902.57	5	3	20 II	616.91		I
3,898.60	8	4	40 II	642.99		I
97.43	2	4		650.70		II
95.65			8 IV	662.42		Fe(?)
92.47	—	3		683.37	(0.00h) 1.4h	II
92.05	—	3		686.15		II
3,886.37	60	150	400 III E	25,723.69	(0.00W) 1.62 A[2]	II

TABLE 1.—*Wave lengths and Zeeman effects in lanthanum spectra*—Continued

λ (air) I. A.	Intensity arc	Intensity spark B. S.	Arc intensity and temperature class K and C	ν (vac.) cm⁻¹	Zeeman effect	Spectrum
3,885.09	1	4		25,732.16		
71.64	100	200	300 III (?) E	821.56	(0.00) 1.08	II
68.35	—	3h		843.52		II
64.49	6	100l		859.33	(0.00h) 1.10h	II
63.11	—	2		878.57		II
60.31	—	2		897.34		II
54.91	15	30		933.62	(0.00) 1.50	II
49.02	40	100	200 III (?) E	973.30	(0.00) 0.69	II
46.00	10	20	20 V (?) E	25,993.69	(0.36) 1.11 B	II
40.72	40	60	50 V (?) E	26,029.43	(0.00) 1.04	II
36.4	—	1		058.7		II
35.09	15	50	20 V E	067.64	(0.00) 1.49	II
17.24	1	8h		189.53	(0.00) 0.82h	II
16.25	2	10h		196.33	(0.00 h) 0.68	II
14.1	—	2		211.1		II
08.79	10	15		247.63	(0.00w) 1.18h	II
07.1	—	1		259.3		II
04.8	—	2h		275.2		II
3,801.0	—	1		301.4		II
3,798.19	—	2		320.88		II
94.78	150	400	600 III E	344.54	(0.00) 1.16	II
90.83	100	300	600 III E	371.99	(0.00) 1.00	II
84.81	8	15	20 V E	413.93	(0.17) 0.79	II
83.06	—	1		426.15		II
80.67	20	50 (?)	50 V E	442.85	(0.00) 1.54	II
80.53	5	50 (?)		443.84	(0.00h) 0.92h	II
73.12	10	150l		495.77	(0.00) 1.00h	II
68.98	1	3h		524.87		II
67.05	1	5h		538.46	(0.47) 1.24 B	II
66.58	1	3h		541.77		II
59.08	100	300	600 III E	594.72	(0.00) 1.25	II
53.04	—	2h		637.52		II
47.96	1	5l		673.63	(0.00w) 0.90h	II
44.85	—	2h		695.78		II
36.41	2	15l		756.08	(0.37) 1.20 B	II
35.85	6	10	20 IV E	760.09	(0.00w) 0.90d	II
35.09	—	1		765.53		II
31.42	1	8h		791.86		II
28.97	—	2h		809.46		II
25.05	10	20	40 IV E	837.67	(**0.00**, 0.38, 0.75) 0.79, 1.16, 1.53, **1.90**	II
24.77			2 V	839.69		
20.75	—	2		868.69		II
17.99	1	2		888.63		II
15.53	20	50	80 IV E	906.44	(0.40, **0.72**) 0.80, **1.13, 1.46,** 1.79	II
14.87	10	40	60 V E	911.22	(0.00) 1.50	II
14.30	2	2		915.34		I
13.54	30	100	300 IV E	920.85	(**0.00**, 0.34, 0.68) 1.00, 1.35, 1.69, **2.03**	II
10.61	—	2		942.11		II
05.81c	25	80	125 V E	977.01	(0.00) 1.51	II
04.54	10	4	40 II	26,986.25	(0.00) 1.08	I
3,701.81	4	40l	4 V E	27,006.15	(0.00W) 0.73A¹	II
3,699.57	4	2	12 III A	022.51		I
96.11	—	2h		047.80		II
95.2	—	2h		054.5		II
94.27	2	7h		061.27	(0.36) 0.88h	II
92.31	—	2h		075.64		II
78.24	—	2h		179.20		II
75.22	—	1		201.54		II
72.02	8	4	30 III	225.24		I
70.23	1	4h		238.52	(0.30) 1.06	II
69.27	—	3h		245.65		II
65.22	2	10l		275.75	(0.00d) 1.92d	II
62.08	15	30	50 IV E	299.14	(0.66) 1.16 B	II
58.40	1	3		326.60	(0.00) 1.0	II
3,658.04	—	1		27,329.29		II

TABLE 1.—*Wave lengths and Zeeman effects in lanthanum spectra*—Continued

λ (air) I. A.	Intensity arc	Intensity spark B. S.	Arc intensity and temperature class K and C	ν (vac.) cm⁻¹	Zeeman effect	Spectrum
3, 652. 62	—	1h		27, 369. 84		II
50. 19	25	80	125 V E	388. 06	(0.48, **0.91**) 0.29, **0.73, 1.18**, 1.62	II
49. 55	10	6	40 II	392. 86	(0.00) 1.00	I
45. 43	50	200	400 IV E	423. 82	(0.00) 0.66	II
41. 66	10	50l		452. 21	(0.00) 1.21	II
41. 53	20 (?)	(?)	100 II (+E)	453. 19		I
41. 10	—	2		456. 43	(0.00) 1.01	II
39. 25	1	3h		470. 39		II
37. 15c	10	40	50 V E	486. 25	(0.00) 1.51	II
36. 67	6	2	40 III	489. 88		I
29. 99	1	2hl		540. 46		II
28. 83	20	60	125 IV E	549. 27	(0.00W) 1.68 A [2]	II
21. 77	2	4	4 V E	602. 97		II
20. 16	1	1		615. 24		II
18. 60	—	1		627. 15		II
13. 08	10	4	30 II	669. 36	(0.00) 0.97	I
12. 34	5	50	8 V E	675. 02	(0.00) 1.11	II
11. 09	1	2		684. 60	(0.00) 1.57h	II
10. 25	4	30 l		691. 04	(0.00) 1.02	II
09. 22	—	4		698. 95	(0.00) 1.00	II
08. 18	—	4		706. 93	(0.00w) 1.08 A [2]	II
06. 42	—	4hl		720. 45		II
3, 601. 07	5	20hl	15 V E	761. 63	(0.00) 1.18	II
3, 598. 93	—	3hl		778. 14	(0.00) 1.15	II
96. 65	—	4hl		795. 75	(0.00) 1.22	II
93. 29			2 V E	821. 74		
92. 42	—	2h		828. 48		II
90. 66	—	1h		842. 11		II
85. 53	—	2		881. 95	(0.00) 1.25	II
81. 68	1	20hl		911. 92	(0.00) 0.74	II
80. 10	—	8h		924. 24	(0.00) 1.52	II
78. 89	—	5 h		933. 68	(0.00) 1.44	II
76. 56	—	2hl		951. 88		II
74. 43	20	6	50 II	27, 968. 53	(0.00) 0.83	I
70. 10	(?)	30hl		28, 002. 38	(0.00) 1.08	II
57. 26	3	8	20 IV (?) E	103. 53		II
50. 82	3	6	15 IV (?) E	154. 49		II
36. 87	—	3h		269. 53		II
33. 67	—	3h		291. 13		II
30. 67	4	8	20 V (?) E	315. 17		II
26. 77	—	2h		346. 48		II
20. 72	2	10hl		395. 19	(0.00) 0.88	II
17. 14c	5e	200	— V E	424. 09	(0.73) 1.36	III
14. 87	—	2h		442. 45		II
14. 07	6	3	20 II A	448. 92		I
12. 93	5	10	25 IV E	458. 15	(0.53) **0.53**, 1.10	II
10. 00	6	15	25 IV E	481. 91		II
3, 507. 90	—	4hl		498. 96		II
3, 493. 97	—	2h		612. 58		II
84. 39	2	10l		691. 25	(0.00) 1.33	II
80. 61	3	2	8 III A	722. 40		I
74. 84	2	8l		770. 10		II
66. 46	—	1h		839. 64		II
62. 32	—	2h		874. 13		II
61. 18	10	3	25 III A	883. 64		I
60. 31	2	5l		890. 90		II
53. 17c	40	50	70 III E	950. 63	(0.93) 0.37, 0.68, **1.00, 1.31**, 1.63, 1.94.	II
52. 18c	30	40	50 III E	958. 94	(0.00) 0.95	II
51. 12	—	3l		967. 83		II
50. 65	5	2	12 III A	28, 971. 78		I
32. 81	2	5		29, 122. 34		II
27. 57	2	8		166. 85		II
23. 9	3	5		198. 1		II
22. 44	1	2		210. 57		II
3, 420. 54	1	5h		29, 226. 80		II

TABLE 1.—*Wave lengths and Zeeman effects in lanthanum spectra*—Continued

λ (air) I. A.	Intensity arc	Intensity spark B. S.	Arc intensity and temperature class K and C	ν (vac.) cm⁻¹	Zeeman effect	Spectrum
3,411.76	2	20hl		29,302.01	(0.00 w) 1.48	II
07.00	1	8hl		342.95	(0.00) 1.50	II
3,404.53	10	3	15 III A	364.24		I
3,398.29	1	2h		418.15		II
97.77	4	40hl	4 V E	422.65	(0.24) 0.85	II
92.94	1	4h		464.54		II
90.40	1	4h		486.61		II
88.61	6	2	12 II A	502.18		I
81.42			15 II A	564.92		I
80.91	200	300	400 III E	569.36	(**0.00**, 0.37) **0.75**, 1.11, 1.47	II
76.33	40	50	40 III E	609.49	(0.00) 0.88	II
74.89	1	3		622.12		II
68.36	3	—		679.54		I
64.88	2	—		710.24		I
62.04	7	3	12 III A	735.33		I
57.50	5	2	7 III A	775.54		I
51.89	—	3		825.37		II
49.82	2	—	3 III A	843.80		I
44.56	150	200	300 III E	890.73	(0.00) 0.53	II
42.23	10	5	20 II A	911.57	(0.00) 1.08	I
37.49	200	300	500 III E	29,954.05	(0.00w) 1.12 A[1]	II
29.07	2	8		30,029.81		II
26.21	1	5		055.63		II
25.33	1	3		063.59		II
10.62	1	4		197.16		II
06.98	7	8	10 IV E	230.40	(0.00) 1.77 R	II
3,303.11c	100	150	200 III E	265.82	(1.00) 0.51, **1.51**	II
3,298.72	—	5h		306.09		II
97.15	1	3		320.52		II
94.44	1	10		345.46		II
83.95	1	8h		442.39		II
77.83	—	4		499.23		II
67.31	1	3		597.43		II
65.67c	80	100	150 III E	612.79	(0.48, **0.80**) 0.82, **1.17**, **1.51**, 1.86	II
63.98	2	5		628.64		II
56.60	2	1		698.05		I
53.41	2	10h		728.15	(0.00) 0.65	II
49.35	60	80	100 III E	766.54	(**0.00**, 0.50), **0.46**, 0.94, 1.44	II
47.06	5	2	8 II A	788.24		I
45.13	100	150	200 III E	806.55	(0.00) 1.04	II
35.66	3	2	5 III A	896.71		I
26.03	1	2		30,988.93		II
24.71	—	1		31,001.62		II
17.12	2	8h		074.76		II
15.81	10	2	15 II A	087.42	(0.00) 1.13	I
12.56	1	5		118.86		II
09.13	2	6		152.12		II
08.13	1	6		161.83		II
05.75	3	4		184.96		II
3,204.55	1	3		196.64		II
3,194.70	—	2		292.83		II
93.02c	15d	25	{ 10(?) IV E 15(?) IV E }	309.29	(**0.00**, 0.96) 0.61, 1.58, **2.54**	II
91.39	1	10h		325.28		II
79.78	4	2	8 III A	439.65		I
75.99	8	2	15 II A	477.17		I
74.88	1	10hl		488.18		II
71.68c	8e	300	— V E	519.94	(0.37) **0.99**, 1.76	III
66.26	1	2		573.90		II
65.19	1	4		584.57		II
60.56	1	3		630.84		II
57.58	1	2		660.69		II
56.35	—	2		673.02		II
48.51	4	2	4 III A	751.89		I
45.7	1	2h		780.3		II
3,142.76	30	40	50 IV E	31,809.98		II

TABLE 1.—*Wave lengths and Zeeman effects in lanthanum spectra*—Continued

λ (air) I. A.	Intensity arc	Intensity spark B. S.	Arc intensity and temperature class K and C	ν (vac.) cm⁻¹	Zeeman effect	Spectrum
3,132.14	—	3		31,917.83		II
30.25	—	2		937.10		II
25.72	1	4hl		31,983.39		II
12.63	1	8h		32,117.88		II
09.42	8	3	12 II A	151.04		I
08.46	6	8	5 IV E	160.97		II
3,104.58	40	50	60 IV E	201.16	(0.00 W) 1.50 A [3]	II
3,096.02	8	2	10 II A	290.19		I
94.76	—	4h		303.34		II
88.53	—	4h		368.49		II
81.42	1	6h		443.18		II
75.51	—	4h		505.52		II
69.45	—	3		569.69		II
68.96	—	4		575.09		II
59.91	1	8		671.23		II
54.02	2	6		734.24		II
49.39	2	5		783.94		II
45.63	—	1		824.41		II
36.43	1	2		923.86		II
35.9[illegible]	—	1		32,930.69		II
28.64	—	2		33,008.54		II
25.88	—	4(?)		038.65		II
22.26	1	5hl		078.22		II
18.95	1	6hl		114.48		II
10.78	4	3	2 IV A	204.34		I
07.32	2	5		242.54		II
04.68	—	5h		271.74		II
3,001.41	2	—		307.99		I
2,992.99	2	—		401.69		I
85.76	1	2		482.57		II
85.43	2	5		486.27		II
84.33	2	3		498.61		II
83.44	—	3		508.61		II
76.83	—	3		583.01		II
71.48	—	1		643.47		II
66.55	1	4		699.33		II
66.08	—	2		704.72		II
62.90	2	15		740.89		II
59.85	2	5		775.65		II
58.71	—	1		788.67		II
51.46	1	3		871.66		II
50.50	8	50	2 V E	882.68	(0.00) 1.04	II
48.82	—	1		901.99		II
43.56	1	6hl		33,962.57		II
39.64	—	3h		34,007.85		II
29.86	1	7		121.37		II
25.15	1	5h		176.31		II
23.90	2	20		190.92	(0.00) 1.23 (?)	II
13.60	—	2		311.78		II
10.05	—	1		353.63		II
09.65	2	—		358.36		I
05.53	1	4hl		407.07		II
2,904.62	1	—		417.85		I
2,899.80	1	4hl		475.06		II
97.76	2	5hl		499.32		II
93.08	10	60	4 V E	555.14	(0.00) 1.12	II
89.11	—	1		602.61		II
85.13	10	50	4 V E	650.35	(0.00) 1.04	II
83.35	—	1		671.74		II
80.65	8	40	3 V E	704.23	(0.00) 1.18	II
76.55	—	1		753.69		II
74.28	—	3		781.14		II
73.20	—	2		794.21		II
67.47	1	2h		863.74		II
2,862.98	5	15hl	1 V E	34,918.41		II

TABLE 1.—*Wave lengths and Zeeman effects in lanthanum spectra*—Continued

λ (air) I. A.	Intensity arc	Intensity spark B. S.	Arc intensity and temperature class K and C	ν (vac.) cm^{-1}	Zeeman effect	Spectrum
2,862.37	3	6		34,925.85		II
59.76	3	5		34,957.73		II
55.90	10	50hl	1 V E	35,004.97	(0.00) 1.13	II
53.72	1	4h		031.71		II
49.51	1	2h		083.47		II
48.34	3	6		097.88		II
46.67	1	5		118.47		II
43.67	1	4		155.51		II
40.51	3	25hl		194.62		II
38.45	3	5l		220.16		II
32.53	1	5		293.77		II
25.82	—	1		377.57		II
25.51	1	5		381.45		II
21.03	1	5		437.64		II
19.73	1	2		453.97		II
18.40	1	3		470.70		II
17.46	2	—		482.54		I
15.36	3	6		509.00		II
13.72	2	5		529.70		II
13.05	1	3		538.16		II
09.35	1	2		584.96		II
08.39	40	150	10 V E	597.13	(0.00) 1.04	II
07.20	—	1		612.22		II
05.58	3	5		632.78		II
2,804.55	2	4		645.86		II
2,798.56	8	40hl	1 V E	722.15	(0.00) 1.08	II
96.40	3	5		749.75		II
94.03	4	1		780.07		I
91.51	8	25		812.37	(0.00) 1.04R	II
81.25	—	1		944.47		II
80.23	4	20		957.66		II
79.78	2	10		963.48		II
78.76	2	10		35,976.68		II
73.86	—	1		36,040.23		II
67.40	1	8		124.35		II
66.46	4	1		136.62		I
61.56	7	1		200.74		I
61.10	1	5		206.77		II
60.51	1	3		214.51		II
59.54	4	1		227.24		I
59.14	—	3		232.49		II
58.65	—	3		238.93		II
56.57	2	—		266.27		I
55.57	—	1		279.43		II
52.84	1	10		315.41		II
49.52	2	—		359.25		I
48.31	1	8		375.26		II
39.25	4	1		495.56		I
37.49	3	1		519.03		I
36.90	—	2		526.90		II
36.41	—	3		533.44		II
32.40	1	10		587.05		II
30.15	2	—		617.20		I
29.85	5	2		621.22		I
27.5	—	2		652.8		II
26.48	—	1		666.49		II
25.57	15	3		678.73		I
22.31	6	2		722.65		I
21.45	—	2		734.25		II
17.33	2	—		789.90		I
15.77	3	—		811.08		I
15.43	1	10hl		815.68		II
14.52	8	1		828.03		I
12.51	—	1		855.32		II
2,710.69	4	1		36,880.06		I

TABLE 1.—*Wave lengths and Zeeman effects in lanthanum spectra*—Continued

λ (air) I. A.	Intensity arc B. S.	Intensity spark B. S.	Arc intensity and temperature class K and C	ν (vac.) cm⁻¹	Zeeman effect	Spectrum
2,709.92	—	3		36,890.54		II
07.07	3	1		929.38		I
06.49	—	2		937.29		II
2,702.13	5	8		36,996.88		II
2,695.47	15	35		37,088.29		II
94.21	—	5		105.64		II
91.60	—	1		141.62		II
87.75	—	2		194.81		II
84.90	—	50hl		234.29		III
84.11	6	1		245.25		I
82.46	—	30hl		268.16		III
81.49	4	10		281.64		II
79.87	—	4h		304.17		II
77.77	2	—		333.43		I
75.66	2	5		362.87		II
73.74	1	3		389.70		II
72.90	15	30		401.45		II
72.06	—	2		413.20		II
71.91	2	—		415.30		I
70.05	—	2		441.37		II
66.54	1	3		490.65		II
66.18	2	6		495.71		II
65.62	—	4		503.59		II
64.75	1	3		515.83		II
62.73	—	1h		544.29		II
61.66	1	3		559.38		II
61.36	1	4		563.61		II
53.48	2	—		675.16		I
51.60	—	300hl		701.87		III
49.61	—	1		730.18		II
47.36	1	4		762.25		II
47.13	2	—		765.53		I
44.70	—	1		800.23		II
42.27	—	1		834.96		II
40.15	—	1		865.37		II
39.00	1	5		881.87		II
36.66	—	1		915.48		II
31.94	2	8		983.47		II
31.52	1	4		37,989.54		II
20.01	2	7		38,156.42		II
17.29	—	1		196.07		II
16.32	2	7hl		210.23		II
13.09	1	4		257.46		II
10.34	50	150		297.76		II
04.18	—	1		388.35		II
02.87	—	1		407.66		II
01.79	1	5		423.60		II
00.86	—	2		437.34		II
2,600.33	1	4		445.18		II
2,596.32	1	3		504.55		II
96.08	6	20		508.11		II
92.87	—	3h		555.78		II
86.35	2	10		652.97		II
82.96	1	8		703.70		II
82.55	2	6		709.85		II
80.82	3	8hl		735.79		II
77.92	—	2		779.36		II
73.47	—	2h		846.42		II
66.09	3	10hl		38,958.13		II
61.84	2	20l		39,022.75		II
60.37	10	50		045.15		II
58.99	—	3		066.21		II
58.72	—	2		070.33		II
53.41	—	3h		151.57		II
2,552.60	—	7		39,164.00		II

TABLE 1.—*Wave lengths and Zeeman effects in lanthanum spectra*—Continued

λ (air) I. A.	Intensity arc	Intensity spark B. S.	Arc intensity and temperature class K and C	ν (vac.) cm⁻¹	Zeeman effect	Spectrum
2,552.36	—	2		39,167.68		II
46.40	4	20hl		259.35		II
42.40	—	6		321.11		II
41.60	1	4		333.49		II
38.40	—	2		383.07		II
36.76	—	3		408.53		II
34.98	2	6		436.21		II
33.14	10	15		464.84		II
31.60	—	8		488.84		II
30.26	—	1		509.76		II
27.84	—	3		547.58		II
23.07	1	5hl		622.34		II
19.22	10	50		682.89		II
15.79	—	4		736.99		II
14.59	—	3		755.95		II
2,501.18	1	15hl		969.08		II
2,499.69	—	1		39,992.91		II
95.82	—	2		40,054.91		II
94.90	—	1		069.68		II
87.59	10	40		187.42		II
83.00	1	5hl		261.71		II
79.85	5?	10l		312.85		II
78.8		20hl		329.9		III
76.72	—	100hl		363.79		III
74.50	—	3		400.00		II
72.44	1	10		433.65		II
71.90	15	20		442.49		II
71.06	—	5		456.23		II
70.55	—	3		464.58		II
68.11	—	1		504.58		II
58.15	—	2		668.69		II
55.88	—	10		706.28		II
54.30	—	1		732.48		II
52.73	1	8		758.55		II
51.59	—	2		777.50		II
45.56	—	10h		878.04		II
43.14	—	2h		918.53		II
42.80	—	3		924.22		II
39.08	—	2		986.63		II
38.42	—	10		40,997.82		II
38.02	2	20		41,004.45		II
37.14	1	10		019.26		II
36.42	1	15		031.37		II
31.40	—	6h		116.08		II
24.53	—	2h		232.58		II
21.61	—	5h		282.29		II
20.01	1	5hl		309.58		II
17.61	—	3h		350.59		II
12.08	—	2h		445.38		II
10.10	—	5hl		479.43		II
07.79	—	5hl		519.22		II
04.65	—	6		573.43		II
03.29	1	7		596.96		II
2,401.46	—	2h		628.66		II
2,399.64	3	20hl		660.22		II
98.70	—	3h		676.55		II
97.26	1	7hl		701.57		II
94.98	—	4		741.27		II
93.27	—	2h		771.10		II
89.84	—	3hl		831.04		II
88.96	—	2		846.45		II
86.26	—	2		893.80		II
84.28	—	3h		41,928.58		II
79.38	5e	200h		42,014.92		III
75.63	—	2h		081.24		II
2,370.47	—	2		42,172.84		II

TABLE 1.—*Wave lengths and Zeeman effects in lanthanum spectra*—Continued

λ (air) I. A.	Intensity arc	Intensity spark B. S.	Arc intensity and temperature class K and C	ν (vac.) cm^{-1}	Zeeman effect	Spectrum
2,369.18	—	2		42,195.79		II
65.50	—	3		261.43		II
58.02	—	3h		395.48		II
56.10	—	1h		430.02		II
55.81	—	5h		435.24		II
53.40	—	2		478.70		II
53.03	—	1		485.48		II
51.93	—	1		505.24		II
48.86	—	2		560.79		II
41.85	—	4		688.18		II
28.75	4	20hl		42,928.29		II
22.78	—	3h		43,038.62		II
19.44	15	20		100.59		II
17.82	5	20hl		130.71		II
2,311.45	—	1		249.56		II
2,297.75	4e	200hl		507.40		III
93.47	—	2h		588.59		II
92.32	1	3		610.45		II
80.94	—	4h		828.01		II
76.06	—	1h		43,921.97		II
65.54	—	3		44,125.90		II
56.77	40	50		297.36		II
30.74	—	7		44,814.20		II
16.08	2e	100hl		45,110.63		III
07.08	—	1		294.56		II
2,202.76	—	1		383.38		II
2,195.91	—	4		524.94		II
90.67	—	1		633.82		II
87.87	30	40		45,692.22		II
63.66	5	20hl		46,203.12		II
61.36	—	4		252.58		II
2,142.81	2	20hl		46,642.94		II

TABLE 2.—*Band heads in the spectrum of lanthanum monoxide (La O)*

λ air I. A.	Intensity	ν vac cm^{-1}	System and v′, v″
8,423.3	2	11,868.6	VII 14, 14
8,994.5	3	11,114.9	VII 14, 15
9,035.9	1	11,063.9	VII 15, 16
9,073.4	1	11,018.2	VII 0, 2
9,111.5	2	10,972.1	VII 1, 3
9,150.1	2	925.9	VII 2, 4
9,188.8	4	879.8	VII 3, 5
9,228.15	4	833.4	VII 4, 6
9,267.8	4	787.1	VII 5, 7
9,307.8	4	740.7	VII 6, 8
9,348.2	3	694.3	VII 7, 9
9,388.8	3	648.1	VII 8, 10
9,429.9	3	601.7	VII 9, 11
9,471.4	3	555.2	VII 10, 12
9,513.3	3	508.7	VII 11, 13
9,555.5	3	462.3	VII 12, 14
9,582.2	3	415.8	VII 13, 15
9,641.1	3	369.4	VII 14, 16
9,684.8	3	322.6	VII 15, 17
9,729.1	3	10,275.6	VII 16, 18

WASHINGTON, June 11, 1932.

NOTE ON THE FREEZING POINT OF "ISO-OCTANE" (2, 2, 4-TRIMETHYLPENTANE) [1]

By Johannes H. Bruun [2] and Mildred M. Hicks-Bruun

ABSTRACT

A high-grade sample of commercial iso-octane was purified by equilibrium melting. The freezing point of the pure hydrocarbon was found to be −107.41° C. The purity of an iso-octane sample may be calculated from the equation: Mole per cent purity $=3.86_2 t_F + 514.8$ in which t_F is the initial freezing point of the sample in ° C.

"Iso-octane" (2, 2, 4-trimethylpentane) is used as the upper reference standard for antidetonation tests of motor fuels. As a

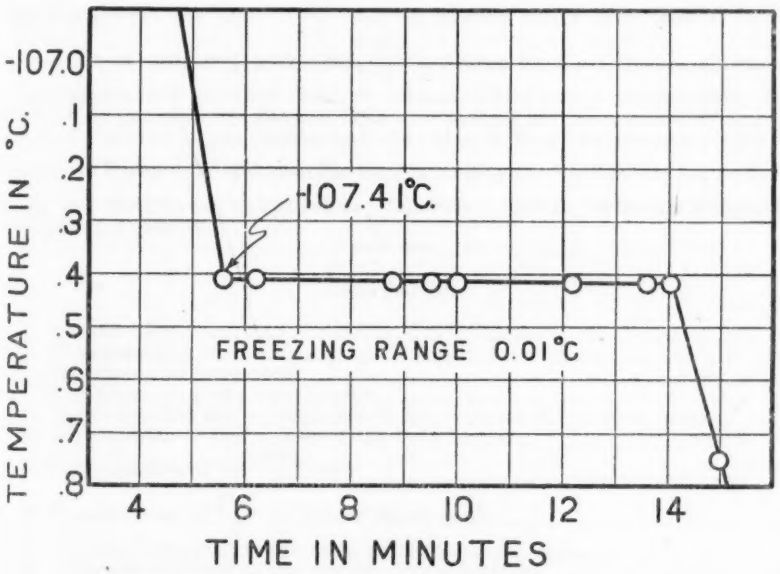

FIGURE 1.—*Time-temperature cooling curve of iso-octane*

criterion for the purity of commercial "iso-octane," it is desirable to have a reliable value for the freezing point of the pure hydrocarbon. The value (−107.8° C.) reported in the literature [3] is apparently too low as many commercial samples were found to freeze at temperatures above this value.

[1] Financial assistance has been received from the research fund of the American Petroleum Institute. This work is part of Project No. 6, "The Separation, Identification, and Determination of the Constituents of Petroleum."

[2] Research Associate representing the American Petroleum Institute at the Bureau of Standards.

[3] G. M. Parks and H. M. Huffman, Ind. Eng. Chem., vol. 23, p. 1139, 1931.

A sample of high-grade commercial "iso-octane" was purified further by subjecting it to a number of fractionations by equilibrium melting in a centrifuge.[4] As a result of these fractionations four different fractions with freezing points ranging from −107.7° to −107.4° C. were obtained. The time-temperature cooling curve of the purest fraction of "iso-octane" was determined, and is shown in Figure 1.

From the value, −107.41° C., found for the freezing point of pure iso-octane and from Parks and Huffman's value [5] (18.9 cal./g) for the heat of fusion, the purity of the iso-octane may be calculated from the laws of ideal solutions and is expressed by the equation: $P=3.86_2t_F+514.8$ in which t_F is the initial freezing point of the sample in ° C., and P is the purity in mole per cent.

Temperatures were determined by means of a platinum-resistance thermometer calibrated at this bureau in accordance with the International Temperature Scale [6] as adopted in 1927.

WASHINGTON, May 4, 1932.

[4] For method see M. M. Hicks-Bruun and J. H. Bruun, B. S. Jour. Research, vol. 8, p. 527, 1932.
[5] See footnote 3, p. 269.
[6] B. S. Jour. Research, vol. 1, p. 635, 1928.

A TWIN-BOMB METHOD FOR THE ACCURATE DETERMINATION OF PRESSURE-VOLUME-TEMPERATURE DATA AND A SIMPLE METHOD FOR THE ACCURATE MEASUREMENT OF HIGH PRESSURES

By Edward W. Washburn

ABSTRACT

By filling one bomb, A, with the system under investigation and a twin bomb, B, with a reference substance and then adjusting the two pressures to exact equality (at a given temperature) with the aid of a pressure equalizer, the ratio of $\frac{PV_0}{T}$ per gram for the two systems can be accurately determined by weighing the two bombs. No pressure measurements are involved. If now the volume of bomb B is known, the value of $\frac{PV_0}{T}$ for the system under investigation can be computed to the accuracy with which $\frac{PV_0}{T}$ is known for the reference substance.

Furthermore, if a gas-filled bomb of volume V at a known temperature, T, is brought into pressure equilibrium with any system at the pressure P and the mass of the contained gas determined, the value of P can be computed with the accuracy to which $\frac{PV_0}{T}$ is known for the gas employed. In this way an ordinary balance and weights can be utilized as a laboratory tool for the accurate measurement of high pressures.

CONTENTS

		Page
I.	Introduction	271
II.	Equipment	272
III.	Experimental procedure	273
IV.	Construction of the twin bombs	273
V.	Determination and equalization of the volumes of the twin bombs	273
VI.	Equalization of the masses of the twin bombs	274
VII.	Computation of the $\frac{PV_0}{T}$ ratio	274
VIII.	Computation of $\frac{PV_0}{T}$ for the reference gas	275
IX.	Accuracy required in the mass determinations	275
X.	Accuracy required in the volume determinations	276
XI.	Selection of the reference gas	276
XII.	Adaptation of the method to liquids and solids and to polyphase systems	277
XIII.	The use of a gas-filled bomb as a pressure gage	277
XIV.	Determination of the mass of the gas after removal from the bomb	277
XV.	Conclusion	278

I. INTRODUCTION

For practical purposes the task of accumulating accurate physical data concerning chemical substances and systems may be roughly divided into two categories. To the first category belong those pri-

mary measurements in which the measuring instruments employed are more or less directly standardized in terms of the fundamental units of science, for example in cgs (e or m) °K. units.[1] Such measurements may be called primary or "absolute" measurements to distinguish them from the second category, which may be designated as secondary or relative measurements.

This category comprises measurements in which the apparatus and instruments employed are in part at least, standardized with the aid of a substance or material for which accurate values are available from primary measurements carried out as outlined above or which is selected by convention as the reference substance.

Measurements in this class are fundamentally relative measurements, but they can be converted to absolute values through the standardizing material employed, and if the accuracy of the relative measurements is sufficient, the absolute values obtained in this way should be as reliable as are the primary data for the standardizing substance. Examples of measurements belonging to the second category are the determination of the viscosity of a liquid with a viscosimeter standardized with water and the determination of the heat of combustion of an organic substance with a bomb calorimetric equipment standardized with benzoic acid.

In some cases the relative measurements are so much more precise than any primary measurements that a conventional value is sometimes adopted for the standardizing substance. This conventional value may be purely arbitrary, as in the atomic weight table, or it may be the best at-the-time available absolute value with zeros assumed in all places following the last known figure, as in the measurement of current in so-called "international amperes" by means of a silver coulometer.

The relative method frequently has the advantage of greater rapidity in the measurements combined with simplicity and relative inexpensiveness in the equipment required, these advantages being sometimes combined with a higher degree of accuracy than that obtainable in the absolute measurements.

So far as the writer is aware, no attempt has been made to determine directly and accurately the ratio of PV/T for two gases at high pressures.[2] The purpose of this paper is to outline a simple method for doing this and to show that this method may be extended to the determination of pressure-volume-temperature data for any system.

II. EQUIPMENT

The equipment to be employed consists of:

1. A pair of twin bombs as nearly identical as possible in all respects.
2. Inexpensive Bourdon gages.
3. A good thermometer.
4. A well-stirred constant-temperature bath, or baths, variable over the temperature range desired.
5. A good balance and set of weights.
6. Means for obtaining the gases under the desired pressures.

No accurate pressure measuring equipment is required.

---

[1] Centimeter, gram, second (electrostatic or electromagnetic), °K.

[2] For very low pressures, below 1 atmosphere, an interesting and accurate relative method has been described by Addingley and Whytlaw-Gray, Trans. Faraday Soc., vol. 24, p. 378, 1928.

III. EXPERIMENTAL PROCEDURE

The investigator first selects, on the basis of available data, a reference gas (or gases) for which satisfactory P–V–T values are available over the pressure and temperature ranges within which he proposes to make his measurements. A typical experiment is carried out as follows: With the aid of an ordinary Bourdon gage one of the bombs is filled at about $t°$ C. with the reference gas, R, at a pressure slightly above that desired for the experiment. The second bomb is filled in the same way with the gas, E, under investigation. Both bombs are placed side by side in the constant-temperature bath regulated to the desired temperature, $t°$ C., and each one is then joined through capillary tubing (and a guard bomb if desired) to a pressure equalizer, for example, a large cylinder containing air (or other suitable fluid) at a pressure slightly below the pressure in the two bombs, and provided with a Bourdon gauge.

The valves of the two bombs are now opened simultaneously and when temperature equilibrium has been attained, the valves are closed, the capillary tubing is disconnected, and the bombs are removed from the bath, dried, and the difference in mass accurately determined. One of the bombs is then evacuated and the difference in mass again determined in the same way, or either of the two may be weighed against a closed dummy bomb of known mass. The ratio of $\frac{PV}{T}$ for unit masses of the two gases can now be calculated, as explained in section VII below.

IV. CONSTRUCTION OF THE TWIN BOMBS

The material used for constructing the bombs will be determined by the nature of the gas to be investigated and the pressure and temperature ranges to be covered.[3] The material selected and the wall thickness adopted should be such that the strain on the bomb will be well within the elastic limit. The thoroughly annealed bomb before calibration is first put through a number of cycles of compression and decompression (filling and emptying) with compressed gas, for the maximum pressure for which it is to be utilized at each temperature. It is now ready for calibration.

The calibration consists in determining the volume of one of the bombs and in determining, or reducing to a negligible amount, two small quantities both of which would be zero, if the bombs were identical twins. These two quantities are the difference in the masses and the difference in the volumes of the two bombs.

V. DETERMINATION AND EQUALIZATION OF THE VOLUMES OF THE TWIN BOMBS

With the aid of the constant-temperature bath and pressure equalizer described above, both bombs are filled with the same gas at the same moderate pressure (preferably a dense gas, such as CO_2,

[3] A discussion of materials suitable for containers for various conditions of temperature, pressure, and corrosive influences has been given by F. G. Keyes (Ind. Eng. Chem., vol. 23, p. 1378, 1931).

purity not essential) or with the same liquid, and the difference, $m_1 - m_2$, in the masses of the fluid, together with the mass, m_1, in one of the bombs is determined as in a regular experiment. The difference in the two volumes is given by the relation

$$\Delta V = V_1 - V_2 = \frac{(m_1 - m_2)V_1}{m_1} \tag{1}$$

To the larger of the two bombs there is now added, in the form of fine shot or wire for example, the right amount of a material, having negligible vapor pressure and negligible (or known) compressibility, to adjust the volumes to exact equality. There is some advantage in using for this purpose the material of the bomb itself.

After this adjustment has been made the now-much-smaller ΔV may be determined as a function of p and T over the proposed experimental range. If the construction and adjustment of the two bombs have been carefully carried out, this value of ΔV should be negligible.

The bombs having been adjusted to equality of volume, the volume of one of them is now determined as a function of pressure and temperature. For atmospheric pressure (zero pressure difference) this value will be known from the above determinations, if the density of the fluid used is known. The temperature coefficient can be calculated from the coefficient of thermal expansion of the bomb or the volume may be determined by calibration at different temperatures.

The small pressure coefficient can, for many purposes, be determined with the necessary accuracy by immersing all but the stem of the bomb in the liquid of a volumeter and reading the increases in volume of this liquid as successively increasing pressures are applied to the bomb. It may also be calculated from the elastic properties of the material composing the bomb. Formulas for this purpose have been given by F. G. Keyes.[4]

For the most accurate work, especially for extreme conditions of temperature and pressure, it may be necessary to check the volume calibration from time to time because of possible hysteresis effects.

VI. EQUALIZATION OF THE MASSES OF THE TWIN BOMBS

The evacuated bombs are now suspended from the arms of a sensitive balance and the masses are adjusted to equality. At the same time a closed dummy bomb can also be provided, if desired, and similarly adjusted to the same mass. This dummy may be employed as a counterpoise for determining the total mass of the gas in one of the bombs, as indicated in the procedure outlined in Section III above.

VII. COMPUTATION OF THE $\frac{PV_0}{T}$ RATIO

From the data obtained by the procedure described in Section III the value of $\pi_E = \frac{PV_0}{T}$ for unit mass of any gas at the pressure and temperature of the experiment is obtained from the relation

$$\frac{\pi_E}{\pi_R} = (1 - \Delta V/V_R)\ (1 + \Delta m/m_E) \tag{2}$$

[4] See footnote 3, p. 273.

in which π_R is the value of $\frac{PV_0}{T}$ for the reference gas at the pressure and temperature of the experiment; V_R is the volume of the reference gas; $\Delta V, = V_R - V_E$, is the difference in the volumes of the two gases; m_E is the mass of the gas under investigation; and $\Delta m, = m_R - m_E$, is the difference in the masses of the two gases. After completing the experiment as described above, it may be repeated by interchanging the gases in the two bombs and ΔV may be eliminated from the two equations thus obtained.

Judging from the precision which should apparently be attainable in the measured quantities, the relative values obtained in this way should be more accurate than many of the absolute values at present available.

VIII. COMPUTATION OF $\frac{PV_0}{T}$ FOR THE REFERENCE GAS

In order to convert into absolute values the relative values obtained by the above procedure, it is necessary to compute the value of π for the reference gas. If the data for this gas have been put into mathematical form by evaluating the parameters of an equation of state in which π is given as a function of V and T, then the value of π is readily calculable since both V and T are known with the necessary accuracy. If only tabulated values of $\frac{PV_0}{T}$ are available for various temperatures and for a series of pressures, then the experimental temperatures employed should include those available for the reference gas and the value of π_R can be obtained by graphing values of $\frac{PV_0}{T}$ against $\frac{T}{V_0}$ in the experimental region and interpolating π_R for the known value T/V_0. At the same time the value of P is obtained to the degree of accuracy corresponding to that of the $\frac{PV_0}{T}$ data of the reference gas.

IX. ACCURACY REQUIRED IN THE MASS DETERMINATIONS

For any specific case the accuracy required in the weighings for any given desired accuracy in π_E/π_R can be judged by inspection of equation (2).

In general, it may be said that an accuracy of 0.01 per cent in π_E/π_R should be practically always attainable, or stated in another way, the masses of the bombs will never need to be so great as to render difficult the attainment of the required accuracy in the weighing operations, and this accuracy will be obtainable with a comparatively inexpensive balance, except possibly in the cases of hydrogen and helium where a balance of high sensitivity might be needed. (See further, Sec. XIV below.)

X. ACCURACY REQUIRED IN THE VOLUME DETERMINATIONS

If the volumes of the two bombs are adjusted to substantial equality, a large percentage error is obviously allowable in both ΔV and V in determining the value of π_E/π_R. For interpolating the absolute value of π_R, V_R must be known with an accuracy which varies with the slope of the $\pi - \frac{T}{V_0}$ curve for the reference gas in the experimental region. Thus, for a considerable region on both sides of the Boyle pressure,[5] large errors in V_R will have but little effect upon the result. In any case V_R can be determined with the required accuracy.

XI. SELECTION OF THE REFERENCE GAS

Since relative values of $\frac{PV_0}{T}$ can be determined with a high degree of accuracy and with comparatively simple equipment, absolute values should be available for one or for a few gases selected on the basis of their advantages as reference gases and these values should be known as accurately as possible and should cover a wide range of temperatures and pressures.

Among the gases which might be selected as suitable reference gases, air has the disadvantages of its oxidizing action at high temperatures and its lack of constancy in composition.[6] In spite of these disadvantages, however, dry, CO_2-free air is likely to be the favored reference gas for measurements of moderate accuracy, say ± 0.1 per cent, because of its ready accessibility. For this reason reliable P–V–T data should be available for air (of known normal density) over wide ranges of temperature and pressure. Furthermore, if the investigator who proposes to use air as a reference gas determines the normal density of the sample of air employed, air would probably be suitable as a reference gas even for measurements of the highest accuracy.

A review of the various other possibilities leads to the conclusion that "atmospheric nitrogen",[6] methane, and carbon dioxide would be suitable as additional reference gases. These gases can be prepared in a high state of purity at reasonable cost. Carbon dioxide could be used for investigations confined to temperatures above, say, 40° C., while methane could be used for temperatures between, say, 200° and −80° C. "Atmospheric nitrogen" could be used at any temperature above, say, −140° C.

---

[5] That pressure at which for a given temperature the PV product is a minimum.

[6] See the extensive data on this question recently obtained by Moles (Gazz. Chim. Ital., vol. 56, p. 915, 1926). This investigator also found that after chemical removal of the oxygen from air, the residue, "atmospheric nitrogen," showed a much more nearly constant density, the maximum variation found being only 1 in 10,000. Apparently, therefore, "atmospheric nitrogen" would be an excellent reference gas for wide ranges of temperature and pressure.

XII. ADAPTATION OF THE METHOD TO LIQUIDS AND SOLIDS AND TO POLYPHASE SYSTEMS

It is obvious from the foregoing discussion that the method described in this paper might also be applied to the determination of P–V–T relations in many systems composed of or containing one or more solid or liquid phases. For this purpose a retaining or immersing liquid may be needed or preferred in the bomb containing the system under investigation and in that case the gas-filled bomb functions purely as a pressure gage.

XIII. THE USE OF A GAS-FILLED BOMB AS A PRESSURE GAGE

If a gas-filled bomb of known volume and temperature is brought into pressure equilibrium with a system at the pressure P, with the aid either of a pressure equalizer such as that described above or with the aid of a nul-point differential gage,[7] and the mass of gas in the bomb determined, then its pressure can be calculated as indicated above and the value thus obtained will be as accurate as are the available PV_0/T data for the gas employed. In this way a balance and weights can be utilized as a laboratory tool for the accurate measurement of high pressures.

The accuracy required in V and T will be determined by the accuracy wanted in P or by the accuracy possessed by $\frac{PV_0}{T}$, whichever happens to be the determining quantity.

The method might also find some application for calibrating an electrical or mechanical pressure gage, in case a dead-weight pressure gage is not available.

XIV. DETERMINATION OF THE MASS OF THE GAS AFTER REMOVAL FROM THE BOMB

The range of pressure over which a given pair of twin bombs can be employed is limited on the high pressure side by the elastic limit of the material of which the bomb is composed and on the low-pressure side by the mass of contained gas which can be determined with the required accuracy by weighing the bomb. If, therefore, a given gas is to be investigated over a very wide range of pressures, a set of bombs would be required. For many gases this necessity can be avoided and a single pair of heavy-walled bombs can be employed in all parts of the pressure range by arranging to remove the gas from the bomb for the purpose of weighing it. Thus CO_2 could be weighed after condensation or after absorption in ascarite (NaOH-asbestos mixture), H_2O and certain alcohols after absorption in Dehydrite ($Mg(ClO_4)_2 \cdot 3H_2O$), a combustible gas after passage through a combustion furnace followed by absorption of CO_2 and/or H_2O as above, etc. These methods are somewhat more time-consuming than direct weighing, but a high degree of accuracy is obtainable and certain other obvious advantages are secured.

[7] For example, the sensitive differential gage described by Osborn, Stimson, and Fiock, B. S. Jour. Research, vol. 5, p. 430, 1930. The differential gage is required whenever direct contact between the system and the fluid of a pressure equalizer is undesirable.

XV. CONCLUSION

The method outlined above will probably find its chief application in chemical laboratories and industrial laboratories which do not have available accurate dead-weight pressure gages, but in which the need occasionally arises of obtaining *P-V-T-* data for gases and vapors and their mixtures. The recent publication of several papers giving rather rough data of this character obtained with Bourdon gages illustrates a growing need for reliable *P-V-T* data for a considerable number of gases and gas mixtures for which no information is at present available. It is hoped that the method described in this paper may be found useful to the occasional investigator who finds it necessary to determine such data for himself.

WASHINGTON, December 28, 1931.

○